PARKIN MEDIATED MITOCHONDRIAL QUALITY CONTROL IN CENTRAL DOPAMINE NEURONS

By

Hae-young Hawong

A DISSERTATION

Submitted to
Michigan State University
in partial fulfillment of the requirements
for the degree of

Biochemistry and Molecular Biology-Doctor of Philosophy

2014

ABSTRACT

PARKIN MEDIATED MITOCHONDRIAL QUALITY CONTROL IN CENTRAL DOPAMINE NEURONS

By

Hae-young Hawong

Parkinson disease (PD) is the second most common neurodegenerative disease. The hallmark pathology of PD is progressive degeneration of nigrostriatal dopamine (NSDA) neurons, but the hypothalamic tuberoinfundibular (TI) DA neurons remain intact. A similar pattern of susceptibility can be seen in these DA neuronal populations following single acute exposure to the mitochondrial Complex I inhibitor, 1-methyl-4-phenyl-1,2,3,6-tetrahydropyridine (MPTP). In this dissertation, mitochondrial structure and function in NSDA and TIDA axon terminals in WT mice were investigated. An increase in mitochondrial bioenergetics, mass, and mitophagosomes were observed in mitochondria derived from medial basal hypothalamus (MBH) containing TIDA neurons as compared to striatum (ST) containing NSDA neurons. The ultrastructure of the mitochondria from the two brain regions did not differ, but MBH had higher numbers of mitochondria per synaptosome than ST. Mitochondrial function differed depending on the brain regions in WT mice. However, mitochondria derived from ST and MBH responded to Complex I inhibition in a similar manner. This suggests that intrinsic differences in the sensitivity of mitochondrial electron transport chain (ETC) enzymes to neurotoxicant inhibition are not responsible for differential susceptibility of NSDA and TIDA neurons to MPTP.

Parkin is a 52Kda cytosolic protein originally identified by linkage analysis in autosomal recessive early onset PD. Parkin is reported to mediate mitochondrial quality control through autophagy of mitochondria, and increased parkin expression is associated with resistance of

TIDA neurons to acute MPTP exposure. Parkin may protect against DA neurodegeneration by maintaining mitochondrial homeostasis in central DA neurons. To test this hypothesis, mitochondrial structure and function in NSDA and TIDA neurons were investigated in parkin null mice. Reduced mitochondrial maximal and spare respirations, mitochondrial mass, number of mitochondria per synaptosome, and disrupted mitochondrial ultrastructure were all observed in the absence of parkin. These results suggest that impaired mitochondrial function is due to decreased numbers of high quality mitochondria in DA axon terminals in the ST of parkin deficient mice. This may be due to loss of parkin-mediated mitochondrial quality control in NSDA neurons.

Parkin rescue via rAAV expression in the midbrain failed to alter impaired mitochondrial function in parkin null mice. However, parkin overexpression prevented inhibition of maximum and spare respiration by MPTP. These results suggest parkin overexpression maintained functional mitochondria likely through autophagy in response to acute neurotoxicant exposure. Therefore, loss of parkin mediated mitochondrial quality control may contribute to loss of NSDA neurons in a neurotoxicant model of DA neuronal degeneration in PD.

ACKNOWLEDGEMENTS

I have always wondered why the doctoral degree is called PhD “Doctor of Philosophy”. PhD is derived from Greek “philosophia” which means love of wisdom. During the PhD training year, I found growing love of wisdom in mitochondria, Parkinson disease, neuroscience, AND love of wisdom in life. I found a growing love for knowledge, responsibility, and ethics as a scientist. In addition, I had a great opportunity to learn American culture and values.

In 2010, due to sudden leave of my previous advisor, I had to choose whether to precede PhD training. I reevaluated and questioned myself, who I was and why I was here. The answer was clear; I chose to continue pursuing a PhD with new project and new adviser. I cannot express my appreciation in any word especially to these two advisers, Drs. Keith Lookingland and John Goudreau. Without these two people, I would not be where I am today. Also, I am very greatful that I had an opportunity to learn and grow so much thanks to these amazing faculties and staffs in DO/PhD program, Drs. McCormick and Maher, and Ms. Bethany Heinlen, and the guidance committee members.

First, I want to thank my advisors Drs. Keith Lookingland and John Goudreau for giving me this opportunity to complete my dissertation under their guidance. Dr. Lookingland, I would like to thank you for guiding me throughout the process. You taught me to be a professional scientist. You guided and taught me to mature into a scientist and when I was mature enough to carry research, you gave me autonomy, where I learned “independence”. This was valuable lesson and experience for me to conduct research and I greatly enjoyed conducting research. I don’t think I can be where I am without your guidance. You are much keened to know how mature the student is as a researcher and what needs she/he requires and provides great guidance. Dr. Goudreau, you have been my role model not only as a scientist but also as a physician. Even with a short

discussion with you, I always felt there was so much more I could learn from you. I hope you could remain as my mentor even after completion of PhD training under you. I thank you so much, Dr. Lookingland and Dr. Goudreau for guiding and supporting me to complete the dissertation.

Also, I want to thank the goudlooking lab members. I want to thank previous lab members, Drs. Benskey, Tiernan, and Simkins and current lab members, Joseph Patterson, Theresa Lansdell, and Brittany Winner for all the supports and help to complete my dissertation. I want to thank, Dr. Kaminsky and Bob for helping me with flow cytometry. Dr. Melinda Frame, thank you very much for helping and teaching me confocal microscope.

I want to thank the DO /PhD program. Dr. McCormick, thank you so much for always supporting me with my decisions to continue PhD and allowing me to complete my dissertation. You always gave me a great insight on science and life. I am blessed to have you as a program director and I always enjoy your positive energy and perspective of life. Bethany, thank you so much for all the support and care. Suzanne, thank you so much for helping me with revisions of my dissertation, I very much enjoyed the process. I also want to special thank to Dr. Maher. I want to thank my committee members, Dr. David N Arnosti, Dr. Zachary F Burton, Dr. John J LaPres, and Dr. John L Wang for all the guidances and supports.

I want to thank my family and friends for all their support. Your support helped me complete the dissertation and made the PhD life more fun and joyous. I want to send a very special thank you to Keith. Keith, I appreciate your intellects, caring, and love. You helped me so much throughout my PhD. You were always there for me, encouraged and motivated me when I was down. You helped me to keep my feet on the ground when I lost my head. I enjoyed sharing knowledge on neuroscience and discussing my results with you. I cannot thank you

enough. Keith, I also thank you for your superior editing skills. I would like to thank Mr. and Mrs. Doud for all the support and care. I also like to thank Suzanne, my surrogate mom/grand mother/friend, thank you for always being there for me. I enjoy discussing widoms of life and philosophy with you and thank you for always supporting and caring for me. Last, I would like to thank my family. Dad, you always had such a big heart and gave me so many wisdoms in each step of my carreer and life. You are my mentor in so many aspects of my life. You are so amazing, I am not sure I could ever be able to surpass what you have accomplished. You have always forgiven me when I made mistake and guided me to do the "right things". Mom, thank you so much for always being there for me. Nothing can be brighter or bigger than your unconditional love. Mom and dad, you both have been such a big support and help me to be who I am today. I love you very much. Sister, my second mom, since I move to US, you always cared for me like mom and helped me. Thank you all and I love you all, brother Moon-ho, brother-in-law, Coco, Sam, Brian, Ppoppy, and Mumu.

TABLE OF CONTENTS

LIST OF TABLES

LIST OF FIGURES

KEY TO ABBREVIATIONS

AAV	adeno-associated virus
AD	autosomal dominant
ADHD	Attention deficit hyperactivity disorder
ANOVA	One-way analysis of variance
AR	autosomal recessive
ARC	arcuate nucleus
ATP	adenosine tri-phosphate
AUF1	AU rich binding protein
BH4	tetrahydrobiopterin
BCA	bicinchoninic acid assay
CCCP	carbonyl cyanide m-chlorophenyl hydrazone
CM	centromedian
COMT	catechol-O-methyl-transferase
CoQ	Coenzyme Q
COX IV	cytochrome c oxidase IV
CSF	cerebral spinal fluid
CSTF2	cleavage stimulation factor, 3' pre-RNA, subunit 2
CYP	cytochrome P450
D2	DA receptor 2
DA	Dopamine
DAT	dopamine transporter

DBS	deep brain stimulation
DMSO	Dimethyl sulfoxide
DNER	Delta/notch-like EGF-related receptor
DNP	2, 4-dinitrophenol
DOPA	L-3,4-dihydroxyphenylalanine
DOPAC	3,4-dihydroxyphenylacetic acid
DOPAL	3,4-dihydroxyphenylacetaldehyde
E1	ubiquitin-activating enzyme
E2	ubiquitin-conjugating enzyme
E3	ubiquitin ligase
EIF1AX	eukaryotic translation initiation factor 1A, X-linked
eIF4G1	eukaryotic translation initiation factor 4 gamma 1
ECAR	Extracellular acidification rate
ETC	electron transport chain
ETS	electron transfer system
FAD	flavin adenine dinucleotide
FCC	forward scatter
FCCP	Carbonyl cyanide 4-(trifluoromethoxy) phenylhydrazone
FMN	flavin mononucleotide
GABA	gamma-aminobutyric acid
GAPDH	Glyceraldehyde 3-phosphate dehydrogenase
GFP	green fluorescent protein
GPe	globus pallidus externa

GPi	globus pallidus interna
GST	glutathione S-transferase
GSTT1	glutathione-S-transferase T1
HDAC6	histone deacetylase 6
HEPES	4-(2-hydoxyethyl)piperazine-1-ethane-1)-sulfonic acid
HPLC-EC	High performance liquid chromatography coupled with electrochemical detection
[^{3}H] TPP^+	[^{3}H]tetraphenylphosphonium
HVA	homovanillic acid
IBR	in-between-ring
IC50	Half maximal inhibitor concentration
IGF-1	insulin-like growth factor 1
IL1RAPL2	interleukin 1 receptor accessory protein-like 2
Ipla2-β	VIA Ca-independent phospholipase A2
IRS1	Insulin receptor substrate 1
KIF1A	Kinesin family member 1A
KO	knockout
LC3	microtubule associated protein1A/1B light chain 3
L-DOPA	L-3,4-dihydroxyphenylalanine
L-DOPA	Levodopa
LNAA	large neutral amino acids
LRRK2	leucine-rich repeat kinase 2
MAM	mitochondrial associated membrane
MAO	monoamine oxidase

MAO-B	monoamine oxidase B
MBH	medial basal hypothalamus
ME	median eminence
mPTP	mitochondrial permeability transition pore
MORF4L2	mortality factor 4 like 2
MPPP	1-methyl-4-phenyl-4-propionoxypiperidine
MPTP	1-methyl-4-phenyl-1,2,3,6-tetrahydropyridine
MPP^+	1-methyl-4-phenylpyridinium
mtDNA	Mitochondrial DNA
MTT	3-[4,5-dimethylthiazol]-2,5-diphenyltetrazolium bromide
NA	nucleus accumbens
NA	numerical aperture
NCX	sodium/Ca^{2+} exchanger
NDUFA10	NADH dehydrogenase (ubiquinone) 1 alpha subcomplex 10
NMDA	N-methyl-D-aspartate
NSDA	Nigrostriatal dopamine
NSM	non-synaptosomal mitochondria
NXT2	nuclear transport factor 2-like export factor 2
OCR	oxygen consumption rate
6-OHDA	6-hydroxydopamine
$OONO^-$	peroxynitrite
PC	Pearson Coefficient
PD	Parkinson disease
PE	phosphotidylethanoamine

PET	positron emission tomography
PGRMC1	progesterone receptor membrane component 1
PINK1	PTEN-induced putative kinase 1
PKPS	parkinsonian-pyramidal syndrome
PLA2G6	phospholipase A2, GroupIV
PLP1	proteolipid protein 1
Δp	proton motive force
POLG1	polymerase gamma 1
PON1	Praoxonase 1
Q	ubiquinone
R1	ring1
R2	ring2
RCR	respiratory control ratio
RET	reverse electron transfer
ROS	reactive oxygen species
SCC	side scatter
SCG2	secretogranin II
SLC6A3	solute carrier family 6 member 3
SM	synaptosomal mitochondria
SNP	single nucleotide polymorphism
SNpc	substantia nigra pars compacta
SNpr	substantia nigra pars reticulate
SPR	sepiapterin reductase
ST	striatum

STN	subthalamic nucleus
SYNJ1	synaptojanin-1
TCA	tricarboxylic acid
Tfam	transcriptional factor A
TEM	Transmission electron microscopy
TH	tyrosine hydroxylase
TIDA	tuberoinfundibular dopamine
TIMM8A	translocase of inner mitochondrial membrane 8 homolog a
TMRE	tetramethylrhodamine, ethyl ester
TPB^-	tetraphenylborate
UBA	ubiquitin associated domain
UBL	ubiquitin like domain
UCH-L1	ubiquitin c-terminal hydrolase
UPS	ubiquitin proteosome system
VA	ventral anterior
VL	ventral lateral
VMAT	vesicular monoamine transporter
VMAT2	vesicular monoamine transporter
VPS35	vacuolar protein sorting 35
VTA	ventral tegmental area
ZCCHC12	zinc finger, CCHC domain containing 12
$\Delta\Psi_m$	mitochondrial inner transmembrane potential

Chapter 1. General Introduction

Statement of Purpose

Nigrostriatal dopamine (NSDA) neuronal degeneration is one of the major pathobiological characteristics of Parkinson disease (PD). Current "first-line' therapy is L-DOPA (L-3,4-dihydroxyphenylalanine), which alleviates symptoms of PD. However, there is no known drug or treatment that halts the degeneration of the DA neurons. Discovery of the unique neurotoxin, 1-methyl-4-phenyl-1,2,3,6-tetrahydropyridine (MPTP) contributed to the overall understanding of the importance of mitochondrial function in PD. Evidence of mitochondrial involvement in PD was identified either genetically or through evidence of environmental neurotoxicant exposure. Although the mechanism of PD pathogenesis is still unknown, there are differential pathological outcomes between two populations of DA neurons; NSDA neurons are susceptible to PD but tuberoinfundibular dopamine (TIDA) neurons are spared. By examining mitochondrial function and characterizing their mitochondrial morphology, differential outcomes of these neurons may explain mitochondrial involvement in the PD process.

The most common cause for autosomal recessive (AR) early-onset PD is a mutation in parkin. Parkin regulates mitochondrial quality control with the help of PTEN-induced putative kinase 1 (PINK1), which is another gene mutation associated with familial AR early-onset PD. However, there is a lack of *in vivo* evidence of parkin involvement and mitochondrial maintenance in DA neurons. TIDA neurons with increased parkin expression are resistant to MPTP. Therefore, understanding the pathogenesis of mitochondria and parkin may provide a way to develop a novel therapeutic regimen for PD.

The goal of my research discussed in this dissertation is to: 1) identify mitochondrial function, morphology, integrity, and mitophagy differences associated with differential

susceptibility to PD between NSDA and TIDA neurons; 2) characterize differential mitochondrial responses to Complex I inhibition in brain regions containing axon terminals of NSDA and TIDA neurons; 3) characterize mitochondrial function impairment in the absence of parkin; and 4) identify possible neuroprotective effects of parkin on DA neurons via mitochondrial maintenance using parkin KO genetic and neurotoxin mitochondrial Complex I inhibitor models.

My overall hypothesis is: **Loss of parkin mediated mitochondrial quality control contributes to DA neuronal degeneration in a neurotoxicant model of PD**.

Parkinson Disease

PD is named after Dr. James Parkinson. In 1817, he first described clinical symptoms of PD in his book "An Essay on the Shaking Palsy" (**Figure 1.1 A**). Historically, a description of PD can be found as early as 1000 BC from an ancient Indian medical text *Basavarajiyam*. PD was called "Kampavata" and patients were treated with Mucuna pruriens seeds that contain a natural source of L-3,4-dihydroxyphenylalanine (L-DOPA), a precursor of DA (Manyam, 1990). PD was also described earlier in a Chinese text in 425 BC, by Silvius de la Böe in 1680, and by Francois Boissier de Sauvages de Lacroix in 1768 (Zhang et al. 2006; Goetz et al. 2011). In 1872, Dr. Jean-Martin Charcot "father of modern neurology" extensively described PD and was able to distinguish PD from other similar neurological diseases with parkinsonism symptoms (Charcot, 1872; Goetz, 2011).

PD is the second most common neurodegenerative disorder affecting more than 1 million in the United States and 4 million worldwide. The prevalence of PD is 13.4 per 100,000 persons a year in United States (Eeden,2003). PD is neurodegenerative disease that generally affects elderly people over age 50 and the prevalence increases as people age. About 1 % of those over 55 years or older are affected and 3 % over 75 years of age are affected (De Rijk, 1997). Early onset PD affects people at age 50 or younger, and PD affecting people of age twenty or younger is called juvenile PD. PD is a progressive motor system disorder that causes four cardinal symptoms; tremor, bradykinesia, rigidity, and postural instability. Two of the four features are required for the diagnosis of the PD.

Seventy-five percent of all PD patients have tremors. The tremors have a frequency of 3 to 7 hz and are prominent during rest, called "resting tremor", and can be differentiated from essential and intention tremors. Resting tremor often improves during intentional actions or

movements. On the other hand, essential tremor (action tremor), also referred to as benign tremor or shaky hand syndrome, occurs with purposeful usage of the affected muscle, and intention tremor (cerebellar tremor) occurs with purposeful move guided by the end points.

Bradykinesia is a movement with reduced amplitude and velocity. It is a "slow movement" due to inability to initiate a movement. Bradykinesia affects the daily life functions of most PD patients in the following ways; buttoning and dressing, handwriting and speech, walking (gait becomes shuffled due to inability to swing arms), and the inability to blink which causes the face to become non-emotive. Bradykinesia can also affect essential functions such as swallowing which can be fatal in later stages of the disease. Patients often complain of fatigue or weakness in movement due to bradykinesia superimposed with rigidity. Rigidity in the muscle tone causes a stop-and-go pattern of movement in the passive range of the motions of muscle movement. This is also called "cog-wheel rigidity". In the later stages of the disease, postural instability commonly occurs with gait disturbances and an increase in falls, which contributes to increased mortality rates in PD patients (**Figure 1.1B**). In addition to these four primary symptoms, depression, hyposmia (loss of sense of smell), sleep disturbances, and autonomic dysfunction such as hypotension with change in posture, and lack of bowel movement can also be present in early PD (Royden, 2005).

A.

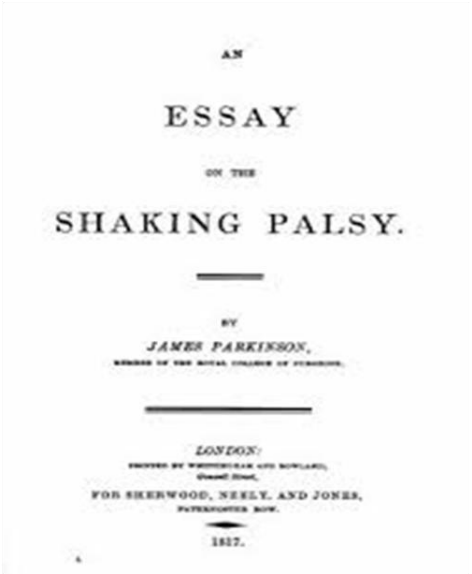

AN

ESSAY

ON THE

SHAKING PALSY.

BY

JAMES PARKINSON,

LONDON:

FOR SHERWOOD, NEELY, AND JONES,

1817.

B.

Figure 1.1. Description of PD. Panel A, "Essay on the Shaking Palsy" written by Dr. James Parkinson (Parkinson, 1817). Panel B, Postural instability and gait disturbance in PD. The picture depicts a small shuffling gait, leaning forward, and absence of swinging of the arms, and increase in postural instability with an altered center of gravity, which increases the risk of falling in PD patients (Gowers, 1886).

Current treatment of PD alleviates symptoms, but there is no treatment that can halt the progression of the disease. PD symptoms are treated pharmacologically and/or surgically. There are five types of medications for PD treatment, dopaminergic, anticholinergic agents, catechol-O-methyl-transferase (COMT) inhibitors, monoamine oxidase B inhibitors, and amantadine. The most commonly used treatment modality is the drug Levodopa (L-DOPA). It is an immediate precursor of DA and beneficial for all four cardinal symptoms. However, L-DOPA can cause nausea/vomiting and orthostatic hypotension as a minor adverse effect in early stage PD. In the later stage, L-DOPA can cause excessive DA stimulation which can result in involuntary movements called dyskinesias, as well as psychosis such as hallucination and delusions. When pharmacological intervention fails, deep brain stimulation (DBS) can be done. DBS on ventralis intermedius of thalamus, globus pallidus, and subthalamic nucleus are reported to be most effective on PD (Royden, 2005).

Major Pathobiological Characteristics of PD

The hallmark pathology of PD is NSDA neuronal degeneration and Lewy body accumulation. NSDA neuronal degeneration causes a decrease in signaling to the caudate and putamen of the striatum (ST) (Uhl et al., 1994; Bernheimer et al., 1973). In patients who demonstrate any two of the four cardinal symptoms of PD described above, 80% of the NSDA fibers are lost in ST and 60% of DA neurons have degenerated in the substantia nigra pars compacta (SNPC) (Bernheimer et al., 1973). Decreased numbers of NSDA neurons can also present as depigmentation of the SNPC due to loss of neuromelanin. Neuromelanin is an oxidized form of DA, so reduction in NSDA neurons decreases in neuromelanin (Marsden, 1961; Zecca et al., 2001). In addition to NSDA neuronal degeneration, another major pathobiological

characteristic of PD is accumulation of Lewy bodies. These are intra-neuronal inclusion bodies that are mostly composed of α-synuclein. Additionally, ubiquitin, parkin, neurofilaments, and other proteins are present in Lewy bodies (**Figure 1.2**).

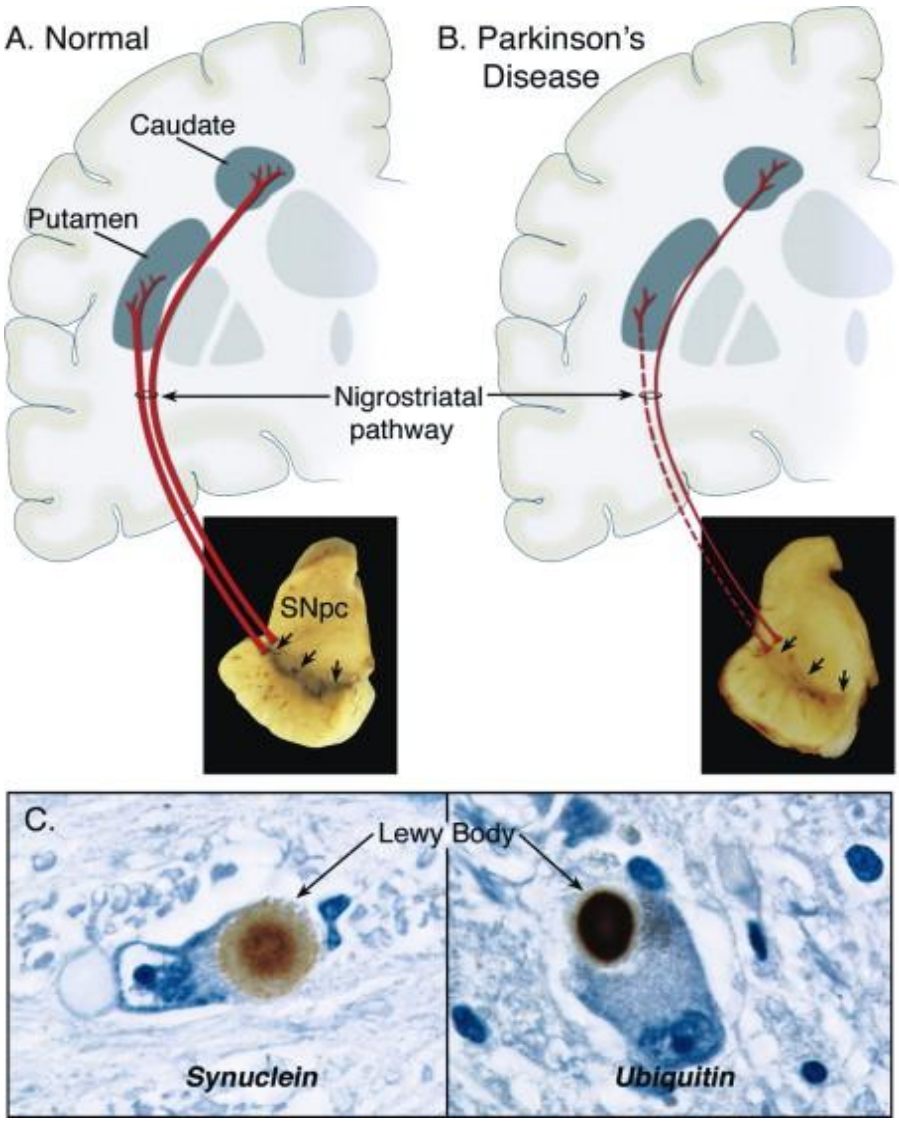

Figure 1.2 Major Pathobiological Characteristics of PD. Panel A, normal nigrostriatal DA pathway. Panel B, Abnormal nigrostriatal DA pathway in PD. Depigmentation of SNpc with decrease signaling to ST, Panel C, Lewy body accumulation. Protein components of Lewy body, α-synuclein and ubiquitin (Dauer et al., 2003).

There are four major DA neuronal pathways in the brain; mesolimbic, mesocortical, TIDA and NSDA neuron (**Figure 1.3**). The mesolimbic cell bodies reside in the ventral tegmental area (VTA) and project axons via the median forebrain bundle that terminate in nucleus accumbens (NA). This pathway is responsible for the reward systems associated with pleasure, euphoria and cocaine addiction. Mesocortical DA neurons also originate from VTA but terminate in the frontal lobe of the pre-frontal cortex and are associated with memory and attention. Attention deficit hyperactivity disorder (ADHD) is affected in this DA pathway. TIDA neurons originate in the arcuate nucleus (ARC) and axons terminate in the median eminence (ME) in the medial basal hypothalamus (MBH). Hypothalamic TIDA neurons regulate anterior pituitary secretion of prolactin. As described above, axons of NSDA neurons originate in the SNpc and terminate in ST of the basal ganglia. These neurons regulate fine motor control functions. In PD, NSDA neurons are affected the most and pathological evidence shows that mesolimbic and mesocortical DA neurons in VTA are also affected, but to a lesser extent. However, TIDA neurons are spared in PD (Matzuk et al.,1985; Langston et al., 1978; Jellinger, 1991; Braak and Braak, 2000). This differential susceptibility is also observed in the neurotoxin 1-methyl-4-phenyl-1,2,3,6-tetrahydropyridine (MPTP) exposure model (Behrouz et al., 2007). Thus, the first part of the dissertation will determine if there are differences in mitochondria function in NSDA and TIDA neurons.

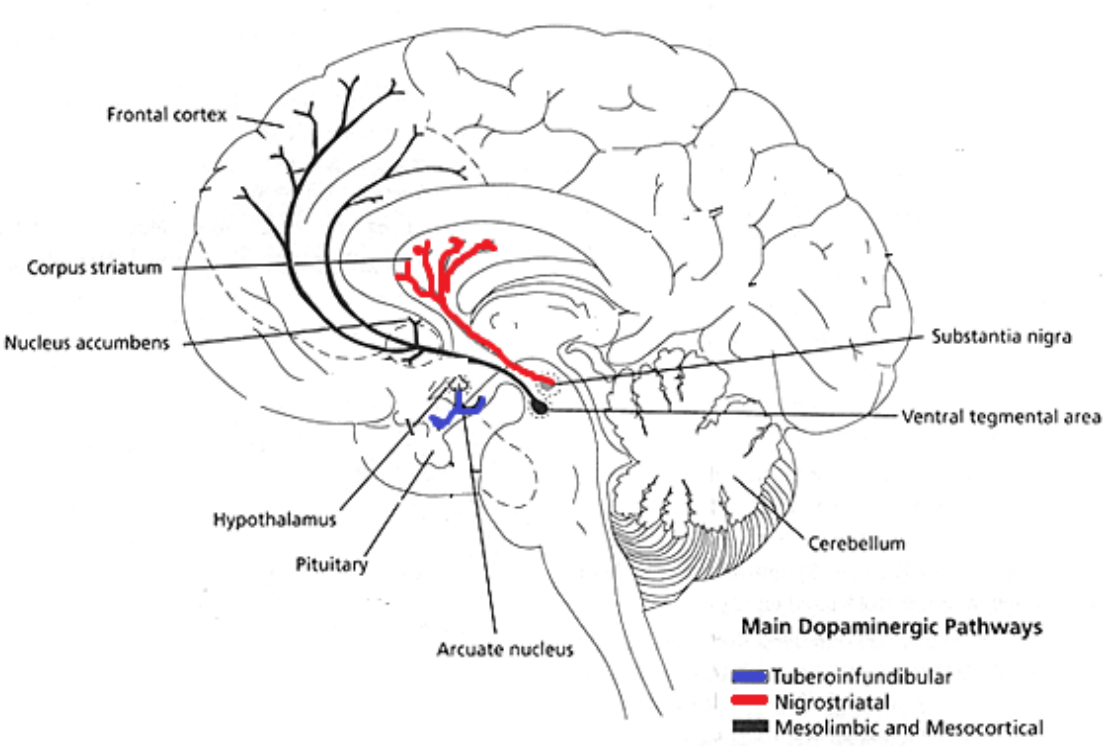

Figure 1.3 Anatomical distribution of central DA neurons (Crocker, 1994) Four major central DA pathways: mesolimbic, mesocortical, nigrostriatal, and tuberoinfundibular pathways. Black indicates mesolimbic and mesocortical pathways, red indicates nigrostriatal pathway, and blue indicates tuberoinfundibular pathway (Crocker, 1994).

Brain and movement control

Synthesis of DA

DA released from NSDA neurons in the brain control the voluntary body movements from finger movements to legs, arms, mouth, etc. DA is synthesized from dietary tyrosine, which is taken up into DA neurons by sodium independent large neutral amino acids (LNAA) transporters (UniProt Consortium, 2013-2014). Tyrosine is converted to L-3,4-dihydroxyphenylalanine (L-DOPA) by tyrosine hydroxylase (TH). This is the rate-limiting step for DA synthesis and is universally utilized to phenotypically identify or visualize DA neurons using immunohistochemistry. TH activity is inhibited by DA receptor 2 (D2) signaling and inhibits DA synthesis in a negative feedback manner. DOPA is converted to DA by L-aromatic amino acid decarboxylase. Newly synthesized DA is taken up into synaptic vesicles by vesicular monoamine transporter (VMAT). VMAT transport of DA into a vesicle occurs through a proton gradient generated by vesicular H^+ ATPase (Wimalasena, 2011; Chaudhry, 2007).

DA release from synaptic vesicles occurs by docking, priming, and fusing with the axon terminal membrane. Synaptic vesicles dock onto the release site at the synaptic cleft and open conformation of t-Snare syntaxin, which induces SNARE complexes and allows rapid fusion of the vesicle into the synaptic membrane in a Ca^{2+} dependent manner (Abraham et al., 2011; Lin, 2010; Südhof, 2004). DA released from pre-synaptic neurons binds to DA receptor 1 (D1) or D2 receptors, and thereby initiates DA signaling onto post-synaptic neurons or provides negative feedback onto pre-synaptic neurons. DA signaling is terminated when released DA is taken up by the DA transporter (DAT) located on the presynaptic axon terminal. DAT is a symporter that moves DA from synapse to the cytosol along with sodium and chloride ions. Na^+/K^+ ATPase equilibrates the synaptic membrane ionic gradient to allow extracellular DA to bind to DAT

(Torres, 2003). DA taken back into cytosol of presynaptic axon terminals is converted to 3,4-dihydroxyphenylacetaldehyde (DOPAL) by mitochondrial enzyme, monoamine oxidase (MAO). DOPAL is metabolized into 3,4-dihydroxyphenylacetic acid (DOPAC), which passively diffuses out of the neurons (**Figure 1.4**).

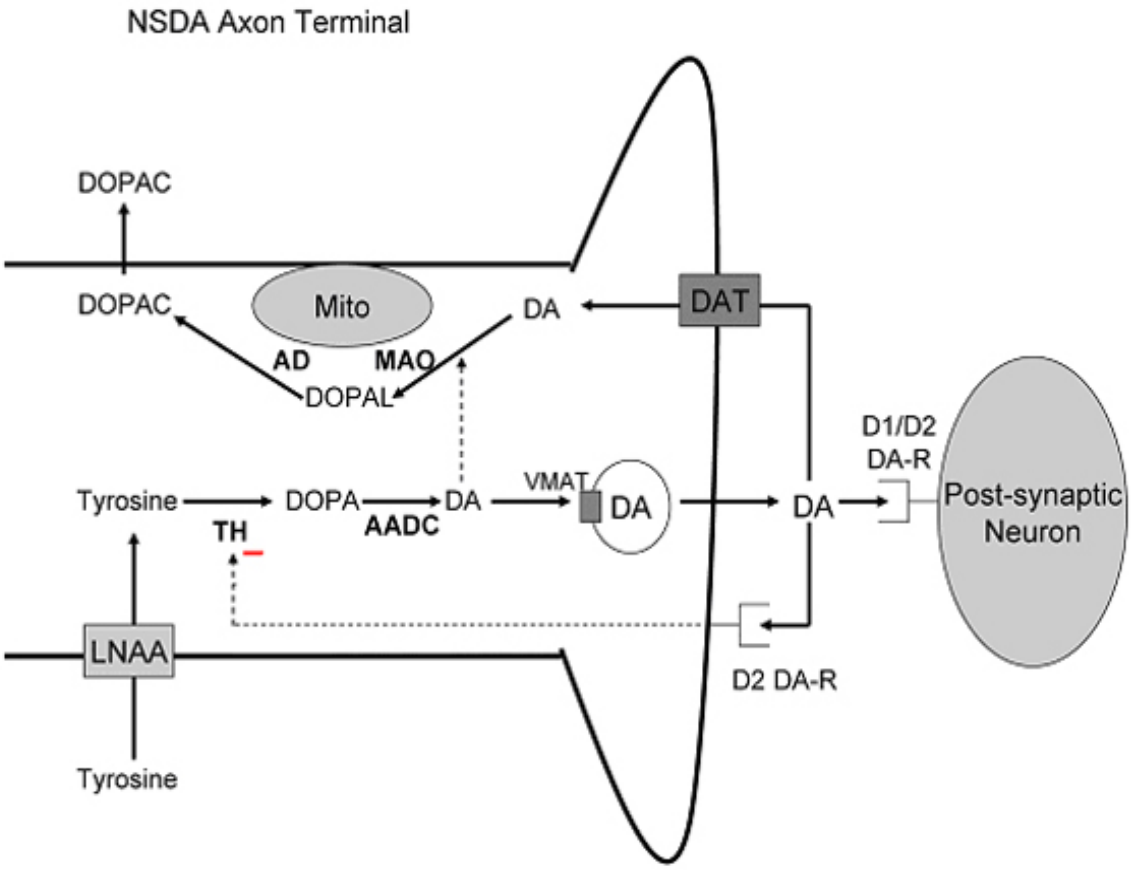

Figure 1.4 DA synthesis and metabolism. Dietary tyrosine is transporter into the cytosol and converted to DOPA by the rate-limiting enzyme in DA synthesis TH. DOPA is rapidly converted to DA by L-aromatic amino acid decarboxylase (AADC). DA is packaged into synaptic vesicles by VMAT and released into synapse. DA in the synapse is taken back into cytosol by DAT and further metabolized to DOPAL and it inactive metabolite DOPAC.

Basal Ganglia Motor System

The voluntary motor system is regulated by the basal ganglia via direct and indirect pathways. The basal ganglia is composed of ST (caudate nucleus and putamen), globus pallidus externa (GPe), globus pallidus interna (GPi), subthalamic nucleus (STN), SNPC, and substantia nigra pars reticulate (SNPR). In the big picture, the pre-motor region of the cerebral cortex sends a signal to the basal ganglia and the basal ganglia sends a signal back to the motor region of the cerebral cortex for movement to occur (**Figure 1.5)**. Here, the basal ganglia mediates communication between the thalamus and cerebral cortex and modulates movement via direct and indirect pathways. The direct pathway facilitates voluntary movement by initiating movement of the muscles, while the indirect pathway inhibits muscles that oppose movement; i.e. during the movement initiation, the direct pathway activates agonist muscle while the indirect pathway inhibits antagonist muscle.

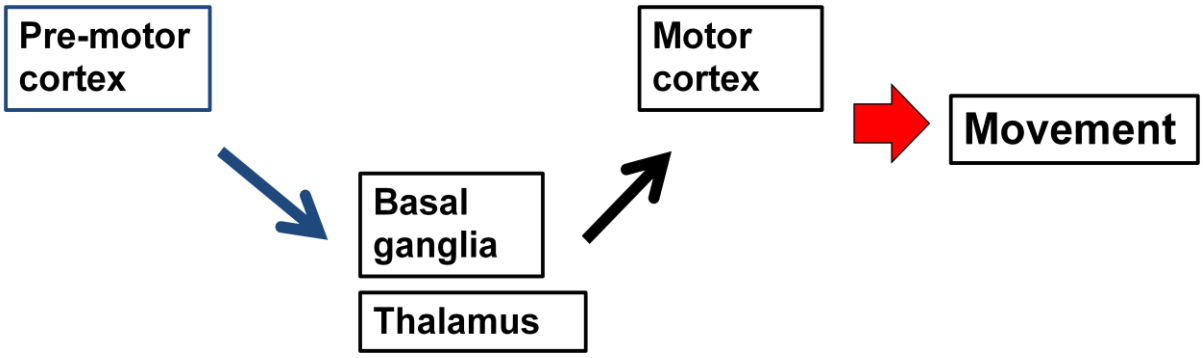

Figure 1.5 Overall voluntary motor circuits. Basal ganglia mediates communication between thalamus and cerebral cortex for coordination of muscle movement.

In the direct pathway, when a person is at **rest**, the GPi and SNPR tonically inhibit the thalamus (centromedian (CM), ventral anterior (VA), ventral lateral (VL) nucleus of thalamus) by releasing the inhibitory neurotransmitter gamma-aminobutyric acid (GABA) (**Figure 1.6**). When the thalamus is activated, glutamate is released to excite the motor cortex for movement. Therefore, inhibition of the thalamus results in no movement during rest. When a person decides to **move**, the pre-motor cortex activates caudate and putamen of the ST. Stimulation of ST inhibits GPi and SNPR halting inhibition of the thalamus. Thus, the thalamus is free to activate the cortex for movement. Here, SNPC plays a critical role as a "kick starter". The pre-motor cortex directly activates SNPC, and SNPC activates ST via the D1 receptor for disinhibition of GPi and SNPR.

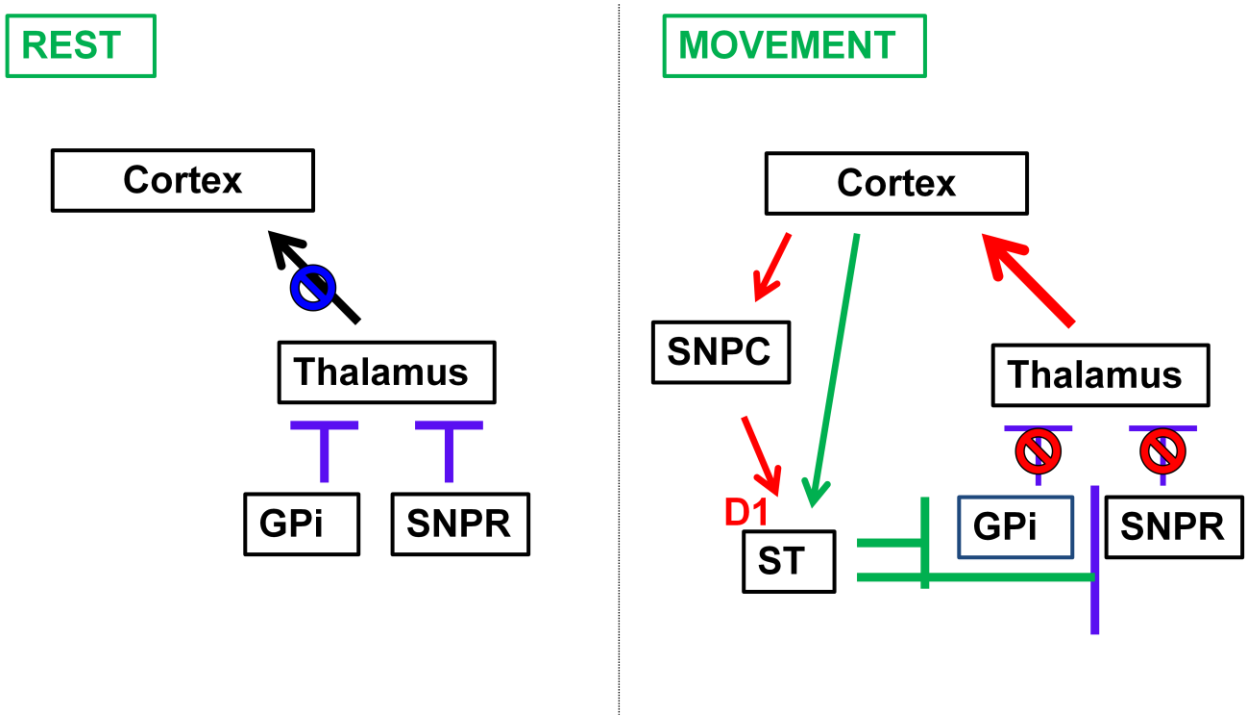

Figure 1.6 Direct pathway for basal ganglia control of motor cortical neurons at rest and during voluntary muscle movement. During the rest, GPi and SNPR neurons inhibit the thalamus. During initiation of voluntary movement, pre-motor cortex and SNPC (via D1 receptors) activates ST for disinhibition of thalamus by GPi and SNPR.

In the indirect pathway, during the **rest**, GPe tonically inhibits the subthalmic nucleus (STN). STN is excitatory to GPi, which inhibits the thalamus tonically as mentioned previously. However, during rest, even if there is no activation of GPi by STN, GPi and SNPR neurons are tonically activated by the direct pathway. Therefore, the net effect of the direct and the indirect pathways is no movement at rest (**Figure 1.7**). In summary of the direct and indirect pathways during rest, the thalamus and STN are tonically inhibited and no movement is initiated. As the pre-motor cortex commands initiation of **voluntary movement** and activates ST. ST inhibits GPe, GPe no longer inhibits STN, and as a result the STN activates GPi, which inhibits the thalamus for antagonist muscle control. Therefore, antagonist muscle is inhibited from firing up during initiation of movement through the indirect pathway while the agonist muscle can initiate movement by the direct pathway.

Here, the SNPC NSDA neurons also play a critical role as a "regulator" of stopping the movement in the indirect pathway during the initiation of the movement. SNPC inhibits ST through D2 receptors and inhibition of the ST frees GPe. GPe inhibits STN and STN no longer can inhibit the thalamus, finally allowing movement. SNPC allows movement in both the direct and the indirect pathway as a "kick-starter" in the direct pathway and is a "regulator" in the indirect pathway. Therefore, when SNPC NSDA neurons are degenerated in PD, these modulations of the SNPC are lost causing over-activity in the indirect pathway. Reduced activation of the D2 receptor causes reduced GPe, an increase in STN, and over stimulation of GPi. This results in inhibition on the thalamus and impairs movement causing bradykinesia or akinesia (failure to initiate movement), and imbalance of the agonist and antagonist muscle regulation causing tremors (Kandel et al., 2000).

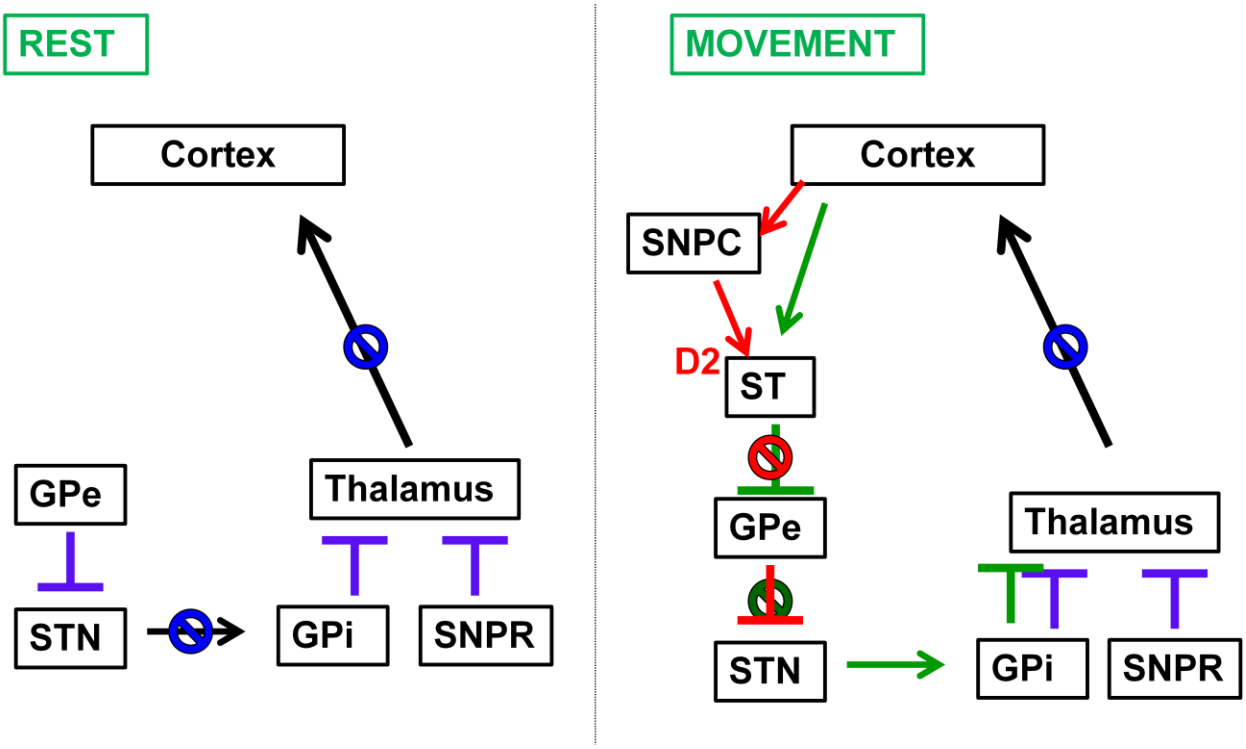

Figure 1.7 Indirect pathway for basal ganglia control of motor cortical neurons at rest and during voluntary muscle movement. During the rest, GPe inhibits STN. During the initiation of the movement, ST inhibits GPe and STN is free to activate GPi and inhibit thalamus for antagonist muscle. SNPC (D2 receptor) regulates inhibition of the movement by inhibition of ST for disinhibition of GPe.

Pathophysiology of PD

Fifteen to twenty-five per cent of PD patients have a family history of relatives with PD and nineteen loci have been identified to be associated with PD and named *PARK1* to *PARK 20.* However, most of the PD cases are sporadic and idiopathic suggesting that in these cases, PD may be caused by complex interactions between environmental and genetic factors. Genetic factors may be undervalued since having a family history of first degree or any other relatives with PD has been shown to be the highest association indicator for PD compared to any other etiological factors. A 3-4 fold increased risk for PD has been verified in biological relatives of PD patients (Noyce et al., 2012). 18F-dopa positron emission tomography (PET) of the twin study revealed underestimation of pre-symptomatic aspects of PD in the cross-sectional study (Burn,1992). In addition to *PARK1* to *PARK20*, early hair color loss and melanoma are also associated with PD (Constantinescu, 2007; Gao, 2009).

Environmental factors, pesticide-exposure, head injury, rural living, beta-blockers, agricultural occupations, and well-water drinking are associated with PD (Kandel, 2000). Prevalence of PD differs depending on sex; males present 1.5 to 2 fold higher risk of PD than females (Tanner and Goldman, 1996). The synthetic drug, 1-methyl-4-phenyl- 1,2,3,6-tetrahydropyridine (MPTP) induces pathophysiology of PD in humans, other primates, and rodents causing parkinsonism (Smeyne et al., 2005). On the other hand, high polyunsaturated fatty acids and low saturated fatty acids, caffeine, exercise, and nicotine reduce risk for PD (Kamel et al., 2014; Liu et al., 2012; Xu, 2010; Chen et al., 2010).

Genetic factors

α-Synuclein (*PARK1*) accumulation in Lewy Bodies was discovered by the finidng of mutation in the *SNCA* gene (Goedert et al., 2012). This led focus to genetic factors associated with PD. Genome-wide association studies identified twenty loci; *PARK1* through *PARK 20* are loci found to have mutation associated with PD (Healy, 2008). The nomenclature was made based on the sequences of the locus was found. Table 1.1 represents summary of loci, genes involved (or candidate genes), inheritance pattern, and atypical clinical features. Among the twenty loci, mutation in *PARK1*, *PARK2*, *PARK6*, *PARK7*, *PARK8*, and *PARK17* have high penetrance (Bonifati,2014).

Locus	Location	Protein	Inheritance pattern	Atypical Features	Lewy bodies
PARK1	4q21	α-Synuclein	AD	Psychosis, early-onset, pyramidal sign	Pos
PARK2	6q25.2–q27	Parkin	AR	Early or juvenile onset More frequent dystonia Slower disease progression	Mostly NE
PARK3	2p13	Sepiapterin reductase	AD	Dementia in some individuals Rapid progression	Pos
PARK4	4q22.1	α-Synuclein	AD	Early onset, rapid, dementia Autonomic dysfunction	Pos
PARK5	4p14	UCH-L1	AD?		UN
PARK6	1p36	PINK1	AR	Early onset, slow progression	UN
PARK7	1p36	DJ-1	AR	Early onset, dementia	UN
PARK8	12q12	LRRK2	AD	Lewy body dementia Fronto temporal dementia	Pos
PARK10	1p34-p32	UN	AR	Supranuclear gaze paralysis	UN
PARK11	2q 37	UN	AD	No substantia nigra degeneration	Pos
PARK12	Xq21-Xq25	UN	X-liked		
PARK13	2p12	HTRA2	AD		
PARK14	22q13	PLA2G6	AR	Adult onset dystonian PD, Brain iron accumulation	Lewy body like
PARK15	22q12-q13	FBXO7 gene	AR	Early onset, parkinsonisan-pyramidal syndrome;PKPS	
PARK16	1q32	UN	UN		
PARK17	16q12	VPS35 gene	AD	Dyskinesia, dystonia, psychosis	
PARK18	3q27	EIF4G1 gene	AD		Pos
PARK19	1p32	DNAJC6 gene	AR	Juvenile PD, mental retardation, seizure	
PARK20	21q22	SYNJ1 gene	AR	Early-onset PD, cognitive decline, seizure, dystonia	

Table 1.1 Summary of genes and loci linked to familial PD
The table is updated and modified from the table published by Vila et al. 2004

PARK1

Mutation of SNCA, α-synuclein gene, is one of the major and the most extensively studied genetic factors in PD that supports evidence for a phathophysiological cause from protein accumulation, unfolded protein response to prion mechanisms (Satake et al., 2009; Simón-Sánchez et al., 2009). *Park1* is the SNCA gene mutation on 4q22 causing autosomal dominant inherited early-onset, rapid progressive PD (Polymeropoulos et al., 1996; Golbe et al.,1990; Lesage et al., 2013). In addition to a mutation in the SNCA gene, duplications of the SNCA are associated with PD (Nishioka, 2006). Other important evidence of association of α-synuclein with PD is that Lewy bodies (Lewy body accumulation is a major pathobiological characteristic) contain α-synuclein. α-Synuclein is ubiquitously expressed and especially abundant in pre-synaptic neurons and synaptosomal membranes (Jakes et al., 1994; Maroteaux et al.,1991). A53T and A30P forms of α-synuclein impair DA storage by inhibiting recycling of the vesicles via phospholipase D2 and/or fatty acid binding properties. This in turn causes oxidative stress in DA neurons due to highly oxidative characteristics of DA (Lotharius et al., 2002; Outeiro et al., 2003). Overexpression of WT α-synuclein has been found to be anti-apoptotic, but anti-apoptotic effect of α-synuclein was reversed by 6-hydroxydopamine (6-OHDA), an oxidized form of DA (Costa et al., 2002). Transgenic mice expressing A53T mutant α-synuclein have motor impairment and pathology similar to PD (Giasson et al.,2002). However, Kuo et al. verified that both A53T and A30P mutant α-synuclein transgenic mice have abnormality in enteric nervous system, but did not show PD phenotypes or NSDA neuronal degeneration (Kuo et al.,2010). Also, The mutation in 4q21 is called *PARK4,* but it revealed as triplication of the α-synuclein gene in locus *PARK 1* causing AD PD *PARK1* (Singleton et al., 2003). Mutation, duplication, triplication, or stability/solubility of the oligomers of α-synuclein are reported to be pathological in PD.

PARK2

Mutation in gene coding parkin on chromosome 6q26 is the most common cause for AR juvenile PD (Takahashi et al., 2003; Jones et al., 1998). *Park2* spans over 1.4 Mb and is the second largest gene in humans. *Park2* has 12 axons and a bidirectional promoter that encodes for parkin and parkin co-regulated gene (PACRG) (Lockhart et al., 2003). Parkin is an E3 ubiquitin ligase involved in proteosomal pathway and autophagy of mitochondria. Details of the function of parkin are described below in **Section 1.6**.

PARK6

Mutation in *pink1* on chromosome 1p36.12 is one of the three genetic factors for AR early onset PD (Valente et al., 2001). PINK1 is mitochondrial serine/threonin kinase and ubiquitin protein ligase that is ubiquitously expressed and degraded in the mitochondrial membrane (Poole et al.,2008). PINK 1 (PTEN-induced putative kinase 1) has no effect on cell growth in PTEN signaling pathway. PINK1 prevents apoptosis by reducing release of cytochrome c oxidase and regulating mitochondrial Ca^{2+} capacity via Na^{+}/Ca^{2+} exchanger (Petit et al., 2005; Gandhi et al.,2009). In addition, PINK 1 maintains mitochondrial integrity by mediating autophagy of mitochondria and mitochondrial fission (Narendra, 2010; Poole, 2008). PINK1 knock out mice have reduced mitochondrial function without alternations in mitochondrial morphology (Gautier et al., 2008). PINK1 knock out Drosophila were observed to have DA neuronal degeneration and mitochondrial dysfunction (Park et al., 2006). PINK1 is localized to mitochondria and help recruit parkin onto damaged mitochondria to regulate mitochondrial quality control via mitophagy.

PARK7

PARK7 is a mutation in the *DJ-1* gene located on chromosome 1p36 causing early onset AR PD (Van Duijn et al., 2001). DJ-1 has various functions as chaperone, transcriptional regulator, and tumorigenesis (*PARK7* is also called "oncogene *PARK7*"). DJ-1 also plays an important role in reducing reactive oxygen species (ROS) as a redox sensor and an antioxidant scavenger. In addition, DJ-1 maintains mitochondrial homeostasis by modulating Ca^{2+} level via mitochondria and endoplasmic reticulum tethering. Mutant DJ-1 transgenic mice have increased ROS and alternated mitochondrial enzymes (Andres-Mateos et al., 2007). DJ1 knock out mice exhibit normal motor behavior and no loss of NSDA neurons. However, these mice are more susceptible to MPTP than WT mice and overexpression of DJ1 in cell culture and DJ1 knock out mice causes resistance to the toxic effects of MPTP (Kim et al., 2005). Presence of DJ-1 was protective against MPTP in NSDA neurons.

PARK8

Mutation in the *leucine-rich repeat kinase 2 (LRRK2)* gene in Locus *PARK8* causes AD PD. *LRRK2* mutations are also found in patients with Lewy body dementia or frontotemporal dementia (Ross et al.,2006). LRRK2 is reported to regulate protein synthesis, involved in cell cycle and survival control, through miRNA (Gehrke et al., 2010). LRRK2 directly interacts with parkin through its COR domain and R2 ring domain of parkin (Smith et al.,2005). Through its interactions with tubulin and key regulators of wnt signaling, LRRK2 modulates axon, dendrite and synapse formation (Gillardon et al.,2009; Sancho et al., 2009).

Mutant LRRK2 disturbs mitochondrial homeostasis by causing Ca^{2+} imbalance and an increase in mitophagy resulting in mitochondrial clearing and shortening of dendrites (Cherra et

al., 2013). LRRK2 expression is associated with membranous structures such as lysosomes, vesicles, golgi, ER, and mitochondria (Gloeckner et al.,2006). LRRK2 plays a role in the endosomal-autophagic pathway; R1441C mutation in LRRK2 caused autophagic imbalance. Autophagic vacuoles with incomplete degradation of the aggregates accumulate and p62, an adapter protein for autophagic cargo and the aggresome, are increased (Alegre-Abarrategui et al., 2009). LRRK2 has also been found to interact with a hydrogen peroxide antioxidant scavenger, so G2029S mutation in LRRK2 results in increased ROS, mitochondrial dysfunction, and cell death (Angeles et al., 2011). In addition, LRRK2 interacts directly with the mitochondrial fission protein, Dlp1 (also called drp1) and causes mitochondrial fragmentation (Wang et al., 2012).

PARK17

The heterozygous mutation in the vacuolar protein sorting 35 (VPS35) gene at 16q13 on *PARK17* locus causes AD PD with incomplete penetrance (not all people with gene mutation present with clinical symptoms) (Wider et al., 2008; Vilariño-Güell et al., 2011). *PARK17* is an adult onset PD with clinical features similar to idiopathic PD with atypical features of diskinesia, distonia, mental retardation, and psychosis (Wider et al., 2008; Zimprich et al., 2011; Kumar et al., 2012). VPS35 is a critical component of the retromer cargo-recognition complex and plays an important role in endosome-trans-Golgi trafficking via interaction with a highly conserved asp residue at N-terminal domain with trans-Golgi network proteins (Vila et al., 2004; Zhang et al., 2000; Edgar et al., 2000). VPS35 is involved in recycling of membrane-associated proteins by interaction with vacuolar protein sorting proteins and recruitment of endosomal proteins (Haft et al., 2000; Seaman et al., 2009).

Environmental factors

1-methyl -4-phenyl-1,2,3,6-tetrahydropyridine (MPTP)

MPTP was first identified when a group of young drug addicts ingested MPTP as "heroin", but were later hospitalized with symptoms identical to PD (Singer et al., 1987). MPTP is a synthetic drug, a by-product of narcotic 1-methyl-4-phenyl-4-propionoxypiperidine (MPPP). Post-mortem analysis of the brain revealed NSDA neuronal degeneration in the absence of Lewy body formation (Dauer et al.,2003). MPTP crosses the blood brain barrier due to its high lipophilic characteristics and is converted to the bioactive metabolite MPP^+ by monoamine oxidase B (MAO-B) in the glial cells (**Figure 1.8**) (Markey et al., 1984). MPP^+ is released to the extracellular space and is selectively taken up by DA neurons due to its high affinity for the DA transporter (DAT).

After MPP^+ enters the DA neurons, it is translocated into the mitochondria in a membrane electrical-chemical gradient dependent manner. Energy driven uptake of MPP^+ has affinity towards mitochondria with K_m of about 5 mM regardless of the low physiological steady-state concentration of MPP^+ in the cells or brain (Ramsay et al., 1986; Ramsay and Singer, 1986). In mitochondria, MPP^+ mostly binds to Complex I NADH dehydrogenase and impairs the electron transport chain (ETC). MPP^+ is also shown to inhibit Complexes III and IV (Mizuno et al.,1988). An impaired ETC results in depleted ATP synthesis and an increase in oxidative stress (Sherer et al., 2002; Dawson and Dawson, 2003). Free radicals generated by mitochondrial impairment can interact with NO forming peroxynitrite ($OONO^-$). Peroxynitrite is one of the strongest oxidants and can target TH, DA, and α-synuclein (Ischiropoulos et al., 1995). Energy depletion and ROS generation by MPTP can result in cell death (Ischiropoulos et al., 1995). MPP^+ also can be taken up by the vesicular monoamine transporter, VMAT2, thereby replacing

DA. Overexpression of VMAT2 allows cells to be resistant to MPP^+ through VMAT2 sequestering of MPP^+ and preventing MPP^+ from entering the mitochondria (Liu et al., 1992). VMAT2 heterozygote mice were more sensitive to MPTP toxicity (Takahashi et al., 1997).

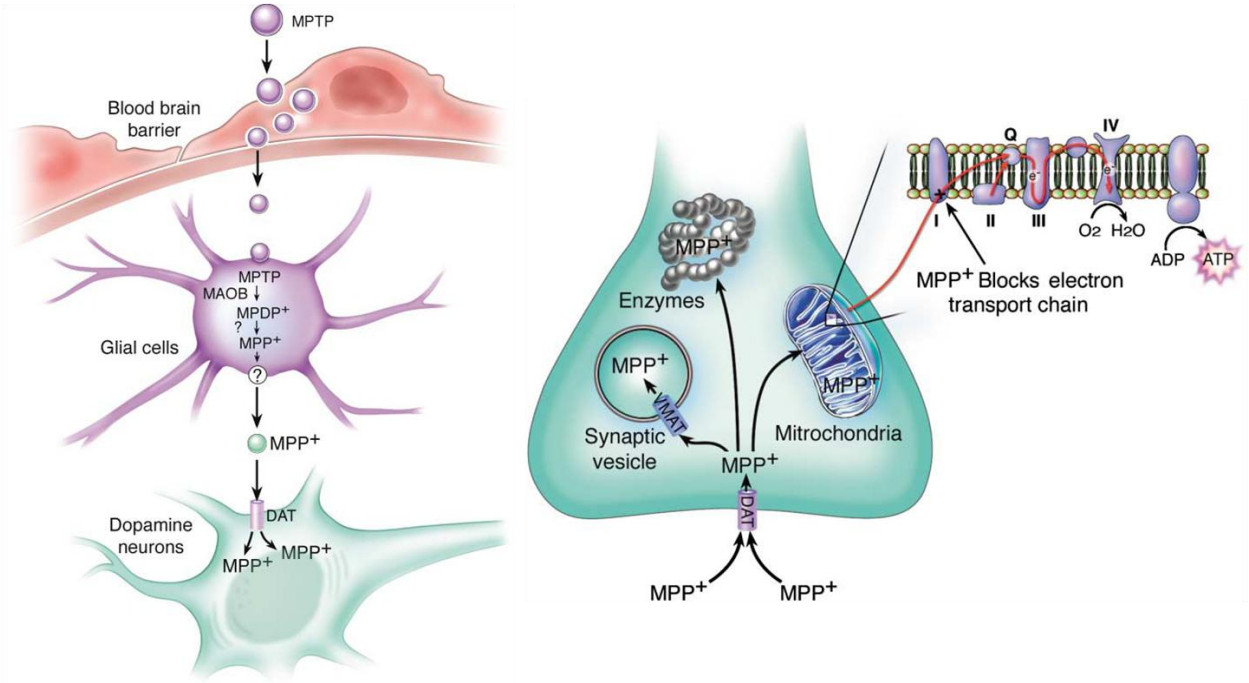

Figure 1.8 Mechanism of action of MPTP on DA neurons. MPTP crosses blood brain barrier and is converted to the active form of MPP^+ by MAOB in glial cells. MPP^+ enters DA neurons via DAT and inhibits the mitochondrial Complex I (Dauer, 2003).

Pesticides and herbicides

Farming, drinking well-water and other rural environmental factors are associated with and increased prevalence of development of PD. It is also known that farmers have an enhanced exposure to pesticides and herbicides which increase the risk of PD. Additionally, some pesticides and herbicides have a structural similarity to neurotoxin MPP^+ suggesting a mechanistic connection.

Organochlorine pesticides

Organochlorides are the most commonly associated pesticides to PD causing about 2 fold higher risk for PD compared to people without any exposure to these chemicals (Hancock et al., 2008). The products were banned in the 1970s, however, organochlorides are highly stable, so they bio-accumulate in the food chain and environment. Among organochloride, dieldrin, hexachlorohexane, dithiocarbamates, organophosphates, and pyrethroids are reported to have an association with mitochondrial dysfunction, ROS, and DA neuronal cell death (Goldman et al., 2014).

Rotenone

Rotenone is a naturally occurring substance in plant leaves and roots, and is often used as a pesticide. Historically, indigenous people used rotenone to catch fish (ATSDR, 2010). Currently, rotenone is commercialized and most commonly utilized as an insecticide. Rotenone (2R,6aS,12aS)-1,2,6,6a,12,12a-hexahydro-2-isopropenyl-8,9-dimethoxychromenol[3,4-b]furo(2,3-h)chromen-6-one), is highly lipophilic and readily crosses the blood brain barrier. Rotenone has a short half-life of approximately 12 h in natural water (Ott, n.d) (**Figure 2.5.3**). Rotenone exposure causes 2.5 fold higher risk of PD (Tanner and Goldman, 1996). Rotenone is a mitochondrial Complex I inhibitor and binds at the same site as MPP^+. It inhibits the transfer of

an electron from iron-sulfur center to ubiquinone (Sherer et al., 2007). In rats, rotenone recapitulated neuropathological features of PD, i.e., NSDA neuronal specific degeneration, α-synuclein accumulation, microglial activation, and movement disorders as well as non-motor symptoms of PD (Cannon et al., 2009; Betarbet et al., 2006). Rotenone impaired mitochondrial function, decrease in ATP, and increase in ROS, in addition to proteosomal dysfunction (Cent. Dis. Control Prev. 2013).

Paraquat

Paraquat (N,N'-dimethyl-4,4'-bipyridinium dichloride) is a member of a redox-active heterocycle family and is one of the most widely used herbicides (Cent. Dis. Control Prev. 2013). Paraquat is structurally very similar to MPP^+ and has similar characteristics (**Figure 1.9**). Once paraquat crosses the blood brain barrier, it is converted to $paraquat^+$ and enters the DA neurons via DAT. Once inside DA neurons low concentrations of $paraquat^+$ can generate extensive ROS through redox cycling and generation of superoxide radicals (McCormack et al., 2005). Reductase in the cell reduces one electron of $paraquat^+$ to a cation radical that interacts with oxygen and forms a superoxide anion (Day et al.,1999). The superoxide anion repeats this process and cycles back again forming increasing amounts of superoxide anions causing an overabundance of ROS from a small amount of $paraquat^+$. Paraquat causes NSDA neuron specific degeneration, accumulation of α-synuclein, mitochondrial dysfunction, lipid peroxidation, and a decrease in antioxidants (Kuter, 2010; McCormack, 2002). In addition, people with a glutathione-S-transferase T1 (GSTT1) gene deletion (~20% of Caucasians, ~40% of Asians) have a much higher risk of PD following paraquat exposure (Goldman, 2012). This suggests a complex interaction between genetic and environmental etiologic distribution to PD.

MPP+

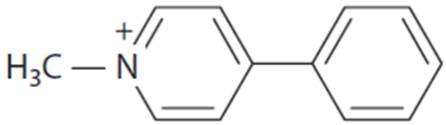

Paraquat

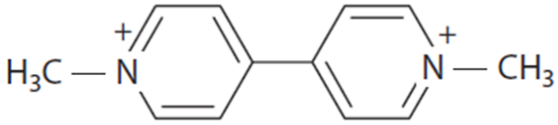

Rotenone

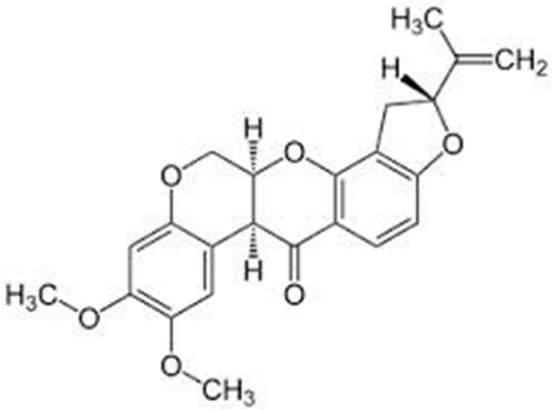

Figure 1.9 Chemical structures of MPP^+, paraquat, and rotenone. MPP^+ and paraquat have similar chemical structures and common factors of MPP^+, paraquat, and rotenone are pathogenesis for mitochondrial dysfunction and development of PD.

Mitochondria

Mitochondrial bioenergetics

Mitochondria are essential in the metabolic function of eukaryotes. Mitochondria regulate cellular Ca^{2+} homeostasis, apoptosis, β-oxidation of fatty acids and oxidative phosphorylation. Mitochondria are composed of outer membrane, inter-membrane space, inner membrane and cristae, and matrix. Oxidative phosphorylation occurs in the inter-membrane space via an electron transport chain (ETC) embedded on the inner membrane. Oxidative phosphorylation is an aerobic respiration which is processed in the presence of oxygen using the redox potential of the molecules transferred by the ETC.

ETC is composed of four Complexes and adenosine tri-phosphate (ATP) synthase (also called Complex V) (**Figure 1.10**) (Brownlee, 2001). Complex I is an NADH dehydrogenase (also called NADH ubiquinone oxidoreductase) which converts NADH generated from glycolysis and TCA cycle to NAD^+ and two electrons. Two electrons convert flavin mononucleotide (FMN) to $FMNH_2$ and are then transferred to a Fe-S cluster. From the Fe-S cluster, electrons are transferred to a lipid soluble carrier, ubiquinone (Q), which later transfers the electrons to Complex III. In the process of the electron transportation in Complex I, four protons ($4H^+$) are pumped into the inner membrane space, creating an electrochemical gradient of protons. Complex II is succinate dehydrogenase. This enzyme oxidizes succinate to fumarate generating additional electrons that are transferred to Q via flavin adenine dinucleotide (FAD) and the Fe-S cluster. Electrons transferred are transferred from Q to Complex III, but no protons are pumped across the inner membrane in this process.

Complex III is a cytochrome bc_1 complex. Electrons reduced from Q to (QH_2) are transferred to cytochrome C, which is a water-soluble electron carrier in the mitochondrial inter-

membrane space. In this process, four protons are pumped across the inner membrane relative to two e^- and transferred in the Q-cycle. Complex IV is cytochrome C oxidase. Four cytochrome C molecules reduced in Complex III reduce the O_2 molecule, which is the final electron acceptor, forming two H_2O; four protons are pumped across the inner membrane. The electrochemical gradient potential of the protons generated during electron transport catalyzes ATP synthesis, which is called "oxidative phosphorylation". ATP synthase is also called Complex V, but it is not considered to be part of ETC. The protons react with hydroxyl ions in the matrix, but this is not the driving source for ATP synthesis or oxygen consumption. Rather it is the proton potential gradient change that drives the reaction. In intact mitochondria, electron transfer is tightly coupled to oxidative phosphorylation. Therefore, mitochondrial respiratory capacity can be measured by measuring oxygen consumption rate and respiratory control ratio as discussed in Chapter 2.

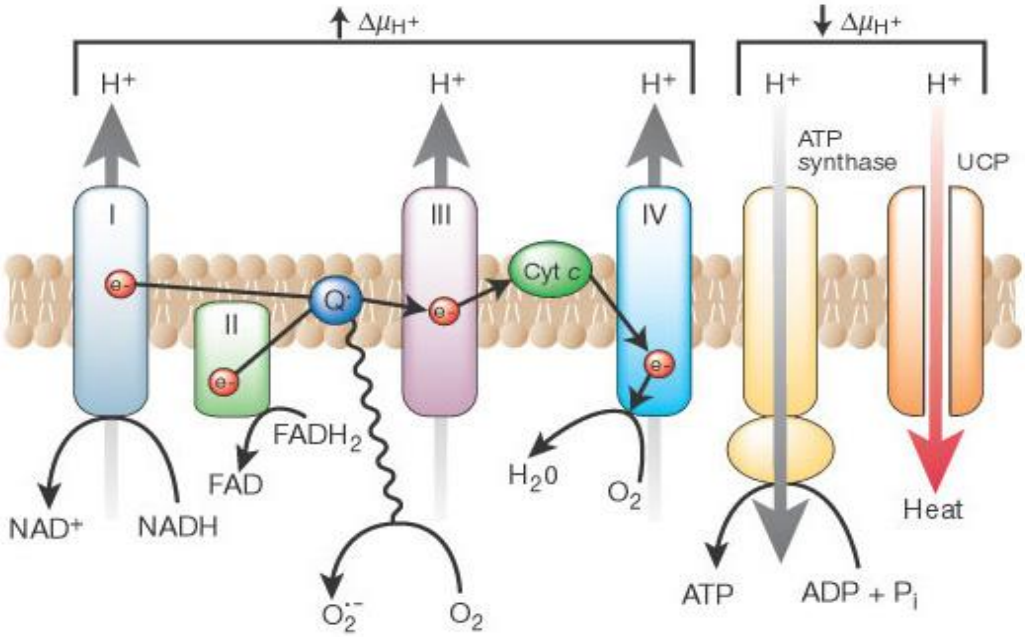

Figure 1.10 Schematic depicting oxygen consumption and ATP synthesis in the mitochondrial ETC (Brownlee,2001) Proton gradients are generated in the process of electron transfer from Complex I though Complex IV, and the coupling of ATP synthesis (see the text for a detailed description).

As electrons are transferred by the ETC in the mitochondrial inner membrane, the proton gradient is generated across the intermembrane space causing differential electric potentials across the inner membrane. The force of the protons moving across the electron chemical gradient (Ψ_m) drives ATP synthesis. The thermodynamics of the proton motive force follows the equation below.

$$\mathbf{\Delta p = \Delta\psi - 60\Delta pH}$$

Δp: proton motive force

$\Delta\psi$: electrical gradient (electrical potential)

ΔpH: pH gradient

Proton motive force depends on the mitochondrial membrane potential and the pH unit change by protons pumped into the intermembrane space. Ψ_m is +150 mV and the pH unit is 0.5 for two protons, therefore, a proton motive force for two protons is 180 mV, while electrons to transfer from NADH to O_2, electropotential drops through 1100 mV. Therefore, ten protons pump into intermembrane space through the two electron transfer is thermodynamically favored and the proton motive force fuels ATP synthesis (Lodish, 2000; Macmillan, 2010). When a mitochondrion is damaged, caspase and nuclear activating proteins are released, which causes the opening of the mitochondrial permeability transition pore (mPTP). Molecules less than 1.5 kDa in size diffuse into the mitochondria freely but swelling of the mitochondria increases inner membrane permeability and decreases mitochondrial inner transmembrane potential ($\Delta\Psi_m$) (Boregaard et al, 1983; Broekman, 1992). As mitochondrial Ψ_m drops in dysfunctional mitochondria, the proton gradient dissipates, and mitochondrial respiration uncouples. Consequently, cells proceed to apoptosis (Del Buono BJ et al., 1989). Thus, measurement of

$\Delta\Psi_m$ provides the information about the integrity of the mitochondria (Cezanne L., 1992; Lpopis J. et al., 1998).

$\Delta\Psi_m$ is generally too small to be measured by microelectrode, thus, monovalent fluorescent cations are utilized to identify negative electrical potential differences across the membrane $\Delta\Psi_m$ (Lemasters and Ramshesh, 2007). Fluorescent lipophilic cations such as MitoTracker rosamine derivatives and tetramethylrhodamine, ethyl ester (TMRE) accumulate in the mitochondrial matrix depending on $\Delta\Psi_m$ following the Nernst equation at equilibrium. The Nernst equation is:

$$\boldsymbol{\Psi = -59 \log \left(\frac{Fin}{Fout}\right)}$$

Ψ: electrical potential (mV)

F_{out}: concentration of the cationic fluorophore in the extracellular or extra-compartment space

F_{in}: intra cellular or intra-compartmental fluorophore concentration

As 61.5 mV of Ψ increases cross the membrane, 10 fold increase of cation concentration in the mitochondria can be predicted. Therefore, $\Delta\Psi$ can be measured by difference in cation concentrations in mitochondria (Zamzami N et al., 2000).

Mitochondria and PD

Much evidence provides insight on the pivotal role of mitochondrial function and reactive oxygen species production in PD pathogenesis. Post mortem analysis and fibrotic cells from PD patients revealed a decrease in mitochondrial Complex I activity in SN, platelets, and skeletal muscle (Schapira et al., 1989; Mizuno et al., 1989; Krige, 1992; Bindoff, 1991). In addition, discovery of MPTP, which is mitochondrial Complex I inhibitor and caused identical features of PD in human, brought a spotlight to mitochondrial dysfunction in PD. Most of the pesticides/insecticides that are associated with PD have a detrimental effect on mitochondrial

function similar to that seen with MPTP. Rotenone is a mitochondrial Complex I inhibitor, paraquat is a potent ROS generator, and many organochlorines cause mitochondrial dysfunction and ROS generation. In addition, to environmental factors, genetic mutations in familiar forms of PD have a pathogenic effect on mitochondrial dysfunction. DJ-1 (*park7*) is a redox sensor and antioxidant scavenger and LRRK2 (*park8*) interacts with the hydrogen peroxide antioxidant scavenger and regulates ROS production in mitochondria. One of the candidate genes of *park11* is *NADH dehydrogenase (ubiquinone) 1 alpha subcomplex 10 (*NDUFA10).

Mitochondria are vital in the cell process as an engine for energy generation. However, when electrons fail to transfer safely through the ETC, electrons that leak from ETC can interact with oxygen and form reactive oxygen radicals causing ROS in mitochondria and cells (Starkov, 2008). This can cause mitochondrial dysfunction and apoptosis (Ozawa,1997). For years, people considered Complex III as major ROS generator within mitochondria (Cadenas et al., 1977; Turrens et al., 1985). Antimycin A, Complex III inhibitor, caused increase oxygen radical formation from Complex III (Cadenas et al., 1977; Turrens et al., 1985; Liu et al., 2002; Zhang et al., 1998; Grigolava et al.,1980). However, in physiological condition, oxygen radical formation in Complex III is negligible compare to Complex I (Liu et al., 2002; Kudin et al.,2004; St-Pierre et al., 2002). Mitochondrial Complex I produces most of the oxygen radicals in the mitochondria through mode 1 and mode 2 *in vivo* (Andreyev et al., 2005; Adam-Vizi et al., 2006; Brand et al., 2004; Murphy and Michael, 2009). Mode 1 is occurs when NADH/NAD^+ ratio is high, and mode 2 occurs when proton motive force (Δp) is high with reduction in CoQ pool (Kussmaul et al., 2006; Kushnareva et al., 2002; Andreyev et al., 2005; Cino et al., 1989; Krishnamoorthy and Hinkle, 1988; Hinkle, 1967). Impaired respiratory chain or slow respiration can induce mode 1 *in vivo*. Mode 2 occurs during reverse electron transfer (RET), in which too

much proton motive force reverses the ETC, and NAD^+ is converted back into NADH (Cino et al., 1989; Chance and Hollunger, 1961). Overloaded ETC, in the mitochondrial matrix can cause high ROS in mitochondria and cytosol (Murphy et al., 2009; Kushnareva et al., 2002). Complex III generates most oxygen radicals in the cytosol of the cells, which leads to damage of cellular processes. ROS can damage polyunsaturated fatty acids causing lipid peroxidation and disrupted membranes. ROS can damage enzymes by oxidizing co-factors or enzymes themselves causing loss of function. ROS also can oxidize DNA and cause mutations. Damaging DNA is especially detrimental for mitochondria due to less efficient DNA repair ability compared to the eukaryotic/nuclear DNA repair system and histone (Richter et al., 1988; Ozawa, 1997).

Mitochondrial DNA (mtDNA) is a small (16.6kb), double stranded, and circular DNA. MtDNA codes for 37 genes including 22tRNAs, 2 rRNAs, and MtDNA encodes for 13 proteins which mostly function in the mitochondrial ETC complexes (**Figure 1.11**). A higher frequency of mtDNA deletions has been detected in older individuals in an age controlled PD patients (Bender, 2006). MtDNA deletions increase depending on age and the etiology of mitochondrial dysfunction. Also, higher mtDNA deletions were observed in pigmented neurons in SNpc than other brain regions (Kraytsberg et al., 2006). Similar findings have been found in MitoPark mice, which have a mitochondrial transcriptional factor A (Tfam) mutation. In MitoPark mice, NSDA neurons with mitochondrial dysfunction present with identical hallmark pathology of PD (motor impairment, intraneural inclusions, and neuronal death) (Ekstrand et al. ,2007). Down regulation of the catalytic subunit of mtDNA polymerase causes mitochondrial respiratory dysfunction, premature aging, and age-related motor impairment (Humphrey et al., 2012). MtDNA polymerase gamma 1 (POLG1) is encoded by nuclear DNA, however, it regulates mtDNA

replication and repair (Ekstrand et al. ,2007). PLOG1 trinucleotide repeat has significant association with PD (Anvret et al., 2010).

In addition, several genetic factors associated with PD are involved in mitochondrial function. *Park12* is translocase of mitochondrial inner membrane protein and is involved in protein transport. EIF4G1 (*Park18*) is involved in the rate-limiting step of the protein synthesis. Mutant eIF4G1 causes mitochondrial dysfunction with decreased membrane potential and increase in ROS. The most common genetic mutation, which causes AR early-onset PD, parkin (*park2*), plays a significant role in the mitochondrial quality control with PINK1 (*park6*). HTRA2 (*park13*) is a mitochondrial serine protease and interacts with PINK1. FBX07 (*park15*) regulated E3 ubiquitin ligase may be involved in mitochondrial quality control. These findings suggest that mitochondrial maintenance may be vital for survival of DA neurons.

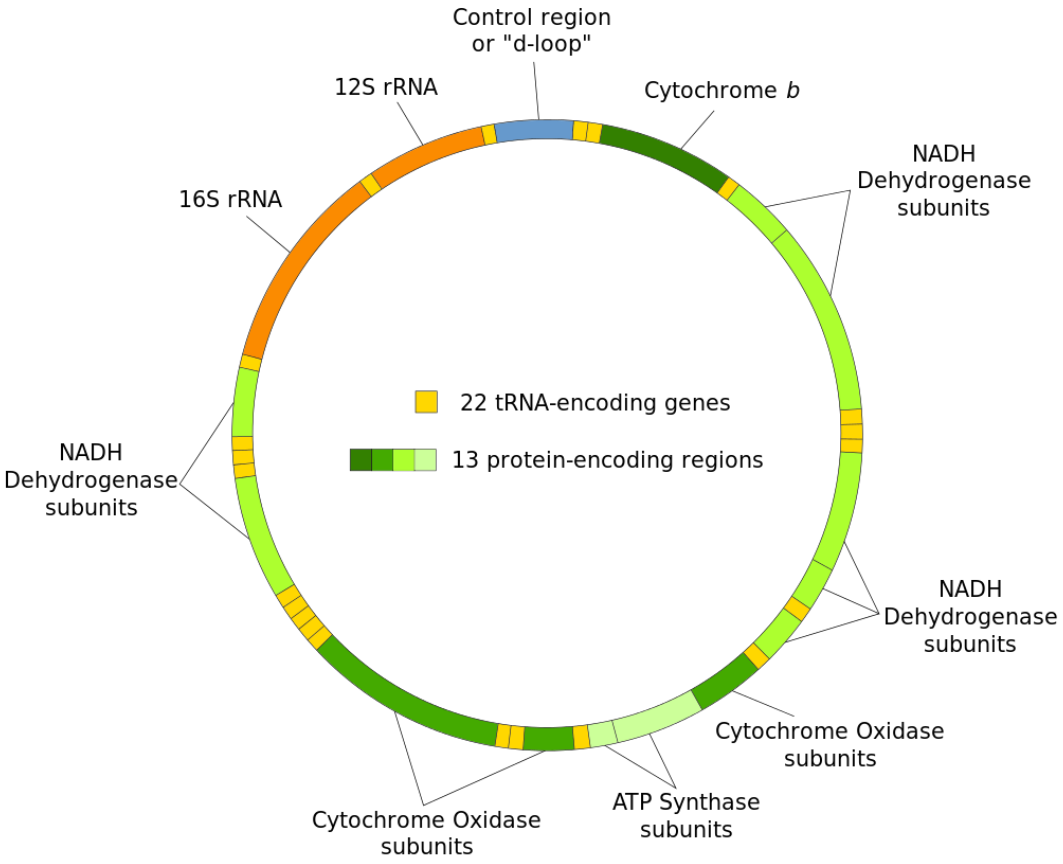

Figure 1.11 Schematic depicting mitochondrial DNA structure (Kalicharan, 2008**).** Double, circular DNA encodes for 13 proteins (mostly mitochondrial ETC complexes), 22 tRNA, and 2 rRNA.

In addition to providing the major source of energy in neurons, mitochondria also play an important role in intracellular Ca^{2+} regulation. Ca^{2+}enters neurons via Ca^{2+} channel openings and N-methyl-D-aspartate (NMDA) receptor activation. Intracellular Ca^{2+} is stored in the endoplasmic reticulum and mitochondria; Ca^{2+} enters mitochondria via Ca^{2+} uniporter and mitochondrial associated membrane (MAM) pores and exits mitochondria via sodium/Ca^{2+} exchanger (NCX) and mPTP, which can trigger apoptosis. Maintenance of intracellular Ca^{2+} concentrations is mediated, in part, by the L-type Cav 1.3 Ca^{2+} channel, which is vital for pacemaking of autonomous activation of NSDA neurons (pulsatile activity in the absence of synaptic input) (Grace and Bunney, 1983). Pacemaking activity and excitotoxity via glutamate NMDA receptor can cause excess Ca^{2+} influx into the NSDA neuronal cells; therefore, mitochondrial Ca^{2+} buffering capacity without induction of apoptosis is essential. Genetic evidence suggests that a mutation in DJ-1 (*park7*), which modulates Ca^{2+}, causes mitochondrial dysfunction and ROS generation. In addition, LRRK2 (*park8*) also modulates Ca^{2+} and regulates mitochondrial function.

Long axons of NSDA neurons have a high energy demand for synapse and dendritic spine formation, and impulse transmission, since the lack of myelin demands more energy for the signal to be transported along the axons (Donkelaar et al., 1998). Therefore, NSDA neurons are more vulnerable to an energy demand on mitochondria as the main source of the energy supply. In addition, the total mass of the mitochondria is much smaller in DA neurons as compared with non-DA neurons in the VMB, and there are less mitochondria in the cytosol of NSDA neurons in the SNpc than in mesolimbic/mesocortical DA neurons in the VTA (Liang et al., 2007). Since mitochondria are responsible for generating and reducing oxidative stress of the cells, mitochondria have a high level of antioxidant buffering capacity to compensate for the electron

radicals generated from Complexes I and III (Koopman et al., 2010). Furthermore, DA in the cytosol is highly oxidative making it sensitive to the levels of ROS in the cells. Therefore, it is vital for DA neurons to maintain mitochondrial health. Unique characteristics of DA neurons including the reactive nature of DA itself, high energy demand, associations of mitochondrial Complex I activity, ROS generation, mtDNA mutation, and Ca^{2+} buffering capacity may explain the importance of loss of mitochondrial maintenance in DA neurons as a contributory factor in PD. A summary of these etiological factors of PD on mitochondria is listed in **Table 1.2**.

Genetic factors		**Action on mitochondria**	**Effect**
PARK2	Parkin	Parkin-pink1 mediated mitophagy	Mitochondrial quality control
PARK6	Pink 1	Parkin-pink1 mediated mitophagy	Mitochondrial quality control
PARK7	DJ-1	Mitochondria and ER tethering, redox, altering of mitochondrial enzymes	Ca^{2+} modulation, ROS
PARK8	LRRK2	Drp1, antioxidant scavenger, Ca^{2+} modulation, autophagy	Mitochondrial fraction, mitophagy, ROS
PARK11	Candidate gene	*NADH dehydrogenase (ubiquinone) 1 alpha sub-complex 10(*NDUFA10)	?
PARK12	Candidate gene	*Translocase of inner mitochondrial membrane 8 homolog a* (TIMM8A)	?
PARK13	HTRA2	HTRA2/Omi mitochondrial serine protease, interacts with pink 1	apoptosis
PARK15	FBX07	Regulate E3 ubiquitin ligase	Possible interaction with parkin
PARK18	eIF4G1	Mitochondrial protein synthesis	Mitochondrial dysfunction, ROS
Environmental factors		**Action on mitochondria**	**Effect**
MPTP		Mitochondrial complex I inhibitor	ATP depletion, ROS
Organochlorine		ROS	ROS
Rotenone		Mitochondrial complex I inhibitor	ATP depletion, ROS
Paraquat		Redox cycle	ROS

Table 1.2 Summary of etiological factors of PD associated with mitochondria

Parkin

Mutation in parkin (*Park2)* is the most common cause for early onset of AR PD (onset at 41 years or less). Early onset PD patients, caused by parkin mutations have motor impairment and NSDA neuronal degeneration. This is similar to late-onset idiopathic PD, however, pathological evidence shows a lack of Lewy body accumulation (Mizuno et al., 2001). Nevertheless, ubiquitin and parkin are identified in Lewy bodies along with α-synuclein in idiopathic PD. Parkin is a E3 ubiqutin ligase, composed of 465 amino acids containing ubiquitin like domain (UBL), and triad domains (ring1 (R1), in-between-ring (IBR), ring2 (R2) domains) (**Figure 1.12 A**). Parkin labels unfolded or damaged proteins with ubiquitin for degradation in ubiquitin proteosome system (UPS).

The first step of the UPS is adenylation of ubiquitin at the c-terminal glycine (gly 76) residue by ubiquitin-activating enzyme (E1). This forms a thioester bond between E1 and ubiquitin and activates ubiquitin. Activated ubiquitin is transferred to ubiquitin-conjugating enzyme (E2) and forms a thioester bond between ubiquitin c-terminus of ubiquitin and cysteine residues of E2. Finally, ubiquitin is transferred from E2 to a substrate protein with the help of ubiquitin ligase (E3) forming an isopeptide bond between lysine residues of the substrate protein and c-terminal carboxylate of ubiquitin (**Figure 1.12 B**). Here, parkin, as an E3 ligase, plays a significant role in the UPS system by recognizing the target substrate protein. Parkin determines which protein will be degraded by the proteosome. The triad domains of parkin bind to E2 and the substrate protein for transfer of the ubiquitin to the target protein. Subsequently, parkin also interacts with 26s proteosome and proteosome degrades the target protein. Ubiquitins in the poly-ubiquitin chain are broken into monomers by UCH-L1 and are recycled (Passmore et al., 2004). UPS regulates protein abundance and their functions.

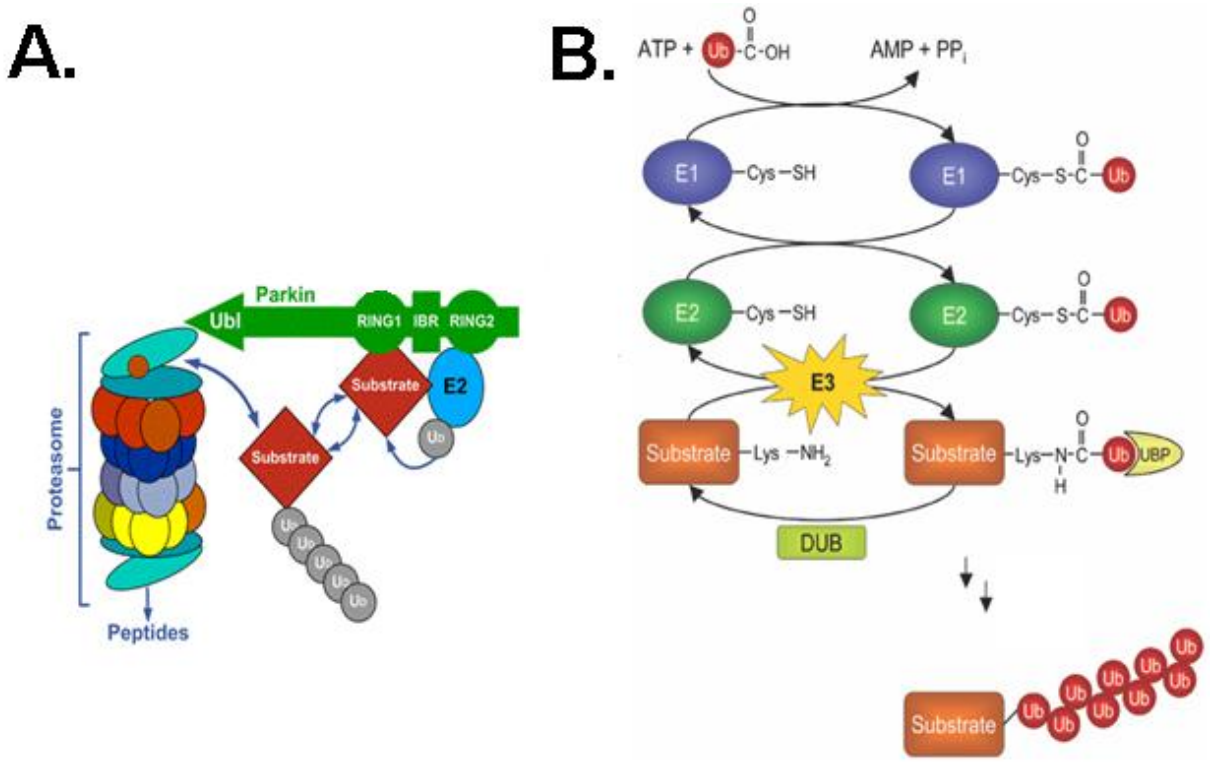

Figure 1.12 Parkin protein structures and ubiquitin proteasomal system (UPS). Panel A, Parkin protein structures in UPS (Schmidt, 2012). Triad domains in parkin, ubiquitin ligase, interacts with substrate protein, E2, and 26s proteosome. Panel B, Biochemical mechanism of UPS (Passmore, 2004). Ubiquitin is activated by the E1 and transfers to the E2 by thioester bond of cysteine (Cys). E3 ligase recognizes substrate protein and allows substrate protein to be poly-ubiquitinated by isopeptide bond of lysine (Lys).

When a protein is misfolded or damaged, chaperones can reform the misfolded protein or it can be tagged by ubiquitin and degraded by proteasomes. When protein aggregates are too large or the UPS is overloaded, aggregates can be degraded by autophagy. Ubiquitin is involved in many cell processes; proteosome, endocytosis, signal transduction, apoptosis, transcription, histone function, and DNA repair. The length of the ubiquitin chain and lysine residue of the poly-ubiquitination chain determines the fate of the protein substrate. Ubiquitin is composed of 76 amino acids with 7 lysine residues, including Lys6, Lys11, Lys27, Lsy29, Lys33, Lys48 and, Lys63. Glycine residues of the ubiquitin molecule bind to lysine residues of the ubiquitin molecule on the substrate protein to form a covalent bond, which is poly-ubiquitinylated chain. Here, parkin is involved in recognizing the target protein and transfers Lys48 poly-ubiquitinated protein to UPS and Lys63 poly-ubiquitinated protein to the autophagy machinery (Olzmann et al. ,2007) (**Figure 1.13**). Autophagy is a catabolic process in which cells get rid of their proteins or cytosolic organelles. When aggregation of the protein load exceeds proteosomal degradation or cells are in higher demand for nutrients, macroscopic autophagy can get rid of aggregated proteins (or cytosolic organelles) and recycle them.

E2 enzyme, Ubc-H13-Uev1a and parkin target Lys63 poly-ubiquitinated protein aggregates and parkin binds to histone deacetylase 6 (HDAC6) (Olzmann et al., 2007). HDAC6 is an adaptor protein for dynein motor complex. This allows microtubule-based retrograde transportation of the Lys63 poly-ubiquitinated proteins to the microtubule-organizing center near the nucleus forming aggresomes. Poly-ubiquitination also promotes recruitment of an isolation membrane, called phagopore, through p62. P62 has an ubiquitin associated domain (UBA) and a LC3-interacting region, and thereby binds to both Lys63 poly-ubiquitinated aggresomes and LC3 on an isolation membrane. LC3, microtubule associated protein1A/1B light chain 3, is an

ubiquitin-like protein and an autophagic marker. LC3-II has WXXL-like sequence recognize autophagic receptors such as p62 (Noda et al., 2010). LC3 conjugates to phosphotidylethanoamine (PE) and this is called LC3-II (Tanida et al., 2008). While interacting with aggresomes with an adaptor protein, LC3-II anchors into an isolated membrane, helps tethering and hemifusion of the membranes, and allows isolated membranes to expand (Nakatogawa et al., 2007). As isolated membrane with LC3-II grows and engulfs protein aggresomes (or organelles) forming "autophagosomes". LC3-II is responsible for recruitment and assembly of autophagosome machinery. Autophagosomes fuse with lysosomes and lysosomal hydrolase degrades aggregated proteins or organelles.

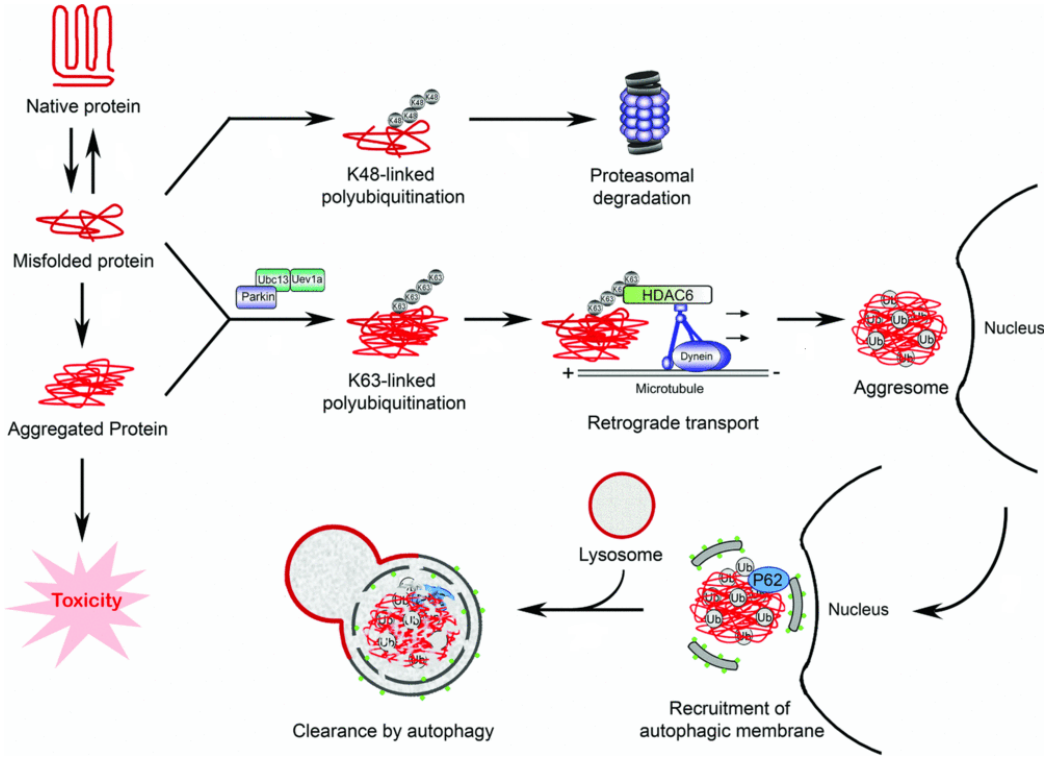

Figure 1.13 Schematic depicting the fate of poly-ubiquitination K48 and K63 and mechanism of autophagy (Chin et al., 2010**).** Parkin transports K48 poly-ubiquitinated aggregates to UPS and K63 poly-ubiquitinated aggregates to autophagy. K63 poly-unbiquitinated aggregates form aggresome and recruited onto isolated membrane by adaptor protein HDAC6 and p62. The isolated membrane expands and engulfs aggresome, fuses with lysosome and clears.

After induction of apoptosis, Tolkovsky et al. prevented cells from executing apoptosis by treating with general caspase inhibitors. The cells that were able to return to a normal state cleared the entire cohort of the mitochondria (Tolkovsky et al., 2002). This provides an insight on the importance of degradation of the damaged mitochondria to prevent initiation of apoptosis. Mitochondria are degraded by autophagy, also called "mitophagy" (Lemasters, 2005). Mitophagy occurs normally in the cells as a maintenance and stress-induced compensatory process (Goldman et al., 2010). Mitochondrial health is maintained by continuous fusion, fission, and mitophagy. An unhealthy mitochondrion is fused with healthy mitochondrion, which distributes nutrients and repairs damaged mitochondrial DNA and mitochondrial biogenesis can occur by mitochondrial fission (division of mitochondria) (Chen and Chan, 2009). However, if a mitochondrion is too damaged to revive, it is segregated and undergoes mitophagy.

Parkin plays a pivotal role in mitochondrial quality control by mitophagy (**Figure 1.14**). PINK1 is ubiquitously expressed and degraded in mitochondrial matrix (Tanaka, 2010; Youle and Narendra, 2011). However, when mitochondria are depolarized by injury, neurotoxin, or oxidative stress causing a change in mitochondrial membrane potential, PINK1 is accumulated on the mitochondrial outer membrane like a "halo" and recruits parkin. Parkin ubiquitinates the mitochondrial outer membrane proteins and recruits the isolated membrane, phagopore. Phagopore expands and engulfs damaged mitochondria forming mitophagosomes (mitochondria in autophagosomes). Mitophagosomes are fused with lysosomes and damaged mitochondria are degraded (Youle and Narendra, 2011).

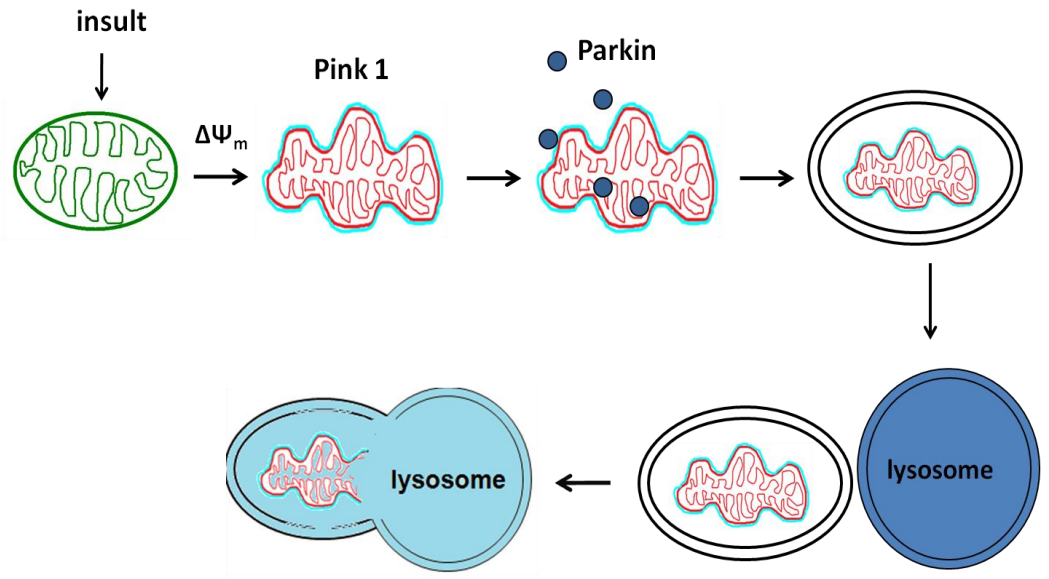

Figure. 1.14 Schematic depicting PINK1-parkin mediated mitophagy. Depolarized mitochondria are surrounded by PINK1 with parkin recruitment. Parkin ubiquitinates damaged mitochondria and are engulfed by autophagosome, fused with lysosome, and degraded.

Experimental paradigm and goal of dissertation research

The differential susceptibility of TIDA and NSDA neurons in PD is also observed following single acute MPTP exposure (Behrouz et al., 2007; Benskey, 2012; Benskey, 2013). MPTP is a mitochondrial Complex I inhibitor causing mitochondrial dysfunction; ATP depletion, and oxidative stress formation (Mizuno, 1988; Sherer,2002; Dawson, 2003; Cleeter, 1992). Several evidences indicate that mitochondria are deeply involved in pathophysiology of PD. Reduced mitochondrial Complex I activities in SN, platelets, and skeletal muscle of PD patients were observed (Schapira et al., 1989; Mizuno et al., 1989; Krige et al., 1992; Bindoff et al., 1991). Mitochondrial Complex I inhibitors, rotenone and MPTP, recapitulated identical pathophysiology of PD in various animal models (Cannon,2009; Smeyne et al., 2004). Mutations in parkin, PTEN-induced kinase I (PINKI), DJ-1 , α-synuclein, and leucine-rich-repeat kinase 2 (LRRK1) that cause PD in humans are also reported to be associated with mitochondrial dysfunction (Devi et al., 2008; Albrecht, 2005; Pendergrass et al., 2004). Therefore, it is natural to study mitochondrial structure and function in NSDA and TIDA neurons and their involvement in differential susceptibility to acute neurotoxicant exposure.

Brain regions containing these DA neurons (i.e. ST and MBH) in mice are too small to investigate mitochondrial respiration using Clark electrode methodology, as this technique requires mg quantities of tissue (Sauerbeck et al., 2011). However, the Seahorse XF Analyzer can measure mitochondrial bioenergetics using samples as small as fifteen µg of mitochondria, which permits measurement of mitochondrial respiration in synaptosomes derived from these discrete brain regions. In the studies described in this dissertation, ST and MBH from WT and parkin null mice were dissected, synaptosomes containing mitochondria were isolated, and basal, spare and maximal respiratory capacities were determined. Synaptosomal mitochondrial mass

and membrane potentials were determined by flow cytometry, and their morphology were analyzed by TEM.

The mechanism of NSDA neurodegeneration is still unknown; over 90 % of PD is idiopathic and genetic factors have incomplete penetrance with variable severity of disease and age of onset. This suggests the mechanisms underlying this disease are complex and multifaceted. The process may require multiple hits for the degeneration of NSDA neurons to occur. To understand mitochondrial involvement in PD better, each of the objectives in this dissertation were tested in both genetic and neurotoxin models. Parkin null mice were utilized to establish genetic evidence of parkin mediated mitochondrial quality control involvement in NSDA neurons, and MPTP and rotenone neurotoxin models were utilized to investigate mitochondrial function in NSDA neurons.

Preliminary investigation of the single acute MPTP exposure model and the time-line of neuronal responses were attained from previous studies in our laboratory (Benskey, 2013; Benskey, 2012; Behrouz, 2007). TIDA and NSDA neurons had reduction in DA level at 4 h after MPTP exposure with highest peak concentration of MPP^+. However, TIDA neurons recover DA levels at 24 h after MPTP exposure, whereas NSDA neuronal axon maintained depleted DA at this time. In addition, by 24 h, MPP^+ was cleared from both NSDA and TIDA neurons. Therefore, mitochondria in NSDA and TIDA neurons were investigated at 4 h and 24 h after MPTP single acute exposure. Studies described in this dissertation utilized these time points to examine the effects of MPTP single acute exposure on mitochondrial structure and function using analytic techniques including immunohistochemistry, confocal microscopy, electron microscopy, seahorse XF24 analyzer, and flow cytometry. Study of mitochondria using these

various approaches allowed identification of the unique characteristics of mitochondria and the involvement of parkin in mitochondrial function in central DA neurons.

Finally, to provide a possible tool for a novel therapy of PD, evidence of neuroprotective role of parkin was tested using parkin gene delivered through adeno-associated virus (AAV). Successful transduction of AAV-parkin into DA neurons in the MBH, SN, and ST was confirmed previously and optimum time of expression was determined as 4 weeks (Manfredsson, 2007; Manfredsson, 2009; Benskey et al., n.d.). rAAV-F-hParkin was stereotaxically delivered into SN in parkin null mice and mitochondrial function change was investigated. In addition, to test neuroprotective effect of parkin in neurotoxin model, rAAV-F-hParkin was delivered into SN in WT mice and mitochondrial bioenergetics and Western blot analysis of mitochondria, TH expression, and level of autophagy were determined.

Summary

A hallmark pathology of PD is differential susceptilibity of NSDA and TIDA neurons. This differential susceptibility is recapitulated following exposure of mice to mitochondrial Complex I inhibitor, MPTP; NSDA neurons are degenerated, while TIDA neurons are spared. In this dissertation, similar regional differential mitochondrial characteristics were revealed in WT mice; reduced mitochondrial bioenergetics, mass, and mitophagosomes were observed in mitochondria derived from regions containing NSDA neurons as compared to those containing TIDA neurons. However, mitochondria derived from both NSDA and TIDA axon terminal regions responded to mitochondrial Complex I inhibit in a similar manner, suggesting that the unique characteristics of mitochondria in axon terminals are not responsible for differential susceptibility of NSDA and TIDA neurons to MPTP. In addition, MPP^+ showed transient

inhibitory effects on mitochondria, and inhibition of MPP+ uptake by DAT did not prevent the inhibitory effects of this active MPTP metabolite. This indicates that the dynamics of MPTP conversion to MPP^+, MPP^+ uptake into cells and mitochondria, and/or a compensatory mechanism to MPTP exposure may play a significant role in determining differential susceptibility of TIDA and NSDA neurons. In addition, possible sequestration of MPP^+ into cells adjacent to TIDA neurons may prevent MPP+ uptake thereby allowing these neurons to be resistant to neurotoxins.

In MPTP-treated mice, previous studies have shown that differential parkin expression is observed; parkin increased in TIDA neurons, but not in NSDA neurons. In the present series of experiments, absence of parkin caused deficits in maximal and spare mitochondrial respirations, mitochondrial mass, mitochondrial number per axon terminals, and the morphology/structures, most plausibly due to loss of the mitophagy-mediated quality control of mitochondria. However, introduction of parkin in parkin null mice did not rescue impaired mitochondrial function. Also, parkin did not rescue reduction in basal respiration by MPTP in NSDA axon terminals. However, parkin overexpression prevented the decrease in the number of viable mitochondria caused by MPTP and maintained functional mitochondria likely through autophagy. This suggests that parkin may protect central DA neurons by maintaining mitochondrial function in long term as neurotoxin is cleared from the brain.

Dissertation objective

Central Hypothesis: Loss of parkin mediated mitochondrial quality control contributes to DA neuronal degeneration in a neurotoxicant model of PD

Specific Aim 1. Comparison of the mitochondrial structure and function in NSDA and TIDA neurons

Hypothesis: Mitochondrial function in axonal terminal regions of central DA neurons differs depending on the brain regions in WT mice

Specific Aim 2. Differential effect of mitochondrial Complex I inhibition on mitochondria in NSDA and TIDA neurons

Hypothesis: Mitochondria in TIDA neurons are resistant to acute exposure to mitochondrial Complex I inhibitor in WT mice

Specific Aim 3. Impaired mitochondrial function and structures in the absence of parkin

Hypothesis: Mitochondrial structure and function in axonal terminal regions of central DA neurons are impaired in the absence of parkin

Specific Aim 4. Neuroprotective effect of parkin on mitochondria in NSDA axon terminals

Hypothesis: Parkin has neuroprotective effect in ST-derived mitochondria following mitochondrial Complex I inhibition and in parkin null mice.

Chapter 2. Material and Methods

Animals

C57BL/6 WT mice: C57BL/6 male WT mice were obtained from Jackson Laboratories and used between 20 – 24 weeks of age. Mice were housed in a room with a 12-h light/dark cycle, with food and water provided *ad libitum*. The Michigan State University Institutional Animal Care & Use Committee approved all experiments using live animals (AUF 01/08-123-00).

Parkin KO: Parkin KO mice (Jackson Laboratories) were bred in house and used between 20 – 24 weeks of age. Mice were housed in a room with a 12-h light/dark cycle, with food and water provided *ad libitum*. The Michigan State University Institutional Animal Care & Use Committee approved all experiments using live animals (AUF 10/11-222-00). Homozygous parkin KO mice were B6.129S4-*Park2*^{tm1Shn}/J strain and confirmed by genotyping DNA isolated from tail snips. PCR was performed with primers 5 -CCTACACAGAACTGTGACCTGG; 5 -GCAGAATTACAGCAGTTACCTGG; 5 –ATGTTGCCGTCCTCCTTGAAGTCG for parkin KO mice from Michigan State University research technology support facility (Goldberg et al., 2003). Mice were randomly allocated to treatment groups.

TH-GFP: TH-GFP mice (RIKEN Bio-Resource Center, #RBRC02095) were bred in house and used between 20 – 24 weeks of age. Mice were housed in a room with a 12-h light/dark cycle, with food and water provided *ad libitum*. The Michigan State University Institutional Animal Care & Use Committee approved all experiments using live animals (AUF 10/13-230-00). Homozygous GFP-TH transgenic mice were B6.B6D2-Tg (Th-EGFP)21-31 transgenic line and confirmed by genotyping DNA isolated from tail snips. PCR was performed with primers 5 -CCTGTGACAGTGGATGCAATT; 5 – CTTGTACAGCTCGTCCATGCCGAG from Michigan

State University research technology support facility (RICKEN BRC). Mice were randomly allocated to treatment groups.

GFP-LC3: GFP-LC3 mice (RIKEN Bio-Resource Center, #BRC00806) were bred in house and used between 20 – 24 weeks of age. Mice were housed in a room with a 12-h light/dark cycle, with food and water provided *ad libitum*. The Michigan State University Institutional Animal Care & Use Committee approved all experiments using live animals (AUF 01/14-001-00). Homozygous GFP-LC3 transgenic mice were GFP-LC3#53 transgenic line and confirmed by genotyping DNA isolated from tail snips. PCR was performed with primers 5-ATAACTTGCTGGCCTTTCCACT-3; 5-CGGGCCATTTACCGTAAGTTAT-3; 5-GCAGCTCATTGCTGTTCCTCAA-3 for GFP-LC3 mice from Michigan State University research technology support facility (Mizushima et al., 2004; 2009). Mice were randomly allocated to treatment groups.

Materials, General Solutions and Drugs

Blocking solution (TEM;0.2% Gelatin, 0.8% BSA): Add 0.02 g Gelatin (Sigma, Cat. No. G1890) and 0.08 g BSA (Sigma, Cat. No. A2153) in warm 0.1 M cacodylate buffer.

5% bovine serum albumin: 5 g of BSA were dissolved into 100 ml of double distilled water.

$CaCl_2$: 1M $CaCl_2$ (Sigma, Cat. No. C1016, MW 110.98) was prepared by adding 110.98 mg $CaCl_2$ to 1 ml.

0.1M Cacodylate buffer: 10.701g Sodium cacodylate trihydrate was added in 500 ml double distilled water.

Odyssey blocking buffer with 0.2% Tween 20: Two hundred µl Tween 20 and 50 ml Odyssey blocking buffer were dissolved into 50 ml double distilled water.

D-Glucose: 1M D-Glucose (Sigma, Cat. No. 47829, MW 180.16) was prepared by adding 18.16 g D-Glucose to 100 ml.

EGTA: 0.5M EGTA·Na_4 (Sigma, Cat. No. E8145, MW 468.3) was prepared by dissolving 1170.75 mg EGTA in 5 ml double distilled water.

2.5% glutaldehyde/2% paraformaldehyde fix solution: 25% glutaldehyde (Sigma, Cat. No. G5882) 20 ml, 32% paraformaldehyde (Fisher, Cat. No. 50-980-494) 12.5 ml was mixed with 167.5 ml 0.1 M cacodylate buffer pH 7.4 to make up for total of 200 ml solution.

HEPES: 1M HEPES (Sigma, Cat. No. H3375, MW 238.31) was prepared by dissolving 3766.2mg HEPES in 20 ml double distilled water.

Incubation media: 3.5 mL of 1M KCl, 120 mL of 1L NaCl, 1.3 mL of 1M $CaCl_2$, 0.4 mL of 1M KH_2PO_4, 1.2 mL of 1M Na_2SO_4, 2 mL of 1M $MgSO_4$, 15mL of 1M D-glucose was added to double distilled water total of 1L. pH of the solution was adjusted to 7.4 at 36°C. The solution was sterilized by filter (Millipore, SCGPU05RE, 0.22 µm) under vacuum and stored at 4°C and made fresh every month. On the day of the experiment, 100 mg of bovine serum albumin (BSA) with free of essentially fatty acid (Sigma, Cat. No. A6003, 4 °C) was dissolved in 250 µL of incubation media (final concentration of 4 mg/ml BSA, 5 mM pyruvate, 2.5 mM malate) and

added freshly before each experiment.

Ionic media: 20 mL of 1 M HEPES, 10 mL of 1M D-Glucose, 1.2mL of 1M Na_2HPO_4, 1 mL of 1M $MgCl_2$, 5 mL of 1M $NaHCO_3$, 5 mL of 1M KCl, 140 mL of 1M NaCl was added to double distilled water. The solution was well mixed and double distilled water was added to total of 1 L and pH of the solution was adjusted to 7.4 at 4°C. The solution was sterilized by filtration (Millipore, SCGPU05RE, 0.22 µm) under vacuum and stored at 4°C and made fresh every month.

Isotonic saline: 9 grams of NaCl was added onto 1 L of twice distilled water to make 0.9% saline and autoclaved.

Ketamine/xylazine: Ketamine:xylazine (26.6 mg/kg : 4 mg/kg; ip) was used for euthanasia and a lower dose (3.3 mg/kg : 2 mg/kg; ip) used for anesthetization.

Ketoprofen (5 mg/kg): 0.1 ml of ketoprofen 100 mg/ml was diluted with 9.9 ml of sterile saline to make 1 mg/ml ketoprofen. The dosage of the ketoprofen for mice 5 mg/kg, so for 25 g mouse 10 unit (100 µl) of ketoprofen was injected subcutaneously (sc) before and 24 h after the surgery.

$MgCl_2$: 1M $MgCl_2$ (Sigma, Cat. No. M8266, MW 95.21) was prepared by adding 95.21 mg $MgCl_2$ to 1 ml double distilled water.

$MgSO_4$: 1M $MgSO_4$ (Sigma, cat. no. M7506, m.w. 120.37) was prepared by adding 120.37 mg

$MgSO_4$ to 1 ml double distilled water .

Mitochondria isolation buffer (MIB): 898.2 ml of sucrose buffer prepared as described above was mixed with 1.8 ml of 0.5 M EGTA. MIB was stored at 4°C for no longer than 4 weeks.

MitoTracker™ Green (Benzoxazolium, 2-[3-[5,6-dichloro-1,3-bis[[4-(chloromethyl)phenyl]methyl]-1,3-dihydro-2H-benzimidazol-2-ylidene]-1-propenyl]-3-methyl-, chloride/ 201860-17-5; Invitrogen, Cat. No. M-7514, MW 671.8): 50 µg of MitoTracker Green was dissolved with 74.4 µl DMSO making 1 mM MitoTracker Green. On the day of the experiment, 1 mM MitoTracker Green was diluted two times, first to 10 µM MitoTracker Green by mixing 10 µl of 1 mM MitoTracker Green with 990 µl KCl assay buffer, and then diluted 250 µl of 10 µM MitoTracker Green with 4.75 ml KCl assay buffer as final concentration of 500 nM.

MPTP: 10 mg/ml of MPTP (1-methyl-4-phenyl-1,2,3,6-tetrahydropyridine, Sigma, Cat. No.) was prepared by dissolving 100 mg MPTP in total of 10 ml saline solution. A 10 mg/ml MPTP working solution was diluted to 2.0 mg/ml with saline solution and a dose of 20 mg/kg MPTP was administered to mice.

2% OsO_4: Dilute 10 ml of 4% OsO_4 (Osmium tetraoxide; Sigma, Cat. No. 75632) in 10 ml double distilled water.

2% Paraformaldehyde: 12.5 ml of 32% paraformaldehyde (Fisher, Cat. No. 50-980-494) was mixed with 187.5 ml 0.1 M cacodylate buffer to make total of 200 ml.

4% Paraformaldehyde for perfusion: First, 8% paraformaldehyde (Sigma, Cat. No. 158127, MW 30.03) solution was prepared by heating 400 mL ddH_2O in a beaker with stirring to 60 °C in the fume hood. When the water reached 60 °C, 32 g of paraformaldehyde was added into the stirring water by slowly adding -15 drops of 10 M NaOH on stir plate at room temperature. When solution was clear , indicating complete dissolution of the paraformaldehyde powder, the solution was filtered and stored in the refrigerator at 4 °C. Four hundred ml 8% paraformaldehyde solution was mixed with 400 ml 0.2 M phosphate buffer and pH was adjusted to 7.4. The solution was made fresh on the day of the experiment.

0.2 M phosphate buffer for perfusion: 0.2 M Monobasic and dibasic sodium phosphate buffers were mixed to make 0.2 M phosphate buffer. Twenty four g anhydrous monobasic sodium phosphate (Sigma, Cat. No. s3139-250G, MW 120) were dissolved in 1 L double distilled water to prepare the monobasic sodium phosphate buffer. 28.4 g of anhydrous dibasic sodium phosphate (Sigma, Cat. No. 71640-250G, MW 142) were dissolved in 1 L doubled distilled water to prepare the dibasic sodium phosphate buffer. Appropriate amounts of 0.2 M monobasic sodium phosphate buffer were added into 300 - 400 ml dibasic sodium phosphate buffer to a pH of 7.4. The pH of the solution was adjusted with monobasic or dibasic sodium phosphate buffers.

40% Percoll solution**:** 8215.2 mg of sucrose were dissolved in 40 ml of ice-cold double distilled water in the ice bucket on the magnetic stirrer. One ml of 1 M HEPES, 200 µl of 0.5 M EGTA, and 40 ml of Percoll ^{Plus} (GE Healthcare, Cat. No. 17-5445-02, stored in 4 °C) were added to the solution. pH of the solution was adjusted to 7.4 with 1 M KOH at 4°C and double distilled ice

cold water was added to solution to total volume of 100 ml. The 40% Percoll solution was stored at 4°C for no longer than 4 weeks.

23% Percoll solution: In order to prepare 30 ml of 23% Percoll solution, 17.25 ml of 40% Percoll solution was mixed with 12.75 ml of MIB solution.

15% Percoll solution: In order to prepare 30 ml of 15% Percoll solution, 11.25 ml of 40% Percoll solution was mixed with 18.75 ml of MIB solution.

PBS for immunohistochemistry and Western blots: Phosphate buffer saline is composed of NaCl 137 mM, KCl 2.7 mM, Na_2HPO_4 10 mM, and KH_2PO_4 1.8 mM in ultra-pure H_2O. Eight g of NaCl, 0.2g of KCL, 1.44g of Na_2HPO_4, and 0.24g of KH_2PO_4 were dissolved into 1 L of double distilled water.

PBS-T (0.1% Tween 20): One ml of Tween-20 (Sigma, Cat. No. P1379-25ML) was added onto 1 L of PBS by stirring for 4 h.

KCl: 1M KCl (Sigma, Cat. No. P9333, MW 74.55) was prepared by adding 7.455 g KCl to 100 ml double distilled water.

KCl Assay buffer (125 mM KCl, 20 mM HEPES, 4 mM $MgCl_2$ and 2 mM KH_2PO_4): 12.5 ml of 1 M KCl, 2 ml 1M HEPES, 400 µl $MgCl_2$ and 200 µl KH_2PO_4 was added to 84.9 ml double distilled water. The buffer was adjusted to pH 7.4 with KOH solution.

KH_2PO_4: 1M KH_2PO_4 (Sigma, Cat. No. P5655, MW 136.09) was prepared by adding 136.09 mg KH_2PO_4 to 1 ml.

1% $NaBH_4$: 0.1g $NaBH_4$ (sodium borohydrate; Sigma, Cat. No. 71321-25G, MW 37.83) was dissolved in 10 ml cacodylate buffer.

NaCl: 1M NaCl (Sigma, cat. no. S7653, m.w. 58.44) was prepared by adding 5.844 g NaCl to 100 ml double distilled water.

$NaHCO_3$: 1M $NaHCO_3$ (Sigma, Cat. No. S5761,MW 84.01) was prepared by adding 84.01 mg $NaHCO_3$ to 1 ml double distilled water.

Na_2HPO_4: 1M Na_2HPO_4 (Sigma, Cat. No. S7907, MW 141.96) was prepared by adding 141.96 mg Na_2HPO_4 to 1 ml double distilled water.

Na_2SO_4: 1M Na_2SO_4 (Sigma, Cat. No. 239313, MW 142.04) was prepared by adding 142.04 mg Na_2SO_4 to 1 ml double distilled water.

Spurr's Resin: 5,72 g of DER (diglycidyl ether of poly (propylene glycol); Ted Pella Inc., Cat. No. 18310) were mixed with 16.4 g ERL (ERL 4221 epoxide resin; Ted Pella Inc., Cat. No. 18306-4221). When DER and ERL were completely mixed, 23.6 g NSA (nonenyl succinic anhydride; Ted Pella Inc., Cat. No. 18301) were added to the solution and mixed for 5 min. When the solutions are completely mixed, 0.4 g of DMAE (2-dimethylaminoethanol; Ted Pella

Inc., Cat. No. 18315) was added drop by drop. The Spurr's resin was made freshly on the day of the experiment.

20% sucrose for perfusion: 20 g sucrose (Sigma, Cat. No. s7903-250G, MW 432.30) were dissolved into double distilled water to final volume of 100 ml.

Sucrose buffer (mitochondrial isolation): 300 mM Sucrose (Sigma, Cat. No. S7903, MW 342.3) with 10 mM HEPS was prepared by dissolving 102.69 g of sucrose in 900 ml of ice-cold double distilled water in the ice bucket on the magnetic stirrer. 10 ml of 1 M HEPES were added and the pH adjust to pH 7.4 with 1 M KOH at 4°C. Ice-cold double distilled water was added to the buffer as total volume of 1 L and sterilized with a micro filter (Millipore, SCGPU05RE, 0.22 µm) under the vacuum. Sucrose buffer was stored at 4°C for no longer than 4 weeks.

0.2% Tannic acid: 0.02g Tannic acid were dissolved into 10 ml of double distilled water.

Tetramethylrhodamine ethyl ester perchlorate (TMRE, Sigma-Aldrich Cat. No. 87917-25MG, m.w. 514.95): 1mM TMRE was prepared by dissolving 25 mg TMRE in 48.5 µl DMSO as the storage concentration. On the day of the experiment, TMRE was diluted two times, first to 10 µM TMRE by combining 10 µl of 1 mM TMRE with 990 µl KCl assay buffer, and then diluting 100 µl of 10 µM TMRE with 4.9 ml KCl assay buffer to a final concentration of 200 nM TMRE

.

Tissue lysis buffer : Tissue lysis buffer is composed with 1% SDS, 0.1mM PMSF (phenylmethanesulfonyl fluoride; Sigma, Cat. No. 93482), 1mM DTT (DL-dithiothreitol; Sigma,

Cat. No. D0632-1G, MW 154.25), protease inhibitor cocktail tablets (Roche Diagnostics, Mannheim, Germany), phophatase inhibitor cocktail (Thermoscientific, Cat. No. 78428). On the day of the experiment, 100 µl SDS (10%[w/v] in double distilled water), 1 µl PMSF, 1 µl of 1 M DTT, 10 µl protease inhibitor, 10 µl phophatase inhibitor was added into 1 ml of TBS buffer.

TBS: Tris-buffered saline was prepared by dissolving 8.77 g of NaCl and 1.211 g Tris-Cl (2-amino-2-(hydroxymethyl)-1,3-propanediol, THAM, and Tris base (hydroxymethyl) aminomethane; Sigma, Cat. No. RDD008, MW 121.14) in double distilled water to final volume of 1 L.

TBS-TX: One ml of Triton x100 (4-(1,1,3,3-Tetramethylbutyl)phenyl-polyethylene glycol, *t*-Octylphenoxypolyethoxyethanol, Polyethylene glycol *tert*-octylphenyl ether; Sigma, cat. No. X100-100ML) was dissolved into 1 L of TBS.

Pyruvate (Sodium Pyruvate; Sigma, Cat. No. P5280-25G, MW 110.04) / Malate (DL-Malic acid disodium salt; Sigma, Cat. No. M6773-5G, MW 178.05): 500 mM pyruvate and 250 mM malate was prepared by adding 110.04 mg pyruvate and 89.02 mg malate into 2 ml of 20 mM HEPES. Two hundred fifty µl of 1 M pyruvate and 500 mM malate stock were diluted with 25 ml incubation media on the day of the experiments yielding a 50 mM working concentration of pyruvate / 25 mM malate with final concentration as 5 mM pyruvate/ 2.5 mM malate in Seahorse plate.

ADP (Adenosine 5′-diphosphate sodium salt): 300 mM ADP (Sigma Cat. No. A2754-1G, powder, MW 427.2) was prepared by dissolving 128.16 mg ADP in 1 ml of 20 mM HEPES (pH7.0) followed by dilution to 1:1000 on the day of use in a final concentration of 300 µM.

Oligomycin A: 10 mM Olygomycin A (Fluka, Cat. No. 75351-5MG, MW 791.06) was prepared by adding 5 mg of oligomycin A to 621.6 µl DMSO and dilute as 1 mM working concentration by diluting 10 mM oligomycin A 100 µl with 900 µl DMSO. On the day of the experiment, 60 µl of 1 mM oligomycin A was added to 2 ml incubation buffer to make a 30 µM oligomycin A solution.

CCCP: 50 mM carbonyl cyanide 3-chlorophenylhydrazone (Sigma, Cat. No. C2759-250MG, MW 204.62) was prepared by dissolving 10.23 mg CCCP in 1 ml DMSO. Twenty µl of 50 mM CCCP stock solution was diluted with 980 µl DMSO to make a final 1 mM CCCP working solution. On the day of the experiment, 40 µl of 1 mM CCCP was added into 2 ml incubation buffer for a final concentration of 20 µM CCCP.

FCCP: 10 mg carbonyl cyanide 4-(trifluoromethoxy)phenylhydrazone (Sigma, Cat. No C2920-10MG, MW 254.17) was dissolved into 787 µ DMSO to make a stock solution of 50 mM FCCP. Twenty µl of 50 mM FCCP was diluted with 980 µl DMSO to make working concentration of 1 mM FCCP. On the day of the experiment, 90 µl of 1 mM FCCP was added into 3 ml incubation buffer for a final concentration of 30 µM FCCP.

Rotenone: 1 mM rotenone (Sigma, Cat. No R8875-1G, MW 394.42) was prepared by dissolving

19.72 mg of rotenone in 1 ml DMSO to make stock solution of 50 mM rotenone. Twenty µl of 50 mM rotenone was diluted with 980 µl DMSO to make working concentration of 1 mM rotenone. On the day of experiment, 75 µl of 1 mM rotenone was added into 3 ml incubation buffer for a final concentration of 25 µM rotenone.

Antimycin A: 25 mg antimycin A (Sigma, Cat. No A8674-25MG, MW 548.63) was dissolved in 911 µl DMSO to make stock solution of 50 mM Antimycin A. Twenty µl of 50 mM antimycin A was diluted with 980 µl DMSO to make working concentration of 1 mM antimycin A. On the day of experiment, 75 µl of 1 mM antimycin A was added into 3 ml incubation buffer for a final concentration of 25 µM antimycin A.

MPP+ iodide: a 1 mM stock solution of **1-methyl-4-phenylpyridinium iodide (**Sigma, Cat. No D048-100MG, MW 297.13) was prepared by dissolving 100 mg MPP+ iodide in 336 µl DMSO. Final dilution was made accordingly depending on the experiments.

Drugs	Action	Mitochondria respiration state	Bioenergetics
Pyruvate/Malate	**ETC substrate**	**State II**	**Basal respiration**
ADP	**ATP synthase substrate**	**State III**	**Maximum respiration**
oligomycin	**ATP synthase inhibitor**	**State IV_o**	**Proton leak**
FCCP	**ETC decoupler**	**State III_μ**	**Maximum respiration**
Antimycin A	**ETC Complex III inhibitor**	**State V**	**Non-mitochondrial respiration**
Rotenone	**ETC Complex I inhibitor**	**State V**	**Non-mitochondrial respiration**
MPP+	**ETC Complex I inhibitor**	**State V**	**Non-mitochondrial respiration**

Table 2.1 Summary of drug actions on mitochondrial bioenergetics. The table describes actions of the drugs on mitochondria and their applications to identify mitochondrial respiratory state and bioenergetics.

Synaptosomal and non-synaptosomal mitochondria isolation

Mice were decapitated and the brain was rapidly removed from the skull. ST and MBH were dissected on ice and SM were isolated from ST and MBH by the method of Dunkley with some modifications for sub-brain regions (Dunkley et al., 2008). ST and MBH were collected in mitochondrial isolation buffer (MIB, 300 mM Sucrose, 10 mM HEPES, 1 mM EGTA, pH 7.4 at 4°C) and homogenated with pre-chilled Teflon/glass homogenizer by 10 strokes on ice (Whittaker & Gray, 1962). The homogenates were transferred to 15 ml tubes and centrifuged at 21,000 g at 4 °C for 10 min in fixed-angle rotor. The hard pellets were re-suspended in 15% Percoll and layered onto the 23% and 40% Percoll with MIB medium 2 ml each. The Percoll gradients were centrifuged 26,000 g at 4 °C for 10 min. Second band was collected for SM and third band was collected for non-synaptosomal mitochondria (NSM) (**Fig 2.3.1**). The mitochondria of the interest were washed with MIB solution and sucrose buffer (300 mM Sucrose and 10 mM HEPES, pH 7.4 at 4°C) by centrifugation, and stored in sucrose buffer. The protein content of individual SM and NSM samples was quantified using a bicinchoninic acid (BCA) assay (Noble & Bailey, 2009).

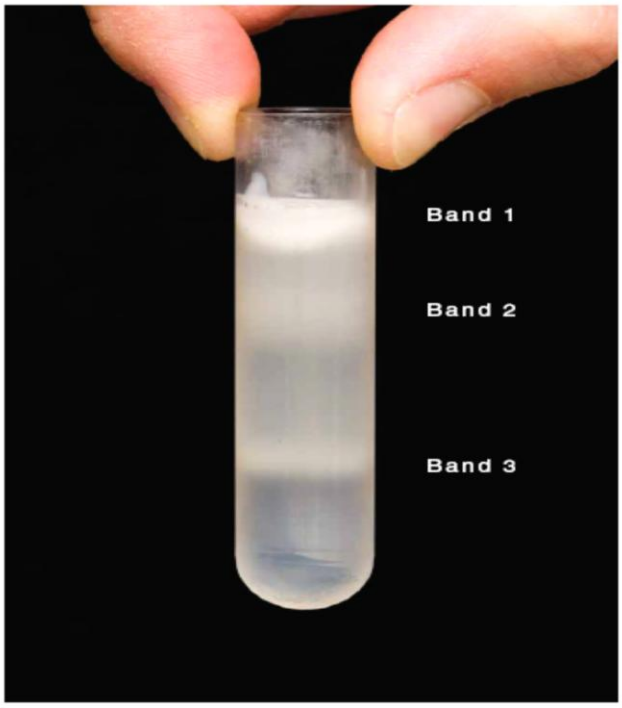

Figure 2.1 Percoll gradient with 3 band formation. Band 1 mostly consists of myelin, band 2 consists of synaptosomes, and band 3 consists of non-synaptosomal mitochondria.

Mitochondrial bioenergetics

Mitochondria plating

Twenty µg SM or 15 µg of NSM in ionic medium (20 mM HEPES, 10 mM D-Glucose, 1.2 mM Na_2HPO_4, 1 mM $MgCl_2$, 5 mM $NaHCO_3$, 5 mM KCl, 140 mM NaCl, pH 7.4) were plated onto 20 wells of the Seahorse XF 24 well plates (Seahorse Bioscience, North Bilerica, MA) and centrifuged at 2,500 rcf for 1 h at 4°C in swinging bucket rotor in a Fisher Scientific 3000R centrifuge. SM attached onto the Seahorse plates were diluted with 600 µl incubation medium (3.5 mM KCl, 120 mM NaCl, 1.3 mM $CaCl_2$, 0.4 mM KH_2PO_4, 1.2 mM Na_2SO_4, 2 mM $MgSO_4$, 4 mg/ml BSA, 15mM D-glucose, 5 mM pyruvate, 2.5 mM Malate) and incubated in a non-CO_2 tank.

Preparation of the Seahorse XF 24 cartridges

A XF 24 cartridge (Seahorse Bioscience, North Bilerica, MA) was incubated with 1 ml calibrant (Seahorse Bioscience, North Bilerica, MA) per well in a non-CO_2 incubator at 37°C overnight for hydration. Before loading the cartridge onto the XF 24 analyzer, 72 µl of rotenone, 80 µl oligomycin, 89 µl FCCP were added onto the cartridges and incubated in a non-CO_2 incubator for 10 min at 37°C. The cartridges were loaded onto the XF 24 analyzer for calibration. **Figure 2.2** depicts the general assay flow chart of the Seahorse XF analyzer for isolated mitochondria.

Mitochondrial respiratory assay by Seahorse XF analyzer

The analyzer creates a microchamber in which mitochondrial oxygen consumption rate (OCR) and extracellular acidification rate (ECAR) were measured by fluorescent probes, which detect oxygen and proton concentrations. A probe is immersed into the micro chamber and measures OCR and ECAR. The microchamber is refreshed after each measurement cycle by oscillation of the emersion and immersion of the probes to replenish ambient oxygen and proton

concentrations for each cycle. OCR and ECAR reflect the mean rates of the measurement cycle. Appropriate mixing and measurement times were pre-set following manufacturer's instructions.

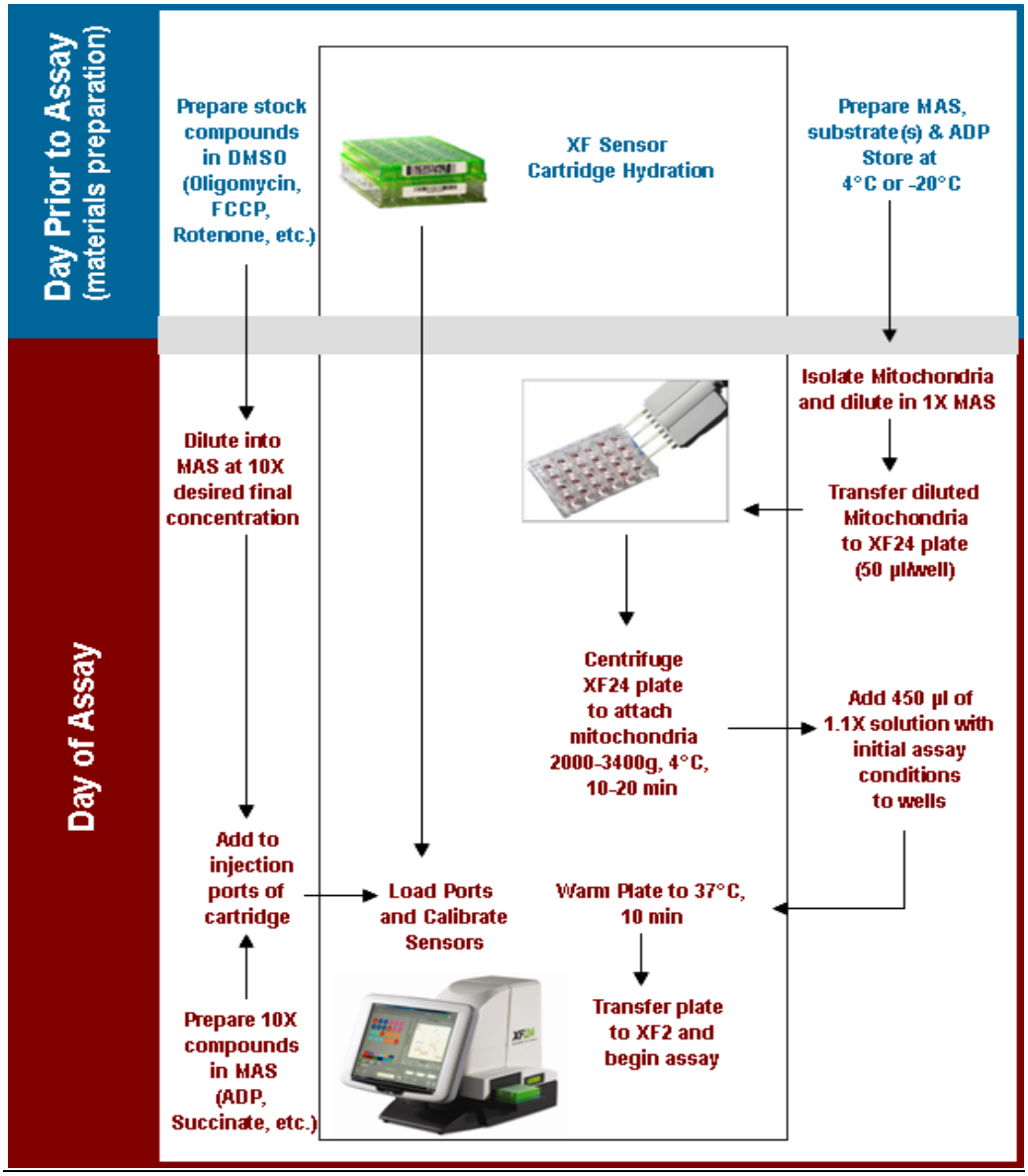

Figure 2.2 General assay flow chart of XF analyzer for isolated mitochondria. Day1: Hydration of the cartilage and turn on of the XF analyzer, Day 2: preparation of the compounds, isolation of the mitochondria and measurement of the respiration of the mitochondria (Rogers et al., 2011).

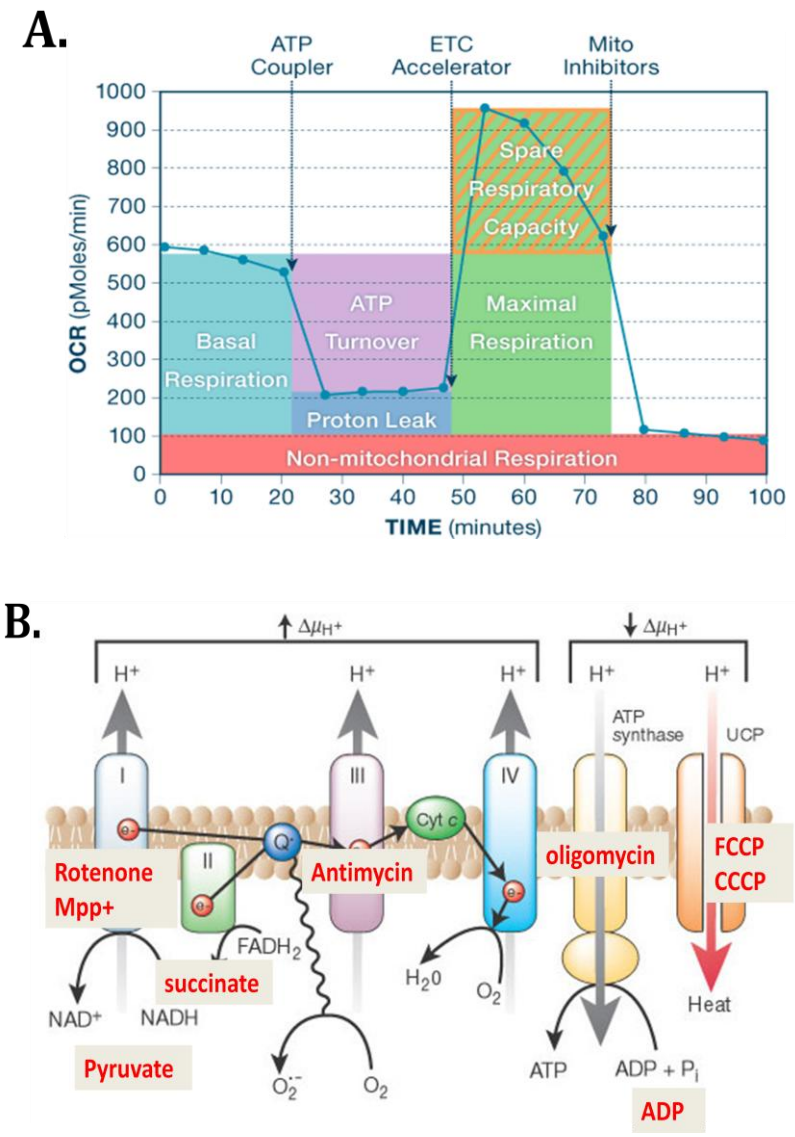

Figure 2.3 Mitochondrial bioenergetics OCR profile. A. Basal respiration: OCR in the absence of any drug treatment, Maximum respiration: OCR after treatment with an uncoupler that accelerates the electron transport chain (ETC), Spare respiratory capacity: OCR difference between basal and maximum respirations, Proton leak: OCR after an ATP synthase inhibitor, ATP turnover: difference between proton leak and basal respiration, Non-mitochondrial respiration: Remaining OCR after inhibition of the ETC. B. ETC and various drugs **(**Brand and Nicholls., 2011**).** Pyruvate is a substrate for ETC Complex I, succinate for Complex II, rotenone and MPP+: Complex I inhibitor, Antimycin A: Complex III inhibitor, olygomycin: ATP synthase inhibitor, FCCP and CCCP: ETC uncouplers.

Data analysis and interpretations

Mitochondrial bioenergetics was measured by changes in the OCR following various drug treatments that affect the ETC (Figure 2.3). Basal respiration was measured when only substrate pyruvate 5 µm and malate 2.5 µM were presented. Here the limiting factor for oxygen consumption rate is ADP availability/demands and the given substrate availability. However, when ATP synthase inhibitor, olygomycin is added, mitochondrial ETC and oxidative phosphorylation are uncoupled, and ATP synthesis no longer occurs from the proton gradients formed by electron transfer. Therefore, remaining OCR indicates proton leak. Mitochondria can leak protons through uncoupling proteins such as thermogenin. In addition, when mitochondrial proton back pressure is elevated, mitochondria leak protons to balance the proton backpressure and the exhaustion of the proton gradient occurs through oxidative phosphorylation. The difference between values for proton leakage and basal respiration gives an index of how much oxygen is consumed to make ATP versus how much is consumed during proton leakage.

Similar to the uncoupling proteins, FCCP or CCCP cause protons to leak from intermembrane space to the matrix of the mitochondria, similar to making a hole in the membrane. Here proton backpressure is no longer a limitation, the ETC can transfer electrons and oxygen accepts electrons. Therefore, the uncouplers provide information regarding the maximal capability of the ETC to transfer electrons, consume oxygen, and undergo maximum respiration. The difference between maximum and basal respiration indicates the mitochondrial spare respiratory capacity. Finally, rotenone, which is an ETC Complex I inhibitor, and antimycin A, which is Complex III inhibitor terminates ETC activity. Maximum doses of rotenone and antimycin A were utilized to completely inhibit ETC. OCR after ETC inhibition

are due to non-mitochondrial cellular oxygen utilization such as oxidative enzymes. Rotenone and antimycin A were utilized to calculate non-mitochondrial respiration.

In each assay, respiratory control ratio' (RCR') was measured as an index of mitochondrial function and health; "Healthier" mitochondria have higher RCR values (Brand and (Nicholls., 2011; Caprette DR., 2008; Guautier C., 2008; Taiz and Zeiger, 2010). RCR measures ability of mitochondria to utilize substrates and convert to oxidative phosphorylation and was calculated according to the following equation:

RCR' = OCR of state III_{μ} / OCR of state IV_o

Respiratory state III_{μ} is OCR for the maximum ability for the ETC to transfer electrons as seen as the OCR following treatment with ADP for NSM, and the OCR following treatment with FCCP or CCCP for SM. State IV_o is OCR when mitochondrial ATP synthesis is decoupled from electron transfer by ETC following treatment with oligomycin. Only mitochondria with RCR' equal to 3 or higher were utilized for analysis.

Mitochondrial density assay

In order to establish the optimal density of non-synaptosomal mitochondria in the bioenergetics experiments, samples were assayed at various concentrations ranging from 2.5 to 40 µg as quantified using a BCA assay. As shown in **Figure 2.4**, basal OCR (pMoles per min) during the first 10 min varied in proportion to the amount of NSM protein added to the analytical chamber. Protein content of 10 µg was considered optimal with an OCR value of approximately 400 pMoles per min for basal respiration. Protein content of 1.25, 2.5 and 5 µg had too low OCR, whereas OCR for 20 and 40 µg was too high. For the 10 µg sample, OCR increased following injection of ADP substrate at Time A, decreased following injection of the ATP

synthase inhibitor oligomycin at Time B, increased in response to ETC uncoupling with CCCP at Time C, and decreased to negligible levels following inhibition of Complex II with antimycin A at Time D, thereby confirming viable NSM in the preparation. The mitochondrial bioenergetic profiles shows injection of ADP increased electron transport demand that OCR was induced. NSM in the 1.25 µg sample exhibited a similar respiratory profile as the 10 µg sample except that administration of substrate ADP does not cause an increase of the OCR. This is likely due to an insufficient number of the mitochondria regardless of its high RCR (10.3).

RCR of 20 and 40 µg NSM are less than the optimal value of 3. This may be due to lack of oxygen availability in the microchamber of the XF analyzer. According to the O_2 concentration profile shown in Figure 2.5, after injection of ADP and CCCP, O_2 crashes in the 20 and 40 µg samples, which represents stalling of the ETC due to the lack of oxygen to accept the transferred electrons. Here, maximum respiration is no longer limited by capability of the ETC but by oxygen availability. Therefore, this protein concentration cannot be utilized, since RCR values were under represented than what actually were or expected. Accordingly, candidate optimal densities are determined to be 2.5, 5, and 10 µg NSM with RCR values of 3.3, 3.4, and 3.1, all within the acceptable range.

Mitochondrial density assay of basal respiration shows a nice linear relationship between the densities of the mitochondria and OCR readings. However, increase in basal respiration or mitochondrial density does not respond to high RCR. The recommended mitochondrial density for OCR of the State II is between 50 and 200 pMoles per min, and for State III of OCR is less than 1,500 pMoles per min. OCR of the State II of 2.5 µg NSM is 69, 5 µg NSM is 107, 10 µg NSM is 222. Thus, 10 µg NSM can be acceptable in this study. The mitochondrial density assay

was repeated again for NSM and SM and consideration of the recommended literature, 5-15 µg NSM and 10-20 µg SM was utilized in subsequent studies.

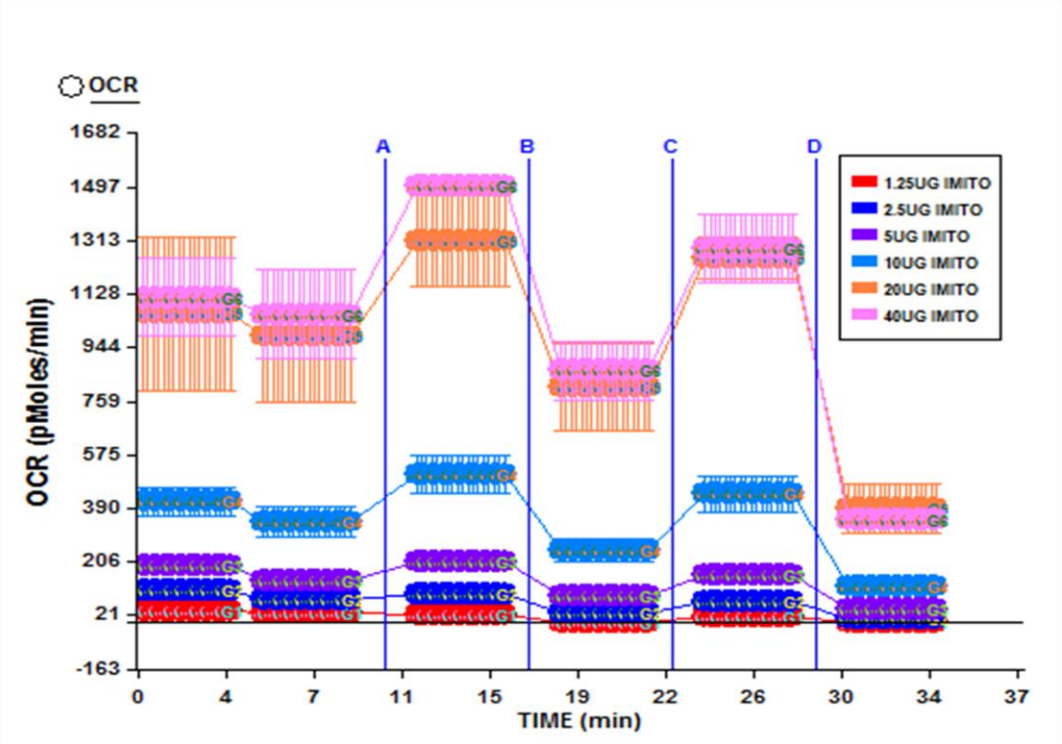

Figure 2.4 Representative respiration profiles of non-synaptosomal mitochondria assay as a function of protein density. Non-synaptosomal mitochondria were isolated from mouse whole brain using a Percoll gradient and following centrifugation, protein content was quantified by BCA assay. Amounts of protein between 1.25 µg to 40 µg were examined by using Seahorse XF24 analyzer to measure oxygen consumption rate (OCR) following (A) ADP, (B) oligomycin A, (C) CCCP, and (D) antimycin A.

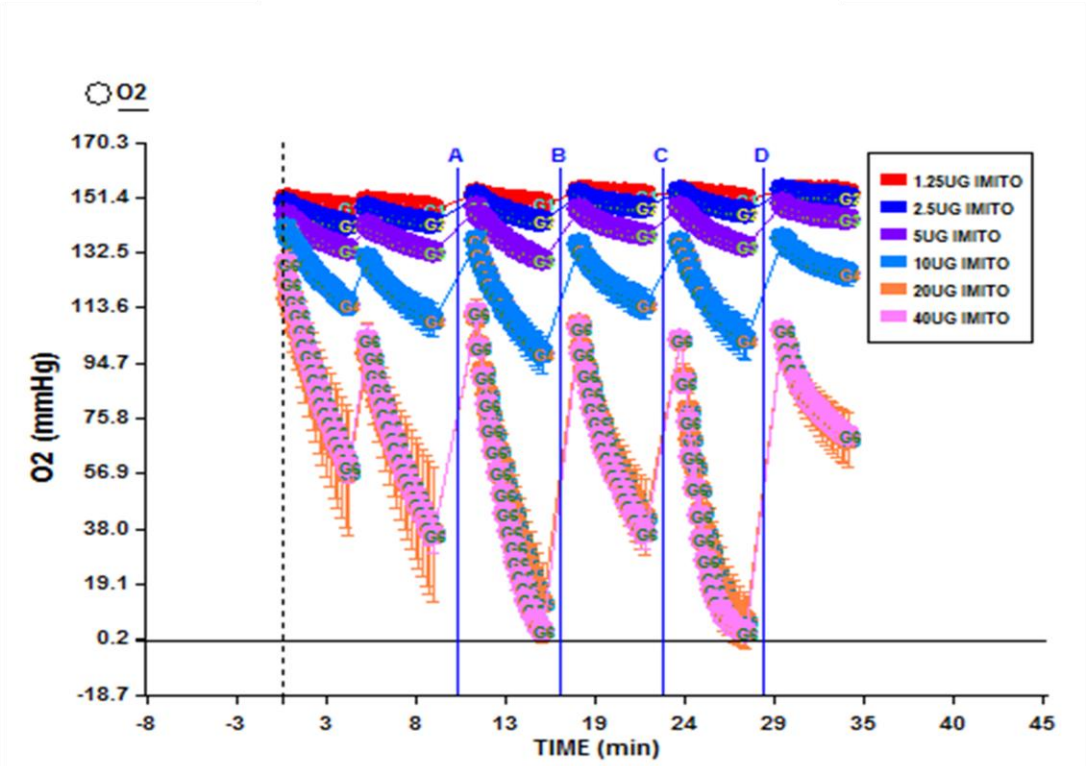

Figure 2.5 O_2 profile during oxygen consumption of NSM as a function of protein density. NSM were isolated from mouse whole brain using a Percoll gradient and following centrifugation, protein content was quantified using a BCA assay. Amounts of protein between 1.25 µg to 40 µg were examined by using Seahorse XF24 analyzer to measure O_2 concentrations via XF 24 analyzer while measuring OCR following (A) ADP, (B) oligomycin A, (C) CCCP, and (D) antimycin A.

Drug and substrate titrations

In addition to mitochondrial density assay, the concentrations of the various drugs used to accurately measure mitochondrial bioenergetics were optimized. Three drug class were tested including uncouplers of mitochondrial energy State III_{μ}, substrates, and storing buffer or dissolving solutions.

Uncouplers: FCCP, CCCP

Carbonyl cyanide 4-(trifluoromethoxy) phenylhydrazone (FCCP) and carbonyl cyanide m-chlorophenyl hydrazone (CCCP) are protonophores that uncouple mitochondrial oxidative phosphorylation by translocating protons from intermembrane space into the matrix of the mitochondria, thereby dissipating electrochemical potential. These drugs are weak lipophilic acids, which can be in anionic or protonated forms (**Figure 2.6**). The ionic forms of the compounds are able to pass the membrane through delocalization of charges by conjugated resonance structures. Therefore, addition of FCCP or CCCP causes depolarization of the mitochondria and allows the ETC to fully turn on regardless of ATP synthase activity, ADP concentration, or oxphos capacity. Therefore, FCCP or CCCP addition allows for estimation of the ETS capacity.

The difference between State III_u maximum respiration induced by uncouplers such as CCCP and FCCP, and basal respiration represents spare respiratory capacity. State III_u also represents electron transfer system capacity (ETS capacity) of non-coupled state of mitochondria. This represents the maximum flux capacity of the ETS and membrane potential in an open-proton-circuit operation of the mitochondrial transmembrane. In viable mitochondria, ETS capacity represents functionality of inner membrane bound ETC as well as transporters

within the membrane, TCA cycle and mitochondrial enzymes that are involved in mitochondrial respiration.

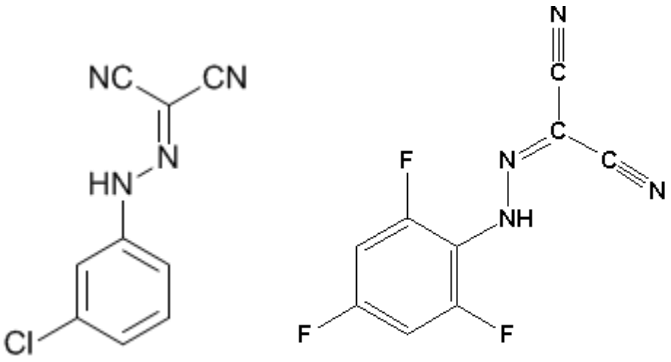

Figure 2.6 Molecular structures of carbonyl cyanide m-chlorophenyl hydrazone (CCCP) and carbonyl cyanide 4-(trifluoromethoxy) phenylhydrazone (FCCP). CCCP and FCCP is uncoupler. The drugs can be utilized to investigate mitochondrial maximum spare respiration (respiratory energy State III_{μ}).

On the other hand, oxphos capacity is assessed by ADP-stimulated mitochondrial respiration in the presence of the substrates and this is a partial coupled state. The proton gradient formed by ETC is utilized to convert ADP to ATP, and the ability of the ETC to generate ATP in given condition is the oxphos capacity. The proton gradient drives ATP synthase in normal mitochondria, but it also creates a leak due to the high backpressure created by protons in the intermembrane space. Also, the state of oxphos capacity causes a dyscoupled respiration state, which is pathological. When ETS capacity is higher, the ability to generate proton motive force is higher than oxphos capacity. However, the difference between the oxphos capacity and ETS capacity is not clearly understood and depends on substrates and substrate combinations. Keeping this in mind, CCCP correction optimization was conducted.

CCCP was titrated from 0.4 to 4 µM and OCR were measured in 20 µg SM. OCR increased incrementally with CCCP concentrations of 0.4 µM to 2 µM. After reaching the maximum OCR of State III_{μ} with 2 µM, OCR decreased with the higher 3 and 4 µM CCCP (**Figure 2.7**). Maximum OCR mitochondrial respiration was attained with 2 µM CCCP. Moreover, 0.8 and 2 µM had the highest RCR' (**Table 2.2**). Both 0.8 and 2 µM CCCP resulted in the maximum RCR' of 6.2 and 6.1, so either can be optimum CCCP concentrations to measure OCR of State III_{μ}. On the other hand, mitochondrial respiration was decreased with higher CCCP concentrations in the 3 and 4 µM ranges. This is likely due to either limited

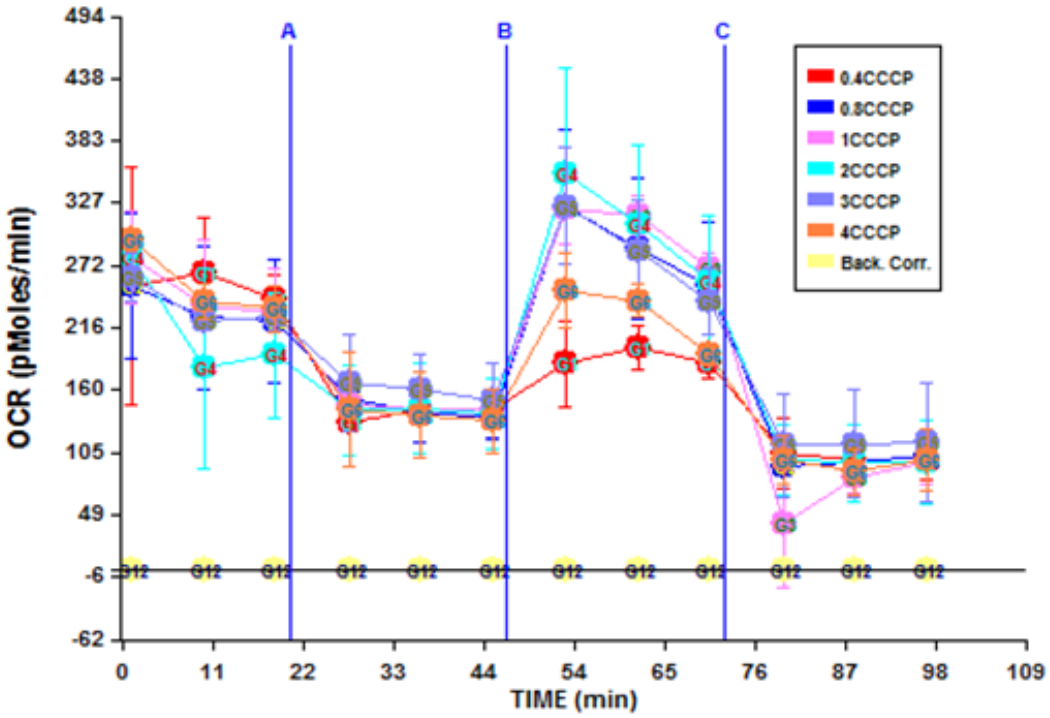

Figure 2.7 Representative respiration profiles of SM with incubation with concentrations of 0.4, 0.8, 1, 2, 3, or 4 µM CCCP injected at Time B. SM were isolated from mouse whole brain using Percoll gradient and centrifugation, and quantified by Bradford protein assay. Ten µg SM respiration was examined by using Seahorse XF24 analyzer measuring OCR: injection port A: oligomycin, injection port B: ● indicates CCCP 0.4 µM, ● indicates CCCP 0.8 µM, ● indicates CCCP 1 µM, ● indicates CCCP 2 µM, ● indicates CCCP 3 µM, ● indicates CCCP 4 µM and injection port C: rotenone.

CCCP µM	OCR state IIIu	OCR state IVo	RCR'
0.4	83	42	2
0.8	222	36	6.2
1	227	48	4.7
2	256	42	6.1
3	212	37	5.7
4	151	35	4.3

Table 2.2 Respiratory control ratios (RCR') of SM following with incubation with concentrations of 0.4, 0.8, 1, 2, 3, or 4 µM CCCP. SM were isolated from mouse whole brain using Percoll gradient and centrifugation, and quantified by Bradford protein assay. Ten µg SM respiration was examined by using Seahorse XF24 analyzer measuring OCR. RCR' was calculated by OCR of State III_{μ}/ State IV_{o}.

oxygen availability in the micro-chambers created by Seahorse XF analyzer, limited substrate availability, or toxicity caused by CCCP. O_2 concentration data shown in **Figure 2.8** indicates that despite CCCP concentrations ranging from 0.4 to 4 µM, O_2 concentrations in the micro-chambers were consistent. Therefore, oxygen availability was not the limiting factor for OCR using higher concentration of CCCP. Accordingly, there may not be sufficient substrate for ETC to attain electrons to consume oxygen at higher rates anticipated with the use of higher CCCP concentrations. Alternatively, this may be due to toxicity of CCCP on mitochondria. Nevertheless, OCR measured by treating with higher CCCP concentrations than 2 µM do not accurately represent maximum respiratory capacity of the mitochondria. This suggests that 2 µM CCCP can maximize ETC in SM and maximum reserve respiration can be measured using this CCCP concentration. Similar to CCCP, optimum concentrations ADP and FCCP were measured for accurate maximum respiratory capacity for SM and NSM. In the experiments described in this dissertation, for 15 µg NSM, 2 µM CCCP was utilized and for 20 µg SM, 2.5 µM CCCP or 3µM FCCP was utilized for the mitochondrial bioenergetics assays.

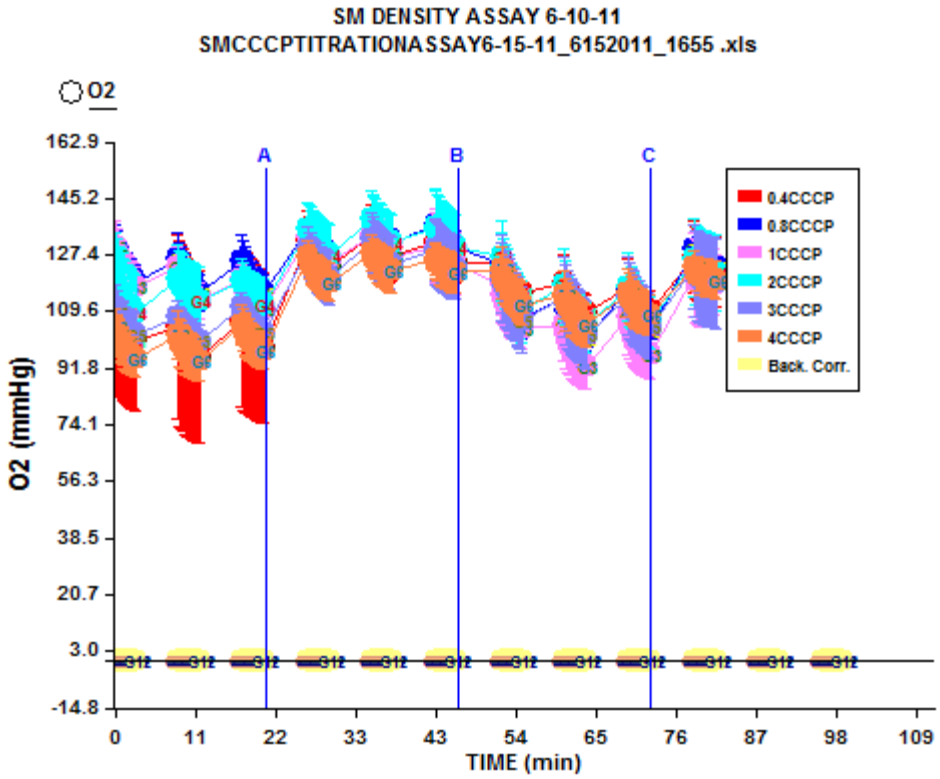

Figure 2.8 Representative oxygen concentrations of SM treated with 0.4, 0.8, 1, 2, 3, or 4 µM CCCP injected at Time B. SM were isolated from mouse whole brain using Percoll gradient and centrifugation. Isolated SM were quantified by Bradford protein assay. Ten µg SM were examined for oxygen concentration using Seahorse XF24 analyzer: injection port A: oligomycin, injection port B: ● indicates CCCP 0.4 µM, ● indicates CCCP 0.8 µM, ● indicates CCCP 1 µM, ● indicates CCCP 2 µM, ● indicates CCCP 3 µM, ● indicates CCCP 4 µM and injection port C: rotenone.

Substrates: Pyruvate/malate, HEPES, DMSO

In preliminary optimization studies, State III_u was small due to little OCR induction following CCCP in isolated mitochondria. This may be due to unhealthy mitochondria that were uncoupled before uncoupler treatment. Alternatively, this could be due to other factors such as substrate availability. To determine if this is the case, pyruvate and malate titrations were investigated on mitochondrial bioenergetics using various ratios of pyruvate/malate including 2.5 mM pyruvate / 1.25 mM malate, 5 mM pyruvate / 2.5 mM malate, 7.5 mM pyruvate / 3.75 malate and 10 mM pyruvate / 5 mM malate using the Seahorse XF analyzer.

As shown in **Figure 2.9**, basal and maximum respiratory capacities increased as a function of pyruvate/malate concentrations. NSM with no Pyruvate/Malate added group had 0 OCR when normalized to background. Basal OCR gradually increased as pyruvate and malate concentrations were increased. **Figure 2.10** represents linear relationship between basal respiration and pyruvate and malate substrate concentrations. NSM OCR following treatment with 2.5-7.5 mM pyruvate / 1.25-3.75 mM malate had similar basal respiration and were in the range of 100 to 200 pMoles per minute (Rogers et al., 2011). Five mM pyruvate / 2.5 mM malate generated the highest maximal respiratory capacity following FCCP treatment among all the different substrate concentrations, and this substrate concentration was utilized for subsequent studies. These results also confirm the presence of healthy mitochondria in our tissue preparations.

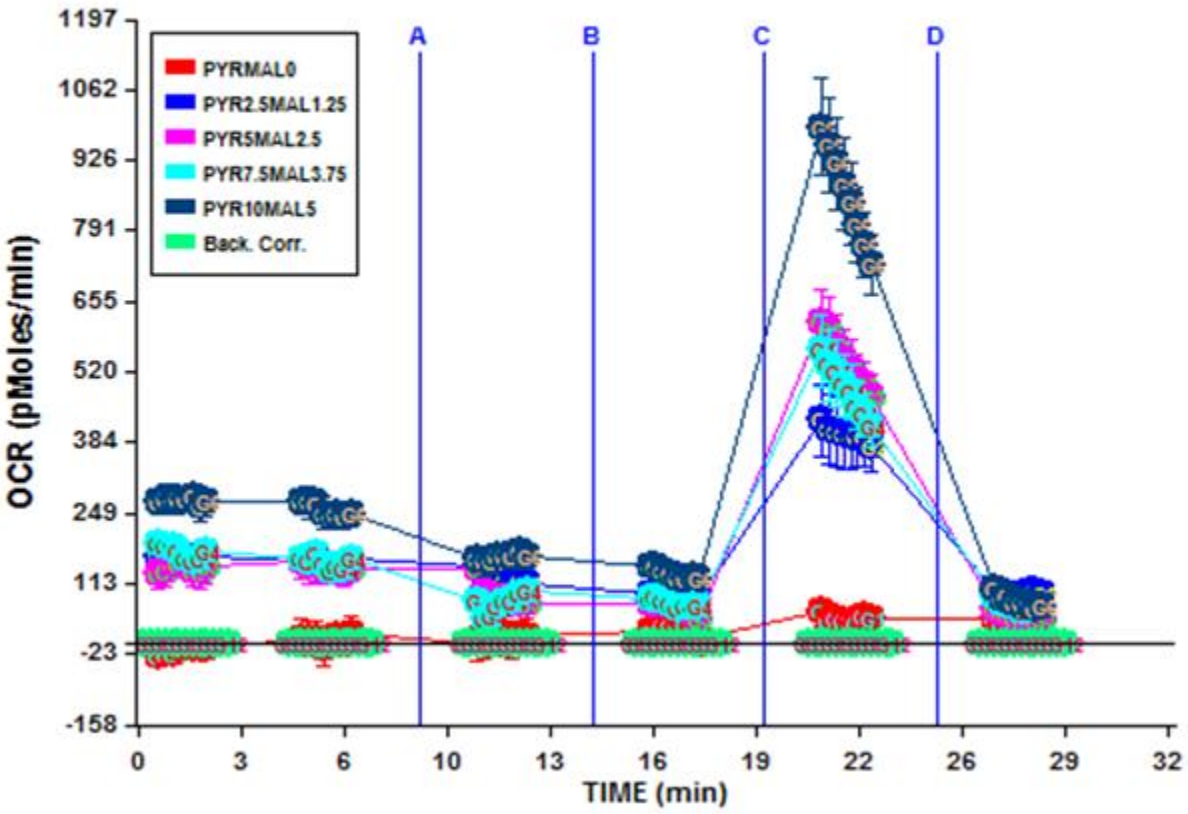

Figure 2.9 Representative respiration profiles of NSM following treatment with various concentrations of pyruvate and malate. NSM were isolated from mouse whole brain using Percoll gradient and centrifugation, and protein was quantified by BCA assay. OCR was measured using 5 µg NSM using Seahorse XF24 analyzer: injection Port A: ADP 500 µM, injection Port B: oligomycin 3 µM, injection Port C: FCCP 2µM and injection Port D: Antimycin A 4 µM. ● indicates pyurvate/malate 0 mM, ● indicates pyruvate 2.5 mM / malate 1.25 mM, ● indicates pyruvate 5 mM /malate 2.5 mM, ● indicates pyruvate 7.5 nM / malate 3.75 mM, ● indicates pyruvate 10 mM / malate 5 mM.

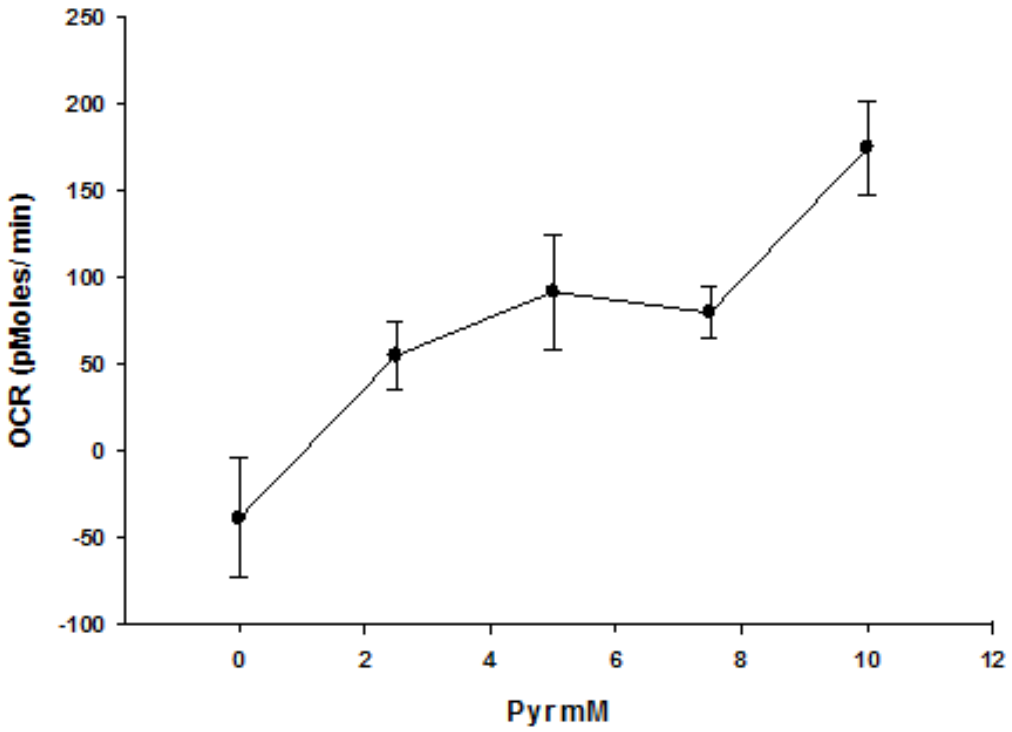

Figure 2.10 Correlation between basal respiration and pyruvate/malate substrate concentrations in NSM. Values represent the means ± 1 SEM of OCR of NSM treated with various concentrations of pyruvate/malate. (n = 3)

In the bioenergetics assay, pyruvate, malate and ADP are dissolved in 20 nM HEPES and oligomycin, CCCP, FCCP, rotenone and antimycin A are dissolved in DMSO. HEPES (4-(2-hydoxyethyl)piperazine-1-ethane-1-sulfonic acid) is a zwitterionic organic molecule with both positive and negative charges (**Figure 2.11**) that is widely used as buffer to maintain physiological pH, especially in the range of pH 6.0 to 8.5. This buffering effect may interfere with Seahorse XF analyzer probes measuring ECAR and pH in addition to interacting directing with CCCP and FCCP. Dimethyl sulfoxide (DMSO) is a polar aprotic solvent that is used to dissolve a wide range of both polar and non-polar organic compounds. Accordingly, DMSO can help mix non-polar organic compounds and water. DMSO does not have an acidic hydrogen center and can accept hydrogen bonds, and can easily be reduced and oxidize other compounds. Therefore, DMSO could interfere with the Seahorse XF analyzer probes, and can also be toxic to mitochondria by dissipating proton gradients in high concentrations. Therefore, effects of 20 mM HEPES and 0.1% DMSO on mitochondrial bioenergetics was investigated. The results showed that neither HEPES or DMSO altered bioenergetic OCR profiles in NSM (**Figure 2.12**).

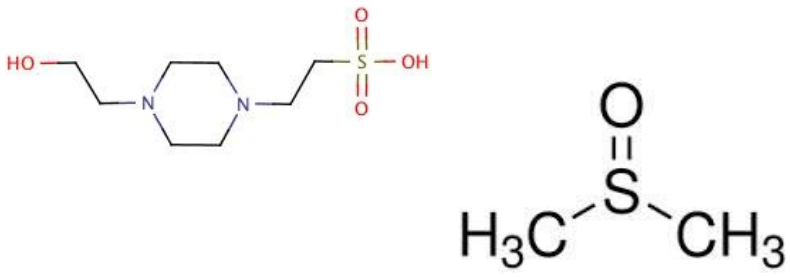

Figure 2.11 Chemical structures of 4-(2-hydoxyethyl)piperazine-1-ethane-1-sulfonic acid (HEPES) and dimethyl sulfoxide (DMSO) (Santa Cruz Biotechnology, 2007; Santa Cruz Biotechnology, 2007) Sigma-Aldrich, 2014)

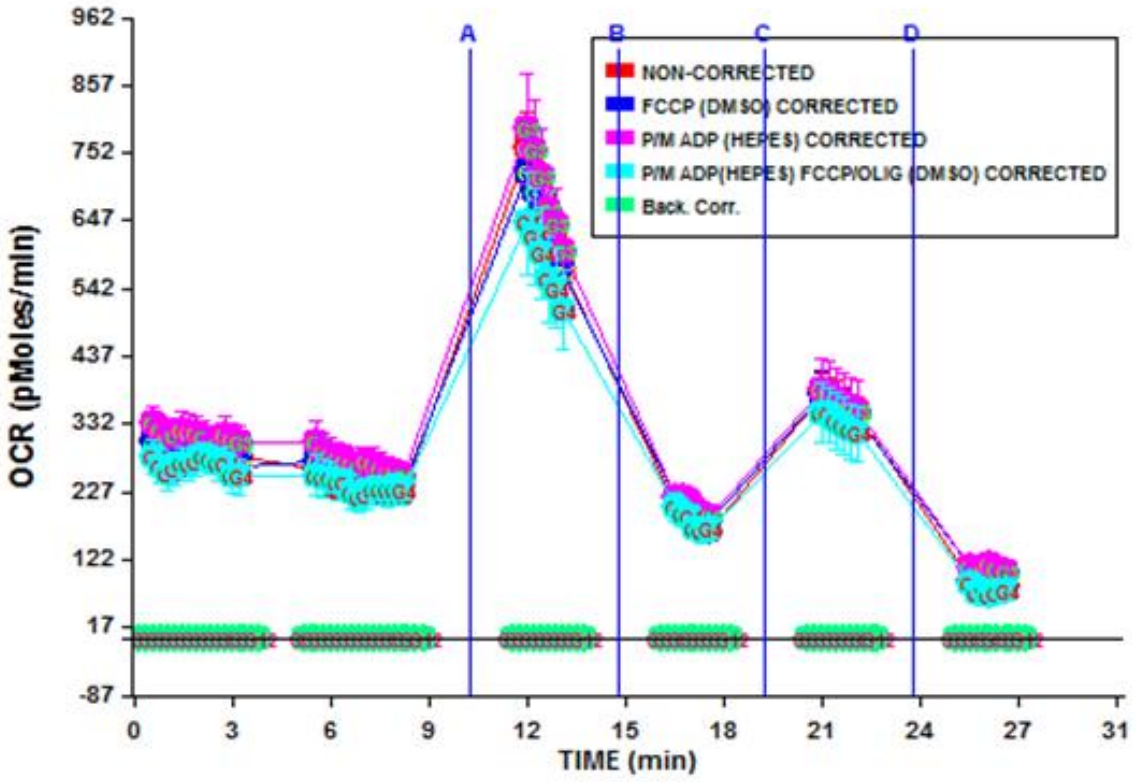

Figure 2.12 Representative OCR of NSM with HEPES/DMSO non-corrected, DMSO corrected, HEPES corrected, HEPES/DMSO corrected. NSM were isolated from mouse whole brain using Percoll gradient and centrifugation. Isolated NSM were quantified by BCA protein assay. 5 µg NSM were examined for oxygen concentration by using Seahorse XF24 analyzer: injection port A: ADP, injection port B: oligomycin, injection port C: ● indicates HEPES/DMSO non-corrected, ● indicates DMSO corrected, ● indicates HEPES corrected, ● HEPES/DMSO corrected, and injection port D: Antimycin A.

Flow cytometry

Twenty μg of isolated SM were added to 1 mL of staining buffer containing 200 nM MitoTracker™ Green (Invitrogen, cat. no. M-7514) or 500 nM tetramethylrhodamine ethyl ester perchlorate (TMRE, Sigma-Aldrich Cat. No. 87917) in KCl assay buffer (125 mM KCl, 20 mM HEPES, 4 mM $MgCl_2$ and 2 mM KH_2PO_4, pH 7.4) supplemented with 5 mM pyruvate / 2.5 mM malate and immediately incubated for 5 min at room temperature. Two μM FCCP was used as a positive control for mitochondrial depolarization. The fluorescent dyes in isolated SM were analyzed with FACS analyzer (BD Biosciences). The MitoTracker™ Green positive mitochondria were measured by FITC (at 488 to 520 nm) and TMRE positive mitochondria were measured by PE (at 488 to 575 nm). The FACS data were analyzed using the FlowJo (Tree Star, Ashland, OR) software.

Transmission electron microscopy (TEM)

Isolated synaptosomes were fixed in 2.5% glutaraldehyde and 2% paraformaldehyde in KCl mitochondria buffer (125 mM KCl, 20 mM HEPES, 4 mM $MgCl_2$, 2 mM KH_2PO_4, pH 7.4), for 1 h at RT. Samples were washed with 0.1 M sodium cacodylate buffer (pH 7.4). Samples were post fixed for 30 min with 1% OsO4 in ddH_2O, treated with 0.2% tannic acid in ddH_2O for 10 min, and washed in ddH_2O. After the last wash, samples were dehydrated in an acetone series, infiltrated and embedded in Spurr's resin, and cured at 65°C for approximately 48 h (Spurr, 1969). Samples were trimmed and sectioned into 85 nm thin sections (or to a silver-gold color), collected on copper grids, stained with 0.2% Reynold's lead citrate and 2% uranyl acetate, and imaged with a JEOL100 CXII transmission electron microscope (Reynolds, 1963). A rastering

pattern, an image is chosen in random pattern of strips such as sine wave, was used to image synaptosomes within a random grid opening and analysis of the images was completed

Confocal microscopy

Perfusion

Mice were anesthetized with ketamine:xylazine (26.6 mg/kg : 4 mg/kg; ip) and perfused with 0.09% saline followed by 4% paraformaldehyde via a transcardial approach. After successful fixation, mice were decapitated and the brains were removed. The whole brains were stored in 4% paraformaldehyde solution overnight and in 20% sucrose in 0.1 M phosphate buffer saline for an additional day.

Preparation of Brain Tissue and Immunohistochemistry

Brains in 20% sucrose were sectioned to 20 μm thick at -20°C using a cryostat. Sections of the MBH and ventral midbrain regions were obtained and immunohistochemistry was performed. The sections were washed with phosphate buffer (PB) followed by 0.05M TBS-TX (pH 7.4). The sections were blocked with 5% bovine serum albumin for 1 h and incubated with 1:500 COX IV (goat monoclonal), 1:2000 TH (rabbit monoclonal) in TBS-TX overnight. Sections were washed with PB-TX and incubated with secondary antibodies 1:500 Alexa Fluor 594 donkey anti-goat IgG (Invitrogen, A11058), 1:500 Alexa Fluor 350 donkey anti-rabbit IgG (Invitrogen, A10039) for 1 h in room temperature. After rinsing with PB, sections were mounted on glass slides with Prolong Gold antifade reagent.

Fluorescent confocal microscope analysis

COX-IV was measured using an Alexafluor 594 *filter* set at 575 to 675 nm, GFP-LC3 using a EGFP filter set at 500 to 545, and TH using a Alexafluor 405 filter set at 425 to

475nm using Olympus FluoView Rv1000 confocal microscope. The threshold was set by background as complete blue in Hi/low setting. TH was set as threshold depending on day of the image taken or due to tissue variance threshold was set depending on the images. Percent mitochondrial distribution in TH+ cells was calculated by dividing pixels colocalized with TH and Cox IV by pixels with TH, and represented as a percent value. The colocalization of mitochondria and TH+ neurons are analyzed using FV1000 ASW software. Mitochondria colocalized with autophagosomes in TH+ neurons were analyzed by Fiji coloc_2 with image J. Using image J, TH+ neurons were masked by converting TH+ fluorescent signal as 225 and background as 0, and only TH+ pixels were analyzed for colocalization by comparing Pearson Coefficients by Fiji Coloc_2 (Pompey et al., 2013). PSF was estimated using equation λ, where λ was 450 for Alexafluor 405, 522.5 for EGFP, and 625 for Alexafluor 594. NA is the numerical aperture of the objective (NA of water-immersion 40x objective = 1.30, NA of oil-immersion 60x = 1.42). A blinded experimenter collected images.

Stereotaxic surgery

Mice were anesthetized using ketamine: xylazine (133mg/kg: 20mg/kg; s.c.) and analgesics ketoprofen (5 mg/kg) and placed onto the stereotaxic frame by ear bars (Mice were pinched at plantar aspect of the feet to make sure they are fully anesthetized). The surgical site was thoroughly cleaned three times with alcohol and Betadine swab in circular pattern along the incision line. The skulls were exposed by the single incision of the tissue overlying the skull. The skulls were drilled about 2mm hole with Dremel drill and parkin-AAV (250 nl of 5.9×10^{12} vg/ml) was injected unilaterally or bilaterally depending on the experiments following coordinates from Bregma: rostro-caudal -3.7 mm, medio-lateral -1.4 mm or ± 1.4 mm, and

dorso-ventral -4.9 mm. Virus was injected two times using automated micropump with 50 nl/min rate via Hamilton syringe (Hamilton, Reno, NV) with a 30 gauge blunt-tip needle and needle was placed for additional 5 min to prevent reflux of the injected virus. The hole in the skull was filled with sterile bone wax and the skin closed by surgical staples. Mice were treated with a triple antibiotic ointment (Bacitracin 400 units, neomycin sulfate equivalent to 3.5 mg of neomycin base, polymyxin B sulfate 5000 units) and kept on heating pads during entire procedure till their awake and returned back to their cages. Analgesics ketoprofen 10 unit injected sc 24 h after the surgery and monitored every day for signs of infection or stress.

High performance liquid chromatography coupled with electrochemical detection (HPLC-EC) analysis

Frozen SM were thawed and sonicated with 3 one-sec bursts (Sonicator Cell Disruptor, Heat Systems-Ultrasonic, Plainview, NY, USA). The samples were centrifuged at 18,000 rpm for 5 min and the 50 µl supernatants were collected with addition of tissue buffer in a final volume of 65 µl. Level of DA and NE in the supernatants was measured by HPLC-EC (Lindley et al., 1990); detector potential set at -0.40 V and the mobile phase: 20 % methanol, pH of 2.64, beginning concentration of 0.020 % sodium octyl sulfate to optimal resolution. The DA and NE content in the ST- and MBH-derived SM were determined by comparison of peak height values (Hewlett Packard Integrator, Model 3395) with those of external standards. Quantification of the protein content of the pellet samples was attained using a BCA assay.

Western blot electrophoresis

The region of interest was dissected from the mice brain and sonicated in the tissue lysis

buffer (1% SDS, 0.1mM PMSF, 1mM DTT, protease inhibitor cocktail tablets (Roche Diagnostics, Mannheim, Germany) in TBS buffer, pH 7.4). The samples were centrifuged at 12,000g for 5 min and supernatants were collected. Based on BCA assay of the supernatants, 15 - 20 μg of samples were prepared for western blot by adding with loading buffer with 5% β-mercaptoethanol and boiled at 100°C for 5 min (Noble and Bailey, 2009). Equal amount of samples were run on 4-20% precast polyacrylamide gels (10% Bio-Rad, Hercules, CA, USA) for 90 V for 30 min, 130 V for 40 min and wet transfer at 70 V for 45 min in activated immobilon-FL PVDF membranes (Millipore, Billerica, MA). Membranes were dried for 1 hour and blocked with 50% Odyssey blocking buffer (ref) and incubated with primary antibody overnight or for 1-4 h at room temperature.

Primary antibodies were diluted in optimal concentrations as **Table 2.3** with BSA blocking buffer. Membranes are washed 4 times for 5 min with PBS-T (0.1 % Tween 20) and incubated with secondary antibodies for 1 h in the dark. The secondary antibodies, HRP-conjugated anti-rabbit (1:1000) or anti-mouse (1:3000) or anti-goat (1:3000; Cell Signaling) were diluted in concentrations following **Table 2.3** in BSA buffer. Membranes are washed for 4 times with PBS-T for 5 min in the dark and finally rinsed with PBS. The samples on the membranes were visualized and quantified by SuperSignal West Femto Chemiluminescent Substrate (Thermo Scientific, Rockford, IL) using Odyssey Fc Infrared Imaging system (Li-Cor, Lincoln, NE). In order to minimize variability due to experimental process, the samples were loaded in equal amount and normalized to GAPDH (G8795, 1:5000, Sigma).

Antibody	dilutions	source	company
Parkin	**1:1000**	**mouse**	**Millipore**
TH	**1:2000**	**rabbit**	**Millipore (Ab152)**
Cox IV	**1:200**	**goat**	**Santa cruz (sc-69359)**
GAPDH	**1:5000**	**mouse**	**Sigma (G8795)**
Rabbit HRP	**1:1000**	**goat**	**Cell signaling (7074)**
Mouse HRP	**1:3000**	**horse**	**Cell signaling (7076)**
Goat HRP	**1:3000**	**donkey**	**Santa cruz (sc-2020)**

Table 2.3 Description of the antibodies. Source, company, and dilution used for Western blot are described in table. TH: tyrosine hydroxylase, Cox IV: cytochrome c oxidase IV, GAPDH: Glyceraldehyde 3-phosphate dehydrogenase.

Statistics

One-way analysis of variance (ANOVA) tests were used to make statistical comparisons among two or more groups with single independent variable using SigmaPlot 12.0. Two way ANOVA equal variant test was performed to compare the samples with three or more independent variables and Tukey's and Holm-Sidak test were utilized for all pairwise multiple comparison tests. Multiple non-parametric groups were statistically analyzed by Kruskal Wallis multiple comparison test or converted to parametric value by equation ASIN(SQRT(% value/100)). For comparing the two parametric groups with equal variance, t-test was performed in two-tailed distribution. The statistical difference with probability of error 0.05 or less is considered statistically significant. A power analysis was performed using expected inter-group difference of 23 % for ANOVA and an α of 0.05. Sample size of 5 yields a power of 0.98 for the mitochondrial bioenergetics end points. Sample size of 3, flow cytometric analysis yields power of 1.00 with 20% group difference. Sample size of 4, TEM analysis yields power of 0.81 with 18% group difference. Investigators performing endpoint assays for flow cytometry, TEM, and confocal microscope were blinded to treatment group.

Chapter 3: Mitochondrial functional and structural differences in NSDA and TIDA neurons in WT mice

Introduction

PD is a progressive movement disorder associated with resting tremor, rigidity, and bradykinesia. PD is the second most common neurodegenerative disease, affecting more than a million people, with a prevalence of 13.4 per 100,000 people a year in the United States (Eeden et al., 2003). One hallmark pathological feature of PD is NSDA neuronal degeneration. In contrast, hypothalamic TIDA neurons are relatively unaffected in PD (Matzuk et al., 1985; Langston et al., 1978; Jellinger and Kurt, 1991; Braak and Braak, 2000). NSDA neurons, located in the SNpc of the ventral midbrain, terminate in the ST and modulate the function of the basal ganglia motor control circuit (Albin, 1989). TIDA neurons, located in the ARC, project to the median eminence of the MBH and regulate anterior pituitary prolactin secretion (Moore et al., 1987).

Mitochondrial dysfunction may play a role in determining NSDA neuronal susceptibility in PD. The differential susceptibility of TIDA and NSDA neurons in PD is also observed following exposure of mice to the mitochondrial toxin MPTP (Behrouz et al., 2007; Benskey et al., 2012). MPTP binds to mitochondrial Complex I (NADH dehydrogenase) and impairs the ETC resulting in depletion of ATP and increased oxidative stress (Sherer et al., 2002; Dawson and Dawson, 2003; Cleeter et al., 1992). There are decreases in mitochondrial Complex I activity in SN, platelets, and skeletal muscle of PD patients (Schapira et al., 1989; Mizuno et al., 1989; Krige et al., 1992; Bindoff et al., 1991). Systemic administration of the mitochondrial Complex I inhibitor, rotenone, causes NSDA neuronal degeneration in mice (Cannon, 2009). Mitochondrial

dysfunction is also involved in familial PD linked to mutations in parkin, PTEN-induced kinase I (PINKI), DJ-1, α-synuclein, and leucine-rich-repeat kinase 2 (LRRK2) (Dodson and Guo, 2007; Devi L, 2008; Albrecht, 2005).

It is plausible that differences in mitochondrial maintenance may play a role in susceptibility of TIDA and NSDA neurons to injury and degeneration. In this study, characteristics of mitochondria in synaptosomes, isolated from brain regions containing axon terminals of NSDA and TIDA neurons, were evaluated in WT mice. Synaptosomes derived from ST have diminished mitochondrial bioenergetics, mass, and membrane potential compared with those derived from the MBH. These deficits were associated with fewer mitochondria and mitophagosomes in TH immunoreactive neurons of the SNpc as compared with the ARC. These results suggest that differences in mitochondrial functional capacity play a role in differential susceptibility of NSDA versus TIDA neurons.

Results

Differential mitochondrial bioenergetics in synaptosomes from MBH and ST in WT mice

When mice are acutely treated with the mitochondrial Complex I inhibitor, MPTP, *in vivo*, TIDA neurons terminating in the ME recover within 24 h, whereas NSDA neurons projecting to the ST remain disrupted (Schapira et al., 1989). This pattern of response to MPTP reflects a differential susceptibility of these neurons to toxin-induced mitochondrial impairment. In this study, differential mitochondrial bioenergetics of synaptosomes derived from NSDA (ST) and TIDA (MBH) axon terminal regions in WT mice were measured. SM were isolated from ST and MBH of WT mice following the procedures described in **Chapter 2, Section 2.3** and mitochondrial bioenergetics, OCR and ECAR were measured using Seahorse XF24 analyze as

described in **Chapter 2, Section 2.4**. Mitochondrial respiration was investigated by measuring OCR of these synaptosomes. Basal respiration of ST- and MBH-derived SM was not statistically different (**Figure 3.1A**). Basal respiration of ST-derived SM was 177 ± 34 (pmoles/min) and basal respiration of MBH-derived synaptosomal mitochondria was 147 ± 33 (pmoles/min). However, maximum respiration, measured by changes in OCR following treatment with FCCP, in MBH-derived SM (915 ± 27 pmoles/min) was higher than in ST-derived SM (719 ± 31 pmoles/min). Moreover, spare respiration of MBH-derived SM was (749 ±57 pmoles/min) higher than ST-derived SM (540 ± 50 pmoles/min).

As one of the possible glycolysis markers ECAR was determined (Wu et al., 2006; Gohil et al., 2010). Basal ECAR was similar in ST-derived SM (5.2±0.7) and MBH-derived SM (7.0±1.0) (**Figure 3.1B**). When mitochondrial ETC was inhibited by rotenone, ECAR increased, but there was no difference between SM derived from these two brain regions. When the mitochondrial proton gradient was dissipated by FCCP, ECAR was further increased in both ST- and MBH-derived SM.

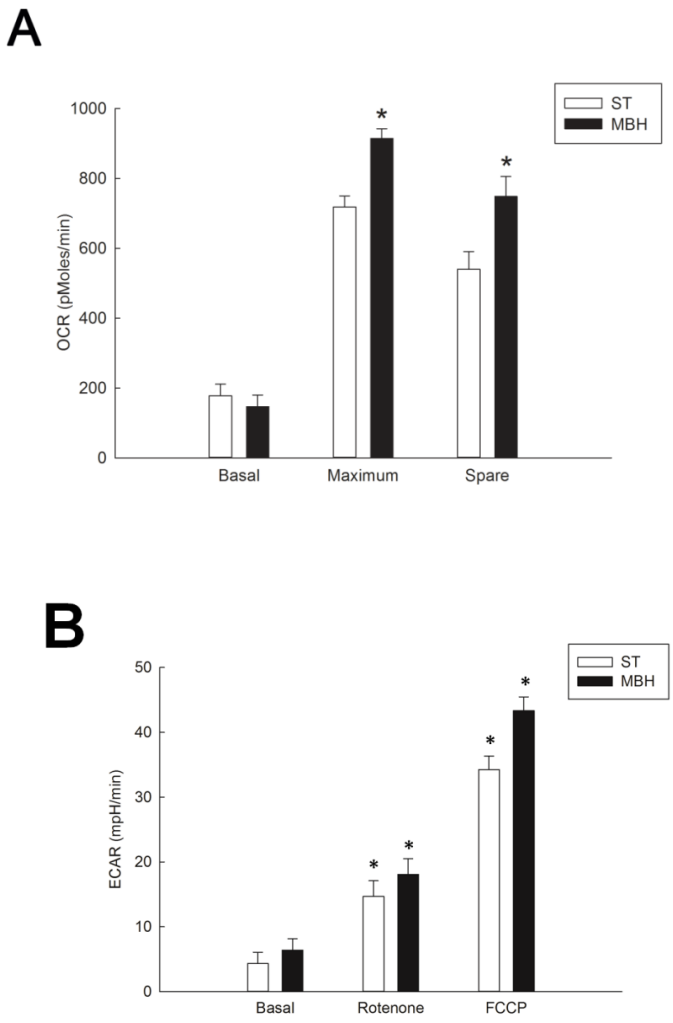

Figure 3.1. Comparison of ST- and MBH-derived SM bioenergetics in WT mice. Panel A, Oxygen consumption rate (OCR) of ST- and MBH-derived SM. Basal, maximum, and spare respirations were measured using a Seahorse XF24 analyzer. Panel B, Extracellular acidification rate (ECAR) of ST- and MBH-derived SM. ECAR of ST- and MBH-derived SM were measured in the presence of 5 mM pyruvate/2.5 mM malate, mitochondrial Complex I inhibitor (rotenone 2.5 µM), and uncoupler (FCCP 3 µM) using a Seahorse XF analyzer. In each assay, 20 µg of SM was used and the respiratory control ratio (RCR) was greater than 3. White columns represent OCR or ECAR of synaptosomal mitochondria from ST (n=5). Black columns represent OCR or ECAR of synaptosomal mitochondria from MBH (n=5). Error bars represent + 1 SEM. In Panel A, * indicates OCR of maximum and spare respirations in MBH are significantly different ($p < 0.05$) from those of ST. In Panel B, * indicates ECAR of FCCP and rotenone are significantly different ($p < 0.05$).

Flow cytometric analysis of SM from ST and MBH in WT mice

Flow cytometric analysis of ST- and MBH-derived SM in WT mice was performed to investigate the underlying reason for differential mitochondrial maximum and spare respiratory capacities between the ST and MBH. The mitochondrial mass in synaptosomes representing mitochondrial density in axon terminals was measured in synaptosomes (20 μg) from each brain region using MitoTracker Green. This fluorescent dye enters and labels mitochondria independent of membrane potential while another fluorescent dye, TMRE, enters mitochondria depending on membrane potential (Pendergrass, 2004). The synaptosomal population from both brain regions is comprised of synaptosomal structures that have similar size/volume (forward scatter) and inner complexity/granularity (side scatter) (**Figure 3.2A**). The histogram of FITC-A for MBH-derived SM showed a right shift of the green fluorescence relative to ST-derived SM (**Figure 3.2B**), suggesting greater mitochondrial mass in MBH-derived SM as compared with ST-derived SM in WT mice. Similar to Mitotracker Green, the histogram of PE-A for MBH-derived synaptosomes showed a right shift of the red fluorescence relative to ST-derived synaptosomes, suggesting greater mitochondrial membrane potential in MBH-derived SM as compared with ST-derived SM (**Figure 3.2C**). A 35 % increase in MitoTracker Green fluorescence and a 30 % increase in TMRE fluorescence were observed in synaptosomes derived from MBH, compared to synaptosomes derived from ST (**Figure 3.2D**).

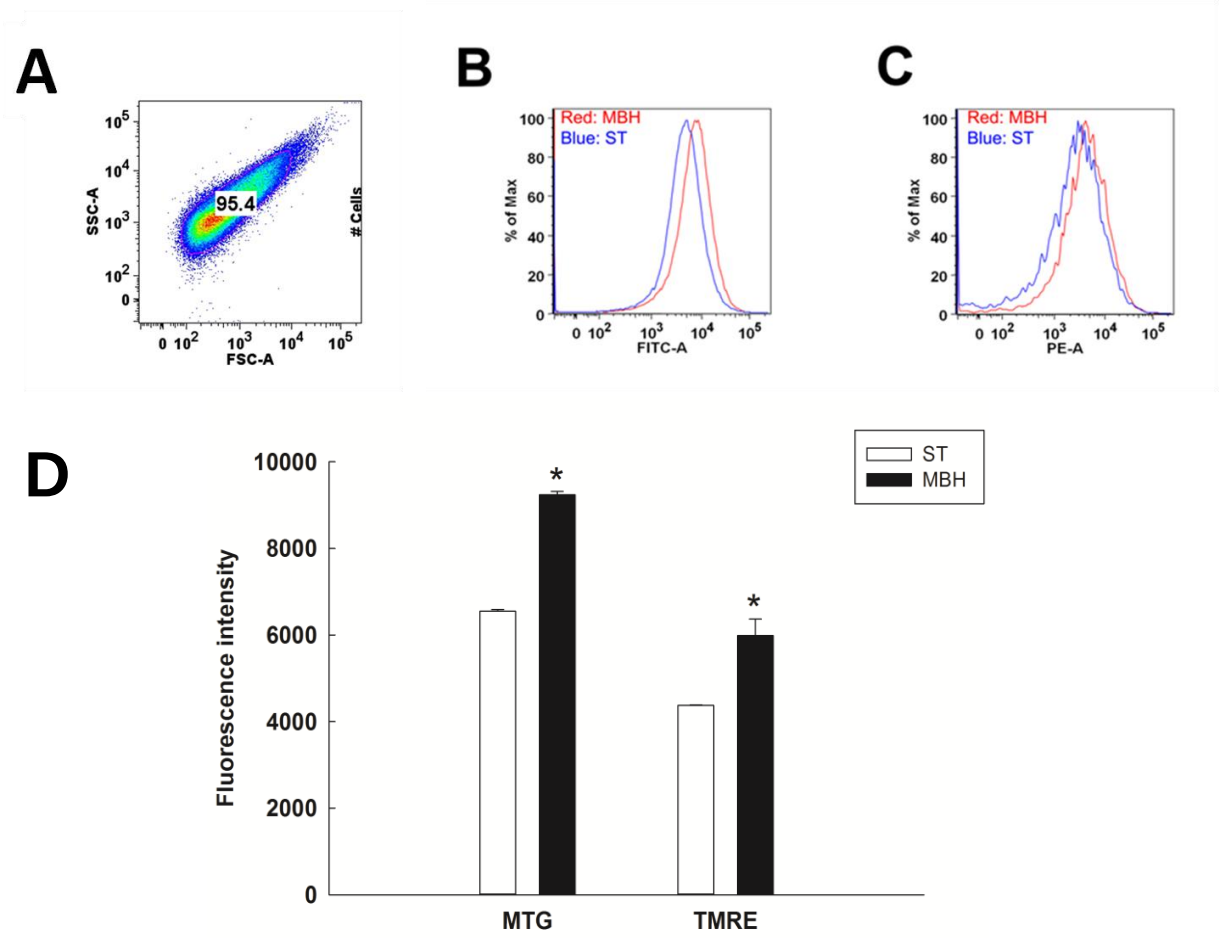

Figure 3.2. Flow cytometric comparison of ST- and MBH-derived SM mass and membrane potential in WT mice. Panel A, Scatter plot of synaptosomes by forward and side scatter. Forward scatter (FSC) indicates size and volume. Side scatter (SSC) indicates complexity and granularity. Panel B, Representative histogram of MitoTracker Green showing a right shift of the green fluorescence toward a higher mode of MitoTracker Green signal relative to the ST derived SM. Panel C, Representative histogram of TMRE showing a right shift toward a higher TMRE signaling in SM derived from MBH compare to those derived from ST. Panel D, Quantitative representation of MitoTracker Green and TMRE presence in ST- and MBH-derived SM. Flow cytometric assessment of SM mass and membrane potential were performed using fluorescent dye MitoTracker Green and TMRE. Twenty µg SM were examined for mitochondrial mass and membrane potential by flow cytometry. The error bar is +1 standard error of the mean. White columns represent ST-derived synaptosomes and black columns represent of MBH-derived synaptosomes in WT mice (n=3) and verticle lines + 1 SEM. * indicates mitochondrial mass or membrane potential of ST-derived SM that are significantly different ($p < 0.05$) from MBH-derived SM in WT mice.

HPLC analysis of DA in synaptosomes derived from the ST and MBH

HPLC-EC analysis measured DA concentrations in synaptosomes derived from both the ST (46 ±8 ng/mg) and MBH (7.1 ±1.1 ng/mg), whereas the secondary DA metabolite homovanillic acid (HVA) was not detected. Since generation of HVA is dependent on glia-derived enzymes, the lack of detectable HVA in the synaptosomes indicates little, if any, glial contamination in the preparations. The synaptosomes are derived from neurons, but not all synaptosomes are of DA neuronal origin exclusively. Mitochondrial flow cytometric sorting of the synaptosomes derived from ST of GFP-TH mice revealed about 20% of the synaptosomes contained GFP-TH. TH is the rate limiting step for DA synthesis and is a phenotypic marker for DA neurons.

Confocal analyses of mitochondrial in DA neurons from SNpc and ARC

Analysis of mitochondria colocalized with TH immunoreactive neurons *in situ* was performed using confocal microscopy. Coronal sections through the ventral midbrain and MBH were immunohistochemically stained for TH using frontal brain sections selected at -3.16 mm and -1.46 mm relative to Bregma for SNpc and ARC, contain the cell bodies of the TIDA and NSDA neurons, respectively (**Figures 3.3A and 3.3B**). TH was labeled with a secondary antibody linked to Alexafluor 405 and visualized as blue. Mitochondria were labeled with Cox IV and a secondary antibody linked to Alexafluor 594 and visualized as red.

Fluorescent intensities of TH and COX IV are represented in scatter plots (**Figures 3.4A and 3.4B**). The X axis represents fluorescent intensity of TH and the Y axis represents fluorescent intensity of COX IV. The lower left quadrant represents background below the threshold of TH and COX IV. The lower right quadrant represents TH immunoreactive neurons

without detectable mitochondria, whereas the upper left quadrant represents mitochondria colocalized with cells that are not immunoreactive to TH. The upper right quadrant represents mitochondria colocalized with TH immunoreactive neurons. The mitochondria were quantified and expressed as a percentage of total TH immunoreactive neurons. The fluorescent intensity of COX IV colocalized with TH immunoreactive neurons in ARC was higher than in SNpc. This was consistent with a higher density of mitochondria in TIDA neurons than in NSDA neurons (**Figure 3.4C**).

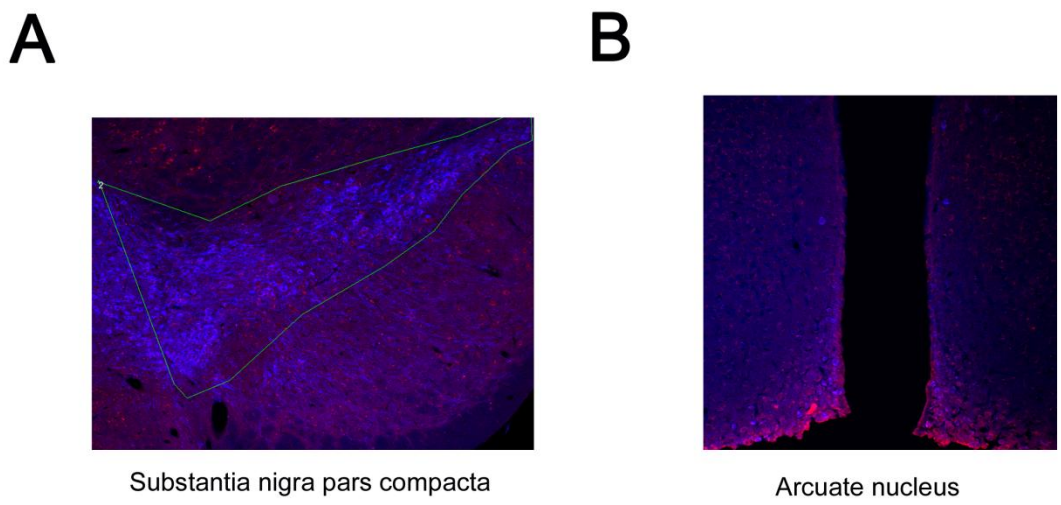

Figure 3.3. Comparison of mitochondrial content in DA neurons in SNpc and ARC. Confocal microscopic single plane focal image of SNpc (Panel A) and ARC (Panel B). GPF-LC3 mice were perfused with fixative and brains were isolated and cut into 20 µm slides for immunohistochemistry. Percent mitochondrial distribution in TH-immunoreactive neurons was performed in SNpc and ARC. SNpc regions were selected using region of interest (ROI) to avoid the ventral tegmental area. Blue staining represents TH neurons and red staining indicates COX IV staining of mitochondria.

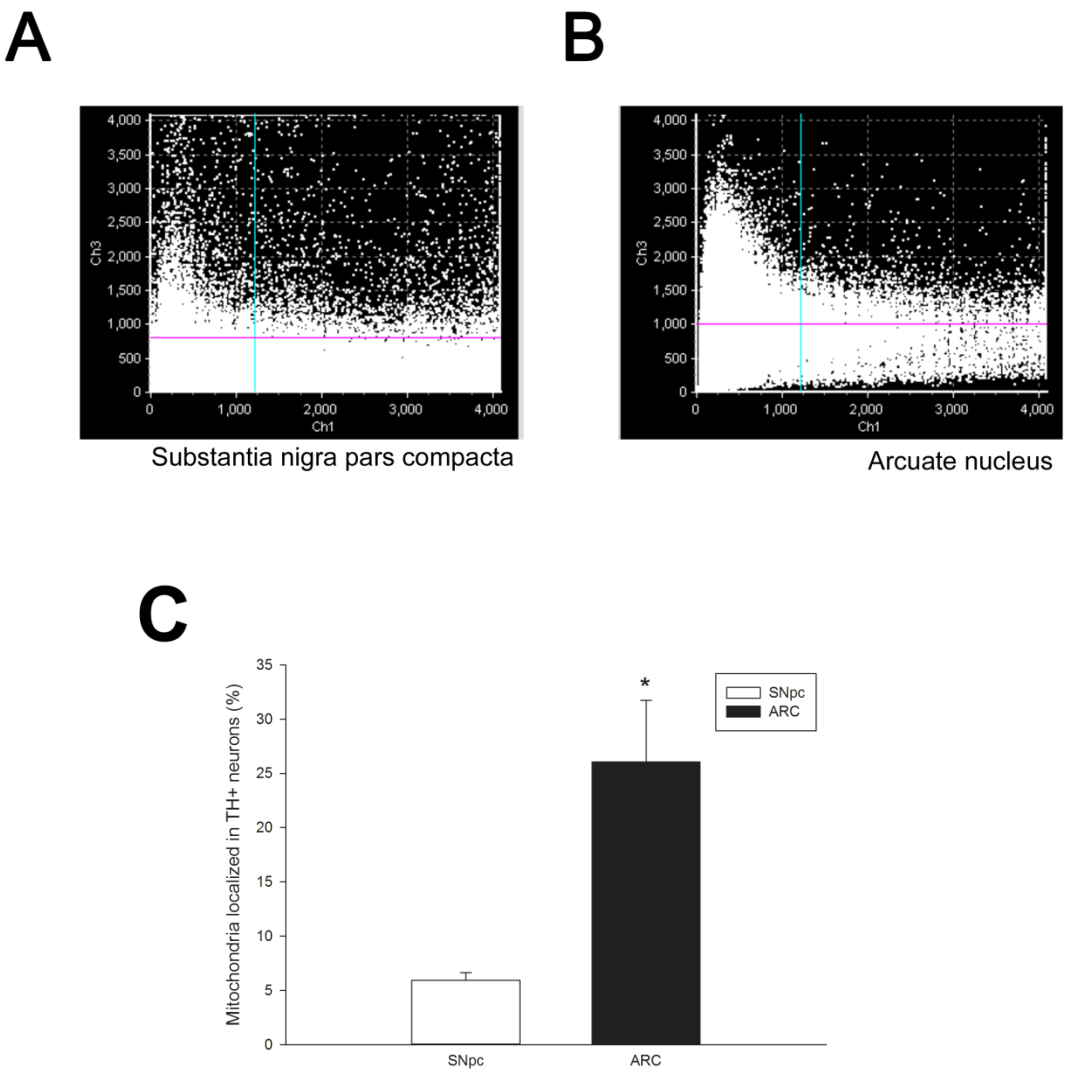

Figure 3.4. Scatter plot of TH and COX IV fluorescent intensity in SNpc and ARC. Panel A, SNpc, Panel B, ARC. Y axis indicates fluorescent intensity of COX IV and X axis indicates fluorescent intensity of TH. The upper quadrant indicates colocalized mitochondria in TH neurons, the lower left quadrant indicates the background, the lower right quadrant indicates population of TH neurons without mitochondria, and upper left quadrant indicates mitochondria in non-TH neurons. Panel C, Representative bar graph of COX IV colocalized with TH in SNpc and ARC. Mitochondria were quantified from the scatter plot upper right quadrant and the percent distribution of these mitochondria within TH neurons was measured. Percent values were converted to parametric value by ASIN(SQRT(% value/100)). The error bar is +1 standard error of the mean. * indicates mitochondrial colocalized with TH in SNpc is significantly different ($p < 0.05$) from in ARC.

Mitophagosome measurements in DA neurons from SNpc and ARC

Mitochondrial dynamic process maintains mitochondrial homeostasis by fusion, fission, and mitophagy. Damaged mitochondria are removed by autophagy (Green and Houten, 2011). Mitophagy, autophagy of mitochondria, was assessed by immunohistochemical colocalization of mitochondria with autophagosomes (mitophagosomes). In this study, mitophagosomes were measured in NSDA and TIDA neurons in SNpc and ARC, respectively, using GFP-LC3 mice. Microtubule-associated protein 1A/1B-light chain 3 (LC3) is an autophagic marker. Mitochondrial protein, COX IV and DA phenotypic marker, TH was immunohistochemically stained. TH immunoreactive neurons were visualized as blue (Alexafluor 405), mitochondria were visualized as red (Alexafluor 594), and autophagosomes were visualized as green punctate structures. GFP-LC3 is a cytosolic protein visualized as diffused green in the cells. When autophagy is activated, GFP-LC3 is a membrane-bound component of autophagosomes, forming green punctate structures (**Figure 3.5A SNpc** and **Figure 3.5B ARC**). The colocalization of COX IV and GFP punctate in TH immunoreactive neurons located in SNpc and ARC were compared using the Pearson Coefficient (PC), which ranges from 0 to 1. PC values represent how likely the two fluorescent signals colocalize with each other, with 1 representing the highest likelihood of colocalization. The PC was higher in ARC compared to SNpc, indicating mitochondria were more likely to colocalize with autophagosomes in TIDA neurons in ARC compared to NSDA neurons in SNpc (**Figure 3.5C**).

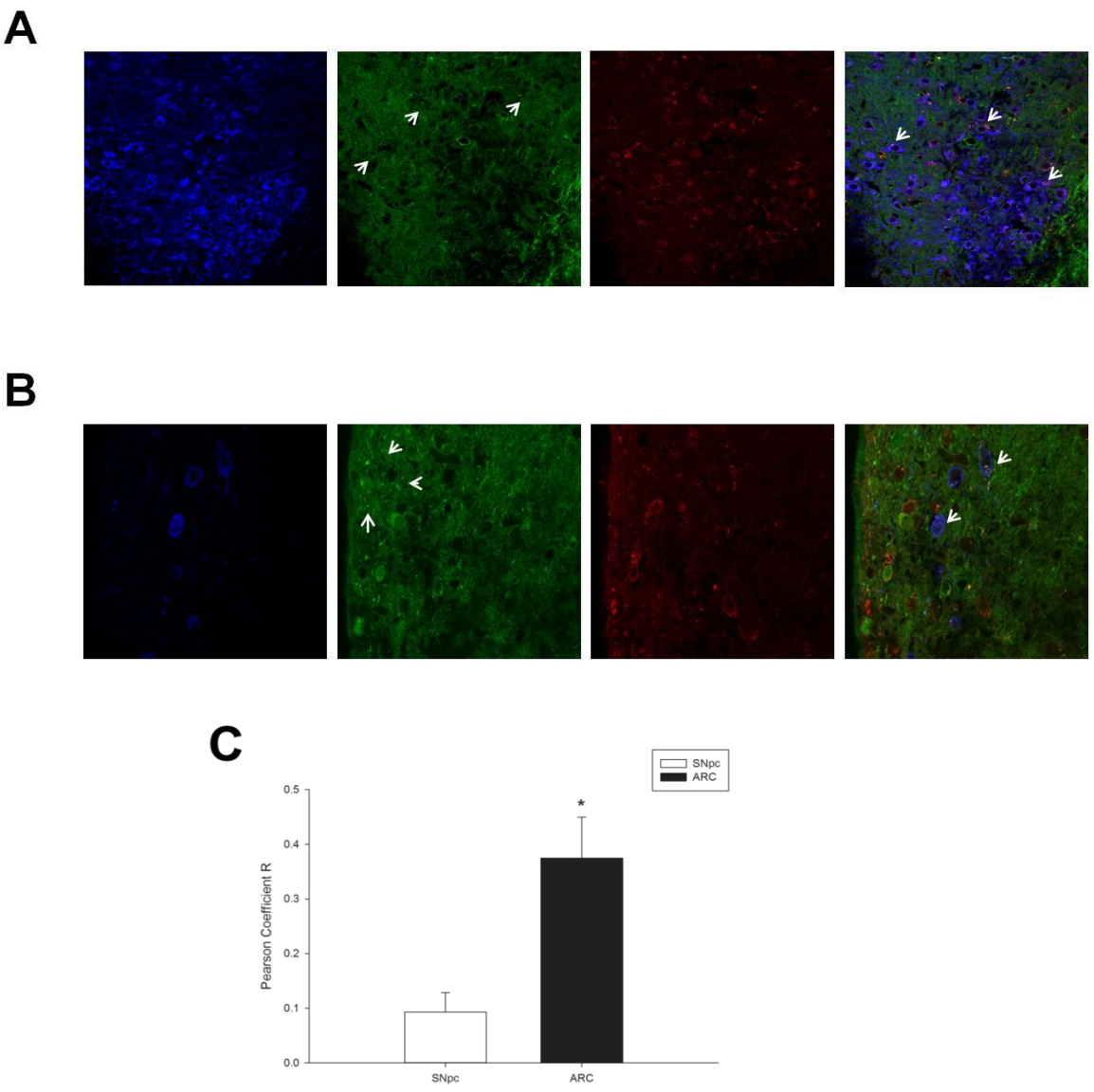

Figure 3.5. Comparison of mitochondrial colocalization with autophagosome in DA neurons in SNpc and ARC. Confocal microscopic single plane focal image of SNpc (Panel A) and ARC (Panel B). Blue represents TH immunoreactive neurons, autophagosomes were visualized as green punctuate structures (arrows) and red indicates Cox IV stained mitochondria. (Panel C) Pearson coefficient of mitochondrial colocalization with autophagosomes in TH immunoreactive cells in SNpc and ARC. Pearson coefficient values of colocalization between mitochondria and autophagosomes were measured using Fiji with image J software. Using image J, TH immunoreactive neurons were masked and pixels with TH immunoreactive neurons were analyzed for colocalization using Fiji Coloc_2. The error bar is +1 standard error of the mean. The statistical difference with probability of error 0.05 or less is considered statistically significant.

Transmission electron microscopy analysis of SM-derived from ST and MBH in WT mice

Bioenergetics, flow cytometric and confocal microscopic analysis represent overall quality and quantity of mitochondria in ST- and MBH-derived synaptosomes. To investigate the ultrastructural integrity of mitochondria, individual mitochondrial morphology was visualized by transmission electron microscopy. Visualized mitochondrial morphology was semi-quantified to evaluate mitochondrial function using Flameng grading (Sun et al., 2012; Flameng, 1980). The Flameng score evaluates mitochondrial function based on the morphology with an ordinal scale of 1 through 5; 1 represents mitochondria with disrupted membranes and broken cristae, 2 represents mitochondria with broken cristae but intact membranes, 3 represents swollen mitochondria with clear matrixes with intact cristae and membranes, 4 represents intact mitochondria, 5 represents intact mitochondria with granules (clusters of ions) (**Figure 3.6**).

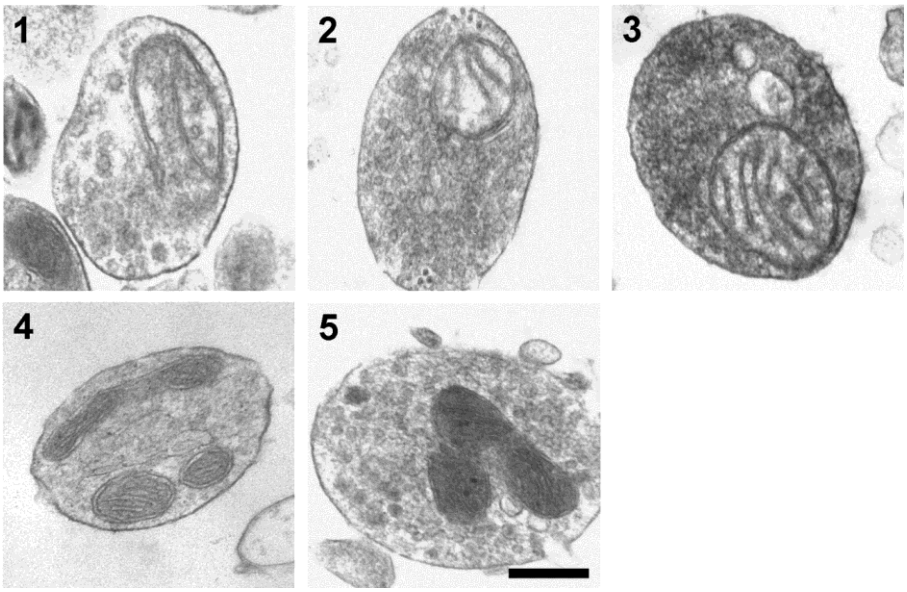

Figure 3.6. Description of transmission electron microscopy analysis of synaptosomes and Flameng mitochondrial functional score. Flameng score 1: broken cristae with ruptured mitochondrial membrane, 2: broken cristae with matrix clearing but membrane intact, 3: swelled mitochondria with cleared matrix but intact cristae and membrane, 4: intact mitochondria, 5: intact mitochondria with mitochondrial granules. (Scale bar = 50 µm)

The mitochondria found in ST-derived synaptosomes and MBH-derived synaptosomes had no difference in morphology. The distributions of mitochondrial functional based on Flameng grading were similar in ST- and MBH-derived synaptosomes. The average of the Flameng score of SM from ST was 3.46 ± 0.07 and MBH was 3.55 ± 0.08 (**Figure 3.7; Table 3.1**). However, fewer mitochondria per synaptosome were observed in ST compare to MBH (**Table 3.1**). ST-derived synaptosomes only contained 1.67 ± 0.11 mitochondria per synaptosome while MBH-derived synaptosomes contained 2.02 ± 0.10 mitochondria per synaptosome.

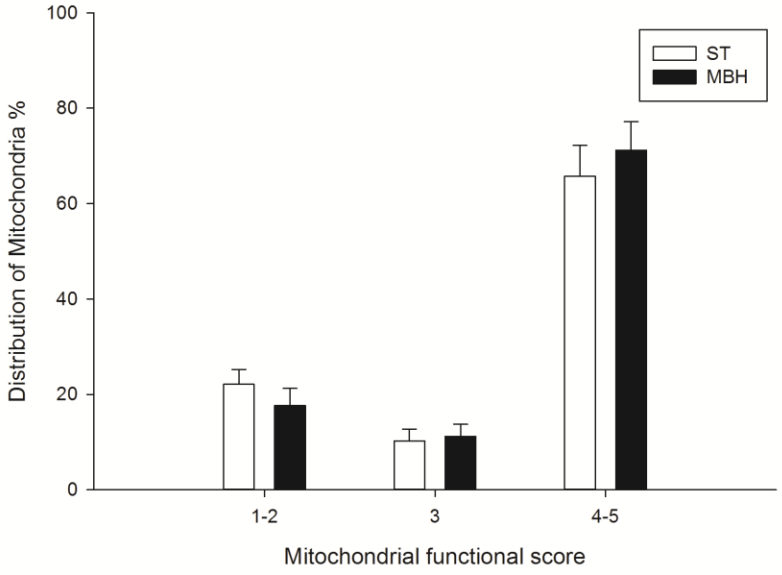

Figure 3.7. Representative bar graph of Fleming mitochondrial functional score of ST-derived SM vs MBH-derived SM. The synaptosomes were fixed, sectioned and at least 200 mitochondria from images were analyzed. Number of mitochondria with score ranged from 1-2 as a dysfunctional mitochondria, 3, and 4-5 as a functional mitochondria are divided by total number of mitochondria and represented as percent value. The graph represents distribution of the mitochondria from each group based on mitochondrial morphology. Statistical analysis was done converting percent value by ASIN(SQRT(% value/100)). White columns represent synaptosomal mitochondria from ST and black columns represent MBH (n=4) and verticle lines + 1 SEM.

	Mean Flameng score	Number of Mitochondria per synaptosomes
ST	3.46 ± 0.07	1.67± 0.11
MBH	3.55 ± 0.08	2.02 ± 0.10*

Table 3.1. Comparison of SM mean Flameng scores and mean number of mitochondrial per synaptosomes in the ST and MBH. Mean mitochondrial functional score was calculated by averaging Flameng mitochondrial functional score utilizing at least 200 mitochondria from each experimental group. Mean number of mitochondria per synaptosomes is derived by dividing total number of mitochondria by total number of synaptosomes in each experimental group. The experiment was repeated four times with $\pm$ 1 standard error of the mean. * indicates mean number of mitochondria per synaptosomes derived from MBH is significantly different ($p<0.05$) from those from ST.

Discussion

The results from this study provide evidence that regional differences in mitochondrial quality control may underlie impaired mitochondrial function. The data presented herein are consistent with the conclusion that differential mitochondrial characteristics may play a crucial role in central DA neurons. TIDA neurons appear to have increased aerobic mitochondrial respiratory capacity associated with increased mitochondrial mass, membrane potential, and mitophagosomes compared to NSDA neurons. Greater availability of mitochondria may play a neuroprotective role in TIDA neurons and explain resistance to toxicant exposure and degeneration in PD.

Characteristics of SM

Although *in vivo* studies offer an opportunity to assess mitochondrial function in an intact nervous system, the heterogeneity of brain tissue may constrain the interpretation of mitochondrial functional end-points. Brain tissue samples contain a variety of non-neuronal components including glial, endothelial, and immune cells, in addition to a variety of phenotypically distinct neuronal cell bodies and axon terminals. Alternatively, synaptosomes derived from brain tissue homogenates are enriched with neuronal axon components; 84 % of ST-derived synaptosomes are reported to be of neuronal origin while only 5-10 % are of glial origin (Wolf and Kaptos, 1989). During homogenization of the brain tissues, vesicles of axon terminal membranes are pinched off forming synaptosomes. They contain cytosolic organelles and key elements of pre-synaptic regulation for neurotransmitters' storage, release, re-uptake and metabolism, including voltage-gated ion channels and neurotransmitter autoreceptors.

In the present study, synaptosome preparations were found to contain DA, but not its metabolite homovanillic acid (HVA). Since HVA is exclusively generated by glial catechol-o-methyl transferase, absence of HVA is consistent with the conclusion that synaptosomes utilized in these experiments do not contain glia (Barrett, 2012). NSDA neurons originate in SNpc and provide major afferent input to ST. Therefore, NSDA neurons are major contributors to the synaptosomes derived from ST (Smith et al., 1994; Moss and Bolam, 2008; Lehéricy, 2012). ST-derived synaptosomes are predominately comprised of presynaptic NSDA axon terminals (Moss and Bolam, 2008). Accordingly, the parameters of mitochondrial function observed in the present study reflect, in large part, bioenergetics, mass, and membrane potential of mitochondria contained within DA axon terminals. Indices of mitochondrial function were obtained specifically in DA neurons *in situ* using confocal microscopy image analysis and the results are in agreement with data derived from the synaptosomes. This latter set of data provides further assurance that the changes observed in synaptosomes reflect changes in DA nerve terminals and that they are sufficiently robust to be apparent using different methods of analysis.

Distinct mitochondrial characteristics in ST and MBH

In the absence of metabolic stress, mitochondrial respiration and glycolysis are similar in ST and MBH in WT mice. However, maximum and spare respiratory capacities increased in MBH-derived synaptosomes as compared to ST-derived synaptosomes. Differences in mitochondrial bioenergetics indicate mitochondrial functions differ depending on brain regions. In previous studies, glucose utilization correlates with mitochondrial function in neurons and varied across brain regions (Shimoji, 2004). Mitochondrial bioenergetics and susceptibility to mitochondrial inhibition has also been shown to differ between brain regions (Brand and

Nicholls, 2011). In another study, mitochondrial function varied depending on level of neuronal activity (Kann and Kovács, 2007).

Increased mitochondrial mass and membrane potential may cause an increase in maximum and spare respiratory capacities in MBH (TIDA axon terminals) compared to ST (NSDA axon terminal). Confocal microscopic analysis revealed a corresponding higher mitochondrial density in ARC than in SNpc which is consistent with the increased mitochondrial mass observed in synaptosomes from MBH. Ultrastructural analysis also suggested a higher number of mitochondria per synaptosome in MBH compared to ST. Consistent with my observation, Liang et al. 2007 found mitochondrial mass in SNpc was also lower compared to ventral tegmental area DA neurons. Mitochondrial mass can vary between distinct DA neuronal subpopulations (Liang, 2007).

In addition to their higher density, mitochondria are also more likely to colocalize with autophagosomes in ARC compared to SNpc. However, transmission electron microscopic analysis revealed no difference in morphology of the mitochondria in synaptosomes derived from ST and MBH. An increased level of autophagosome may indicate an increase in autophagy or it may indicate low autophagic flux. In ARC, an increase in mitophagosomes could be due to the higher mitochondrial mass. However, the level of mitophagosomes may also be dependent on mitochondrial quality control. Mitochondrial quality control is mediated by autophagy of mitochondria, which is regulated by parkin. Differential parkin expression was observed in NSDA and TIDA neurons after a single acute exposure to MPTP (Benskey et al., 2013). Therefore, mitochondrial quality control was examined in axonal terminal regions of central DA neurons in the absence of parkin (**Chapter 5**).

Conclusion

Synaptosomes derived from MBH (containing TIDA axon terminals) were found to have greater mitochondrial mass and mitochondrial respiratory capacities compared to synaptosomes derived from ST (containing NSDA axon terminals). These region-specific differences in mitochondria may explain the differential susceptibility of distinct DA neuronal populations to mitochondrial neurotoxins and underscores the importance of mitochondrial quality control in NSDA neurons.

Chapter 4. Differential effects of Complex I inhibition on mitochondria in NSDA and TIDA neurons

Introduction

Six young adults from Santa Clara, California were hospitalized with sudden onset of PD in 1982. Langston and coworkers investigated the incidents and discovered the use of MPTP, which is a contamination of a synthetic opioid drug (Langston et al., 1983; Fahn et al., 1996). MPTP is a highly lipophilic compound that easily crosses the blood brain barrier and is converted to its metabolically active form MPP^+ by mitochondrial MAO B in glial cells. MPP+ is taken up into DA neurons DAT and binds to mitochondrial Complex I, interfering with the mitochondrial ETC (Sherer et al., 2002; Dawson and Dawson, 2003). Mitochondrial Complex I inhibition by MPTP has been observed in primate and mouse models (Nakamura et al., 1989; Mizuno et al., 1988). In addition to animal models, post-mortem analysis of the SNpc in PD patients revealed a reduction in mitochondrial Complex I and NADH cytochrome c reductase activities (Krige et al., 1992). Like MPTP, some pesticides used in farming are reported to have causal links to PD (Noyce et al., 2012). Rotenone is a pesticide that can cause PD (Tanner and Goldman, 1996). Exposure of rats to rotenone causes neuropathological features of PD including NSDA neuronal specific degeneration, α-synuclein accumulation, microglial activation, and movement disorders similar to parkinsonism (Cannon et al., 2009; Betarbet et al., 2006). Similar to MPTP, rotenone is a mitochondrial Complex I inhibitor causing mitochondrial dysfunction and generating ROS (Javitch et al., 1985). This implicates the importance of mitochondrial dysfunction in the etiology of PD.

Data presented in **Chapter 3** revealed higher maximum spare respiration and mitochondrial mass in the TIDA neuronal cell body and axonal terminal regions compared to those of NSDA neurons. Therefore, in this chapter, the differential mitochondrial responses to Complex I inhibitors will be examined. Mitochondria in NSDA and TIDA neuron axonal terminal regions showed concentration-dependent mitochondrial respiratory inhibition to rotenone in an *ex vivo* study. In addition, an MPP^+ *ex vivo* study revealed possible uncoupling of mitochondrial MPP^+ and cytosolic MPP^+ accumulation. Mitochondria in tyrosine hydroxylase (TH) immunoreactive cells from both ARC and SNpc are reduced at 24 h after MPTP treatment with no change in overall TH expression. However, neurons that express TH are recovered in ARC but are lost in SNpc. On the other hand, mitochondria in cells that do not express TH are lost in ARC, though there was no mitochondrial change in non-TH neurons in the SNpc. These results suggest that TIDA neurons are resistant to acute exposure to mitochondrial Complex I inhibitors in WT mice due to 1) sequestration of MPP^+ by non-DA cells; 2) different activity-dependent MPP^+ accumulation in cells; and/or 3) possible upregulation of mitochondrial quality control.

Results

Concentration response of mitochondria from TIDA and NSDA neuronal axonal terminal regions to rotenone

As discussed in **Chapter 3**, TIDA neurons are resistant to MPTP while NSDA neurons are susceptible, which may be due to differences in mitochondria in these different populations of DA neurons. Therefore, mitochondrial respiratory response to *ex vivo* rotenone treatment in SM in TIDA and NSDA axonal terminal regions was investigated. Synaptosomal mitochondria

were isolated from ST and MBH as described in **Chapter 2, Sections 2.3 & 2.4**. Using a Seahorse XF analyzer, the OCR in SM was determined after treatment with vehicle (SM ionic media) or 0.0125, 0.25, or 2 µM rotenone. SM derived from ST and MBH both responded similarly to rotenone. Mitochondrial basal respiration from both ST and MBH was inhibited in a similar concentration-dependent manner (**Figure 4.1 A**). Rotenone 0.0125, 0.25 and 2 µM inhibited mitochondrial basal respiration 23%, 67%, and 89%, respectively, in ST-derived SM. Rotenone 0.0125, 0.25 and 2 µM inhibited mitochondrial basal respiration 21%, 64%, and 73%, respectively in MBH-derived SM. Half maximal inhibitor concentration (IC50) was calculated using Microsoft excel add in software ED50 plus (v1.0) (Lockwood et al., 2012). Fifty percent of the basal respiration from ST-derived synaptosomes was 0.22 µM and 0.91 µM from MBH-derived synaptosomes (**Figure 4.1 B**). However, there was no statistically significant difference between ST and MBH.

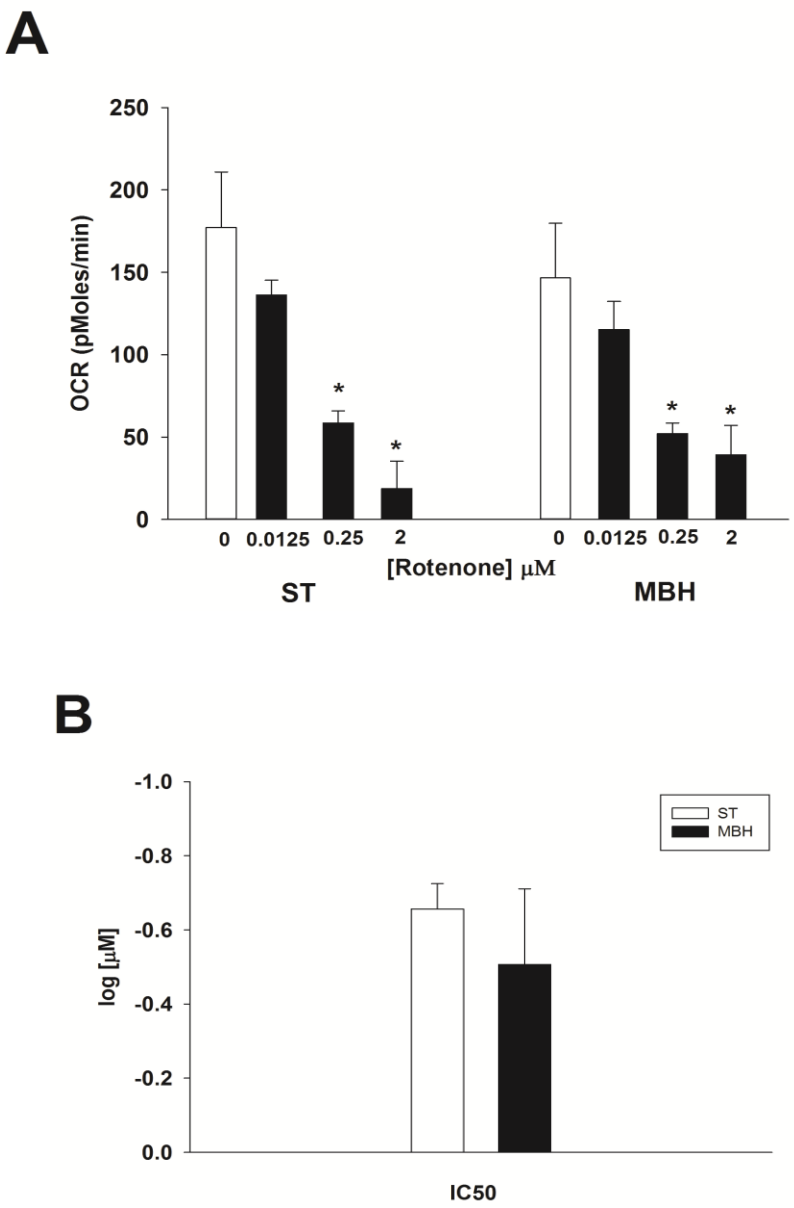

Figure 4.1 Comparison of concentration response of rotenone on SM <u>basal</u> respiration in the ST and MBH. Panel A, Representative bar graph of mitochondrial bioenergetics. Rotenone concentration dependent basal respiration inhibition measured using a Seahorse XF24 analyzer. Panel B, Representative bar graph of IC50 of rotenone. IC50 is expressed as a logarithmic value. ST and MBH were dissected in male C57B1/6J mice (n=4). Synaptosomes were isolated from the ST and MBH using Percoll gradients and centrifugation. Twenty µg of synaptosomes was examined. Basal respirations of SM from ST and MBH were measured after vehicle (SM ionic media) or rotenone (0.0125, 0.25, or 2 µM) treatment and OCR was measured using a Seahorse XF24 analyzer. The respiratory control ratio' (RCR') of SM was greater than 3. IC50 was calculated using software ED50 plus (v1.0) (Heikkila et al., 1985). The error bar is +1 standard error of the mean. * indicates values in rotenone-treated SM that were significantly different from vehicle-treated controls, $p < 0.05$.

Similar to basal respiration, maximum and spare respirations were inhibited by rotenone in a concentration-dependent manner (**Figure 4.2 A** and **4.3 A**). The difference between ST and MBH in maximal and spare respirations was not present with any concentration of rotenone. Rotenone at 0.0125 µM did not decrease maximal respiration, but 0.25 µM and 2 µM rotenone reduced maximal respiration by 85% and 96%, respectively, in ST-derived SM. In MBH-derived SM, rotenone 0.0125 µM, 0.25 µM, and 2 µM reduced maximal respiration by 19%, 87%, and 96%, respectively. Rotenone showed stronger inhibition in spare respiration; 2 µM rotenone reduced spare respiration by 98% in ST-derived SM and by 99.7% in MBH-derived SM. However, the IC50 of maximum respiration and spare respiration were similar. Fifty percent of the maximal respiration was inhibited by 0.11 µM rotenone for both synaptosomes from ST and MBH (**Figure 4.2 B**). Fifty percent of the spare respiration was inhibited by rotenone 0.093 µM and 0.096 µM for ST-derived and MBH-derived synaptosomes (**Figure 4.3 B**). There was no difference in the IC50 between maximal and spare respirations of SM from ST and MBH.

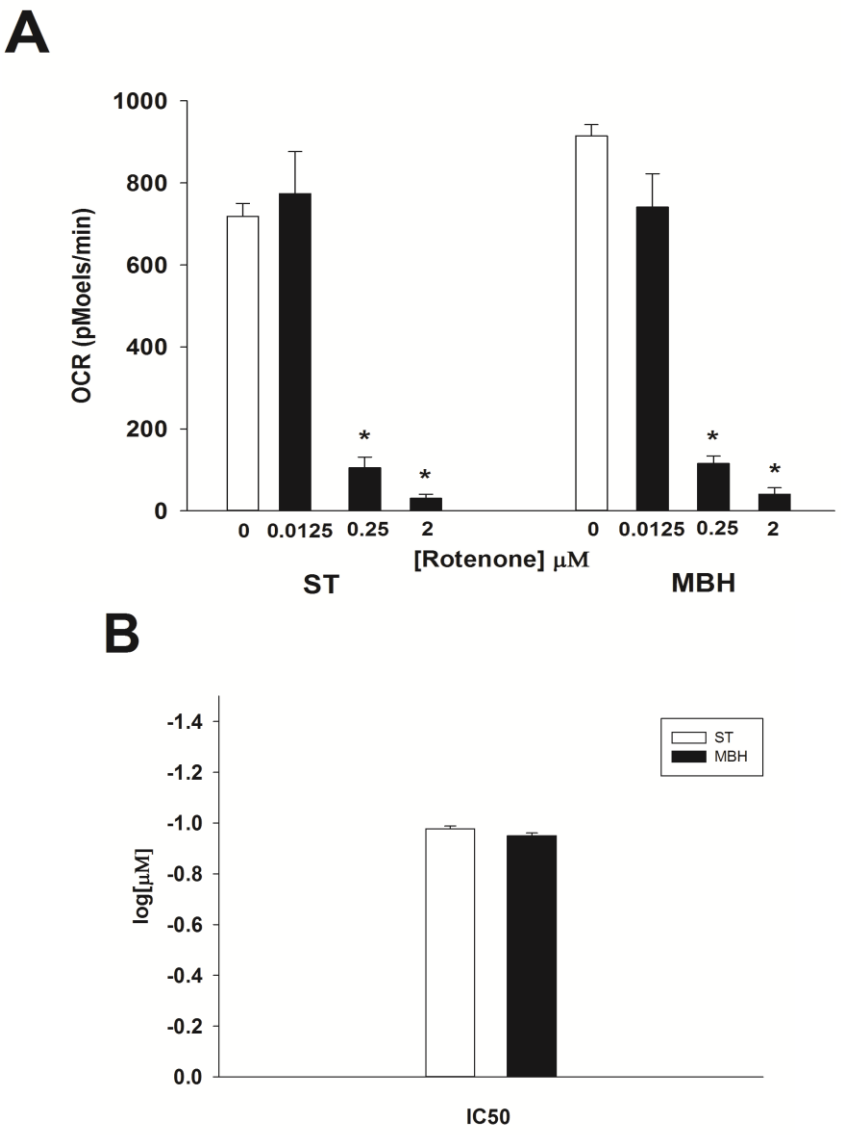

Figure 4.2 Comparison of concentration response of rotenone on SM <u>maximal</u> respiration in ST and MBH. Panel A, Representative bar graph of mitochondrial bioenergetics. Rotenone concentration-dependent maximal respiration inhibition measured using a Seahorse XF24 analyzer. Panel B, Representative bar graph of IC50 of rotenone. IC50 is expressed as a logarithmic value. ST and MBH were dissected in male C57B1/6J mice (n=4) and synaptosomes were isolated from the ST and MBH using Percoll gradients and centrifugation. Twenty µg synaptosomes were examined. Maximal respirations from ST and MBH were measured after vehicle (SM ionic media), or rotenone (0.0125, 0.25, or 2 µM) treatment and OCR was measured using a Seahorse XF24 analyzer. The respiratory control ratio' (RCR') of SM was greater than 3. IC50 was calculated using ED50 plus (v1.0) software (Heikkila et al., 1985). The error bar is +1 standard error of the mean. * indicates values in rotenone-treated SM that were significantly different from vehicle-treated controls, $p < 0.05$.

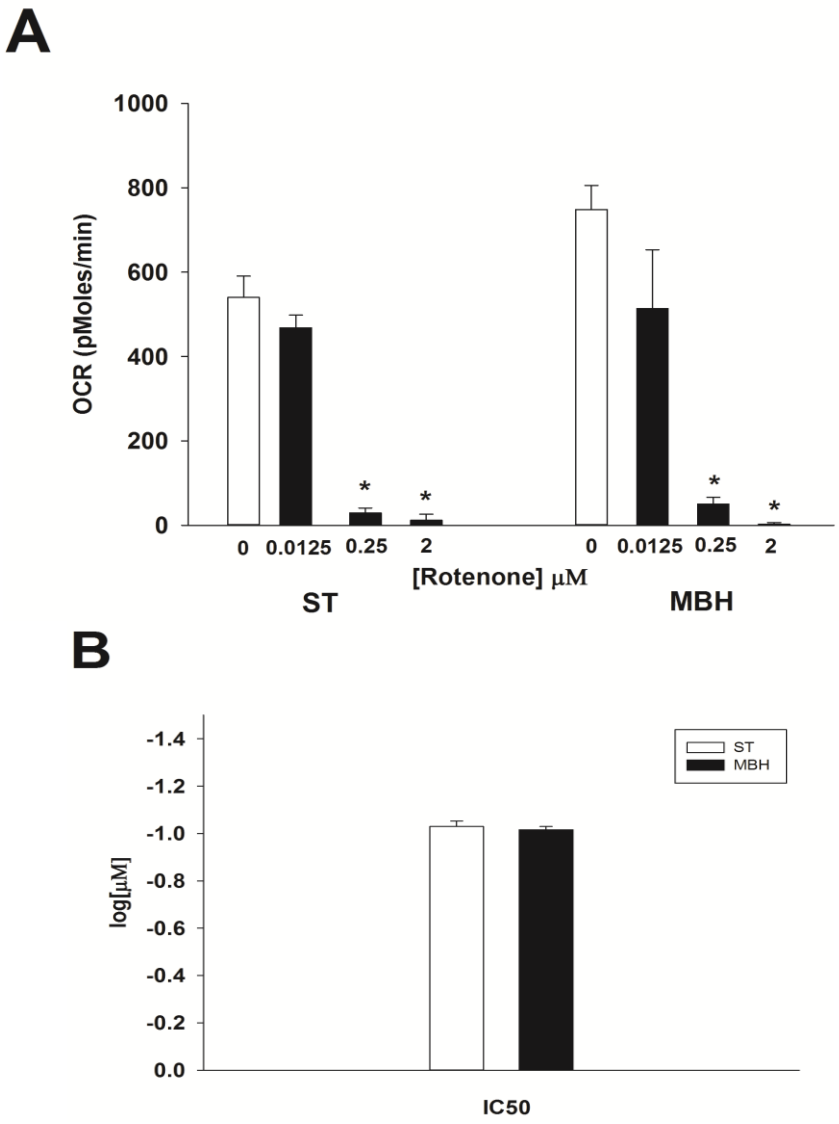

Figure 4.3 Comparison of concentration response of rotenone on SM <u>spare</u> respiration in ST and MBH. Panel A, Representative bar graph of mitochondrial bioenergetics. Rotenone concentration dependent spare respiration inhibition measured using a Seahorse XF24 analyzer. Panel B, Representative bar graph of IC50 of rotenone. IC50 is expressed as a logarithmic value. ST and MBH was dissected in male C57B1/6J mice (n=4) and synaptosomes were isolated from the ST and MBH using Percoll gradients and centrifugation. Twenty µg synaptosomes were examined. Spare respiration of SM from ST and MBH were measured after vehicle (SM ionic media) or rotenone (0.0125, 0.25, or 2 µM) treatment and OCR was measured using a Seahorse XF24 analyzer. The respiratory control ratio' (RCR') of SM was greater than 3. IC50 was calculated using ED50 plus (v1.0) software (Heikkila et al., 1985). The error bar is +1 standard error of the mean. * indicates values in rotenone-treated SM that were significantly different from vehicle treated controls, $p < 0.05$.

Ex vivo effect of MPP^+ on ST-derived SM

Like rotenone, MPTP can cause parkinsonian symptoms in humans. MPTP is converted to a bioactive form, MPP^+ by glial cells. Because synaptosomal *in vitro* preparations lack glial cells necessary to convert MPTP to MPP^+, the concentration response of SM derived from ST to 1, 5, 10, 50, and 100 µM MPP^+ was investigated (**Figure 4.4**). Although, a concentration-dependent inhibition of ST-derived SM maximal respiration by MPP^+ was observed, the differences were not statistically significant.

To test whether MPP^+ is able to inhibit mitochondrial function, mitochondrial respiratory capacities were measured following exposure to 1 mM MPP^+ concentration (**Table 4.1**). Basal and maximum respirations in ST-derived synaptosomes after MPP^+ treatment differ from vehicle treatment by 66.5% and 34.5%, respectively. Spare respiratory capacity was reduced 30% by MPP^+, however, the difference was not statistically significant.

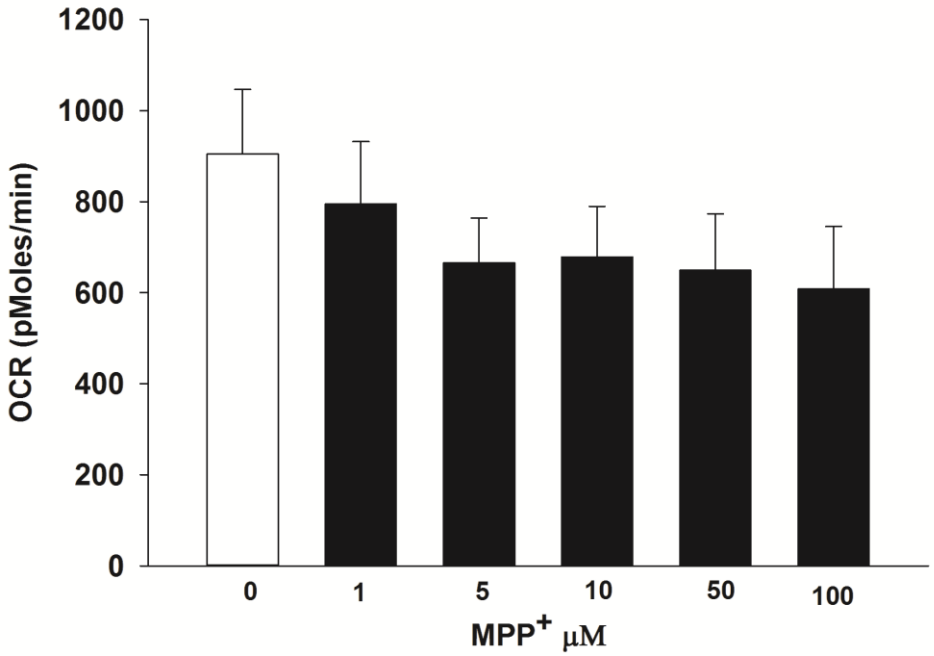

Figure 4.4 Concentration response of MPP^+ on maximum respiration of ST-derived SM. ST was dissected in male C57B1/6J mice (n=4) and synaptosomes were isolated from the ST using Percoll gradient and centrifugation. Fifteen to twenty µg synaptosomes were examined for OCR using a Seahorse XF24 analyzer. Synaptosomes were treated with either vehicle (SM ionic media), or MPP^+ 1, 5, 10, 50, or 100 µM and maximum respiration was measured. The respiratory control ratio' (RCR') of SM was greater than 3. The error bar is +1 standard error of the mean.

	Vehicle	1 mM MPP^+	Inhibition (%)
Basal respiration	163 ± 18.3	50.8 ± 5.63*	33.5 ± 5.59*
Maximum respiration	983 ± 111	627± 94.7*	65.5 ± 8.66*
Spare respiration	865 ± 109	583 ± 92.2	70.0 ± 10.7

Table 4.1 Effects of MPP^+ on basal, maximum, and spare respirations in SM derived from the ST. Basal, maximum, and spare respirations of ST-derived SM were measured after 1 mM MPP^+ or vehicle using a Seahorse XF24 analyzer. ST was dissected from male C57B1/6J mice (n=6) and synaptosomes were isolated from the ST using Percoll gradient and centrifugation. Isolated synaptosomes were quantified by BCA protein assay. Fifteen µg synaptosomes were examined for OCR using a Seahorse XF24 analyzer. The respiratory control ratio' (RCR') of SM was greater than 3. The error bar is ±1 standard error of the mean. * indicates values in MPP^+-treated SM that were significantly different from vehicle-treated controls, $p < 0.05$.

MPP^+ is transported specifically into DA neurons by DAT (Javitch et al., 1985; Heikkila et al., 1985; Sanchez-Ramos et al., 1986). To investigate the effect of DAT uptake on MPP^+ inhibition in synaptosomes derived from ST, the DAT inhibitor GBR12909 was utilized. GBR12909 is 1-(2-(bis (4-fluorophenyl)-methoxy)-ethyl)-4-(3-phenylpropyl) piperazine, a derivative of diphenyl-substituted piperazine (Van der Zee et al., 1980). GBR12909 selectively inhibits synaptosomal DA uptake by DAT with $K_I = 1$ nM. Mitochondrial respiration of synaptosomes derived from ST was determined in four independent treatment groups 1) vehicle, 2) MPP^+ 1 mM, 3) 50 nM GBR12909, and 4) MPP^+ 1 mM and 50 nM GBR12909. MPP^+ 1mM treatment reduced mitochondrial respiration independent of the presence of GBR12909. MPP^+ 1mM treatment reduced basal respiration by 66% and MPP^+ 1mM with GBR12909 reduced basal respiration by 80%. There was no statistically significant difference in basal respiration between the GBR12909 treated and non-treated groups.

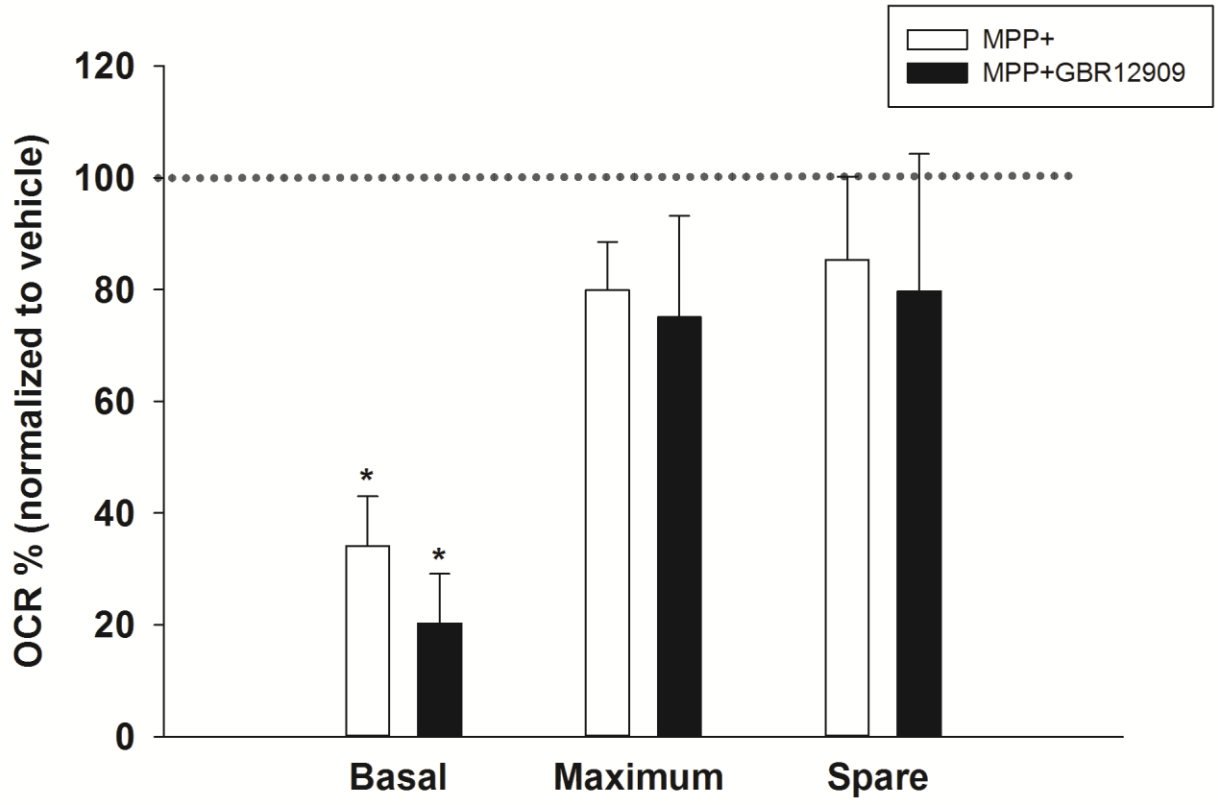

Figure 4.5 Lack of an effect of GBR12909 on mitochondrial inhibition by MPP^+ 1 mM in SM derived from striatum. After incubation of ST-derived SM with 50 nM GBR12909, basal, maximum, and spare respirations of SM from ST with MPP^+ 1 mM or vehicle were measured using a Seahorse XF24 analyzer. Control (100% values) indicates OCR of the vehicle-treated SM. Basal, maximum, and spare respirations of MPP^+ and MPP^+ with GBR12909-treated synaptosomal mitochondria were calculated by dividing each OCR measurement by that of vehicle-treated synaptosomes with conversion to %. ST was dissected from male C57Bl/6J mice (n=3) and synaptosomes were isolated from the ST using Percoll gradients and centrifugation. Isolated SM were quantified by BCA protein assay. Fifteen µg SM were examined for OCR by using a Seahorse XF24 analyzer. The respiratory control ratio' (RCR') of SM was greater than 3. The error bar is +1 standard error of the mean. * indicates values in MPP^+-treated SM that were significantly different from vehicle-treated controls, $p < 0.05$.

Effect of MPTP on mitochondria in NSDA and TIDA neuronal cell bodies

Mitochondria in axonal terminal regions of NSDA and TIDA neurons did not differ in response to mitochondrial Complex I inhibitor, rotenone. Moreover, MPP^+ failed to inhibit more than 50% of the mitochondrial maximum and spare respiratory capacities in an *ex vivo* study. Therefore, the effect of MPTP on mitochondria in NSDA and TIDA neurons *in vivo* was investigated using immunohistochemistry and confocal microscopy using the procedures described in **Chapter 2, Section 2.7**. SNpc at Bregma -3.16 and ARC at Bregma -1.46 were visualized by confocal microscopy at 10x and 20x magnification respectively and these images were utilized to determine TH immunoreactive cell counts (**Figure 4.6 A and B**). DA neurons are visualized by TH as blue fluorescence, and mitochondria are visualized by cytochrome C oxidase subunit IV (COX IV) as red punctuate fluorescence in confocal magnification of 20x for SNpc and 40x for ARC (**Figure 4.6 C and D**).

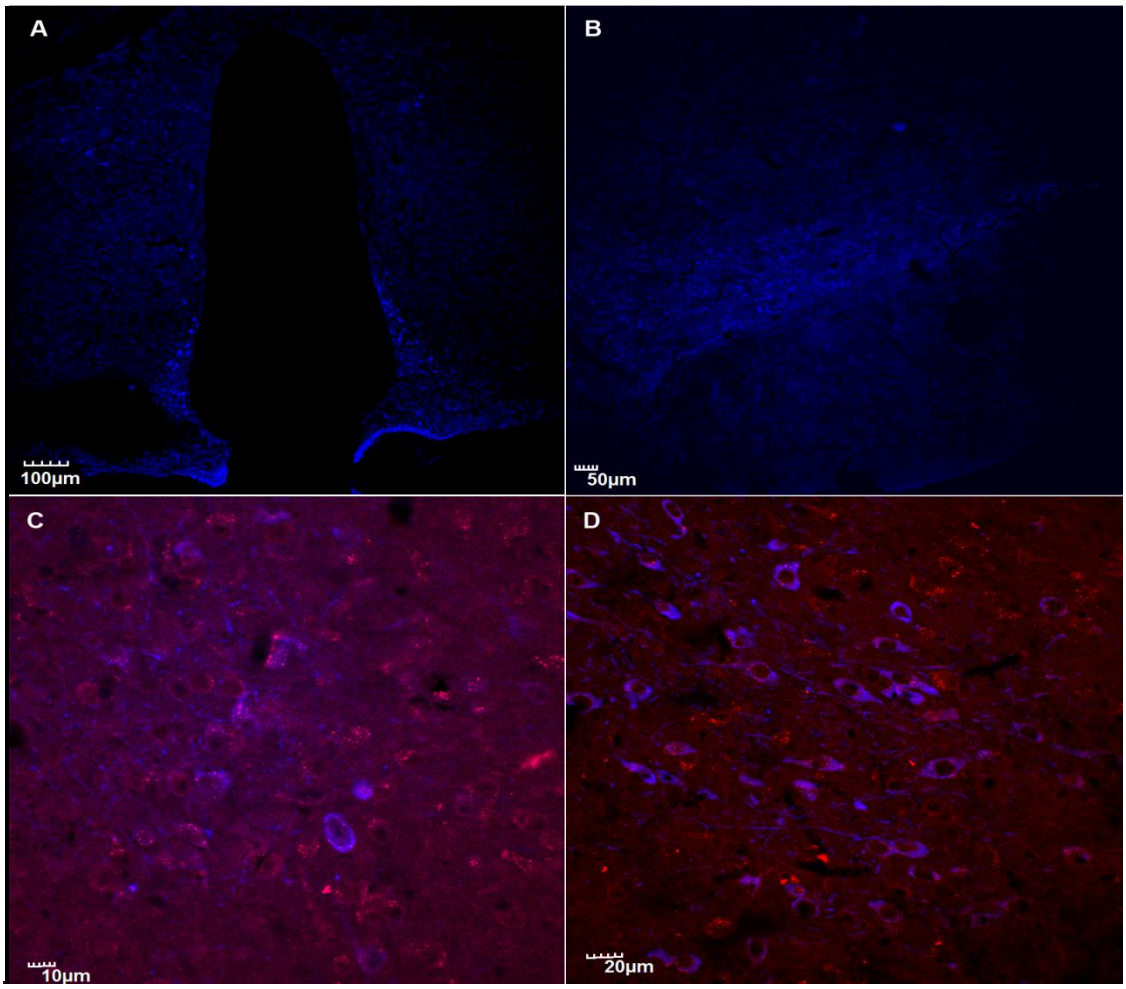

Figure 4.6 Confocal microscopic single plane focal images of ARC and SNpc. Mitochondria colocalized with TH immunoreactive neurons in ARC and SNpc. Mice were treated with MPTP for 4 h or 24 h, or with saline for 4 h, and then rapidly perfused and fixed. Brains were isolated and cut into 20 µm coronal sections for immunohistochemistry. The confocal images were attained from the sections that contain SNpc at Bregma -3.16 and ARC at Bregma -1.46. TH immunoreactivity is visualized as blue and represents DA neuronal cell bodies. Immunoreactivity to COX IV is visualized as red and represents mitochondria. **Panel A** is the confocal image of ARC at 20x and **Panel B** is the confocal image of SNPC at 10x. **Panel C** shows colocalization of mitochondria with TH immunoreactive neurons in ARC at 40x and **Panel D** shows the colocalization of mitochondria with TH immunoreactive neurons in SNpc at 20x.

Mice were exposed to 20 mg/kg MPTP for 4 h or 24 h, or saline (10 ml/kg) for 4 h. Mitochondria in TH immunoreactive cells were investigated. COX IV colocalization with TH was measured using scatter plots as shown in **Chapter 3**. Mitochondria in TH immunoreactive cells in both SNpc and ARC are reduced at 24 h compared to the vehicle (**Figure 4.7**). MPTP reduced mitochondria protein by 20% in SNpc and 17% in ARC.

The MPTP effect on mitochondria in cells that are not immunoreactive to TH was determined in ARC and SNpc. Mitochondria in non-TH immunoreactive cells of SNpc did not differ between MPTP- and vehicle-treated mice (**Figure 4.8**). However, mitochondria in non-TH immunoreactive cells of ARC were reduced at 24 h following exposure to MPTP. Similar to mitochondria in TH-immunoreactive cells, MPTP treatment reduced mitochondria by 20% at 24 h in non-TH immunoreactive cells from ARC.

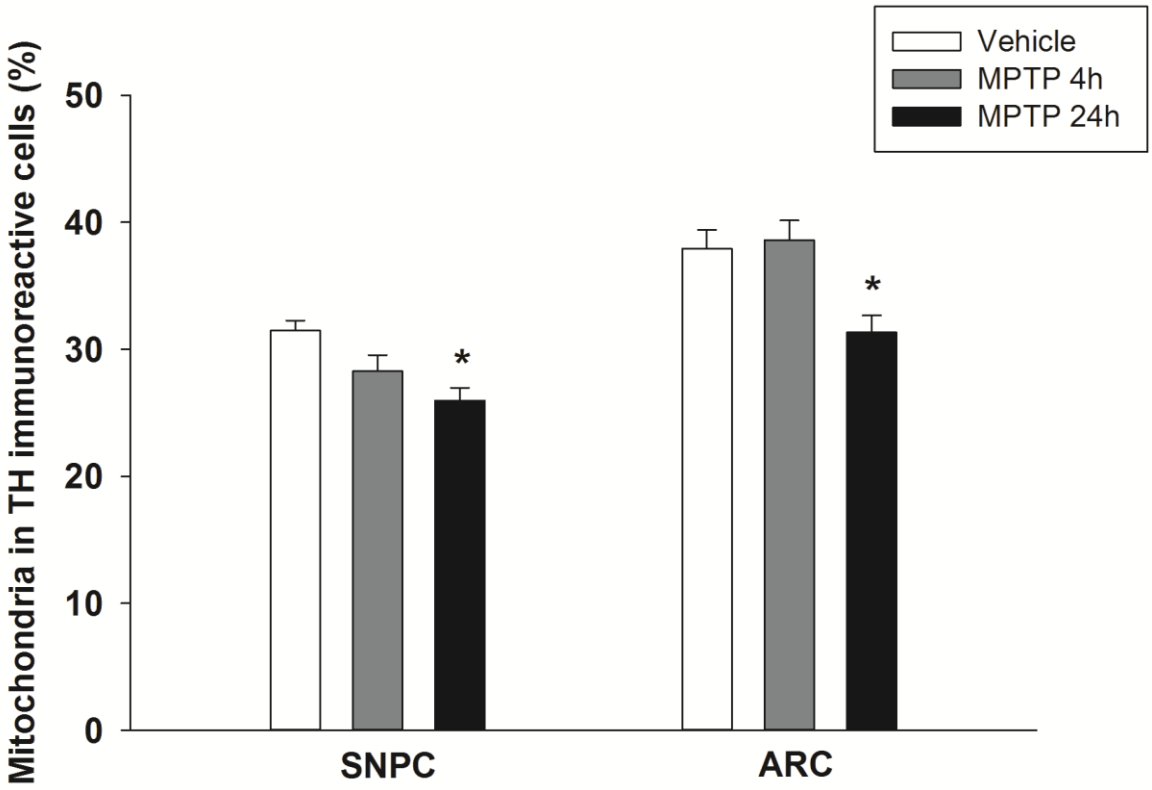

Figure 4.7 Representative bar graph of COX IV colocalized with TH in SNpc and ARC following acute MPTP exposure. Mice were treated with MPTP for 4 h or 24 h, or with saline for 4 h, and then rapidly perfused and fixed. Brains were isolated and cut into 20 µm coronal sections for immunohistochemistry. Mitochondria were quantified from the scatter plot upper right quadrant attained from confocal image using Olympus Fluoview v3.0 software. The colocalization image of ARC is 40x and SNpc is 20x. The percent distribution of these mitochondria within TH neurons was measured. Percent values were converted to parametric value by ASIN(SQRT(% value/100)) for statistic analysis. The error bar is +1 standard error of the mean. * indicates values in MPTP-treated COX IV that were significantly different from vehicle-treated controls, $p < 0.05$.

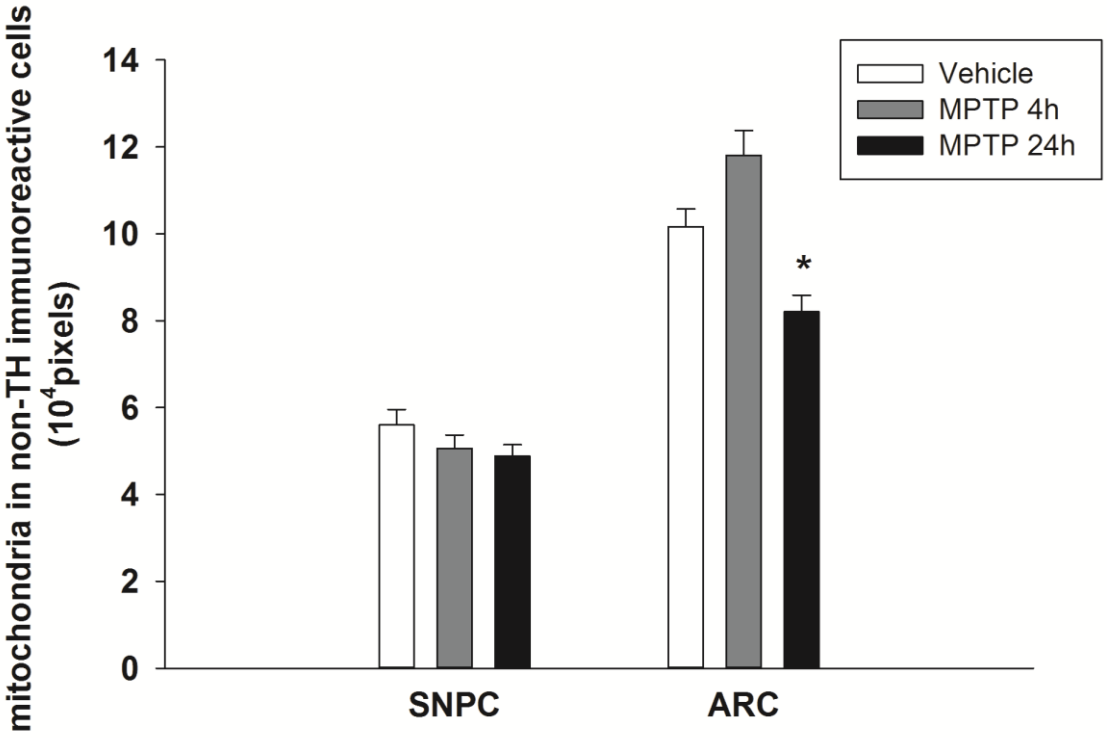

Figure 4.8 Representative bar graphs of COX IV colocalized with non-TH immunoreactive cells in SNPC and ARC following acute MPTP exposure. Mice were treated with MPTP for 4 h or 24 h, or with saline for 4 h, and then rapidly perfused and fixed. Brains were isolated and cut into 20 µm coronal sections for immunohistochemistry. Mitochondria colocalized in the cells that are not immunoreactive to TH were attained using Olympus Fluoview v3.0 software in SNpc and ARC. The colocalization image of ARC is 40x and SNpc is 20x (n=72). The error bar is +1 standard error of the mean. * indicates values in MPTP-treated SM that were significantly different from vehicle-treated controls, $p < 0.05$.

In vivo effect of MPTP on TH expression in NSDA and TIDA neurons

To investigate the effect of MPTP on TH expression in DA neurons in the SNpc and ARC, the numbers of cells that are immunoreactive to TH were counted and overall TH expression was measured. MPTP reduced TH immunoreactive cells in SNpc in a time-dependent manner. After 24 h of MPTP exposure, TH immunoreactive cells were reduced by 27%. MPTP reduced TH immunoreactive cells were reduced after 4 h in ARC, however, the cells recovered after 24 h MPTP exposure. Overall TH expression was measured in ARC and SNpc after MPTP exposure for 4 h, 24 h, or 4 h vehicle treatment (**Figure 4.10**). MPTP did not reduce TH expression in either the SNpc or ARC.

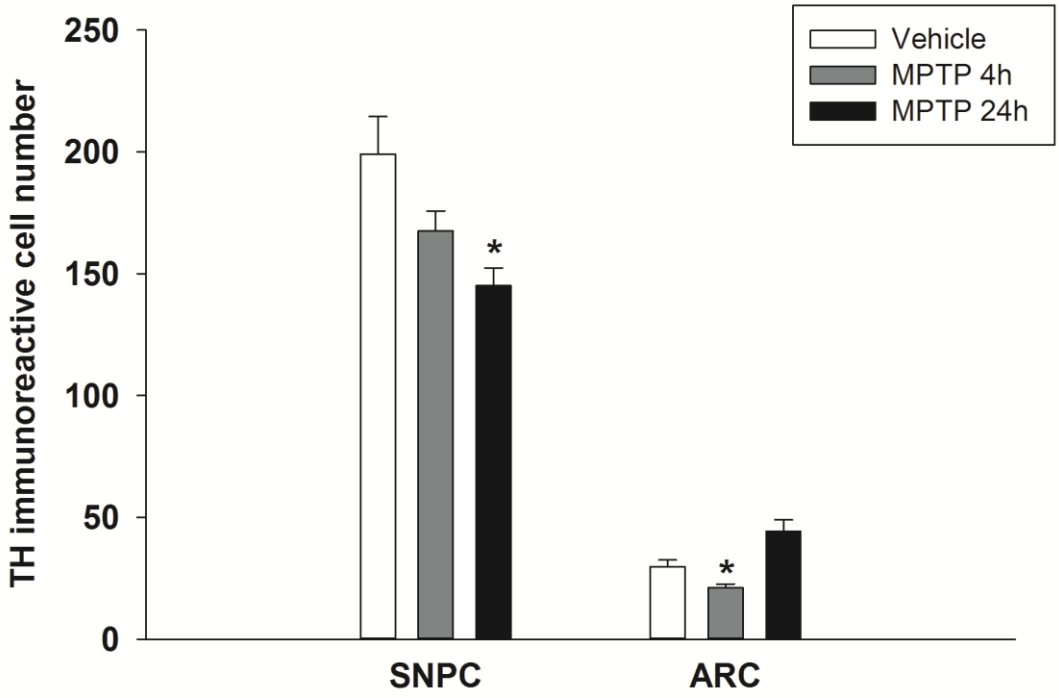

Figure 4.9 Representative bar graphs of TH immunoreactive cell numbers in SNpc and ARC following acute MPTP exposure. Mice were treated with MPTP for 4 h or 24 h, or with saline for 4 h, and then rapidly perfused and fixed. Brains were isolated and cut into 20 µm coronal sections for immunohistochemistry. Cells immunoreactive to TH in SNpc and ARC were counted. Fluorescent intensity of TH was measured in sections of all the regions of ARC (n=18) at 20x magnification and SNpc at 10x magnification (n=30). The error bar is +1 standard error of the mean. * indicates values in MPTP-treated SM that were significantly different from vehicle-treated controls, $p < 0.05$.

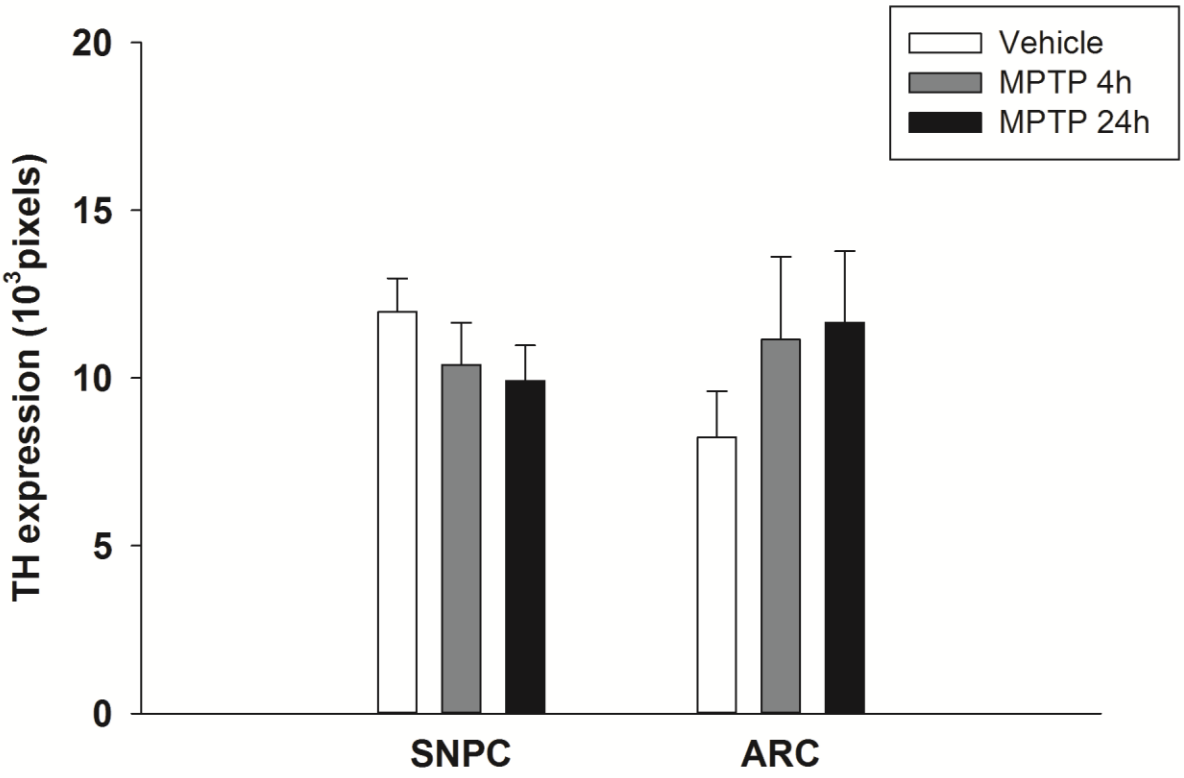

Figure 4.10 Representative bar graphs of fluorescent intensity of TH in SNpc and ARC following acute MPTP exposure. Mice were treated with MPTP for 4h or 24h, or with saline for 4 h, and then rapidly perfused and fixed. Brains were isolated and cut into 20 µm coronal sections for immunohistochemistry. Mitochondria colocalized in the cells that were not immunoreactive to TH were attained using Olympus Fluoview v3.0 software in SNpc and ARC. Fluorescent intensity of TH was measured in sections of all the regions of ARC (n=18) at 20x magnification and half side of SNpc at 10x magnification (n=36). The error bar is +1 standard error of the mean.

The effect of MPTP on NSDA neuron axonal terminal regions was measured using high performance liquid chromatography coupled with electrochemical detection (HPLC-EC). The mean DA concentration in ST from the vehicle group was 220 ± 80.4 ng/mg and at 4 h, DA was reduced to 87.6 ± 37.4 ng/mg and at 24 h to 80.4 ± 35.8 ng/mg. MPTP was reduced by 60% of the DA concentration in the ST at 4 h and 24 h (**Figure 4.11**). At 24 h, the result is not statistically significant due to the small sample size (n=4). Sample size calculation indicated 60% mean difference with sigma of 120 ng/mg requires n=7 for α=0.05 level of significance. In previous study from this laboratory found statistically significant difference between MPTP 24 h and vehicle treatment, n=7 (Schapira et al., 1989).

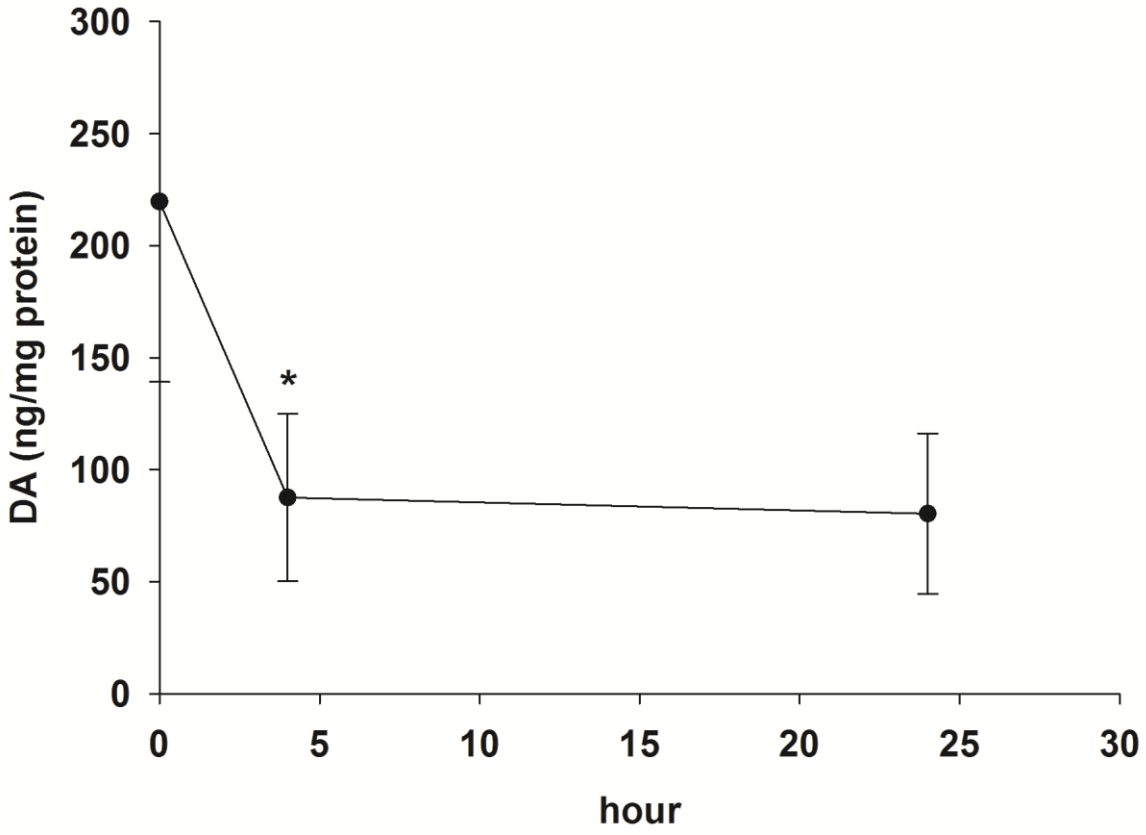

Figure 4.11. Time course effect of MPTP on DA concentrations in the ST. DA concentrations in the ST were measured at 4 h and 24 h after MPTP (20 mg/kg) sc injection in male C57B1/6J mice (n=4). Zero time indicates mice treated with saline-vehicle (10 ml/kg) and killed 4 h post-injection. The error bar is ±1 standard error of the mean. * indicates values in MPTP-treated mice that were significantly different from vehicle-treated controls, $p < 0.05$.

Discussion

Similar "local" response to mitochondrial Complex I inhibitor

The difference in mitochondria between NSDA and TIDA neurons in WT mice was discussed in **Chapter 3**. Maximum and spare respiratory capacities were higher in mitochondria in MBH-derived synaptosomes compared to ST-derived synaptosomes. This corresponds with TIDA neuronal resistance to MPTP and PD. In the present chapter, inhibition of mitochondrial Complex I activity with rotenone reduced mitochondrial respiration in a concentration-dependent manner in both ST and MBH. This *ex vivo* study demonstrated that mitochondria from these two brain regions responded similarly to rotenone 0.0125 µM, 0.25 µM and 2 µM concentrations and showed no difference in the IC50. This indicates that SM derived from the ST and MBH respond to rotenone in a similar manner and degree. Thus, regional differences in maximal and spare respiratory responses are not due to a difference in responsiveness of mitochondria to Complex I inhibition.

When brain tissue is homogenized, pre-synaptic membranes of the axonal terminal breaks off, it forms a vesicle containing cytosolic contents including cytoskeleton, synaptic vesicles and mitochondria (Whittaker and Gray, 1962). Since synaptosomal membranes are derived from axonal terminal plasma membrane, synaptosomes contain ion channels, transporters and receptors. Therefore, SM may mimic the plasma membrane potential and ion homeostasis of the axonal terminals that it is isolated from (Whittaker, 1993; Morgan, 1976; Balázs, R. et al., 1975). Synaptosomes contain functional synaptic vesicles, which can release neurotransmitters of the axonal terminal that they originated from (Dunkley et al., 1987; Ashton & Ushkaryov, 2005). Functional enzymes of the axonal terminals, such as an acetylcholinesterase or protein kinases, are also present in synaptosomes (De Robertis et al., 1962; Dunkley et al., 1988; Dunkley &

Robinson, 1986). Synaptosomes contain functional mitochondria from axonal terminals which give them the ability to generate ATP by consuming oxygen. The SM contains various enzymes involved in the TCA cycle producing metabolites as discussed in **Chapter 3**. However, the use of synaptosomes has some limitations. Due to the absence of a nucleus and other organelles, synaptosomes cannot synthesize proteins except for some of mitochondrial proteins (e.g. mitochondrial ETC, Complex I (Dunkley, 2008). Cytosolic proteins involved in mitochondrial maintenance mechanics contained in synaptosomes may be insufficient due to the lack of protein synthesis and mitochondrial quality control. Therefore, mitochondria, within the cells or *in vivo*, may respond differently to the neurotoxin MPTP (Polosa & Attardi, 1991).

Mechanism of MPP^+ entry of mitochondria in NSDA neurons

In synaptosomes, MPP^+ is shown to reduce mitochondrial membrane potential and cause ATP depletion. ATP depletion indicates that mitochondrial respiration is no longer coupled to ATP synthesis. In addition, mitochondrial dysfunction via MPP^+ has been demonstrated by measuring the amount of the mitochondrial dye 3-[4,5-dimethylthiazol]-2,5-diphenyltetrazolium bromide (MTT) or [^{3}H]tetraphenylphosphonium ([^{3}H] TPP^+) in a mitochondria matrix after MPP^+ treatment (Virmani et al., 2004; Stephans et al., 2002). In addition to mitochondrial membrane potential reduction, the inhibitory effect of MPP^+ on NADH dehydrogenase is seen by measuring NADH oxidation or NAD-linked substrates oxidation and lactate accumulation (Hoppel et al., 1987; Nicklas et al., 1987).

In the present study, treatment of synaptosomes with high concentrations of MPP^+ (1 mM) caused a reduction in both basal and maximal mitochondrial respirations in ST-derived synaptosomes, and MPP^+ was more effective in the inhibition of basal respiration than maximal

or spare respiration. The steady state MPP^+ concentrations in cells from SN are low (Ramsay and Singer, 1986). In MPTP-treated mice, the tissue concentrations of MPP^+ was 30 µM and MPP^+ peaked in mice treated with 20 mg/kg MPTP acutely in ME and ST at 4 h with 365 ± 37 pg/µg protein in ME and 78 ± 9 pg/µg in the ST (Schapira et al., 1989). In contrast to the low physiological concentrations of MPP^+ *in vivo,* mitochondrial function was inhibited *ex vivo* only with a high concentration of MPP^+ (1mM). In addition, there was no effect of the DAT inhibitor, GBR12909, on MPP^+ inhibition of mitochondrial function. This suggests that the amount of MPP^+ accumulated in synaptosomes occurs independently of uptake via the DAT, and may not be coupled to amount of MPP^+ accumulating into mitochondria.

The concentrations of MPP^+ inhibition of NADH oxidase activity in synaptosomes or cells has been reported to vary from 0.2 µM to 10 mM and the IC50 of mitochondria isolated from the mouse liver was 100 µM (Lambert and Bondy, 1989; Gluck et al, 1994). MPP^+ accumulates in synaptosomes in a time- and concentration-dependent manner, and catecholamine uptake inhibitors such as mazindol and nomifensine do not inhibit MPP+ entry. However, the accumulation rate increases when MPP^+ is treated with the lipophilic anion, tetraphenylborate (TPB^-) following passive Nernstian transportation. Therefore, MPP^+ accumulation is dependent on polarization of the membrane (**Figure 4.12**).

Similar to transportation into synaptosomes in a membrane potential-dependent manner, MPP^+ also crosses the mitochondrial membrane depending on the electrochemical gradient (Ramsay et al. 1986). When the mitochondrial inner membrane was destroyed by sonication, MPP^+ failed to affect NADH oxidation. Moreover, when the mitochondrial membrane was depolarized by valinomycin with K^+, MPP^+ entry also failed. When the mitochondrial uncoupler 2, 4-dinitrophenol (DNP) was added, MPP^+ no longer accumulated into the mitochondria and the

outflow of MPP^+ was promoted. MPP^+ entry is also energy dependent (Sherer et al., 2007; Cannon et al. 2009). MPP^+ accumulation is promoted by the availability of the oxidative metabolites of ATP or malate, glutamate and succinate. Once MPP^+ enters the mitochondria, it binds to the rotenone site of NADH dehydrogenase between the Fe-S cluster of NADH dehydrogenase and Q (Ramsay et al., 1987).

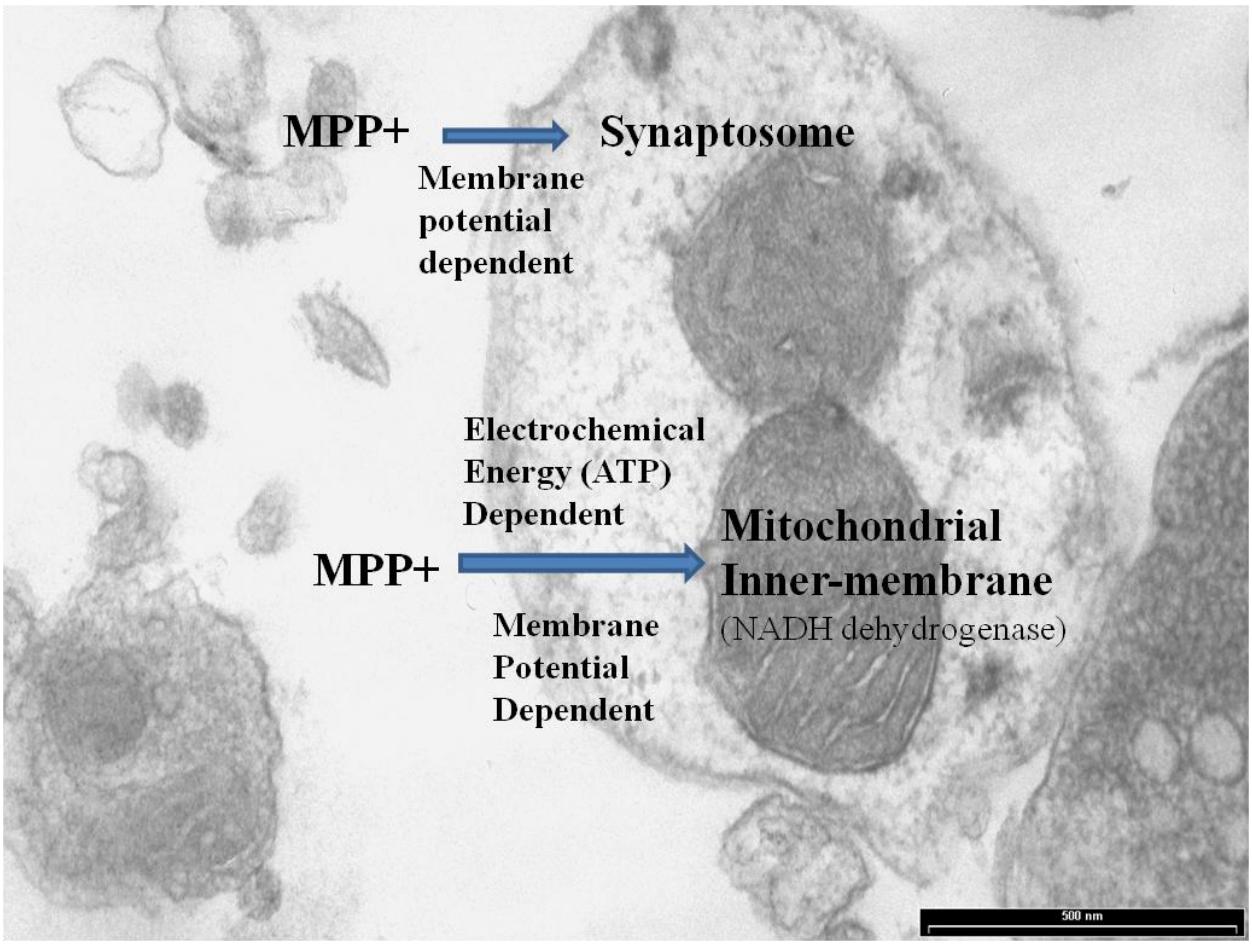

Figure 4.12. Pathway of MPP^+ entry into synaptosomes. MPP^+ enters synaptosomes in a membrane potential dependent manner. Once in the synaptosome, MPP^+ enters into mitochondria in an electrochemical, energy, and mitochondrial membrane potential dependent mechanism, and inhibits electron transport chain Complex I (NADH dehydrogenase).

MPP^+ was found to exhibit limited toxicity in this study. This may be because it does not accumulate in sufficient concentrations to cause toxicity in mitochondria. Synaptosomes in *ex vivo* preparations may lack a sufficient substrate such as pyruvate/malate to provide energy or induce a hyperpolarized energetic state for mitochondria. In addition, decreased inhibition of maximal respiration by MPP^+ provides a clue that binding of MPP^+ or accumulation of MPP^+ is not permanent. FCCP, an uncoupler, decreases membrane potential causing loss of accumulation of MPP^+ in mitochondria regardless of the MPP+ uptake into synaptosomes through DAT. This explains why there is no difference in mitochondrial respiration after inhibition of DAT by GBR12909. GBR12909 causes inhibition of MPP^+ entry by DAT (Andersen, 1989; Czoty et al., 2000; Preti, 2000). Synaptosomal uptake of MPP+ does not result in MPP+ accumulation in mitochondria. This provides an important insight into the DA neuronal characteristics of NSDA and TIDA neurons and their differential susceptibility to MPTP.

Tonic and phasic DA release occurs commonly in NSDA neurons, while TIDA neurons have a diurnal change in release following a circadian rhythm (Dreyer et al., 2010; Mai et al., 1994; Shieh and Pan, 1995). It is generally understood that NSDA neurons are continuously activated to regulate the motor system even during rest while TIDA neurons are not. In addition, DA synthesis and release demands high ATP production by the mitochondria. High ATP demand is a driving force for producing proton gradients by the ETC causing increased membrane potential. Therefore, electrochemical energy assisted and membrane potential dependent MPP^+ entry allows the accumulation of a high concentration of MPP^+ in the NSDA neurons. This may allow mitochondria in NSDA neurons to accumulate MPP^+ in higher concentrations than in TIDA neurons due to different levels of DA neuronal activity.

A previous report from our laboratory showed that MPP^+ peaks at 4 h after MPTP single acute exposure and it clears by 24 h in both ST and ME. TIDA neurons recover levels of DA, but NSDA neurons still exhibit reduced levels of DA 24 h later (Schapira et al., 1989). NSDA neurons may have accumulated MPP^+ in mitochondria independent of tissue MPP^+ concentration. Therefore, MPP+ may accumulate to different levels depending on DA neuronal activity in mitochondria causing a differential neurotoxic effect on the NSDA and TIDA neurons.

Differential effect of MPTP on mitochondria in TIDA and NSDA neurons

Acute MPTP exposure causes progressive TH immunoreactive cell loss in SNpc with decreased DA levels in ST at both 4 h and 24 h. On the other hand, TH immunoreactive cells in ARC were also reduced at 4 h, but recovered cell numbers by 24 h. Since neurons do not progress through mitosis, they lack the ability to regenerate. Recovery of TH immunoreactive cells indicates that MPTP does not cause cell death in ARC.

The differential toxicity of MPTP on TIDA and NSDA neurons after acute and chronic exposures has been reported previously by our laboratory. DA levels in ST and TH immunoreactive cells in SNpc were reduced, while DA levels in ME and TH immunoreactive cells in ARC recovered (Behrouz et al., 2007; Schapira et al., 1989; Benskey et al., 2013). In the present IHC study, TH expression did not change in either SNpc or ARC, however, the amount of mitochondrial protein in TH immunoreactive cells in both regions were reduced at 24 h.

After 24 h MPTP treatment, cells in SNpc that are not immunoreactive to TH showed no difference in the mitochondrial protein levels. However, in ARC, non-TH immunoreactive cells showed an equivalent mitochondrial protein level reduction to TH immunoreactive cells. As noted in **Chapter 1**, MPP^+ can also be sequestered into DA vesicles by VMAT which prevents

MPP^+ inhibition of mitochondria. Similar to MPP^+ sequestration by VMAT, cells nearby DA neurons may take-up MPP^+. This reduces uptake of the MPP^+ into DA neurons preventing cells from degenerating in ARC.

TIDA neuronal axon terminals lay outside the blood-brain-barrier below the third ventricle, so they may adapt more readily to exposure to foreign bodies or toxins and develop compensatory mechanisms to handle these insults. Interstitial solutes are cleared by cerebral spinal fluid (CSF) influx and efflux via astrocytic water transport, so toxins and metabolites can be removed from the parenchyma of the brain (Xie et al., 2013). Enhanced clearing of toxins and the sequestering of toxins via astrocytes or nearby glial cells may also provide resistance to toxin in DA neurons from ARC.

Since MPP^+ is toxic to mitochondria, TIDA neurons may upregulate compensatory mechanisms to repair mitochondria through mitochondrial quality control such as mitophagy. Increased mitochondrial deletion and reduced mitochondrial/nuclear DNA-repair capability has been observed with aging as well as in SNpc (Imam, 2006; Kraytsberg et al., 2006; Bender et al., 2006). In addition, various genetic factors associated with PD such as parkin, pink 1, Omi/HtrA2 play a significant role in mitochondrial quality control (Narendra et al., 2008; Tanaka, 2010; Trempe et al., 2013; Dagda et al., 2009). Increased mitochondria in autophagosomes were measured in TH immunoreactive cells in ARC compared to SNPC (**Chapter 3**). This suggests differential mitochondrial quality control may also be an important factor for survival of DA neurons to MPTP exposure.

Conclusion

Although there are different mitochondrial characteristics between NSDA and TIDA neurons in WT mice, mitochondria isolated from axonal terminal regions responded to mitochondrial Complex I inhibitor in a similar manner and mitochondrial respiratory inhibitory ability was similar between the ST and MBH. This indicates that unique characteristics of mitochondria in axonal terminals are not responsible for differential susceptibility of NSDA and TIDA neurons to MPTP. In addition, the unique SM responses to MPP^+ *ex vivo* suggest the importance of DA neuronal activity dependent MPP^+ accumulation. Tonic and phasic activation of NSDA neurons may cause high accumulation of MPP^+ in mitochondria independent of its low systemic concentration. In addition, in the ARC, possible sequestration of MPP^+ into non-DA cells near the DA neurons may prevent MPP^+ uptake into TIDA neurons.

Chapter 5. Altered mitochondrial structure and function in axonal terminal regions of central DA neurons in the absence of parkin

Introduction

Previous studies from our laboratory have revealed that the differential susceptibility of TIDA and NSDA neurons is correlated with the expression of parkin in response to the mitochondrial toxin, MPTP (Schapira et al., 1989; Behrouz et al., 2007). There is an increase in parkin expression in TIDA neurons that corresponds with the time frame of DA recovery, whereas NSDA neurons did not increase parkin expression and do not recover DA stores in axon terminals. In the previous studies described in **Chapter 3** of this dissertation it was found that mitochondrial characteristics and function differ in axon terminals of TIDA and NSDA neurons suggesting a role for parkin in mitochondrial maintenance in central DA neurons.

Parkin is E3 ubiquitin ligase that tags misfolded proteins with ubiquitin for degradation by the ubiquitin proteasome system. Parkin also plays a role in maintenance of mitochondrial integrity through regulation of mitophagy. When the mitochondrion is damaged, it is segregated and engulfed into an autophagosome, and the resulting mitophagosome is degraded following fusion with lysosomes. Mitochondrial quality control, in part, is regulated by parkin through binding to Pink-1 in the outer membrane thereby tagging damaged mitochondria for mitophagy (Tanaka, 2010; Youle & Narendra, 2011). Parkin not only regulates mitochondrial quality control through mitophagy, but also selectively regulates turnover of the electron transport chain (ETC) (Vincow et al., 2013). A relative parkin deficiency could account for impair mitochondrial function in NSDA neurons (Palacino et al., 2004). Therefore, the loss of parkin-mediated

maintenance of mitochondrial homeostasis is a plausible explanation for the altered mitochondrial function and structure in NSDA neurons.

In the present study, maintenance of mitochondrial homeostasis was evaluated by measuring mitochondrial bioenergetics, mass, membrane potential, and morphology in synaptosomes isolated from brain regions containing axon terminals of NSDA and TIDA neurons in WT and parkin knockout mice. The findings that parkin deficient mice have reduced mitochondrial bioenergetics, mass, and quality in ST-derived synaptosomes suggests that parkin mediated mitochondria quality control may be vital for maintenance of NSDA neurons.

Results

Differential mitochondrial bioenergetics in SM derived from ST and MBH in WT and parkin KO mice

WT and B6.129S4-*Park2*^{tm1Shn}/J strain parkin KO mice (**Chapter 2.1**) were decapitated and brain regions that contain NSDA axon terminals (ST) and TIDA axon terminals (MBH) were dissected. SM were isolated from ST and MBH as described in **Chapter 2, Sections 2.3 & 2.4**. Using a Seahorse XF analyzer, the OCR in 20 µg of SM was examined. Basal respiration was measured in the presence of 5 mM pyruvate and 2.5 mM malate. Maximum respiration was attained after FCCP ex vivo injection. Finally, spare respiration was attain by the difference between basal and maximum respiration. The detailed analysis of mitochondrial bioenergetics attained from Seahorse XF24 Analyzer is described in **Chapter 2, Section 2.4.4.**

There was no difference in ST-derived SM basal respiration between WT and parkin KO mice (169 ± 45 versus 177 ± 34 pmoles/min, respectively; **Figure 5.1 A**). However, both maximum and spare respirations of ST-derived synaptosomes from parkin KO mice were lower

than WT mice (maximum respiration: 555 ± 31 versus 719 ± 32 pmoles/min, respectively; spare respiration: 381 ± 40 versus 540 ± 50 pmoles/min, respectively). Basal ECAR levels were similar in ST SM from WT and parkin KO mice (**Figure 5.1 B**). ECAR increased to a similar extent in both WT and parkin KO mice following application of a mitochondrial ETC inhibitor (rotenone) or uncoupler (FCCP).

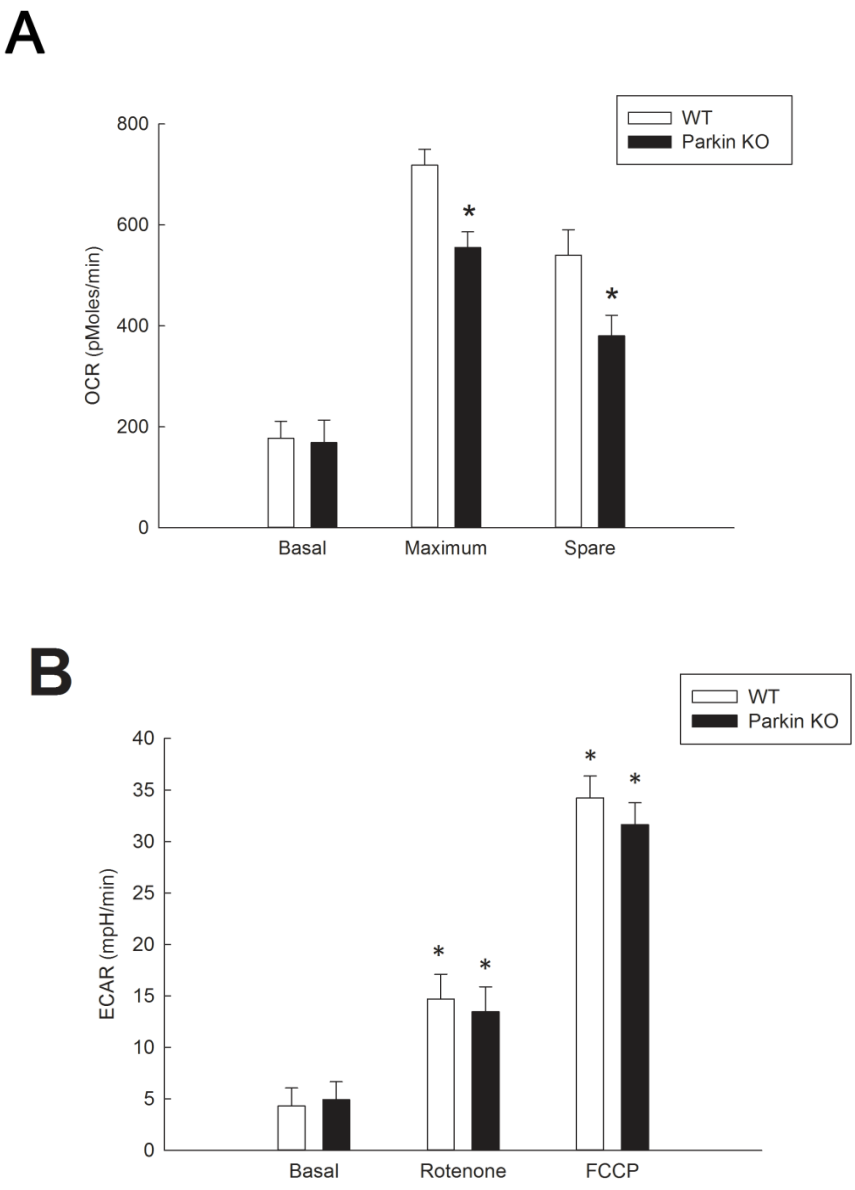

Figure 5.1 Comparison of ST-derived SM bioenergetics of mitochondrial respirations and glycolysis in WT and parkin KO mice. Panel A, OCR representing ST-derived SM aerobic respiration from WT and parkin KO mice. Basal, maximum (uncoupler; FCCP), and spare respirations (difference in OCR of basal and maximum respiration) were measured using Seahorse XF analyzer. Panel B, ECAR of ST-derived SM from WT and parkin KO mice. ST-derived SM from WT and parkin KO mice under basal levels, presence of mitochondrial Complex I inhibitor (rotenone), and uncoupler (FCCP) were measured by Seahorse XF24 analyzer. Twenty µg SM were examined for OCR and ECAR. The respiratory control ratio (RCR) of SM were greater than 3. White columns represent OCR or ECAR of synaptosomal mitochondria from WT mice and black columns represent OCR or ECAR of parkin KO mice (n=5) and verticle lines + 1 SEM. * indicates OCR of maximum and spare respiration in parkin KO mice that are significantly different ($p < 0.05$) from those of WT mice.

In MBH-derived SM, there was no difference in basal respiration between WT and parkin KO mice (147 ± 33 versus 142 ± 26 pmoles/min, respectively). Both the maximum and spare respiratory capacities of parkin deficient SM from the MBH were much lower than those of WT mice (**Figure 5.2 A**). Maximum respiration of parkin KO mice was 649 ± 48 (pmoles/min) versus 915 ± 27 (pmoles/min) for WT mice. Spare respiration of parkin KO mice was 512 ± 24 (pmoles/min) versus 749 ± 97 (pmoles/min) in WT mice. ECAR was similar in SM from WT and parkin KO mice under basal conditions and also following inhibition of Complex I activity with rotenone or dissipation of the proton gradient with FCCP (**Figure 5.2 B)**. Maximum and spare respirations of SM-derived from ST and MBH were reduced in the absence of parkin, however ECAR did not differ depending on parkin presence.

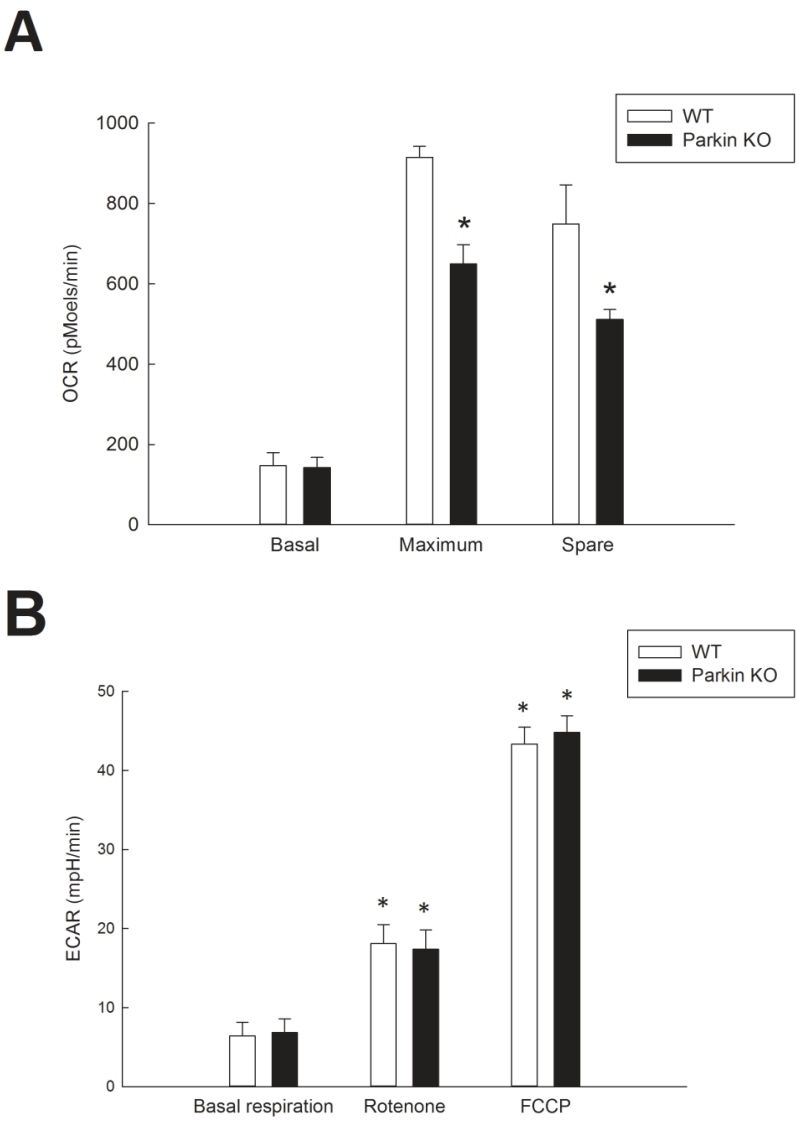

Figure 5.2 Comparison of MBH-derived SM bioenergetics of mitochondrial respirations and glycolysis in WT and parkin KO mice. Panel A, OCR representing MBH-derived SM aerobic respiration from WT and parkin KO mice. Basal, maximum (uncoupler; FCCP), and the spare respiration (difference in OCR between basal and maximum respiration) were measured using seahorse XF analyzer. Panel B, ECAR of MBH-derived SM from WT and parkin KO mice. MBH-derived SM from WT and parkin KO mice under basal levels, presence of mitochondrial Complex I inhibitor (rotenone), and uncoupler (FCCP) were measured by Seahorse XF24 analyzer. Twenty µg SM were examined for OCR and ECAR. The respiratory control ratio (RCR) of SM were greater than 3. White columns represent OCR or ECAR of synaptosomal mitochondria from WT mice and black columns represent OCR or ECAR of parkin KO mice (n=5) and verticle lines + 1 SEM. * indicates OCR of maximum and spare respiration in parkin KO mice that are significantly different ($p < 0.05$) from those of WT mice.

Flow cytometric measurement of the ST- and MBH-derived SM mass and membrane potential in WT and parkin KO mice

Twenty µg SM isolated following method described on **Chapter 2, section 2.3** was examined for flow cytometric analysis following method described in **Chapter 2, Section 2.5**. Flow cytometric assessment of ST- and MBH-derived SM in WT and parkin KO mice was performed using MitoTracker Green and TMRE fluorescent dyes to measure mitochondrial mass and membrane potential. Histograms (**Figures 5.3 A** and **5.3 B)** indicate a left shift of the green fluorescence corresponding to Mitotracker green in both ST- and MBH-derived SM from parkin KO mice as compared to WT mice. Parkin KO mice had lower SM mass compared to WT mice in both ST- and MBH-derived SM based on quantification of MitoTracker Green fluorescence (**Figure 5.3 C**).

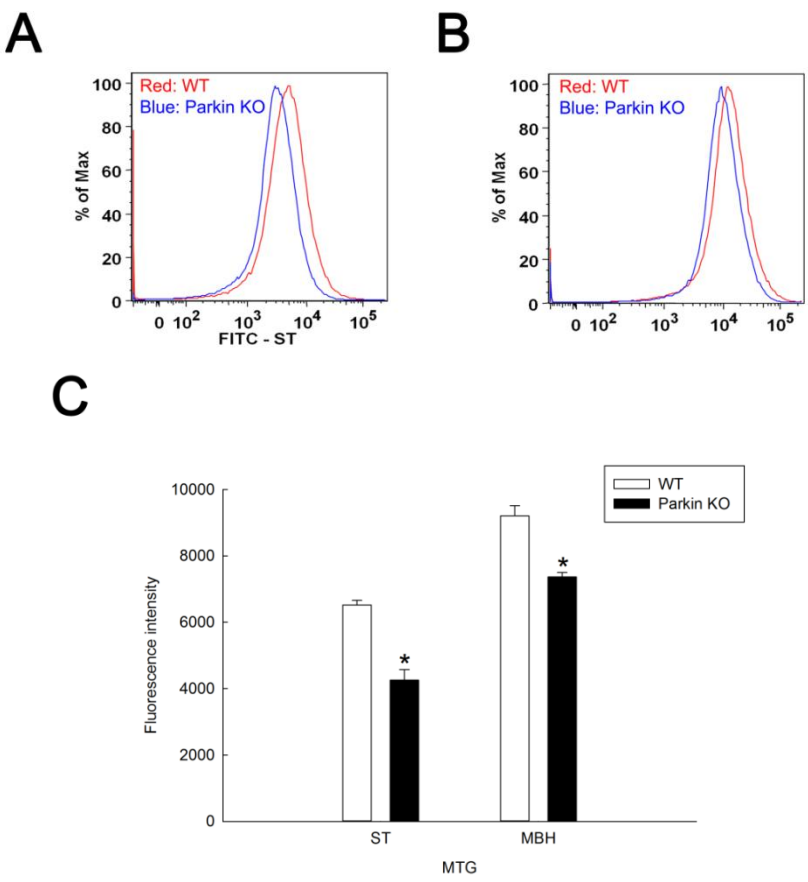

Figure 5.3. Comparison of ST- and MBH-derived SM mass in WT and parkin KO mice. Panel A, Representative histogram of MitoTracker Green measurement of ST derived SM from WT and parkin KO mice. Panel B, Representative histogram of MitoTracker Green measurement of MBH-derived SM from WT and parkin KO mice. Panel C, Quantification of mitochondrial mass of ST- and MBH-derived SM in WT and parkin KO mice. Flow cytometric assessment of SM mass of ST and MBH in WT and parkin KO mice was performed using fluorescent dye MitoTracker Green. Twenty µg SM were examined for mitochondrial mass by flow cytometry. White columns represent synaptosomal mitochondria from WT mice and black columns represent parkin KO mice (n=3) and verticle lines + 1 SEM. * indicates mitochondrial mass of SM from parkin KO mice that are significantly different ($p < 0.05$) from those in WT mice.

Flow cytometry-based TMRE uptake in ST- and MBH-derived synaptosomes from WT and parkin KO mice was used to compare differences in mitochondrial membrane potential in the absence of parkin. There is no difference in the TMRE histogram between synaptosomes from WT and parkin KO mice, an observation that was consistent for both ST- and MBH-derived SM (**Figures 5.4 A** and **5.4 B**). Quantitative analysis of the TMRE signal obtained by flow cytometry in ST- and MBH-derived SM produced similar results in both WT and parkin KO mice, which suggests there is no difference in membrane potential in the presence or absence of parkin, regardless of the brain regions (**Figure 5.4 C**).

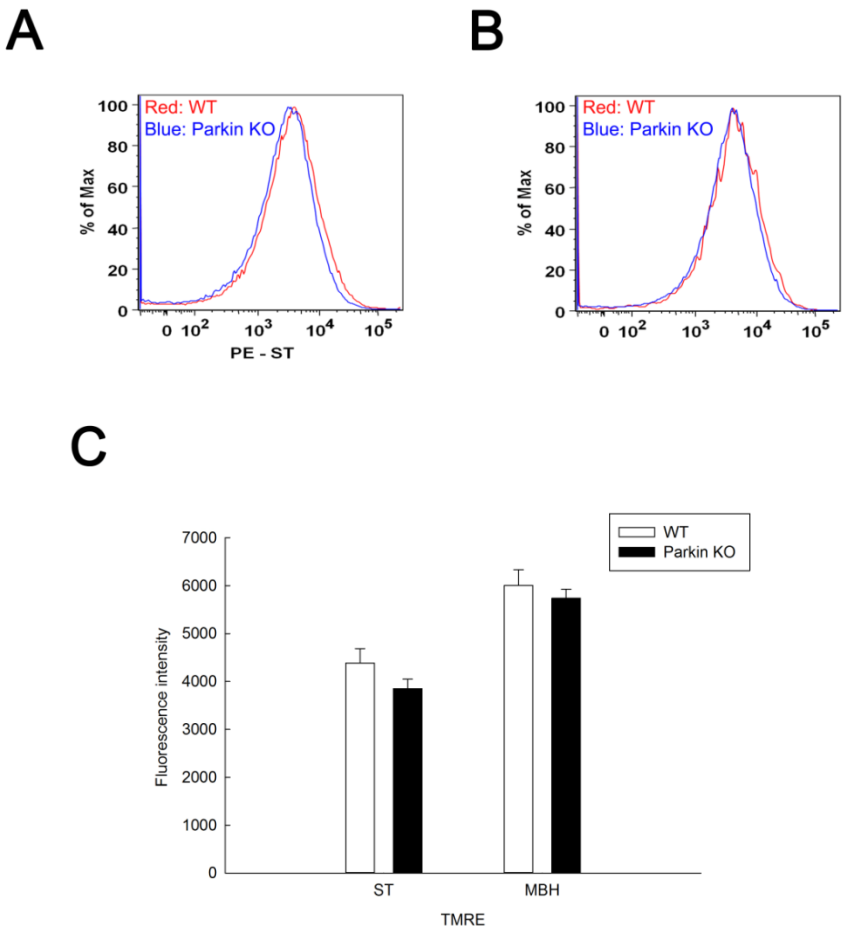

Figure 5.4 Comparison of ST- and MBH-derived SM membrane potential in WT and parkin KO mice. Panel A, Representative histogram of TMRE measurement of ST-derived SM from WT and parkin KO mice. Panel B, Representative histogram of TMRE measurement of MBH-derived SM from WT and parkin KO mice. Panel C, Quantification of mitochondrial membrane potential between WT and parkin KO mice of ST- and MBH-derived SM. Flow cytometric assessment of membrane potential were performed using fluorescent dye TMRE. Twenty µg SM were examined for mitochondrial membrane potential by flow cytometry. White columns represent synaptosomal mitochondria from WT mice and black columns represent parkin KO mice (n=3) and verticle lines + 1 SEM.

Transmission electron microscopy analyses of ST- and MBH-derived SM morphology and integrity in WT and parkin KO mice

Parkin mediates mitochondrial quality control, therefore, in order to investigate quality of morphology of mitochondria, transmission electron microscopic analysis of SM from parkin KO and WT mice was performed following methods described in **Chapter 2, Section 2.6**. Mitochondrial function was scored based on their ultrastructure using Flameng functional scoring system as described in **Chapter 3**. The evaluation of the Flameng mitochondrial score and corresponding morphology was depicted in **Figure 3.6**. The distribution of the mitochondrial morphology represents a quality of mitochondrial function. Mitochondria with Flameng score of 1-2 indicates mitochondria population with low quality, score 1 as the mitochondria with the lowest quality, score 3, swollen mitochondria, which process can be reversed or irreversible depending on the pathologic cause of the swelling, score 4 – 5 as high quality mitochondria populations, score 5 as the highest quality mitochondria.

The mitochondria found in ST-derived synaptosomes from parkin KO mice were more dysmorphic compared to mitochondria from WT-derived synaptosomes. The distribution of mitochondrial morphology scores indicate relatively poorer quality control in parkin deficient mice compared with WT mice. The average of the Flameng score of SM from parkin KO mice was lower (2.83 ± 0.08) compared to WT mice (3.46 ± 0.07) (**Figure 5.5 A; Table 5.1**). In contrast, the mitochondrial morphology scores were similar in MBH-derived SM in WT (3.55 ± 0.08) and parkin KO mice (3.31 ± 0.09) (**Figure 5.5 B, Table 5.1**). Fewer mitochondria per synaptosome were observed in parkin KO mice compare to WT mice in ST-derived synaptosomes, while the numbers of mitochondrial per synaptosome were similar in the MBH of parkin KO and WT mice (**Table 5.1**).

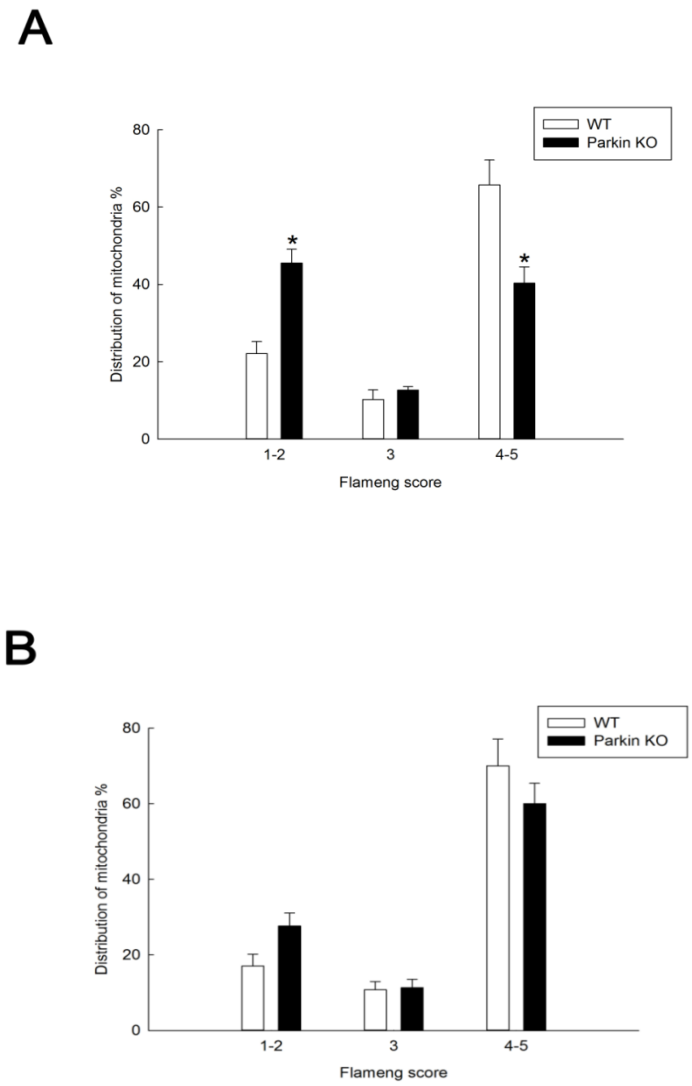

Figure 5.5 Transmission electron microscopic analyses of ST- and MBH-derived SM in WT and parkin KO mice. Panel A, Representative bar graph of Fleming mitochondrial functional score of ST-derived SM from WT and parkin KO mice. Panel B, Representative bar graph of Fleming mitochondrial functional score of MBH-derived SM from WT and parkin KO mice. The synaptosomes were fixed, sectioned and at least 200 mitochondria from images were analyzed. Number of mitochondria with score ranged from 1-2 as a dysfunctional mitochondria, 3, and 4-5 as a functional mitochondria are divided by total number of mitochondria and represented as percent value. The graph represents distribution of the mitochondria from each group based on mitochondrial morphology. Statistical analysis was done converting percent value by ASIN(SQRT(% value/100)). White columns represent synaptosomal mitochondria from WT mice and black columns represent parkin KO mice (n=4) and verticle lines + 1 SEM. * indicates mitochondrial distribution of SM from parkin KO mice that are significantly different ($p < 0.05$) from those in WT mice.

	Mean Flameng score	Number of Mitochondria per synaptosomes
ST – WT	3.46 ± 0.07	1.67± 0.11
ST – KO	2.83 ± 0.08*	1.37± 0.03*
MBH – WT	3.55 ± 0.08	2.02 ± 0.10
MBH - KO	3.31± 0.09	1.78 ± 0.13

Table 5.1. Comparison of SM mean Flameng scores and mean number of mitochondrial per synaptosomes in the ST and MBH of WT and parkin KO mice. Mean mitochondrial functional score was calculated by averaging Flameng mitochondrial functional score utilizing at least 200 mitochondria from each experimental group. Mean number of mitochondria per synaptosomes is derived by dividing total number of mitochondria by total number of synaptosomes in each experimental group. The experiment was repeated four times with $\pm$ 1 standard error of the mean. * indicates mean Flameng score or mean number of mitochondria per synaptosomes in parkin KO mice that are significantly different ($p<0.05$) from those in WT mice.

Weight comparison of WT and parkin KO mice

Mitochondrial maximum and spare respiratory capacities, mass, number per synaptosome, and quality were much lower in ST of parkin KO mice as compared with WT mice. These findings raise the question if there is any consequential phenotype in parkin null mice. Mitochondria are essential for cellular metabolic processes by providing the major source of energy through oxidative phosphorylation. Therefore, as an indirect measure of general body metabolism the weight of parkin KO and WT mice were compared. The mean weight of age-matched WT mice (20-24 weeks old) was 33.1 g, while parkin KO mice weighed 28.6 g (**Figure 5.6**). The difference was higher as the mice were older. WT mice with 36-40 weeks old weighed 38 g while parkin KO mice only weighed 29.5 g.

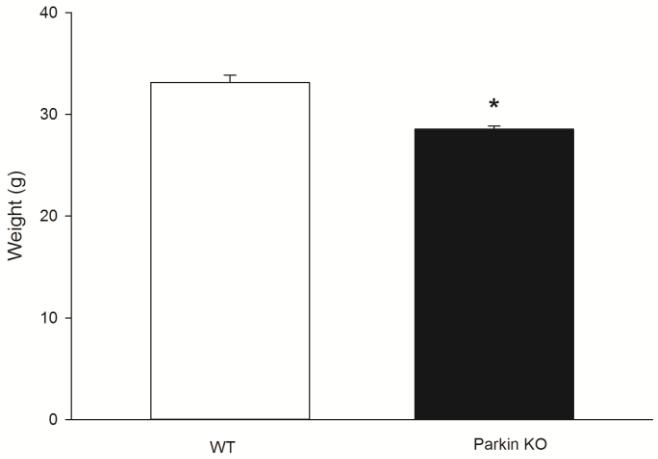

Figure 5.6 Weight comparison of WT vs parkin KO mice. Weights were obtained from age-matched, 20-24 weeks old, untreated mice (n = 7 for WT mice; n= 10 for Parkin KO mice) within our colony.

Discussion

The data presented herein are consistent with the hypothesis that parkin plays a neuroprotective role in central DA neurons during metabolic stress through maintenance of the number and quality of mitochondria in axon terminals. NSDA neurons appear to have reduced aerobic mitochondrial respiratory capacity associated with diminished mitochondrial mass, number of healthy intact mitochondria, and total numbers of mitochondria per synaptosome in the absence of parkin. A relative parkin deficiency following acute injury in NSDA neurons may impair mitochondrial aerobic respiration in axon terminals by decreasing the numbers and quality of viable mitochondria. A limited capacity of parkin-mediated mitochondrial maintenance may, in part, explain unique susceptibility of NSDA neurons and resistance of TIDA neurons to toxicant exposure and to degeneration in PD.

Parkin does not appear to regulate basal aerobic respiration within axon terminals in the ST, although parkin does influence the number of viable mitochondria in NSDA axon terminals. There are fewer mitochondria in NSDA axon terminals in parkin KO mice compared to WT type mice, and existing mitochondria appear more dysmorphic in the absence of parkin. It is likely that under conditions of basal respiration, mitochondrial numbers may be sufficient in NSDA neurons of parkin deficient mice to generate energy to meet physiological demand. This as well as parkin independent regulation of basal anaerobic respiration may explain why only mild behavioral phenotypes are observed in parkin KO mouse models in the absence of metabolic stress (Harvey et al., 2008; Perez and Palmiter, 2005). The similar TMRE-derived estimations of membrane potential for WT and parkin KO mice in the context of a decrease in mitochondrial mass suggest a compensatory increase mitochondrial potential in parkin KO mice.

When mitochondrial respiration is uncoupled by FCCP, in the absence of proton back pressure, parkin deficient mice have an impaired capacity to increase energy production; i.e., maximum and spare respirations are lower in ST-derived SM from parkin KO as compared with WT mice. The reduced numbers of available mitochondria in NSDA neurons in parkin deficient mice result in diminished overall maximal electron transport chain activity and, consequently, less oxygen consumption and ATP generating capacity under high-demand conditions. On the other hand, the absence of parkin has no impact on non-mitochondrial respiration in ST axon terminals; i.e., when the ETC is no longer functional following inhibition of Complex I with rotenone or dissipation of the proton gradient by FCCP.

Impaired mitochondrial morphology and reduced numbers of mitochondria per synaptosome in ST from parkin KO compared to WT mice were observed by transmission electron microscopy suggesting that parkin plays a significant role in maintenance of mitochondrial integrity. These results are consistent with previous reports showing that mitochondrial dysfunction, in the absence of parkin in Drosophila *parkin* null mutants, is associated with reduced lifespan, locomotor defects, and male sterility (Greene et al., 2003). In addition, parkin loss of function mutations are associated with increased levels of DA-induced oxidative stress in induced pluripotent stem cells obtained from both normal human subjects and PD patients (Jiang et al., 2012).

While there are limitations to toxicant-induced models of DA neurodegeneration, there is a direct correlation between susceptibility of NSDA neurons to the acute and chronic toxic effects of MPTP and the inability of these neurons to upregulate parkin (Schapira et al., 1989; Benskey et al., 2013). On the other hand, increased expression of parkin bolsters mitochondrial function providing a neuroprotective effect. Indeed, neuron-specific over-expression of parkin in

Drosophila increases mean and maximum lifespan by improving mitochondrial morphology and mitochondrial dynamics (Rana et al., 2013). In murine models, adenovirus mediated upregulation of parkin expression appears to protect NSDA neurons from toxicants-induced injuries (Vercammen et al., 2006; Manfredsson et al., 2007). The protective effects of exogenous upregulation of parkin expression against neurotoxicant-induced injury is consistent with our observations in **Chapter 3** that mitochondrial respiratory capacity, mass, and quality control are increased in TIDA neurons that have relatively higher parkin expression, particularly following an acute injury, compared to NSDA neurons.

Dysfunctional mitochondria cause impaired ATP synthesis while increasing the generation of oxygen free radicals and oxidative stress in NSDA neurons (Scotcher et al.,1990; Keane et al., 2011). NSDA neurons are susceptible to oxidative stress due, in part, to highly oxidative characteristics of DA (Lin and Beal, 2006; Floor and Wetzel, 1998; Spina and Cohen, 1989; Cohen, 2002). In addition, altered mitochondrial bioenergetics may impact energy metabolism. Low body mass index is also observed in Parkinson disease patients compared to normal age matched healthy subjects (Bachmann and Trenkwalder, 2006). Moreover, abnormal glucose tolerance was observed in 50 – 80% of Parkinson patients in addition to decreased dopaminergic transmission in ST with chronic hyperglycemia (Sandyk, 1993). Differential mitochondrial function in parkin deficient mice may play a role in differential energy metabolism and consequent difference in weight change, as observed in the present study. Therefore, parkin-mediated maintenance of mitochondrial homeostasis may be an important mechanism underlying the unique susceptibility of NSDA neurons to PD-related neurodegeneration.

When mitochondrial degradation is reduced, an increased accumulation of damaged mitochondria would be expected, along with an increase in total number of mitochondria in axonal terminals. However, we observed increased numbers of impaired and damaged mitochondria in ST from parkin KO mice compared to WT controls, but no apparent increase in the overall number of mitochondria were detected in the parkin KO mice. It is possible that, in parkin KO mice, there is a decrease in mitochondrial biogenesis or slowed transport of newly formed mitochondria to the nerve terminals. Our data would be consistent with the concept that mitochondrial biogenesis and degradation are tightly coupled as part of the overall strategy to maintain mitochondrial homeostasis. Further studies would be required to determine if there are regional and/or parkin-dependent mechanisms for mitochondrial biogenesis and transport in TIDA versus NSDA neurons.

Conclusion

In previous chapters, region-specific difference in mitochondria bioenergetics corresponding with different amounts of mitophagosomes was observed. In the present chapter, basal aerobic mitochondrial respiration was found not to be parkin-dependent in either TIDA or NSDA neurons. The presence of parkin, however, facilitates maximal respiration during mitochondrial stress, most plausibly by maintaining the quality of mitochondria through mitophagy of defective mitochondria. Our data reveals the importance of parkin on mitochondrial structure and function in central DA neurons. Furthermore, the differences in parkin-mediated mitochondrial maintenance may be linked to the differential susceptibility of neurons to toxicant-induced injury and to neurodegeneration in PD disease.

Chapter 6. Neuroprotective effect of parkin on mitochondria in NSDA axonal terminals

Introduction

The bioactive form of MPTP, MPP^+ inhibits the ETC and inhibits mitochondrial function in various animal models (Sherer et al., 2002; Krige et al., 1992; Mizuno Y et al., 1988; Nakamura et al., 1989). Mitochondrial Complex I plays a significant role in generating the oxygen radicals that are transported into mitochondrial matrix *in vivo* Kudin et al., 2004; Adam-Vizi et al., 2006; Brand et al., 2004; Murphy, 2009). Thus, impairment of mitochondrial respiration following inhibition of mitochondrial Complex I can cause ROS in mitochondria, which may be detrimental for mitochondrial function (Murphy, 2009; Ozawa, 1997). Therefore, maintenance of mitochondrial quality control following MPTP exposure is essential for DA neuronal health. The data presented in this chapter supports the hypothesis that parkin plays a vital role in maintenance of homeostasis of the mitochondria following acute MPTP exposure.

Parkin maintains mitochondrial quality control by regulation of "mitophagy" or autophagy of mitochondria. Mitophagy successfully gets rid of damaged mitochondria, which may induce initiation of cell death programming or further ROS production Tanaka A, 2010; Chen and Chan, 2009; Youle and Narendra, 2011). In **Chapter 5**, altered mitochondrial structure and function were observed in parkin deficient mice; i.e., mitochondrial bioenergetics, mass, and the number of healthy intact mitochondria were reduced in the absence of parkin. In addition, mitochondrial Complex I inhibitor, rotenone is reported to induce mitophagy and impaired level of mitophagy was revealed in parkin KO mice (Kubli et al., 2013). Parkin is reported to have a neuroprotective role in neuronal cells and increases mean and maximum

lifespan by improving mitochondrial morphology and mitochondrial dynamics (Rana et al., 2013). Therefore, in the present study, the neuroprotective effects of parkin on mitochondria in NSDA axonal terminals was investigated by; 1) introducing parkin via adeno-associated virus (rAAV)-hParkin in parkin deficient mice and determining mitochondrial respiratory capacity in NSDA axonal terminal regions, and 2) overexpressing parkin in WT mice and determining the effect of mitochondrial Complex I inhibition on mitochondrial function and mitophagy.

AAV is a single stranded DNA dependovirus, which can infect both mitotic and post-mitotic cells such as neurons without pathogenesis (Xiao et al., 1998; Tenenbaum et al., 2004). In this dissertation, AAV serotype 2/5 was utilized based on previous studies from the collaborators and our laboratory. AAV2 is extensively characterized and utilized in clinical trials with the highest biosafety level among viral vector systems currently in use (Grimm et al., 2003). For the maximum efficiency for viral infection and its expression, AAV2 mixed with capsid from AAV5, AAV2/5 was utilized in this study. Successful transduction of AAV-parkin into DA neurons in the hypothalamus, SN and ST was confirmed previously (McFarland et al., 2009; Manfredsson et al., 2009; Manfredsson et al., 2007; Benskey et al., n.d.).

The results from these studies reveal that human parkin tagged with flag was successfully packaged into AAV and delivered into the SNpc by unilateral or bilateral stereotaxic injection. Exogenous parkin expression in parkin null mice had no effect on mitochondrial respiratory capacity or the inhibitory effect of MPTP on basal respiration in WT mice. MPTP reduced maximum and spare respirations associated with a decrease in mitochondrial protein in WT mice, however, MPTP did not have an effect on maximum or spare respirations or level of mitochondrial protein in parkin overexpressed mice. MPTP exposure and parkin overexpression upregulated the autophagy activation marker, LC3-II. Therefore, parkin may have

neuroprotective effect on NSDA neurons by maintaining viable mitochondria through mitophagy following acute MPTP exposure.

Results

Effect of parkin rescue on mitochondria from NSDA axon terminals in parkin KO mice

Mitochondria in NSDA axon terminals had altered function and structure in parkin KO mice. Mitochondrial respiratory capacity, mass, and the number of healthy, intact mitochondria were all lower in parkin KO mice compare to WT mice (**Chapter 4**). To test whether parkin is able to rescue altered mitochondrial function, parkin was expressed in parkin null mice by stererotaxic unilateral injections of rAAV-F-hParkin into SNpc as described in **Chapter 2**. Four weeks later mitochondrial function was examined. rAAV-F-hParkin was injected into left SNpc – ipsilateral to the parkin injection site (ipsi parkin). The right or contralateral SNpc (contra parkin) did not receive an injection and was utilized as an internal control. The sham group followed same procedures of surgery and care, but was injected with saline. The success of transduction of the virus in DA neurons was validated by immunoreactivity to TH and FLAG in the ventral mesencephalon and confirmed by immunohistochemistry and Western blot (Tanida et al., 2008). SM were isolated from ST and mitochondrial bioenergetics was measured using a Seahorse XF 24 analyzer.

OCR of ST-derived synaptosomes from rAAV-F-hParkin injected (parkin ipsi), non-injected (parkin contra), and saline injected (sham) mice were measured. Compound A: olygomycin, B: FCCP, C: rotenone were injected *ex vivo* into the synaptosomes (**Figure 6.1 A**). The parkin contra uninjected control group had the lowest OCR following 5mM pyruvate /2.5mM malate (basal respiration), than either parkin ipsi or sham groups. Oligomycin treatment (proton leak) did not change the trend. FCCP injection (maximum respiration) caused similar

OCR between parkin ipsi and sham, but parkin contra had much lower OCR and this trend was also observed with rotenone injection. This experiment was repeated 5 more times and based on these mitochondrial bioenergetics profile, mitochondrial basal, maximum, and spare respirations were calculated. Basal respiration of sham was 233 ± 19.7 pMoles/min, parkin contra was 161 ± 25.1 pMoles/min, and parkin ipsi was 188 ± 17.7 pMoles/min (**Figure 6.1 B**). Maximum respiration of sham was 494 ± 33.1 pMoles/min, parkin contra was 428 ± 52.8 pMoles/min, and parkin ipsi was 528 ± 41.1 pMoles/min (**Figure 6.1 C**). Spare respiration of sham was 259 ± 29.7 pMoles/min, parkin contra was 273 ± 28.3 pMoles/min, parkin ipsi was 345 ± 37.9 pMoles/min (**Figure 6.1 D**). There was a trend that maximum and spare respirations of parkin ipsi was higher than parkin contra, however, the differences was not statistically significant.

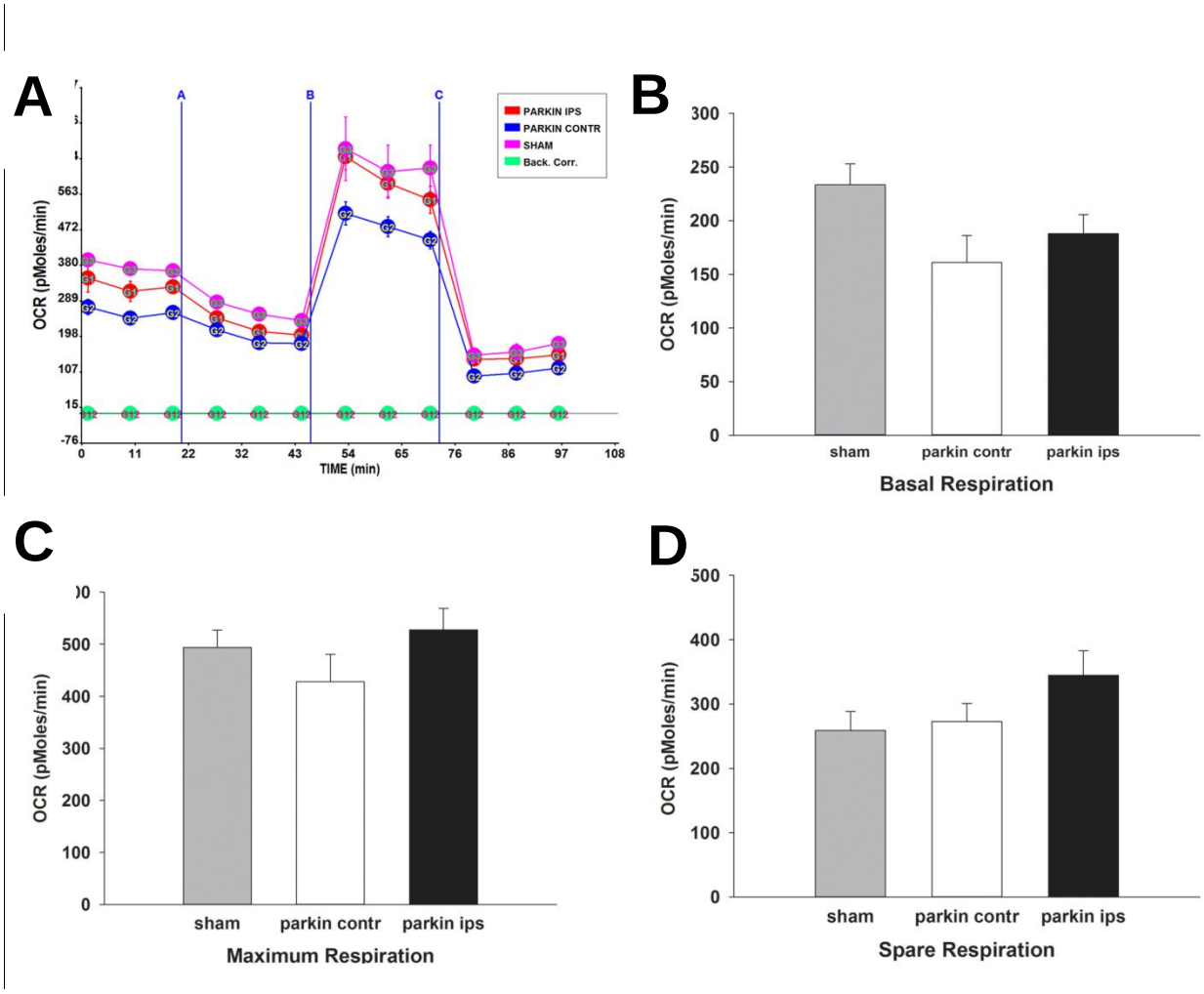

Figure 6.1 Effect of exogenous parkin expression on ST-derived SM containing NSDA axonal terminals in parkin null mice. Panel A, Mitochondrial bioenergetics profile of Seahorse XF analyzer. Eighteen parkin null mice (n=6 per group) received unilateral stereotaxic injections of 500 nl rAAV-F-hParkin (3.4 x 10^{13} vg/ml) or 500 nl saline in ipsilateral SNpc. Parkin contralateral was not injected and used as an internal control. Four-weeks following stereotaxic surgery, synaptosomes were isolated from mouse ST using Percoll gradient and centrifugation, and quantified by BCA assay. Fifteen to 20 µg SM respiration was examined by using Seahorse XF24 analyzer measuring OCR: injection port A: oligomycin 3 µM, injection port B FCCP 3 µM, and port C: Rotenone 2.5 µM. ● indicates ST-derived SM from ipsilateral side to SN injected with rAAV-F-hParkin. ● indicates ST-derived SM from contralateral side SN, which does not have any injection. ● indicates sham, which is injected with saline. Representative bar graph of basal respiration (Panel B), maximum respiration (Panel C), spare respiration (Panel D). Columns represent mean OCR of synaptosomal mitochondria + 1 SEM. Sham is stereotaxically injected with saline. Parkin contr (parkin contralateral) has no injection. Parkin ips (parkin ipsilateral) has rAAV-F-hParkin injection.

Effect of parkin overexpression on mitochondria in NSDA axon terminals following single acute MPTP exposure in WT mice

Differential toxic effects on TIDA and NSDA neurons are correlated with differential parkin expression following acute single MPTP exposure (Schapira et al., 1989; Imam et al., 2006). In **Chapter 4** the effects of MPTP were compared in mitochondria and cells in ventral mesencephalon and MBH where NSDA and TIDA cell bodies reside. In these studies, SM respiratory capacities were reduced by mitochondrial Complex I inhibitor *ex vivo* exposure and mitochondria are diminished in SNpc *in vivo* exposure. Therefore, in the present study, possible protective effect of parkin overexpression following MPTP acute single exposure was investigated. Parkin was overexpressed in WT mice by stereotaxic bilateral injections of rAAV containing flag tagged hParkin in the SNpc and the effect of parkin on mitochondrial function was determined. rAAV-F-hParkin was injected into both sides of SNpc with sham mice receiving saline injections, which does not contain rAAV-F-hParkin. Four weeks after the surgery, the mice were treated with MPTP or saline vehicle and killed 24 h later. ST was dissected and synaptosomes containing mitochondria are isolated and mitochondrial bioenergetics were measured using a Seahorse XF analyzer (**Figure 6.2**).

Success of rAAV-F-hParkin transduction in SN was confirmed by quantitative immuno blotting. Parkin expression by rAAV-F-hParkin injection was revealed by increased immunoreactivity to parkin in rAAV-F-hParkin injected mice compare to vehicle-injected mice (**Figure 6.3**).

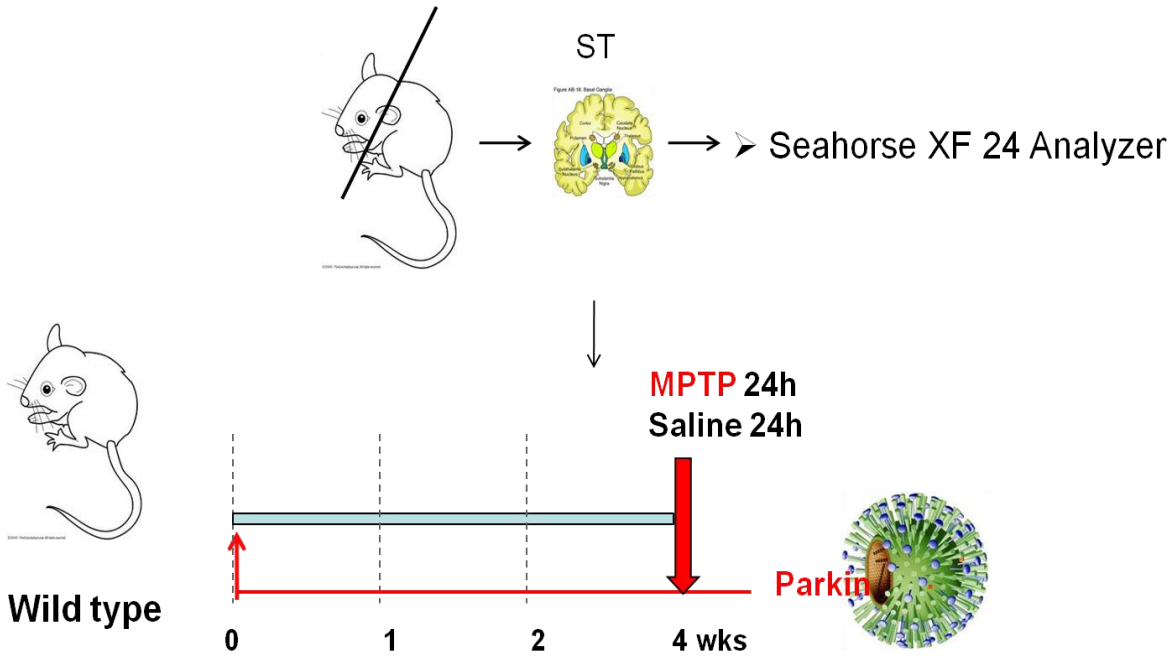

Figure 6.2 Schematic depicting the experimental design of MPTP treatment in parkin overexpressed WT mice. Mice were stereotaxically injected with either 500 nl of rAAV-F-hParkin (3.4×10^{13} vg/ml) or saline bilaterally into the SNpc. Four weeks after stereotaxic surgery, 8 mice (4 injected with rAAV-F-hParkin and 4 with saline) were injected sc with MPTP and the other 8 with saline for 24 h before killing (n=4). ST will be dissected and SM were isolated from ST. Isolated SM bioenergetics will be examined by a Seahorse XF analyzer.

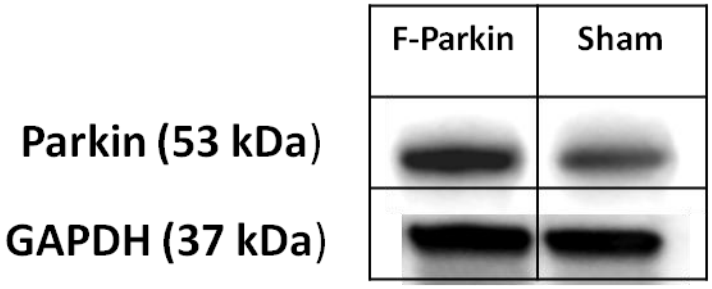

Figure 6.3 Confirmation of rAAV-F-hParkin expression within the SNpc. Twenty-four mice (n=6 per group) received bilateral 500 nl stereotaxic injections of rAAV-F-hParkin (3.4×10^{13}) or saline (sham group) in SNpc. Four weeks following injection, mice were sacrificed and parkin protein was measured in the SNpc of rAAV-F-hParkin injected and sham group.

SM bioenergetics profile of the four groups was determined using a Seahorse XF analyzer (**Figure 6.4 A**). The four groups are: 1) MPTP parkin - parkin expressed mice treated with MPTP. 2) MPTP sham - sham mice treated with MPTP. 3) vehicle parkin – parkin expressed mice treated with saline. 4) vehicle sham - sham mice treated with saline. MPTP reduced OCR in sham mice, but not in parkin expressed mice when OCR is measured in SM incubation media with substrate 5 mM pyruvate and 2.5 mM malate (basal respiration). There was no difference among all four groups in olygomycin *ex vivo* injection (proton leak). FCCP *ex vivo* injection induced difference in OCR among groups; MPTP reduced OCR in sham mice, but did not change OCR in parkin expressed mice (maximum respiration). The experiment was repeated 5 more times and basal, maximum, spare respiratory capacities of MPTP treated groups were normalized to vehicle groups. However, SM of one experiment group did not have RCR' greater than 3 indicating poor mitochondrial quality, and another experiment group failed to measured repeated OCR measurement. The total sample size of the experiments was four.

MPTP reduced basal respiration in both sham (to 81 ± 5.7 % control) and parkin expressed mice (to 76.8 ± 6.2 % of control) (**Figure 6.4 B**). Maximum respiration of sham mice was reduced to 71.9 ± 4.1 % by MPTP treatment, but in parkin expressed mice the effect of MPTP was attenuated (94.0 ± 9.0 %) (**Figure 6.4 C**). Spare respiration of sham was reduced to 68.5 ± 3.86 %, whereas in parkin expressed there was no change (102 ± 11.8 %) compared with OCR following vehicle treatment (**Figure 6.4 D**). In sham mice, MPTP reduced maximum and spare respirations by about 30 %. However, in parkin expressed mice, MPTP failed to reduce maximum or spare respirations.

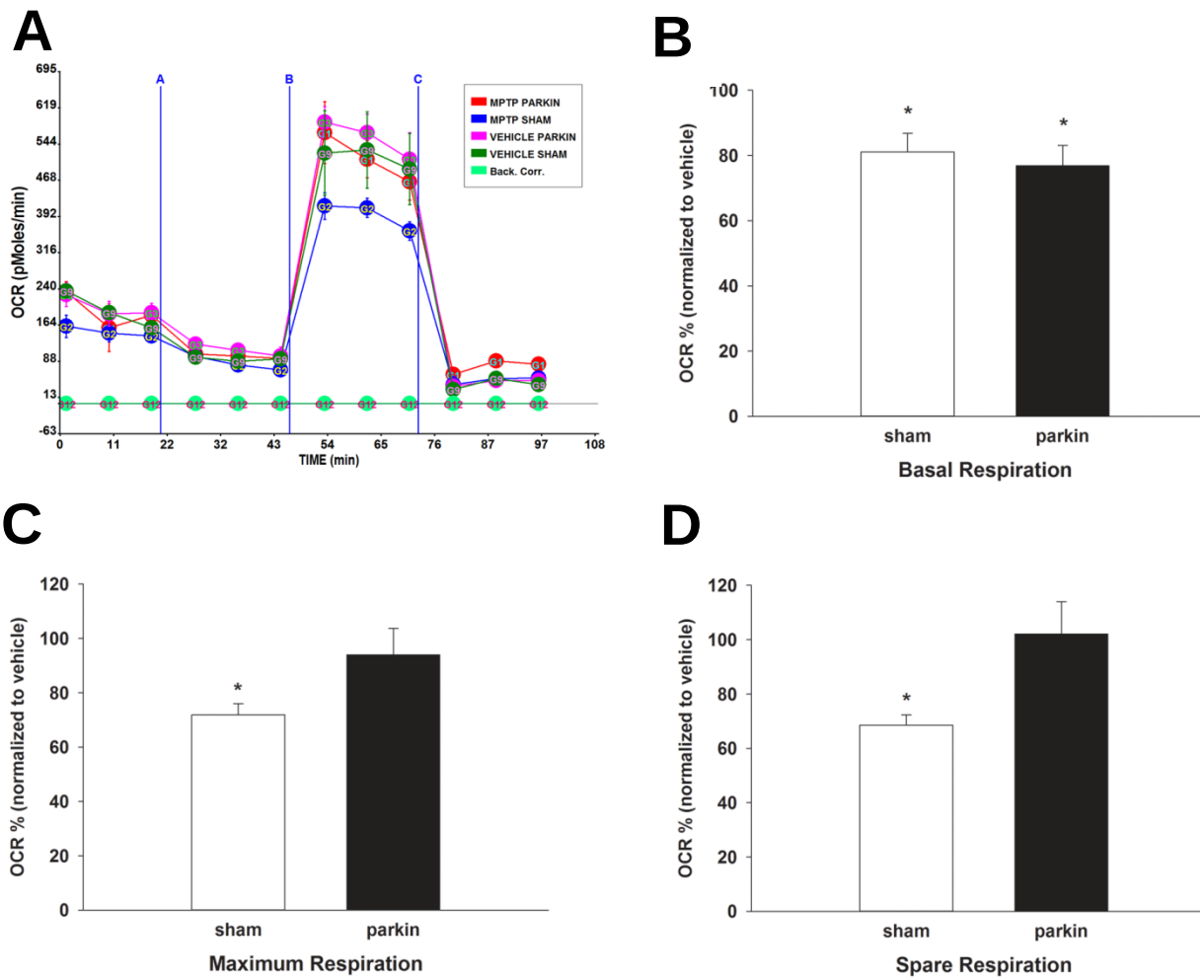

Figure 6.4 Effects of parkin expression on SM respiration following single acute exposure to MPTP in WT mice. Panel A, Mitochondrial bioenergetics profile of Seahorse XF analyzer Synaptosomes were isolated from mouse ST using Percoll gradient and centrifugation, and quantified by BCA assay. Fifteen to 20 µg SM respiration was examined by using Seahorse XF24 analyzer measuring OCR: injection port A: oligomycin 3 µM, injection port B FCCP 3 µM, and port C: Rotenone 2.5 µM. ● indicates SM derived from ST injected with rAAV-F-hParkin in MPTP treated mice. ● indicates SM derived from ST injected with saline in MPTP treated mice. ● indicates SM derived from ST injected with rAAV-F-hParkin in vehicle treated mice. ● indicates SM derived from ST injected with saline in vehicle treated mice. Representative bar graph of basal respiration (Panel B), maximum respiration (Panel C), and spare respiration (Panel D). Columns represent mean OCR of MPTP treated groups were normalized by vehicle group + 1 SEM. OCR of MPTP treated divide by vehicle treated group of sham or rAAV-F-hParkin group. The values are expressed in % . (*) OCR of synaptosomal mitochondria with single acute MPTP exposure is significantly different from saline-treated controls with $p < 0.05$.

Effect of MPTP in mitochondria mass in the SNpc was investigated by quantifying immunoreactivity to cytochrome oxidase subunit IV (COX IV). COX IV expression was normalized to glyceraldehyde 3-phosphate dehydrogenase (GAPDH) as a housekeeping gene (Barber et al., 2005). COX IV expression was reduced in sham mice with a single acute exposure to MPTP; about 20% of COX IV expression was lost (**Figure 6.5**). COX IV expression in sham mice was different from both of the vehicle groups (parkin overexpressed and sham mice). Parkin overexpressed mice showed somewhat of a reduction in COX IV expression, however, the difference was not statistically significant.

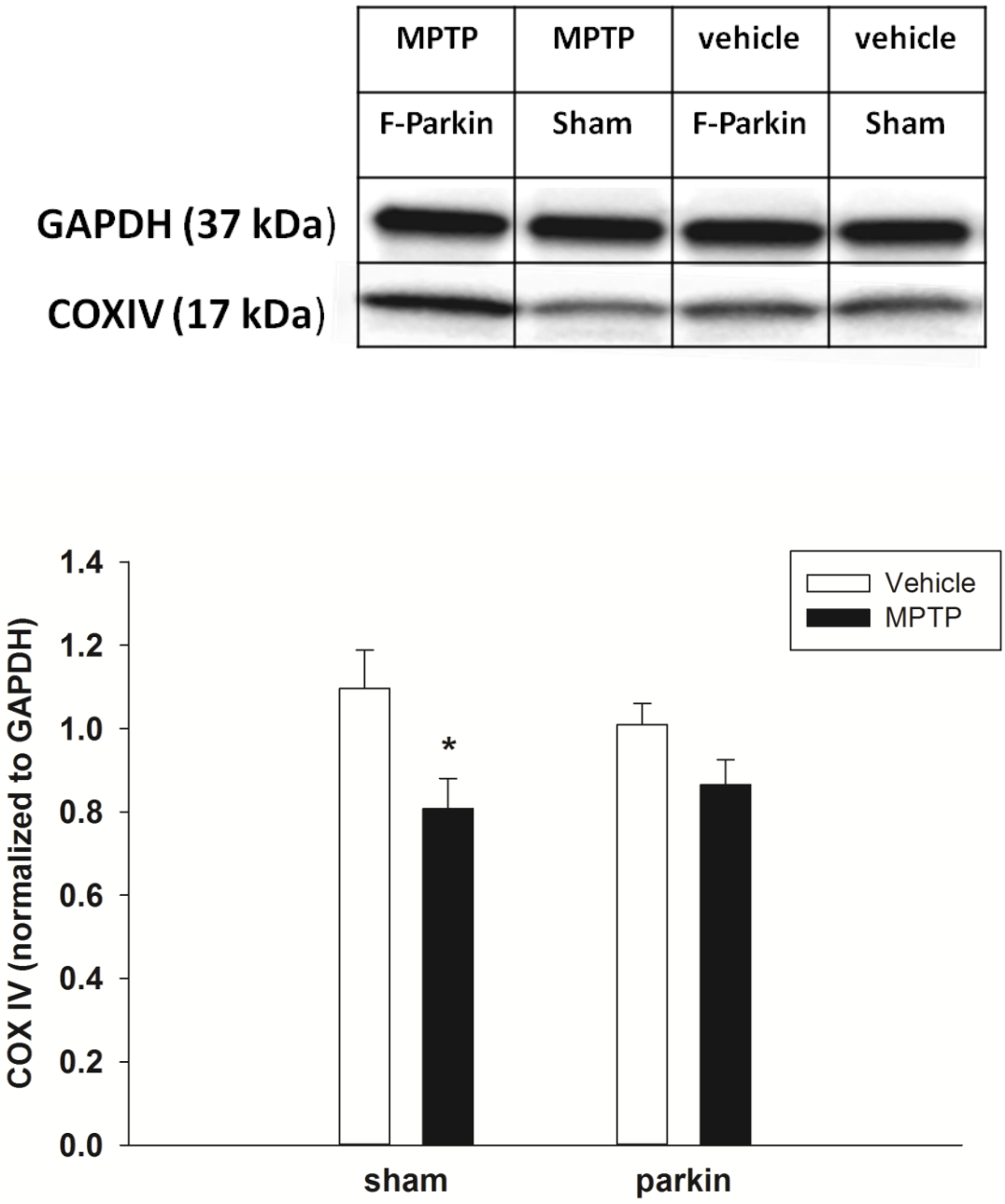

Figure 6.5 The effects of parkin expression on COX IV in SNpc following single-acute MPTP exposure. Twenty-four mice (n=6 per group) received bilateral 500nl stereotaxic injections of AAV-hParkin (3.4×10^{13}) or saline (sham group) in SN. Four-weeks following injection, mice were injected with saline (10ml/Kg; s.c.) or MPTP (20mg/Kg; s.c.) and were sacrificed 24 h later. Cox IV expression in SN were determined by Western blot and were normalized to GAPDH. Columns represent mean COX IV expressions + 1 SEM. (*) Cox IV expression in SN with single acute MPTP exposure is significantly different from saline-treated controls ($p < 0.05$).

Neuroprotective effect of parkin on mitochondria via upregulation of autophagy with single acute MPTP exposure

Parkin plays an important role in mitochondrial quality control via mitophagy (Sauerbeck et al., 2011; Rogers et al. 2011). Pink-1 surrounding damaged mitochondria recruits parkin onto the mitochondria. Parkin ubiquitinates mitochondrial outer membrane proteins and promotes mitochondria engulfing into autophagosomes. Parkin recognizes its substrate protein (or cytosolic organelles) and recruits the substrates to autophagy machinery via lys63 poly-ubiquitination (Olzmann et al., 2007). Therefore, the protective effect of parkin on mitochondria may be mediated by autophagy. In this study, the level of autophagy was identified by measuring the level of microtubule-associated protein 1A/1B-light chain 3 (LC3) activity (Nakatogawa et al. 2007).

LC3 is a cytosolic protein with a molecular mass of 17kDa and is well known molecular marker for autophagy. When the cells undergo autophagy, LC3-I is conjugated at the c-terminus with phosphatidylethanolamine in autophagic membranes and forms LC3-II, which can be found in autophagosomal membranes or isolated membranes (Tanida et al., 2008). Therefore, autophagy can be measured by the relative expression of LC3-I and LC3-II. The ratio of LC3-II to LC3-I was increased approximately 60 % following single acute MPTP exposure in sham mice (**Figure 6.6**). However, the difference was not statistically significant due to small sample size. The power analysis indicated that the mean LC3-II/LC3-I ratio in MPTP-treated mice (0.20) and the mean LC3-II/LC3-I ratio in vehicle-treated mice (0.13) with 0.08 sigma required a sample size of 10 mice per group with $\alpha = 0.05$. The ratio was upregulated with parkin expression alone and there was no difference following MPTP exposure.

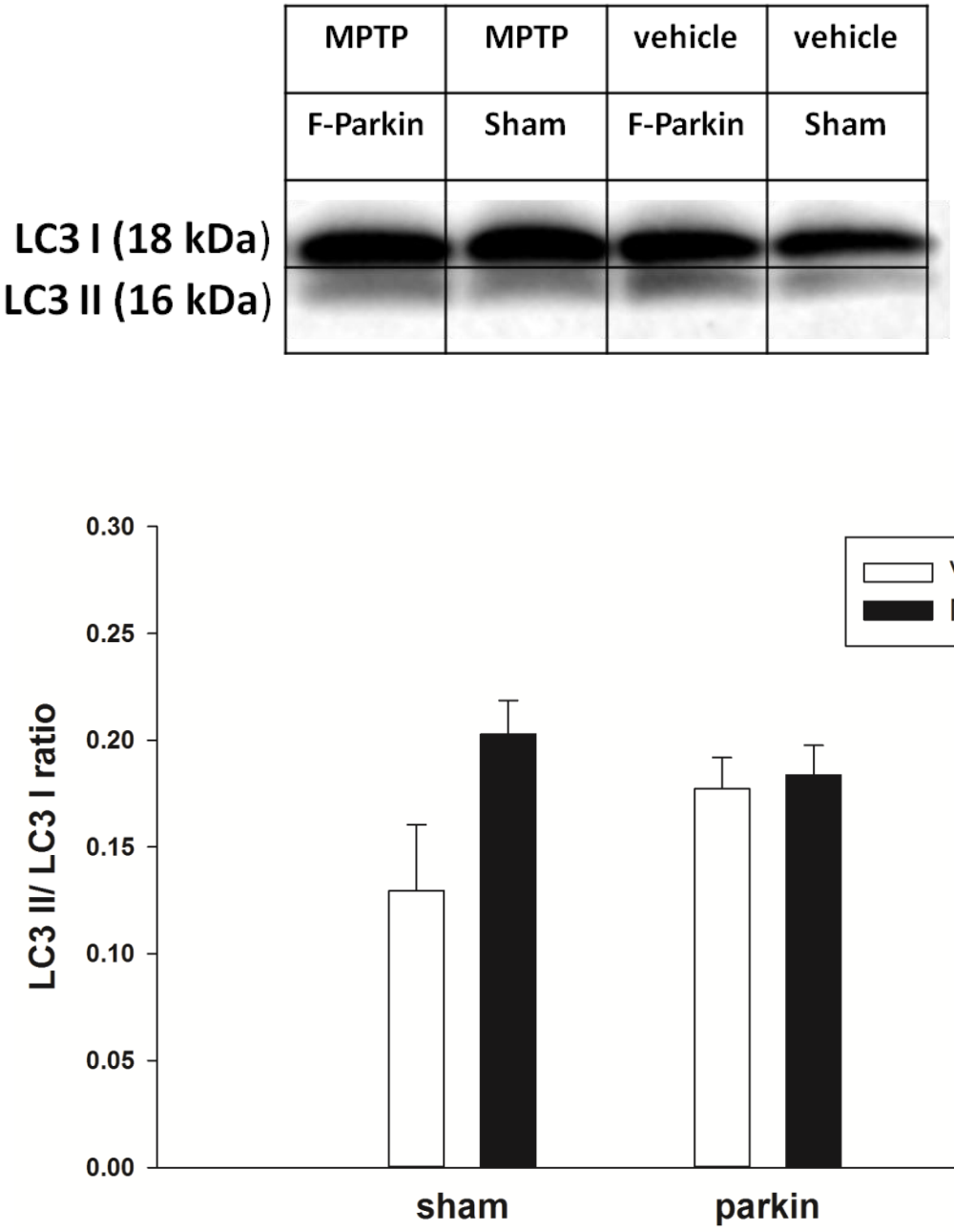

Figure 6.6 The effects of parkin expression on markers of autophagy in SN following single-acute MPTP exposure. Twenty-four mice (n=6 per group) received bilateral 500 nl stereotaxic injections of AAV-hParkin (3.4×10^{13}) or saline (sham group) in SNpc. Four-weeks following injection, mice were injected with either saline (10ml/kg; s.c.) or MPTP (20mg/kg; s.c.) and were sacrificed 24 h later. Levels of LC3-II and LC3-I in SN were determined by Western blot and ratio of LC3-II and LC3-I was calculated; LC3-II divided by LC3-I. Columns represent mean ratio of LC3-II to LC3-I expression + 1 SEM.

Effect of parkin expression on TH in NSDA axon terminals following single acute MPTP exposure

The above results suggest that parkin expression has a protective effect on mitochondria. Next, the effect of parkin expression on TH expression in SNpc following single acute exposure to MPTP was investigated. TH is rate-limiting step for DA synthesis and a phenotypic marker for NSDA neurons. TH was reduced to a similar extent by MPTP treatment in sham and parkin expressed mice (**Figure 6.7**). MPTP reduced about 30 % of TH expression in SN of sham mice and about 20 % of TH expression in SN of parkin expressed mice.

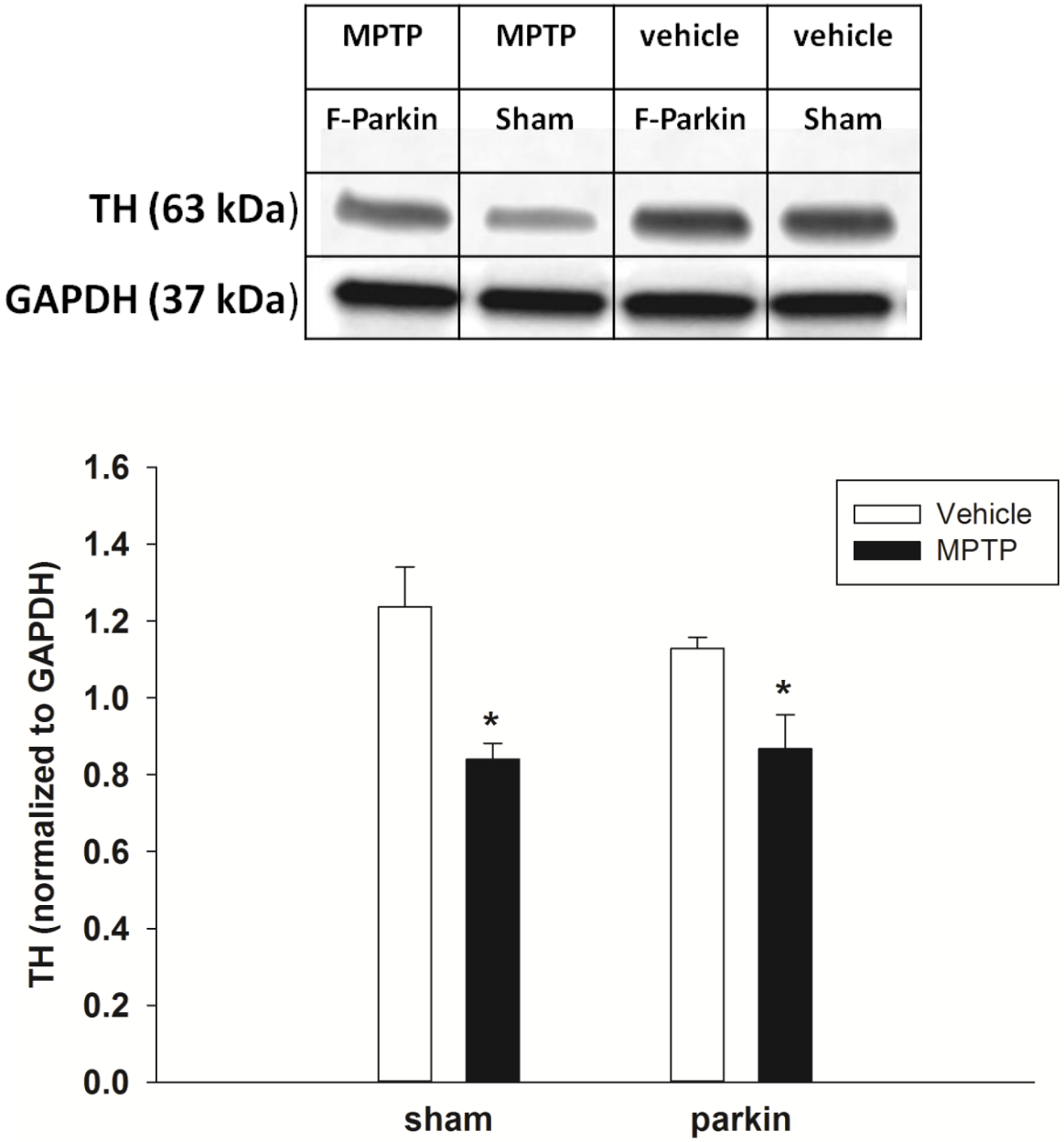

Figure 6.7 The effects of parkin expression on TH expression in SN following single-acute MPTP exposure. Twenty-four mice (n=6 per group) received bilateral 500 nl stereotaxic injections of AAV-hParkin (3.4×10^{13}) or saline (sham group) in SN. Four weeks following injection, mice were injected with either saline (10ml/kg; s.c.) or MPTP (20mg/kg; s.c.) and were sacrificed 24 h later. TH expression in SN was determined by Western blot and normalized to GAPDH. Columns represent mean TH expression + 1 SEM. (*) TH expression in SN with single acute MPTP exposure is significantly different from saline-treated sham and parkin expressed controls ($p < 0.05$).

Discussion

Parkin null mice (B6.129S4-*Park2*^{tm1Shn}/J strain) have EGFP replaced in exon 3, which results in a frame shift and absence of full parkin gene product; mRNA contains exon 2 spliced to exon 4 (omitting exon 3) and premature stop codon in exon 5 (Zhang Z-X et al., 2006). Parkin KO mice had increased sensitivity to cardiovascular disease morbidity and mortality caused by abnormal mitochondria morphology in myocytes (Kubli et al., 2013). Myocytes of parkin null mice contained large clusters of small round mitochondria, and myocardial infarction is associated with swollen and severe cristae remodeling due to impaired mitophagy. Mitochondrial dysfunction with an absence of parkin was also reported in a Drosophila model. Parkin null mice show only mild impaired coordination without loss of DA neurons, however, abnormal mitochondrial physiology, morphology and less mitochondria are identified from NSDA axonal terminals (Greene et al., 2003) (**Chapter 5**).

Data presented in this chapter show that parkin exogenous expression in the SN of parkin null mice did not rescue mitochondrial respiratory capacity. In parkin null mice, other parallel pathways of mitochondrial quality control may compensate for maintaining mitochondrial function. RNF185 and GIDE (also called MULAN) are identified as other E3 ubiquitin ligases of mitochondria (Goetz 2011; Charcot 1872). RNF185 is shown to mediate mitochondrial autophagy and MULAN is reported to regulate mitochondrial dynamics and signaling between mitochondria and nucleus through NF-κB. Another factor to consider is that the parkin null mice used in these studies were housed free from environmental toxins, stress, injury, or infections. Over 90 % of PD is idiopathic and there is no known family history of PD (Goetz 2011). PD shows a complex relationship between genetic and environmental factors. For example, people with genetic polymorphisms of cytochrome P450 (CYP)2D6 (a liver enzyme that metabolizes

xenobiotics), solute carrier family 6 member 3 (SLC6A3) (DAT gene), Praoxonase 1 (PON1) are reported to have increased risk of developing PD by pesticides exposure (Goetz 2011; Charcot 1872; Eeden 2003). Conversely, people with mitochondrial enzyme MAO-B and antioxidant glutathione S-transferase (GST) polymorphisms had lower risk of developing PD with smoking (Goetz 2011; Checkoway et al., 1998). Ageing can be an additional factor for altered mitochondrial phenotype in parkin null mice. A four week time period may not be sufficient time for the cells to adapt to synthesize more mitochondria and change in mitochondrial bioenergetics. In addition, the amount of parkin expression by AAV may not be sufficient for parkin null mice to recover mitochondrial function.

In contrast to parkin expression in parkin null mice, mitochondria in parkin expressed WT mice revealed a protective effect of parkin on mitochondria in ST and SN following single acute exposure to MPTP. Inhibition of basal respiration was not prevented by parkin expression. MPTP inhibited basal respiration of both sham and parkin expressed mice to the same extent. This confirms inhibitory effect of MPTP on mitochondrial function in NSDA axon terminal and explains reduced TH expression in both sham and parkin expressed mice. Intriguingly, MPTP inhibited maximum and spare respirations in sham mice, but MPTP did not inhibit maximum and spare respiration in parkin expressed mice.

In **Chapter 4**, transient accumulation of MPP^+ *ex vivo* and mitochondrial membrane potential and energy dependent transportation of MPP^+ to mitochondria was discussed (Bernheimer et al., 1973; Scotcher et al., 1991; Ramsay et al., 1986; Ramsay and Singer 1986). One hundred µM MPP^+ *ex vivo* treatment failed to inhibit basal, maximum, and spare respirations, and synaptosomes in high MPP^+ concentration showed less inhibitory effect on maximum and spare respirations compare to basal respiration. Uncouplers are reported to not

only prevent MPP^+ uptake into mitochondria but also induce exportation of MPP^+ from mitochondria and prevent MPP^+ from binding to mitochondrial Complex I (Goetz 2011; Ramsay and Singer 1986). Therefore, FCCP *ex vivo* injection may trigger outflow of MPP^+ and dissipate MPP^+ accumulation in mitochondria. This explains the recovered maximum and spare respiration with FCCP *ex vivo* treatment in parkin expressed mice. However, OCR was continuously reduced with FCCP *ex vivo* treatment in sham mice. This suggests the difference in mitochondrial capacity in sham mice is not from inhibitory toxicity of MPP^+, but from reduced viable mitochondria in sham mice. This is consistent with the results presented in **Chapter 4**; i.e., MPTP reduced mitochondrial protein in TH immunoreactive cells from SN. In the study presented in this chapter, Western blot analysis confirmed reduced mitochondrial protein COX IV following MPTP exposure in sham mice, however, MPTP failed to reduce COX IV in parkin expressed mice. This indicates that even though MPP^+ is still bound to mitochondria and inhibits mitochondrial respiration, parkin expression prevented loss of functional/viable mitochondria. Parkin expression prevented further damage to mitochondria in NSDA neurons by MPTP. This suggests that when NSDA neurons are free of neurotoxin, parkin promotes mitochondrial recovery but the endogenous level of parkin in NSDA neurons are not able to recover due to loss in viable mitochondria.

Mitochondrial Complex I inhibitor, rotenone was reported to induce mitophagy and the absence of parkin caused impaired mitophagy in cardiocytes exposed to rotenone (Kubli et al., 2013). In my study, similar mitochondrial Complex I inhibitor, MPTP increased autophagy markers and parkin overexpression upregulated autophagy markers as well. This indicates increase in autophagy of mitochondria may play a significant role in the protective effect of parkin in single acute MPTP exposure.

Autophagy has a neuroprotective role in ageing and neurodegenerative diseases. Increases in the autophagy protein Atg8 induced increased life span in drosophila and resistance to oxidative stress (Goetz 2011). However, in the absence of the autophagic protein Atg 7, drosophila were vulnerable to starvation and oxidative stress and showed a decrease in life span and an increase in ubiquitin-positive aggregates in the brain (Goetz 2011). Atg 7 KO mice are reported to have massive neuronal loss with impairment of coordination of the movement. The mice died early and the pathology of the neurons contained inclusion bodies composed with polyubiquitinated proteins without any proteosomal dysfunction (Goetz 2011). Lewy body, a neuronal inclusion body in PD, is composed of α-synuclein accumulations. Aberrant α-synuclein caused inhibition of autophagy, but when autophagy was induced by Beclin 1, α-synuclein accumulation was reduced (Goetz 2011; Charcot 1872). Aberrant α-synuclein expression is also reported to be associated with mitochondrial dysfunction and an increase in colocalization of autophagosomes and mitochondria (Goetz 2011). In addition to α-synuclein, genetic factors of PD, LRRK2, DJ-1, PINK1, and PARKIN are also involved in mitophagy (Goetz 2011; Charcot 1872; Eeden et al., 2003). Therefore, upregulation of autophagy in mitochondria by parkin overexpression may a play significant role in protecting mitochondria from mitochondrial Complex I inhibitor.

Intriguingly, in parkin overexpressed mice, MPTP did not induce higher levels of autophagy than vehicle-treated controls. Parkin overexpression had increased basal levels of autophagy and the level of autophagy did not alter with MPTP exposure, but the mitochondrial protein level was still protected from MPTP single acute exposure. Increase in autophagy markers can be due to either reduction in clearance of autophagosomes (also called "autophagic stress") or true increases in autophagy. Autophagic stress may cause increased autophagy

markers in response to MPTP exposure, however, overexpression of parkin may prevent autophagic stress and the basal level of autophagy may not be altered. Since autophagosomes are cleared as soon as the autophagosomes are formed, the level of autophagosomes may not be altered. In addition, this may also indicate that parkin overexpression does not overly activate autophagy; parkin overexpression maintained the balance of autophagy induction. Although autophagy has neuroprotective effects, overactivation of autophagy can be toxic to neurons. Excessive autophagy activation can cause axonal dystrophy, neurite degeneration, neuronal atrophy, and cell death (Goetz 2011; Charcot 1872). Autophagy-related therapies in neurodegenerative disease are limited by the inability to regulate autophagy activation. Therefore, parkin, allowing neurons to maintain homeostasis of autophagy while protecting mitochondria from neurotoxin, may provide a novel therapy for PD.

Conclusion

Parkin exogenous expression in parkin null mice failed to restore altered mitochondrial function in axon terminals of NSDA neurons. This suggests that reversal of genetic factor parkin deficiency alone is not sufficient to affect pathophysiology in PD, and another mitochondrial E3 ubiquitin ligase such as RNF185 and GIDE may compensate for absence of parkin in parkin null mice. Mitochondrial Complex I inhibitor, MPTP, impacted mitochondria in NSDA axon terminals even with parkin overexpression in WT mice. However, parkin overexpression rescued viable mitochondria from MPTP exposure, and mitochondrial function was restored with uncoupler *ex vivo* treatment in parkin overexpressed mice possibly through activation of autophagy. Therefore, **loss of parkin mediated mitochondrial quality control may contribute to DA neuronal degeneration in MPTP single acute exposure and pathogens of PD.**

Chapter 7. General Discussion and Concluding Remarks

Insights on the role of mitochondria in pathophysiology of PD

Mitochondrial dysfunction is involved in the pathogenesis of PD as indicated by 1) the reduction of mitochondrial Complex I activity in SN and various tissues (Schapira et al., 1989; Mizuno et al., 1989; Goetz 2011; Bindoff et al., 1991), 2) an increased mtDNA deletion, 3) the role of environmental factors such as organochlorines, rotenone, paraquat, and MPTP, 4) the role of genetic factors such as parkin (*park2*), PINK1 (*park6*), DJ-1 (*park7*), LRRK2 (*park8*), NDUFA10 (candidate gene of *park11*), TIMM8A(candidate gene of *Park12),* HTRA2 (*park13*), FBX07 (*park15*),and EIF4G1 (*Park18*). These findings suggest that mitochondrial maintenance is critical to prevent NSDA neuronal degeneration in PD.

Mitochondria are essential organelles that regulate eukaryotic cellular metabolism of β-oxidation of fatty acids, oxidative phosphorylation, ROS, Ca^{2+} homeostasis, and apoptosis. ATP produced by mitochondria (oxidative phosphorylation) is the major energy source for eukaryotic cells. Since NSDA neurons have long axons lacking myelin, they require high ATP levels for the synapse and dendritic spine formations, and impulse transmission along the axons (Donkelaar 1998). DA synthesis, DA uptake into vesicles, and release into synapse requires ATP. Therefore, healthy, functional mitochondria, as the main energy supply, are vital for the maintenance of NSDA neurons. However, in my studies, mitochondrial function and mass were much lower in NSDA neurons than in TIDA neurons which could explain why NSDA neurons are more susceptible to cell death resulting in PD.

Another important role of mitochondria is the regulation of ROS. Oxygen radicals are generated through ETC during the re-dox process. Mitochondria also remove ROS by various

antioxidants, such as glutathione, and function as a ROS buffer (Koopman et al., 2010) . Therefore, mitochondria are exposed to high levels of ROS, which can damage lipid, protein, and DNA. This inhibits various cellular processes and cytosolic organelles causing apoptosis (Ozawa 1997). Since intracellular DA is highly oxidative, mitochondrial regulation and vulnerability to ROS may contribute to NSDA neuronal degeneration in PD.

In addition to mitochondria as the regulators of ATP synthesis and ROS, mitochondria have intracellular Ca^{2+} buffering capacity, which is vital for DA neurons. In autonomous pacemaking activation (pulsatile activity in the absence of synaptic input) Ca^{2+} enters NSDA neurons via the L-type Cav 1.3 Ca^{2+} channel. Excitotoxity activation of the gluatamate N-methyl-D-aspartate (NMDA) receptor can cause excess Ca^{2+} influx into the NSDA neuronal cells (Grace et al., 1983). Furthermore, Ca^{2+} influx into mitochondria can cause the opening of permeability transition pores, which releases cytochrome c resulting in apoptosis. Therefore, mitochondrial homeostasis is vital for maintenance of NSDA neuron function.

Basal mitochondrial differences between TIDA and NSDA neurons

NSDA neurons play a significant role in regulating the motor system, functioning as a "kick starter" of initiation for the motor response and a " modulator" of motor neuron inhibitory signaling (as described in **Chapter 1)** (Goetz 2011). In PD, these NSDA neurons are lost. By the time PD patients present with clinical symptoms about 60 % of their NSDA neurons have been lost with a 70-90 % reduction in DA signaling in ST (Goetz 2011; Bernheimer et al., 1973). Similar to NSDA neurons, mesolimbic and mesocorical neurons are also partially affected by PD, however, TIDA neurons are not affected (Matzuk et al., 1985; Langston et al., 1978; Jellinger 1991; Braak et al. 2000).

Therefore, in my research, mitochondrial structure and function of NSDA and TIDA neurons in WT mice were characterized. Maximum and spare respiratory capacities were higher in synaptosomes containing TIDA axon terminals compare to NSDA axon terminals. Higher mitochondrial bioenergetics was correlated with increased mitochondrial mass and membrane potential in axons terminals in MBH compared to ST. Also, the difference in mitochondrial mass between brain regions SNpc (NSDA neuronal cell body) and ARC (TIDA neuronal cell body) was confirmed by confocal microscopy. In addition, TEM analysis revealed a higher number of mitochondria per synaptosome, but no morphological differences were observed in MBH compared to ST similar to previous findings among different subpopulations of DA neurons (Fahn1996). In addition, mitochondrial function differed across brain regions (cortex, striatum, hippocampus, and cerebellum) (Brand et al., 2011). Therefore, TIDA neuronal resistance may relate to increased mitochondrial function and mitochondrial mass.

From basal mitochondrial differences to the big picture: neuronal and environmental toxicants

Although mitochondrial function and mass differ between NSDA and TIDA neurons in WT mice, mitochondria isolated from the brain regions containing NSDA and TIDA axon terminals showed no difference in response to the mitochondrial Complex I inhibitor, rotenone. Mitochondrial respiratory capacities were reduced by rotenone in a concentration-dependent manner with similar percent reductions and IC50. This suggests the axon terminal mitochondrial characteristics are not responsible for the differential susceptibility of NSDA and TIDA neurons to neurotoxicant exposure. Differential susceptibility of the central DA neurons may be due to differences in compensatory mechanism or characteristics of the cells and their environments.

Previous studies in our laboratory have shown that single acute exposure to MPTP caused a loss of DA concentration and TH expression in NSDA neurons. However, TIDA neurons had a loss of DA but recovered and did not have any loss of TH expression (Schapira et al. 1989). The steady state of MPP^+ concentrations in central DA neurons are low; cytosolic concentrations of MPP^+ was 30 μM and peak MPP^+ concentration in ST was only 78 ± 9 pg/μg (Ramsay et al.,1986; Ramsay and Singer 1986; Cleeter 1992). However, MPP^+ showed a transient inhibitory effect on mitochondria. Pharmacological blockade of DAT did not affect the inhibition of MPP^+. This indicates that MPP^+ accumulation into mitochondria was independent of MPP^+ uptake into synaptosomes. Entry of MPP^+ into the mitochondria depends on membrane potential, electrochemical gradient, and is most importantly, energy-dependent (Komatsu 2006; Ramsay and Singer 1986; Andersen 1989; Ramsay et al., 1986). Therefore, mitochondria under limited *ex vivo* conditions (restricted substrate availability and ATP demand), did not accumulate MPP^+ in high concentration. ATP demand is the driving force for ETC to generate proton gradients for ATP synthesis in the cells. DA neuronal activity requires high ATP. NSDA neurons are often activated for tonic or and phasic DA release while TIDA neurons are activated diurnally (Shieh et al., 1995; Benskey et al., 2013; Xie 2013). Mitochondrial bioenergetics, membrane potential, and energy production can differ depending on neural activities (Liang et al., 2007; Langston et al., 1983). This may allow mitochondria in NSDA neurons to accumulate MPP^+ in higher concentrations than in TIDA neurons in an electrochemical energy assisted or membrane potential dependent manner. Therefore, MPP^+ can accumulate in mitochondria depending on DA neuronal activity, resulting in a differential neurotoxic effect on the NSDA and TIDA neurons.

Another unique characteristic difference between TIDA and NSDA neurons are their locations. TIDA neurons are located next to the third ventricle, so they are readily exposed to

foreign bodies or toxins and may develop compensatory mechanisms to the exposure to metabolites or toxins. The astrocytic water transport system can remove interstitial solutes or toxins by cerebral spinal fluid (CSF) influx and efflux from the ventricles (Narendra et al., 2008). Sequestering of toxins by glial cells, such as astrocytes, and clearance of toxins via CSF flow may provide resistance to toxins in DA neurons from ARC. This explains a mitochondrial protein level reduction in non-TH immunoreactive cells of ARC while there is no difference in non-TH immunoreactive cells in SNpc after MPTP acute exposure. Sequestration of MPP^+ by non-TH cells explains recovery of TH cells in ARC, but TH cells are lost in SN. This is also consistent with recovery of DA levels in TIDA neurons and loss of DA levels in NSDA neurons after MPTP acute exposure. TIDA neurons may adapt to upregulate mitochondrial quality control to maintain mitochondrial homeostasis.

Parkin mediated mitochondrial quality control in NSDA neurons

Region-specific differences in mitochondria along with different levels of mitophagosomes were observed in ARC and SN. The differential mitophagic level in NSDA and TIDA neurons may underlie the differential susceptibility of central DA neurons in PD. Consistent with my results, differential parkin expression was observed in NSDA and TIDA neurons after a single acute exposure to MPTP (Schapira et al., 1989).

Mutation in parkin is the most common cause for autosomal recessive early-onset PD. Parkin plays a significant role in the ubiquitin proteosomal system as an E3 ubiquitin ligase, but also plays a role in maintenance of mitochondrial integrity through regulation of mitophagy. Parkin recognizes damaged mitochondria through PINK-1 and recruits autophagic machinery to mitochondria. This results in autophagosomes engulfing damaged mitochondria and fusing with lysosomes, degrading damaged mitochondria (Tanaka 2010; Youle et al., 2011). Parkin is also

reported to regulate turnover of the ETC (Vincow et al., 2013). Therefore, parkin may play a pivotal role in mitochondrial maintenance in central DA neurons and loss of parkin-mediated maintenance of mitochondrial homeostasis may alter mitochondrial function and structure in NSDA neurons.

In my study, in the absence of parkin, mitochondrial maximum and spare respiratory capacities were reduced due to the decrease in mitochondrial mass and number of mitochondria in NSDA axon terminals. In addition, impaired mitochondrial morphology with lower Flameng mitochondrial functional score was observed in the absence of parkin. Consistent with my study, dysmorphic mitochondria in the absence of parkin is also found in drosophila and myocytes (Kubli et al., 2013; Zhang et al., 2008). Therefore, during the metabolic stress or exposure to pathogenesis, parkin may play a neuroprotective role in central DA neurons by maintaining the number and quality of mitochondria in axon terminals.

Increased parkin expression is reported to have a neuroprotective effect in various models by maintaining mitochondrial function. For example, neuron-specific overexpression of parkin in drosophila increases mean and maximum lifespan by improving mitochondrial morphology and mitochondrial dynamics (Rana et al., 2013). Also, in murine models, AAV mediated upregulation of parkin expression appears to protect NSDA neurons from toxicant-induced injuries (Vercammen et al., 2006; Manfredsson 2007). The protective effect of exogenous upregulation of parkin expression against neurotoxicant-induced injury is consistent with my observations.

In the MPTP neurotoxin model, parkin overexpression did not prevent inhibition of basal respiration. However, after acute exposure to MPTP, parkin overexpression prevented inhibition of maximum and spare respirations. MPP^+ uptake into the mitochondria was prevented by an

uncoupler, FCCP. Depolarization of the mitochondria by FCCP also triggered outflow of MPP^+ from the mitochondria (Komatsu et al., 2006; Ramsay and Singer 1986). This suggests OCR with FCCP *ex vivo* treatment, reflects maximal respiratory capacity of the viable mitochondria. Parkin overexpression has a protective effect on the number of viable and functional mitochondria. After acute exposure to MPTP, recovery of mitochondrial mass in SN by parkin overexpression was confirmed by Western blot analysis. Parkin overexpression may prevent further damage in mitochondria in NSDA neurons by up-regulating mitochondrial quality control through mitophagy.

Mitochondrial Complex I inhibitors, rotenone and MPTP induced autophagy (Kubli et al., 2013). Aberrant α-synuclein expression is associated with mitochondrial dysfunction and with an increase in colocalization between autophagosomes and mitochondria (Wang et al., 2006). In addition to α-synuclein, other genetic factors of PD such as *LRRK2, DJ-1*, *Pink-1,* and *Parkin* are involved in mitophagy (Krige et al., 1992; Tong et al., 2010; Yang et al., 2007; Thomas et al., 2011). In my study, parkin overexpression upregulated autophagy in SN. Therefore, parkin overexpression protects mitochondria in NSDA neurons from the Complex I inhibitor, MPTP possibly by upregulation of mitophagy.

In Drosophila and mice, lack of autophagy caused neuronal loss with movement disorder, formation of ubiquitin-positive aggregates, and a decrease in life span. However, in Drosophila, an increase in autophagy caused resistance to oxidative stress and increased life span (Simonsen et al., 2008; Martinez-Vicente et al., 2008; Spencer et al., 2009). Aberrant α-synuclein, which is a component of Lewy bodies in PD, caused inhibition of autophagy and autophagy activation reduced α-synuclein accumulation (Tong et al., 2010; Spencer et al., 2009). In contrast, overly activated autophagy can be detrimental to neurons by axonal dystrophy, neurite degeneration,

neuroal atrophy, and even cell death (Yang et al., 2007; Wang et al., 2006). This is one of the limitations in autophagy-related therapies in neurodegenerative disease. Therefore, parkin, allowing neurons to maintain homeostasis of autophagy while protecting mitochondria from neurotoxin, may provide a novel therapy for PD. In my study, upregulated mitochondrial quality control by parkin overexpression protected functional mitochondria in SN after a single acute MPTP exposure. Therefore, it would be intriguing to investigate the effect of parkin overexpression on mitochondria in a chronic or subacute MPTP exposure.

In my study, altered mitochondrial function and structures were observed in the absence of parkin and the alteration was not restored with exogenous parkin expression. This may be due to: 1) genetic factors alone may not determine the pathology of PD, and/or 2) there may be a compensatory mechanism for loss of parkin in mice, and/or 3) the level of parkin expression or the time is not sufficient for mitochondrial functional recovery. Etiology of PD is not conclusive to genetic or environmental factors alone; over 90 % of PD is idiopathic and the molecular mechanism underlying NSDA neurodegeneration in PD is not known (Kelada et al., 2006). The impact of environmental factors on PD risk can be modulated by an individuals' genetic polymorphisms. Patient with cytochrome P450 (CYP)2D6, solute carrier family 6 member 3 (SLC6A3), and Praoxonase 1 (PON1) genetic polymorphism had increased risk to develop PD with pesticide exposure (Manthripragada et al., 2010; Checkoway et al., 1998). Males with MAO-B and glutathione S-transferase polymorphisms had a synergic effect with smoking to lower the risk of developing PD (Juhasz et al., 2007; Checkoway 1998). In animal studies that I conducted, mice were in cages free from known stress and environmental factors. In addition, restricted space allowing less movement may have an impact on DA neuronal activities and their results. Second, there may be alternative enzymes for parkin to maintain mitochondrial function

via mitochondrial quality control in mice. Recently, other mitochondrial E3 ubiquitin ligases, RNF185 and GIDE (also called MULAN), were disovered (Tang et al., 2011; Zhang et al., 2008; Elbaz et al., 1999). RNF185 and MULAN are found to be involved in mitophagy and mitochondrial homeostasis. Therefore, investigating these alternative enzymes that may play a role in mitochondrial maintenance in DA neurons could be important in understanding the mechanism of PD.

Concluding Remarks

The lack of parkin-mediated mitochondrial maintenance correlated with DA neuronal degeneration was observed in my study. Similar to differential susceptibility of DA neurons in PD, mitochondria had different bioenergetics and mass in TIDA and NSDA neurons. However, mitochondrial Complex I inhibitors exhibited equal inhibition in mitochondria isolated from the axonal terminals of NSDA and TIDA neurons. The differential susceptibility of the two types of DA neurons may not be due to underlying quality of mitochondria themselves, but the difference in MPTP metabolism, transport, and/or compensatory response to the toxicant exposure. Furthermore, region-specific differences in colocalization of autophagosomes and mitochondria were observed, which suggests mitochondrial quality control difference in these neurons.

Mitochondrial quality control is mediated by parkin. Therefore, in the absence of parkin, mitochondrial structures and functions were altered; mitochondrial maximum, spare respirations, mass, and number of mitochondria per synaptosome were reduced with increase in dysmorphic mitochondria in ST-derived synaptosomes. This suggests parkin may play a pivotal role in maintenance of mitochondria in central DA neurons. However, parkin rescue in parkin null mice failed to restore mitochondrial function. This may be due to an alternative enzyme, which

functions as parkin to regulate mitochondrial quality control, as a compensatory mechanism in the absence of parkin or due to complex interaction between genetic factors and environmental factors in PD. In the MPTP single acute exposure model, parkin overexpression in WT mice had a protective effect on viable mitochondria, possibly through autophagy. Therefore, parkin-mediated maintenance of mitochondrial homeostasis may be an important mechanism underlying the unique susceptibility of NSDA neurons to PD-related neurodegeneration.

The molecular mechanism of NSDA neuronal degeneration in PD process is not understood to this days and there is no treatment that halts the neurodegenerative process. My study helps understand basic mechanism underlying parkin-mediated mitochondrial maintenance in central DA neurons. Mitochondrial pathology in the absence of the parkin was not reversed by parkin exogenous expression by AAV-hParkin, however, parkin overexpression had protective role in mitochondrial maintenance in NSDA neurons with MPTP single acute exposure. Introduction of parkin may play a neuroprotective role to prevent further damage but the reversal of the pathological outcomes in NSDA neurons may not be rescued. This provides potential evidence for novel gene therapy using AAV-hParkin and importance of early finding of the disease process and diagnosis of PD.

REFERENCES

REFERENCES

Abraham, C.; Bai,L.; Leube, R.E. (2011). "Synaptogyrin-dependent modulation of synaptic neurotransmission in Caenorhabditis elegans." Neuroscience 190; 75-88.

Adam-Vizi, Vera, and Christos Chinopoulos. "Bioenergetics and the Formation of Mitochondrial Reactive Oxygen Species." *Trends in Pharmacological Sciences* 27, no. 12 (December 2006): 639–45. doi:10.1016/j.tips.2006.10.005.

Agency for toxic substances and disease registry, "ATSDR - Toxicological Profile: Toxaphene." Accessed July 18, 2014. http://www.atsdr.cdc.gov.proxy1.cl.msu.edu/toxprofiles/tp.asp?id=548&tid=99.

Albin, Roger L., Anne B. Young, and John B. Penney. "The Functional Anatomy of Basal Ganglia Disorders." *Trends in Neurosciences* 12, no. 10 (1989): 366–75. doi:10.1016/0166-2236(89)90074-X.

Albrecht, M. (2005). LRRK2 mutations and Parkinsonism. The Lancet *365*, 1230.

Alegre-Abarrategui, Javier, Helen Christian, Michele M. P. Lufino, Ruxandra Mutihac, Lara Lourenço Venda, Olaf Ansorge, and Richard Wade-Martins. "LRRK2 Regulates Autophagic Activity and Localizes to Specific Membrane Microdomains in a Novel Human Genomic Reporter Cellular Model." *Human Molecular Genetics* 18, no. 21 (November 1, 2009): 4022–34. doi:10.1093/hmg/ddp346.

Alegre-Abarrategui, Javier, and Richard Wade-Martins. "Parkinson Disease, LRRK2 and the Endocytic-Autophagic Pathway." *Autophagy* 5, no. 8 (November 2009): 1208–10.

Andersen PH. The dopamine uptake inhibitor GBR 12909: selectivity and molecular mechanism of action. European Journal of Pharmacology.1989; 166: 493-504

Andres-Mateos, Eva, Celine Perier, Li Zhang, Beatrice Blanchard-Fillion, Todd M. Greco, Bobby Thomas, Han Seok Ko, et al. "DJ-1 Gene Deletion Reveals That DJ-1 Is an Atypical Peroxiredoxin-like Peroxidase." *Proceedings of the National Academy of Sciences* 104, no. 37 (September 11, 2007): 14807–12. doi:10.1073/pnas.0703219104.

Andreyev, A. Yu, Yu E. Kushnareva, and A. A. Starkov. "Mitochondrial Metabolism of Reactive Oxygen Species." *Biochemistry. Biokhimiia* 70, no. 2 (February 2005): 200–214.

Angeles, Dario C., Bong-Hwa Gan, Luisa Onstead, Yi Zhao, Kah-Leong Lim, Justus Dachsel, Heather Melrose, et al. "Mutations in LRRK2 Increase Phosphorylation of Peroxiredoxin 3 Exacerbating Oxidative Stress-Induced Neuronal Death." *Human Mutation* 32, no. 12 (December 1, 2011): 1390–97. doi:10.1002/humu.21582.

Anvret, Anna, Marie Westerlund, Olof Sydow, Thomas Willows, Charlotta Lind, Dagmar Galter, and Andrea Carmine Belin. "Variations of the CAG Trinucleotide Repeat in DNA Polymerase Gamma (POLG1) Is Associated with Parkinson's Disease in Sweden." *Neuroscience Letters* 485, no. 2 (November 2010): 117–20.

Ashton, A.C.& Ushkaryov, Y.A. Properties of synaptic vesicle pools in mature central nerve terminals.J. Biol.Chem. 280, 37278-88 (2005).

Bachmann, C.G., and Trenkwalder, C. (2006). Body weight in patients with Parkinson's disease. Mov. Disord. *21*, 1824–1830.

Balazs, R. et al. Subcellular fractionation of rat cerebellum: an electron microscopic and biochemical investigation. III. Isolation of large fragments of the cerebellar lomeruli. *Brain Res.* 86, 17–30 (1975).

Barber, Robert D., Dan W. Harmer, Robert A. Coleman, and Brian J. Clark. "GAPDH as a Housekeeping Gene: Analysis of GAPDH mRNA Expression in a Panel of 72 Human Tissues." *Physiological Genomics* 21, no. 3 (May 11, 2005): 389–95. doi:10.1152/physiolgenomics.00025.2005.

Barrett KE. Barman SM. Boitano S. Brooks HL., 2012, *Ganon's review of medical physiology*, McGraw-Hill companies, China, 24th ed, p.146

Behrouz, B., Drolet, R.E., Sayed, Z.A., Lookingland, K.J., and Goudreau, J.L. (2007).Unique responses to mitochondrial complex I inhibition in tuberoinfundibular dopamine neurons may impart resistance to toxic insult. Neuroscience *147*, 592–598.

Bender, Andreas, Kim J. Krishnan, Christopher M. Morris, Geoffrey A. Taylor, Amy K. Reeve, Robert H. Perry, Evelyn Jaros, et al. "High Levels of Mitochondrial DNA Deletions in Substantia Nigra Neurons in Aging and Parkinson Disease." *Nature Genetics* 38, no. 5 (May 2006): 515–17. doi:10.1038/ng1769.

Benskey et al. The Role of Parkin in the Differential Susceptibility of Tuberoinfundibular and Nigrostriatal Dopamine Neurons to Acute Toxicant Exposure. Unpublished.

Benskey, M., Behrouz, B., Sunryd, J., Pappas, S.S., Baek, S.-H., Huebner, M., Lookingland, K.J., and Goudreau, J.L. (2012). Recovery of hypothalamic tuberoinfundibular dopamine neurons from acute toxicant exposure is dependent upon protein synthesis and associated with an increase in parkin and ubiquitin carboxy-terminal hydrolase-L1 expression. NeuroToxicology *33*, 321–331.

Benskey, Matthew, Ki Yong Lee, Kevin Parikh, Keith J. Lookingland, and John L. Goudreau. "Sustained Resistance to Acute MPTP Toxicity by Hypothalamic Dopamine Neurons Following Chronic Neurotoxicant Exposure Is Associated with Sustained up-Regulation of Parkin Protein." *Neurotoxicology* 37 (July 2013): 144–53. doi:10.1016/j.neuro.2013.04.002.

Bernheimer, H., Birkmayer, W., Hornykiewicz, O., Jellinger, K., and Seitelberger, F. (1973). Brain dopamine and the syndromes of Parkinson and Huntington. Clinical, morphological and neurochemical correlations. J. Neurol. Sci. 20, 415–455.

Betarbet, Ranjita, Rosa M. Canet-Aviles, Todd B. Sherer, Pier G. Mastroberardino, Chris McLendon, Jin-Ho Kim, Serena Lund, et al. "Intersecting Pathways to Neurodegeneration in Parkinson's Disease: Effects of the Pesticide Rotenone on DJ-1, A-synuclein, and the Ubiquitin–proteasome System." *Neurobiology of Disease* 22, no. 2 (May 2006): 404–20. doi:10.1016/j.nbd.2005.12.003.

Bindoff, L.A., Birch-Machin, M.A., Cartlidge, N.E.F., Parker Jr., W.D., and Turnbull, D.M. (1991). Respiratory chain abnormalities in skeletal muscle from patients with Parkinson's disease. Journal of the Neurological Sciences *104*, 203–208.

Bonifati, Vincenzo. "Genetics of Parkinson's Disease – State of the Art, 2013." *Parkinsonism &Related Disorders*, Proceedings of XX World Congress on Parkinson's Disease and Related Disorders, 20, Supplement 1 (January 2014): S23–S28. doi:10.1016/S1353-8020(13)70009-9.

Boregaard N. et al. (1983) Subcellular localization of the b-cytochrome component of the human neutrophil microbicidal oxidase: translocation during activation. *J. Cell Biol*. 97:52-61

Braak, H., and Braak, E. (2000). Pathoanatomy of Parkinson's disease. J. Neurol. *247*, 3–10.

Brand, Martin D., Charles Affourtit, Telma C. Esteves, Katherine Green, Adrian J. Lambert, Satomi Miwa, Julian L. Pakay, and Nadeene Parker. "Mitochondrial Superoxide: Production, Biological Effects, and Activation of Uncoupling Proteins." *Free Radical Biology & Medicine* 37, no. 6 (September 15, 2004): 755–67. doi:10.1016/j.freeradbiomed.2004.05.034.

Brand, Martin D., and David G. Nicholls. "Assessing Mitochondrial Dysfunction in Cells." *Biochemical Journal* 435, no. Pt 2 (April 15, 2011): 297–312. doi:10.1042/BJ20110162

Broekman MJ. Homogenization by nitrogen cavitation technique applied to platelet subcellular fractionation.*Methods Enzymol*. 215. 21 (1992)

Brownlee, Michael. "Biochemistry and Molecular Cell Biology of Diabetic Complications." *Nature* 414, no. 6865 (December 13, 2001): 813–20. doi:10.1038/414813a.

Burn, D. J., M. H. Mark, E. D. Playford, D. M. Maraganore, T. R. Zimmerman, R. C. Duvoisin, A. E. Harding, C. D. Marsden, and D. J. Brooks. "Parkinson's Disease in Twins Studied with 18F-dopa and Positron Emission Tomography." *Neurology* 42, no. 10 (October 1, 1992): 1894–1894. doi:10.1212/WNL.42.10.1894.

Cadenas, E., A. Boveris, C. I. Ragan, and A. O. Stoppani. "Production of Superoxide Radicals and Hydrogen Peroxide by NADH-Ubiquinone Reductase and Ubiquinol-Cytochrome c

Reductase from Beef-Heart Mitochondria." *Archives of Biochemistry and Biophysics* 180, no. 2 (April 30, 1977): 248–57.

Cannon, Jason R., Victor Tapias, Hye Mee Na, Anthony S. Honick, Robert E. Drolet, and J. Timothy Greenamyre. "A Highly Reproducible Rotenone Model of Parkinson's Disease." *Neurobiology of Disease* 34, no. 2 (May 2009): 279–90. doi:10.1016/j.nbd.2009.01.016.

Cannon, J.R., Tapias, V., Na, H.M., Honick, A.S., Drolet, R.E., and Greenamyre, J.T. (2009). A highly reproducible rotenone model of Parkinson's disease. Neurobiology of Disease *34*, 279–290.

Caprette DR., 2008, Experimental bioscience Bios211, Rice University, http://www.ruf.rice.edu/~bioslabs/studies/mitochondria/mitostate3.html (1/2/10)

Cent. Dis. Control Prev. 2013. Facts about paraquat. Cent. Dis. Control Prev., Atlanta, Ga. http://www.bt.cdc.gov/agent/paraquat/basics/facts.asp

Cezanne L. (1992) Isolation of the plasma membrane and organelles from Chinese hamster ovary cells. *Biochem. Biophys. Acta*. **1112**. 205-214

Chance, B., and G. Hollunger. "The Interaction of Energy and Electron Transfer Reactions in Mitochondria. I. General Properties and Nature of the Products of Succinate-Linked Reduction of Pyridine Nucleotide." *The Journal of Biological Chemistry* 236 (May 1961): 1534–43.

Charcot J-M. 1872. De la paralysie agitante. In Oeuvres Comple`tes (t 1) Lec¸ons sur les maladies du syste`me nerveux, pp. 155–188. A Delahaye, Paris. [In English: Charcot J-M. 1877. On Parkinson's disease. In Lectures on diseases of the nervous system delivered at the Salpeˆtrie`re (transl. Sigerson G), pp. 129–156. New Sydenham Society, London.

Chaudhry FA, Edwards RH, Fonnum F. (Dec 2007). " Vesicular neurotransmitter transporters as targets for endogenous and exogenous toxic substances." *Ann Rev Pharmacol Toxicol*. 48:280

Checkoway, H., G. M. Franklin, P. Costa-Mallen, T. Smith-Weller, J. Dilley, P. D. Swanson, and L. G. Costa. "A Genetic Polymorphism of MAO-B Modifies the Association of Cigarette Smoking and Parkinson's Disease." *Neurology* 50, no. 5 (May 1998): 1458–61.

Chen H, Chan DC. Mitochondrial dynamics--fusion, fission, movement, and mitophagy—in neurodegenerative diseases.Hum mol genet.2009;18(R2):R169-76

Chen, H., X. Huang, X. Guo, R. B. Mailman, Y. Park, F. Kamel, D. M. Umbach, et al. "Smoking Duration, Intensity, and Risk of Parkinson Disease." *Neurology* 74, no. 11 (March 16, 2010): 878–84. doi:10.1212/WNL.0b013e3181d55f38.

Cherra, Salvatore J., and Charleen T. Chu. “Autophagy in Neuroprotection and Neurodegeneration: A Question of Balance.” *Future Neurology* 3, no. 3 (May 2008): 309–23. doi:10.2217/14796708.3.3.309.

Cherra, Salvatore J., Erin Steer, Aaron M. Gusdon, Kirill Kiselyov, and Charleen T. Chu. “Mutant LRRK2 Elicits Calcium Imbalance and Depletion of Dendritic Mitochondria in Neurons.” *The American Journal of Pathology* 182, no. 2 (February 2013): 474–84. doi:10.1016/j.ajpath.2012.10.027.

Chin, Lih-Shen, James A. Olzmann, and Lian Li. “Parkin-mediated Ubiquitin Signalling in Aggresome Formation and Autophagy.” *Biochemical Society Transactions* 38, no. 1 (February 1, 2010): 144. doi:10.1042/BST0380144.

Choubey, Vinay, Dzhamilja Safiulina, Annika Vaarmann, Michal Cagalinec, Przemyslaw Wareski, Malle Kuum, Alexander Zharkovsky, and Allen Kaasik. “Mutant A53T α-Synuclein Induces Neuronal Death by Increasing Mitochondrial Autophagy.” *The Journal of Biological Chemistry* 286, no. 12 (March 25, 2011): 10814–24.

Cino, M., and R. F. Del Maestro. “Generation of Hydrogen Peroxide by Brain Mitochondria: The Effect of Reoxygenation Following Postdecapitative Ischemia.” *Archives of Biochemistry and Biophysics* 269, no. 2 (March 1989): 623–38.

Cleeter, M.W.J., Cooper, J.M., and Schapira, A.H.V. (1992). Irreversible Inhibition of Mitochondrial Complex I by 1-Methyl-4-Phenylpyridinium: Evidence for Free Radical Involvement. Journal of Neurochemistry *58*, 786–789.

Cohen, G. (2002). Oxidative Stress and Parkinson’s Disease. In Reactive Oxygen Species in Biological Systems, (Springer US), pp. 593–608.

Constantinescu, Radu, Megan Romer, and Karl Kieburtz. “Malignant Melanoma in Early Parkinson’s Disease: The DATATOP Trial.” *Movement Disorders* 22, no. 5 (April 15, 2007): 720–22. doi:10.1002/mds.21273.

Costa, Cristine Alves da, Erwan Paitel, Bruno Vincent, and Frédéric Checler. “α-Synuclein Lowers P53-dependent Apoptotic Response of Neuronal Cells ABOLISHMENT BY 6-HYDROXYDOPAMINE AND IMPLICATION FOR PARKINSON′S DISEASE.” *Journal of Biological Chemistry* 277, no. 52 (December 27, 2002): 50980–84. doi:10.1074/jbc.M207825200.

Crocker AD. (1994). “Dopamine- Mechanisms of Action.” Australian Prescriber.17:17-21.

Cuervo, Ana Maria, Leonidas Stefanis, Ross Fredenburg, Peter T. Lansbury, and David Sulzer. “Impaired Degradation of Mutant Alpha-Synuclein by Chaperone-Mediated Autophagy.” *Science (New York, N.Y.)* 305, no. 5688 (August 27, 2004): 1292–95. doi:10.1126/science.1101738.

Czoty PW. Justice JB Jr. Howell LL. Cocaine-induced changes in xtracellular dopamine determined by microdialysis in awake quirrel monkeys. Psychopharmacology (Berl). 2000;148(3):299-306.

Dagda, Ruben K., and Charleen T. Chu. "Mitochondrial Quality Control: Insights on How Parkinson's Disease Related Genes PINK1, Parkin, and Omi/HtrA2 Interact to Maintain Mitochondrial Homeostasis." *Journal of Bioenergetics and Biomembranes* 41, no. 6 (December 2009): 473–79. doi:10.1007/s10863-009-9255-1.

Dauer, William, and Serge Przedborski. "Parkinson's Disease: Mechanisms and Models." *Neuron* 39, no. 6 (September 11, 2003): 889–909. doi:10.1016/S0896-6273(03)00568-3.

Dawson TM and Dawson VL. Molecular pathways of neurodegeneration in Parkinson's disease.Sience. 2003;302:819-821

Day, Brian J., Manisha Patel, Lisa Calavetta, Ling-Yi Chang, and Jonathan S. Stamler. "A Mechanism of Paraquat Toxicity Involving Nitric Oxide Synthase." *Proceedings of the National Academy of Sciences of the United States of America* 96, no. 22 (October 26, 1999): 12760–65.

De Rijk, M C, C Tzourio, M M Breteler, J F Dartigues, L Amaducci, S Lopez-Pousa, J M Manubens-Bertran, A Alperovitch, and W A Rocca. "Prevalence of Parkinsonism and Parkinson's Disease in Europe: The EUROPARKINSON Collaborative Study. European Community Concerted Action on the Epidemiology of Parkinson's Disease." *Journal of Neurology, Neurosurgery, and Psychiatry* 62, no. 1 (January 1997): 10–15.

De Robertis, E., Pellegrino de Iraldi, A., Rodriquez de Lores Arniaz, G. & Salganicoff, L. Cholinergic and noncholinergic nerve endings in rat brain. I. Isolation and subcellular distribution of acetylcholine and acetylcholinesterase. J. Neurochem. 9, 23-35 (1962)

Del Buono BJ Et al. (1989) Preparation and characterization of plasma membrane vesicles from human polymorphonuclear leukocytes. *J. Cell. Physiol*. **141**: 636-644

Deng, Yifu, Beth Newman, Michael P. Dunne, Peter A. Silburn, and George D. Mellick. "Further Evidence That Interactions between CYP2D6 and Pesticide Exposure Increase Risk for Parkinson's Disease." *Annals of Neurology* 55, no. 6 (June 2004): 897.

Devi L, Raghavendran V, Prabhu BM, Avadhani NG, Anandatheerthavarada HK (2008) Mitochondrial import and accumulation of alpha-synuclein impair complex I in human dopaminergic neuronal cultures and Parkinson disease brain. J Biol chem.2008;283:9089-9100

Dodson, M.W., and Guo, M. (2007). Pink1, Parkin, DJ-1 and mitochondrial dysfunction in Parkinson's disease. Current Opinion in Neurobiology *17*, 331–337.

Donkelaar and Nicholson, Structure and organization of fibre systems: Chapter 3. The central nervous system of vertebrates. 1998;1:113– 157

Dreyer, Jakob K., Kjartan F. Herrik, Rune W. Berg, and Jørn D. Hounsgaard. "Influence of Phasic and Tonic Dopamine Release on Receptor Activation." *The Journal of Neuroscience* 30, no. 42 (October 20, 2010): 14273–83. doi:10.1523/JNEUROSCI.1894-10.2010.

Dunkley, P.R. et al. The preparation and use of synaptosomes for studying secretion of catecholomines. In The Secretory Process Vol.3 309-328 (Eds. A. Poisner and J.M. Triataro. Elsevier, Amsterdam, 1987)

Dunkely P.R., Jarvie, P.E. & Rostas, J.A. Distribution of calmodulin-and cyclic AMP-stimulated protein kinases in synaptosomes. J. Neurochem. 51, 57-68 (1988).

Dunkley PR, Jarvie PE, Robinson PJ. A rapid Percoll gradient procedure for preparation of synaptosomes. Nat Protoc.2008;3(11):1718-28.

Dunkley PR & Robinson PJ. Depolarisation-dependent protein phosphorylation in synaptosomes: mechanisms and significance. Prog. Brain Res. 69, 273-293 (1986).

Edgar, Alasdair J., and Julia M. Polak. "Human Homologues of Yeast Vacuolar Protein Sorting 29 and 35." *Biochemical and Biophysical Research Communications* 277, no. 3 (November 2, 2000): 622–30.

Eeden, S.K.V.D., Tanner, C.M., Bernstein, A.L., Fross, R.D., Leimpeter, A., Bloch, D.A., and Nelson, L.M. (2003). Incidence of Parkinson's Disease: Variation by Age, Gender, and Race/Ethnicity. Am. J. Epidemiol. *157*, 1015–1022.

Ekstrand, Mats I., Mügen Terzioglu, Dagmar Galter, Shunwei Zhu, Christoph Hofstetter, Eva Lindqvist, Sebastian Thams, et al. "Progressive Parkinsonism in Mice with Respiratory-Chain-Deficient Dopamine Neurons." *Proceedings of the National Academy of Sciences* 104, no. 4 (January 23, 2007): 1325–30. doi:10.1073/pnas.0605208103.

Elbaz, A., F. Grigoletto, M. Baldereschi, M. M. Breteler, J. M. Manubens-Bertran, S. Lopez-Pousa, J. F. Dartigues, A. Alpérovitch, C. Tzourio, and W. A. Rocca. "Familial Aggregation of Parkinson's Disease: A Population-Based Case-Control Study in Europe. EUROPARKINSON Study Group." *Neurology* 52, no. 9 (June 10, 1999): 1876–82.

Elbaz, Alexis, Clotilde Levecque, Jacqueline Clavel, Jean-Sébastien Vidal, Florence Richard, Philippe Amouyel, Annick Alpérovitch, Marie-Christine Chartier-Harlin, and Christophe Tzourio. "CYP2D6 Polymorphism, Pesticide Exposure, and Parkinson's Disease." *Annals of Neurology* 55, no. 3 (March 2004): 430–34. doi:10.1002/ana.20051.

Encyclopedia of Movement Disorders, Three-Volume Set. Academic Press, 2010.

Fahn, S. (1996). Book Review. New England Journal of Medicine *335*, 2002–2003.

Fields, J. Z., R. R. Albores, E. J. Neafsey, and M. A. Collins. “Inhibition of Mitochondrial Succinate Oxidation--Similarities and Differences between N-Methylated Beta-Carbolines and MPP+.” *Archives of Biochemistry and Biophysics* 294, no. 2 (May 1, 1992): 539–43.

Flameng, W., Borgers, M., Daenen, W., and Stalpaert, G. (1980). Ultrastructural and cytochemical correlates of myocardial protection by cardiac hypothermia in man. J. Thorac. Cardiovasc. Surg. *79*, 413–424.

Floor, E., and Wetzel, M.G. (1998). Increased Protein Oxidation in Human Substantia Nigra Pars Compacta in Comparison with Basal Ganglia and Prefrontal Cortex Measured with an Improved Dinitrophenylhydrazine Assay. Journal of Neurochemistry *70*, 268–275.

Gandhi, Sonia, Alison Wood-Kaczmar, Zhi Yao, Helene Plun-Favreau, Emma Deas, Kristina Klupsch, Julian Downward, et al. “PINK1-Associated Parkinson’s Disease Is Caused by Neuronal Vulnerability to Calcium-Induced Cell Death.” *Molecular Cell* 33, no. 5 (March 13, 2009): 627–38.

Gao, Xiang, Kelly C. Simon, Jiali Han, Michael A. Schwarzschild, and Alberto Ascherio. “Genetic Determinants of Hair Color and Parkinson’s Disease Risk.” *Annals of Neurology* 65, no. 1 (January 1, 2009): 76–82. doi:10.1002/ana.21535.

Gautier, Clement A., Tohru Kitada, and Jie Shen. “Loss of PINK1 Causes Mitochondrial Functional Defects and Increased Sensitivity to Oxidative Stress.” *Proceedings of the National Academy of Sciences* 105, no. 32 (August 12, 2008): 11364–69.

Gehrke, Stephan, Yuzuru Imai, Nicholas Sokol, and Bingwei Lu. “Pathogenic LRRK2 Negatively Regulates microRNA-mediated Translational Repression.” *Nature* 466, no. 7306 (July 29, 2010): 637–41. doi:10.1038/nature09191.

Giasson, Benoit I., John E. Duda, Shawn M. Quinn, Bin Zhang, John Q. Trojanowski, and Virginia M.-Y. Lee. “Neuronal α-Synucleinopathy with Severe Movement Disorder in Mice Expressing A53T Human α-Synuclein.” *Neuron* 34, no. 4 (May 16, 2002): 521–33.

Gillardon, Frank. “Leucine-Rich Repeat Kinase 2 Phosphorylates Brain Tubulin-Beta Isoforms and Modulates Microtubule Stability – a Point of Convergence in Parkinsonian Neurodegeneration?” *Journal of Neurochemistry* 110, no. 5 (September 1, 2009): 1514–22. doi:10.1111/j.1471-4159.2009.06235.x.

Gloeckner, Christian Johannes, Norbert Kinkl, Annette Schumacher, Ralf J. Braun, Eric O’Neill, Thomas Meitinger, Walter Kolch, Holger Prokisch, and Marius Ueffing. “The Parkinson Disease Causing LRRK2 Mutation I2020T Is Associated with Increased Kinase Activity.” *Human Molecular Genetics* 15, no. 2 (January 15, 2006): 223–32. doi:10.1093/hmg/ddi439.

Goedert, Michel, Maria Grazia Spillantini, Kelly Del Tredici, and Heiko Braak. “100 Years of Lewy Pathology.” *Nature Reviews Neurology* 9, no. 1 (November 27, 2012): 13–24. doi:10.1038/nrneurol.2012.242.

Goetz, Christopher G. “The History of Parkinson’s Disease: Early Clinical Descriptions and Neurological Therapies.” *Cold Spring Harbor Perspectives in Medicine:* 1, no. 1 (September 2011).

Golbe, L. I., G. Di Iorio, V. Bonavita, D. C. Miller, and R. C. Duvoisin. “A Large Kindred with Autosomal Dominant Parkinson’s Disease.” *Annals of Neurology* 27, no. 3 (March 1990): 276–82.

Goldberg, Matthew S., Sheila M. Fleming, James J. Palacino, Carlos Cepeda, Hoa A. Lam, Anushree Bhatnagar, Edward G. Meloni, et al. “Parkin-Deficient Mice Exhibit Nigrostriatal Deficits but Not Loss of Dopaminergic Neurons.” *The Journal of Biological Chemistry* 278, no. 44 (October 31, 2003): 43628–35.

Goldman, Samuel M. “Environmental Toxins and Parkinson;s Disease.” *Annual Review of Pharmacology and Toxicology* 54, no. 1 (2014): 141–64.

Goldman, Samuel M., Freya Kamel, G. Webster Ross, Grace S. Bhudhikanok, Jane A. Hoppin, Monica Korell, Connie Marras, et al. “Genetic Modification of the Association of Paraquat and Parkinson’s Disease.” *Movement Disorders* 27, no. 13 (November 1, 2012): 1652–58.

Goldman, Scott J., Robert Taylor, Yong Zhang, and Shengkan Jin. “Autophagy and the Degradation of Mitochondria.” *Mitochondrion* 10, no. 4 (June 2010): 309–15.

Gowers, W. R. (William Richard). *A Manual of Diseases of the Nervous System*. London : J. & A. Churchill, 1886. http://archive.org/details/manualofdiseases02goweuoft.

Grace, A. A., and B. S. Bunney. “Intracellular and Extracellular Electrophysiology of Nigral Dopaminergic neurons—2. Action Potential Generating Mechanisms and Morphological Correlates.” *Neuroscience* 10, no. 2 (October 1983): 317–31.

Greene, Jessica C., Alexander J. Whitworth, Isabella Kuo, Laurie A. Andrews, Mel B. Feany, and Leo J. Pallanck. “Mitochondrial Pathology and Apoptotic Muscle Degeneration in Drosophila Parkin Mutants.” *Proceedings of the National Academy of Sciences of the United States of America* 100, no. 7 (April 1, 2003): 4078–83.

Grigolava, I. V., M. Iu Ksenzenko, A. A. Konstantinob, A. N. Tikhonov, and T. M. Kerimov. “Tiron as a spin-trap for superoxide radicals produced by the respiratory chain of submitochondrial particles.” *Biokhimiĭa (Moscow, Russia)* 45, no. 1 (January 1980): 75–82.

Grimm, Dirk, Mark A. Kay, and Juergen A. Kleinschmidt. “Helper Virus-Free, Optically Controllable, and Two-Plasmid-Based Production of Adeno-Associated Virus Vectors of Serotypes 1 to 6.” *Molecular Therapy* 7, no. 6 (June 2003): 839–50. doi:10.1016/S1525-0016(03)00095-9.

Gluck MR, Youngster SK, Ramsay RR, Singer TP, Nicklas WJ. Studies on the characterization of the inhibitory mechanism of 4'-alkylated 1-methyl-4-phenylpyridinium

and phenylpyridine analogues in mitochondria and electron transport particles. J Neurochem. 1994;63(2):655-61.

Guautier C., 2008, Protocol for polarographic respiration assay, Harvard University

Haft, Carol Renfrew, Maria de la Luz Sierra, Richard Bafford, Maxine A. Lesniak, Valarie A. Barr, and Simeon I. Taylor. "Human Orthologs of Yeast Vacuolar Protein Sorting Proteins Vps26, 29, and 35: Assembly into Multimeric Complexes." *Molecular Biology of the Cell* 11, no. 12 (December 1, 2000): 4105–16.

Hancock, Dana B, Eden R Martin, Gregory M Mayhew, Jeffrey M Stajich, Rita Jewett, Mark A Stacy, Burton L Scott, Jeffery M Vance, and William K Scott. "Pesticide Exposure and Risk of Parkinson's Disease: A Family-based Case-control Study." *BMC Neurology* 8, no. 1 (2008): 6. doi:10.1186/1471-2377-8-6.

Hao, Ling-Yang, Benoit I. Giasson, and Nancy M. Bonini. "DJ-1 Is Critical for Mitochondrial Function and Rescues PINK1 Loss of Function." *Proceedings of the National Academy of Sciences of the United States of America* 107, no. 21 (May 25, 2010): 9747–52. doi:10.1073/pnas.0911175107.

Harvey, B.K., Wang, Y., and Hoffer, B.J. (2008). Transgenic rodent models of Parkinson's disease. Acta Neurochir Suppl *101,* 89–92.

Healy, Daniel G, Mario Falchi, Sean S O'Sullivan, Vincenzo Bonifati, Alexandra Durr, Susan Bressman, Alexis Brice, et al. "Phenotype, Genotype, and Worldwide Genetic Penetrance of LRRK2-Associated Parkinson's Disease: A Case-Control Study." *The Lancet Neurology* 7, no. 7 (July 2008): 583–90. doi:10.1016/S1474-4422(08)70117-0.

Heikkila RE, Youngster SK, Manzino L, Cabbat FS, Duvoisin RC. Effects of 1-methyl-4-phenyl-1,2,5,6-tetrahydropyridine and related compounds on the uptake of [3H]3,4-dihydroxyphenylethylamine and [3H]5-hydroxytryptamine in neostriatal synaptosomal preparations. J Neurochem. 1985;44(1):310-3.

Hinkle, P. C., R. A. Butow, E. Racker, and B. Chance. "Partial Resolution of the Enzymes Catalyzing Oxidative Phosphorylation. XV. Reverse Electron Transfer in the Flavin-Cytochrome Beta Region of the Respiratory Chain of Beef Heart Submitochondrial Particles." *The Journal of Biological Chemistry* 242, no. 22 (November 25, 1967): 5169–73.

Hoppel CL, Grinblatt D, Kwok HC, Arora PK, Singh MP, Sayre LM. Inhibition of mitochondrial respiration by analogs of 4-phenylpyridine and 1-methyl-4-phenylpyridinium cation (MPP+), the neurotoxic metabolite of MPTP. Biochem Biophys Res Commun.1987;148(2):684-93.

Humphrey, D. M., R. B. Parsons, Z. N. Ludlow, T. Riemensperger, G. Esposito, P. Verstreken, H. T. Jacobs, S. Birman, and F. Hirth. "Alternative Oxidase Rescues Mitochondria-

Mediated Dopaminergic Cell Loss in Drosophila." *Human Molecular Genetics* 21, no. 12 (June 15, 2012): 2698–2712.

Imam, Syed Z., Bensu Karahalil, Barbara A. Hogue, Nadja C. Souza-Pinto, and Vilhelm A. Bohr. "Mitochondrial and Nuclear DNA-Repair Capacity of Various Brain Regions in Mouse Is Altered in an Age-Dependent Manner." *Neurobiology of Aging* 27, no. 8 (August 2006): 1129–36.

Ischiropoulos, Harry, and Abu B. Al-Mehdi. "Peroxynitrite-mediated Oxidative Protein Modifications." *FEBS Letters* 364, no. 3 (May 15, 1995): 279–82. doi:10.1016/0014-5793(95)00307-U.

Jakes, Ross, Maria Grazia Spillantini, and Michel Goedert. "Identification of Two Distinct Synucleins from Human Brain." *FEBS Letters* 345, no. 1 (May 23, 1994): 27–32. doi:10.1016/0014-5793(94)00395-5.

Javitch JA, D'Amato RJ, Strittmatter SM, Snyder SH. Parkinsonism-inducing neurotoxin, N-methyl-4-phenyl-1,2,3,6 -tetrahydropyridine: uptake of the metabolite N-methyl-4-phenylpyridine by dopamine neurons explains selective toxicity.Proc Natl Acad Sci U S A. 1985;82(7):2173-7.

Jellinger, Kurt A. "Pathology of Parkinson's Disease." *Molecular and Chemical Neuropathology* 14, no. 3 (June 1, 1991): 153–97.

Jiang, H., Ren, Y., Yuen, E.Y., Zhong, P., Ghaedi, M., Hu, Z., Azabdaftari, G., Nakaso, K., Yan, Z., and Feng, J. (2012). Parkin Controls Dopamine Utilization in Human Midbrain Dopaminergic Neurons Derived from Induced Pluripotent Stem Cells. Nat Commun *3*, 668.

Jones, Alison C., Yasuhiro Yamamura, Laura Almasy, Saeed Bohlega, Bülent Elibol, Jean Hubble, Shigeki Kuzuhara, et al. "Autosomal Recessive Juvenile Parkinsonism Maps to 6q25.2-q27 in Four Ethnic Groups: Detailed Genetic Mapping of the Linked Region." *The American Journal of Human Genetics* 63, no. 1 (January 7, 1998): 80–87.

Juhasz, Gabor, Balazs Erdi, Miklos Sass, and Thomas P. Neufeld. "Atg7-Dependent Autophagy Promotes Neuronal Health, Stress Tolerance, and Longevity but Is Dispensable for Metamorphosis in Drosophila." *Genes & Development* 21, no. 23 (December 1, 2007): 3061–66.

Kamel, Freya, Samuel M. Goldman, David M. Umbach, Honglei Chen, Gina Richardson, Marie Richards Barber, Cheryl Meng, et al. "Dietary Fat Intake, Pesticide Use, and Parkinson's Disease." *Parkinsonism & Related Disorders* 20, no. 1 (January 2014): 82–87.

Kandel, Eric, James Schwartz, and Thomas Jessell. *Principles of Neural Science*. 4 edition. New York: McGraw-Hill Medical, 2000. Chapter 43

Kann, O., and Kovács, R. (2007). Mitochondria and neuronal activity. Am J Physiol Cell Physiol *292*, C641–C657.

Keane, P.C., Kurzawa, M., Blain, P.G., and Morris, C.M. (2011). Mitochondrial Dysfunction in Parkinson's Disease. Parkinson's Disease *2011*.

Kelada, Samir N. P., Harvey Checkoway, Sharon L. R. Kardia, Christopher S. Carlson, Paola Costa-Mallen, David L. Eaton, Jordan Firestone, et al. "5' and 3' Region Variability in the Dopamine Transporter Gene (SLC6A3), Pesticide Exposure and Parkinson's Disease Risk: A Hypothesis-Generating Study." *Human Molecular Genetics* 15, no. 20 (October 15, 2006): 3055–62.

Kalicharan, "Human Mitochondrial Genetics." *Wikipedia, the Free Encyclopedia*, (2008). http://en.wikipedia.org/w/index.php?title=Human_mitochondrial_genetics&oldid=5935083 11.

Kim, Raymond H., Patrice D. Smith, Hossein Aleyasin, Shawn Hayley, Matthew P. Mount, Scott Pownall, Andrew Wakeham, et al. "Hypersensitivity of DJ-1-deficient Mice to 1-methyl-4-phenyl-1,2,3,6-tetrahydropyrindine (MPTP) and Oxidative Stress." *Proceedings of the National Academy of Sciences of the United States of America* 102, no. 14 (April 5, 2005): 5215–20.

Komatsu, Masaaki, Satoshi Waguri, Tomoki Chiba, Shigeo Murata, Jun-ichi Iwata, Isei Tanida, Takashi Ueno, et al. "Loss of Autophagy in the Central Nervous System Causes Neurodegeneration in Mice." *Nature* 441, no. 7095 (June 15, 2006): 880–84. doi:10.1038/nature04723.

Koopman WJ, Nijtmans LG, Dieteren CE, Roestenberg P, Valsecchi F, Smeitink JA, Willems PH. Mammalian mitochondrial complex I: biogenesis, regulation, and reactive oxygen species generation.Antioxid Redox Signal. 2010 ;12(12):1431-70.

Kordower, J. H. et al. Disease duration and the integrity of the nigrostriatal system in Parkinson's disease. Brain 136, 2419–2431 (2013).

Kraytsberg, Yevgenya, Elena Kudryavtseva, Ann C. McKee, Changiz Geula, Neil W. Kowall, and Konstantin Khrapko. "Mitochondrial DNA Deletions Are Abundant and Cause Functional Impairment in Aged Human Substantia Nigra Neurons." *Nature Genetics* 38, no. 5 (May 2006): 518–20.

Krige D, Carroll MT, Cooper JM, Marsden CD, Schapira AH. Platelet mitochondrial function in Parkinson's disease. The Royal Kings and Queens Parkinson Disease Research Group. Ann Neurol.1992;32:782-788

Krishnamoorthy, G., and P. C. Hinkle. "Studies on the Electron Transfer Pathway, Topography of Iron-Sulfur Centers, and Site of Coupling in NADH-Q Oxidoreductase." *The Journal of Biological Chemistry* 263, no. 33 (November 25, 1988): 17566–75.

Kubli, Dieter A., Xiaoxue Zhang, Youngil Lee, Rita A. Hanna, Melissa N. Quinsay, Christine K. Nguyen, Rebecca Jimenez, Susanna Petrosyan, Anne N. Murphy, and Asa B. Gustafsson. "Parkin Protein Deficiency Exacerbates Cardiac Injury and Reduces Survival Following Myocardial Infarction." *The Journal of Biological Chemistry* 288, no. 2 (January 11, 2013): 915–26.

Kudin, Alexei P., Nana Yaw-B. Bimpong-Buta, Stefan Vielhaber, Christian E. Elger, and Wolfram S. Kunz. "Characterization of Superoxide-Producing Sites in Isolated Brain Mitochondria." *The Journal of Biological Chemistry* 279, no. 6 (February 6, 2004): 4127–35.

Kumar KR, Weissbach A, Heldmann M, and et al. "FRequency of the D620n Mutation in Vps35 in Parkinson Disease." *Archives of Neurology* 69, no. 10 (October 1, 2012): 1360–64.

Kuo, Yien-Ming, Zhishan Li, Yun Jiao, Nathalie Gaborit, Amar K. Pani, Bonnie M. Orrison, Benoit G. Bruneau, et al. "Extensive Enteric Nervous System Abnormalities in Mice Transgenic for Artificial Chromosomes Containing Parkinson Disease-associated A-synuclein Gene Mutations Precede Central Nervous System Changes." *Human Molecular Genetics* 19, no. 9 (May 1, 2010): 1633–50.

Kushnareva, Yulia, Anne N Murphy, and Alexander Andreyev. "Complex I-Mediated Reactive Oxygen Species Generation: Modulation by Cytochrome c and NAD(P)+ Oxidation-Reduction State." *Biochemical Journal* 368, no. Pt 2 (December 1, 2002): 545–53.

Kussmaul, Lothar, and Judy Hirst. "The Mechanism of Superoxide Production by NADH:ubiquinone Oxidoreductase (complex I) from Bovine Heart Mitochondria." *Proceedings of the National Academy of Sciences of the United States of America* 103, no. 20 (May 16, 2006): 7607–12.

Kuter, Katarzyna, Przemysław Nowak, Krystyna Gołembiowska, and Krystyna Ossowska. "Increased Reactive Oxygen Species Production in the Brain After Repeated Low-Dose Pesticide Paraquat Exposure in Rats. A Comparison with Peripheral Tissues." *Neurochemical Research* 35, no. 8 (August 1, 2010): 1121–30.

Lambert CE, Bondy SC. Effects of MPTP, MPP+ and paraquat on mitochondrial potential and oxidative stress. Life Sci. 1989;44(18):1277-84.

Langston, J. W., P. Ballard, J. W. Tetrud, and I. Irwin. "Chronic Parkinsonism in Humans due to a Product of Meperidine-Analog Synthesis." *Science (New York, N.Y.)* 219, no. 4587 (February 25, 1983): 979–80.

Langston, J. William, and Lysia S. Forno. "The Hypothalamus in Parkinson Disease." *Annals of Neurology* 3, no. 2 (February 1, 1978): 129–33. doi:10.1002/ana.410030207.

Lehéricy, S., Sharman, M.A., Santos, C.L.D., Paquin, R., and Gallea, C. (2012). Magnetic resonance imaging of the substantia nigra in Parkinson's disease. Movement Disorders *27*, 822–830.

Lemasters, John J. "Selective Mitochondrial Autophagy, or Mitophagy, as a Targeted Defense Against Oxidative Stress, Mitochondrial Dysfunction, and Aging." *Rejuvenation Research* 8, no. 1 (2005): 3–5.

Lemasters JJ. Ramshesh VK. (2007) Imaging of mitochondrial polarization and depolarization with cationic fluprophores. *Methods in cell bio*. **80**:283-95

Lesage, Suzanne, Mathieu Anheim, Franck Letournel, Luc Bousset, Aurélie Honoré, Nelly Rozas, Laura Pieri, et al. "G51D A-synuclein Mutation Causes a Novel Parkinsonian–pyramidal Syndrome." *Annals of Neurology* 73, no. 4 (April 1, 2013): 459–71.

Li, Wei, Mario H. Bengtson, Axel Ulbrich, Akio Matsuda, Venkateshwar A. Reddy, Anthony Orth, Sumit K. Chanda, Serge Batalov, and Claudio A. P. Joazeiro. "Genome-Wide and Functional Annotation of Human E3 Ubiquitin Ligases Identifies MULAN, a Mitochondrial E3 That Regulates the Organelle's Dynamics and Signaling." *PLoS ONE* 3, no. 1 (January 23, 2008): e1487. doi:10.1371/journal.pone.0001487.

Liang, C.-L., Wang, T.T., Luby-Phelps, K., and German, D.C. (2007). Mitochondria mass is low in mouse substantia nigra dopamine neurons: Implications for Parkinson's disease. Experimental Neurology *203*, 370–380.

Liang, Wang, Luby-Phelps and D.C. German, Mitochondria mass is low in mouse substantia nigra dopamine neurons: implications for Parkinson's disease, Exp. Neurol. 2007;203: 370–380.

Lin, M.T., and Beal, M.F. (2006). Mitochondrial dysfunction and oxidative stress in neurodegenerative diseases. Nature *443*, 787–795.

Lin, X. G.; Ming, M.; Chen, M.R.; Niu, W. P.; Zhang, Y.D.; Liu, B.; Jiu, Y.M.; Yu, J. W.; Xu, T.;Wu, Z. X. (2010). "UNC-31/CAPS docks and primes dense core vesicles in C. Elegans neurons". Biochemical and Biophysical Research Communications 397 (3): 526-531.

Liu, Rui, Xuguang Guo, Yikyung Park, Xuemei Huang, Rashmi Sinha, Neal D. Freedman, Albert R. Hollenbeck, Aaron Blair, and Honglei Chen. "Caffeine Intake, Smoking, and Risk of Parkinson Disease in Men and Women." *American Journal of Epidemiology* 175, no. 11 (June 1, 2012): 1200–1207.

Liu, Yongjian, Doris Peter, Ali Roghani, Shimon Schuldiner, Gilbert G. Prive, David Eisenberg, Nicholas Brecha, and Robert H. Edwards. "A cDNA That Suppresses MPP+ Toxicity Encodes a Vesicular Amine Transporter." *Cell* 70, no. 4 (August 21, 1992): 539–51.

Liu, Yuanbin, Gary Fiskum, and David Schubert. “Generation of Reactive Oxygen Species by the Mitochondrial Electron Transport Chain.” *Journal of Neurochemistry* 80, no. 5 (March 2002): 780–87.

Lockhart, Paul J., Andrew B. West, Casey A. O’farrell, and Matthew J. Farrer. “Identification of a Novel Gene Linked to Parkin via a Bidirectional Promoter.” *Annals of the New York Academy of Sciences* 991, no. 1 (June 1, 2003): 311–14.

Lockwood, William W., Kreshnik Zejnullahu, James E. Bradner, and Harold Varmus. “Sensitivity of Human Lung Adenocarcinoma Cell Lines to Targeted Inhibition of BET Epigenetic Signaling Proteins.” *Proceedings of the National Academy of Sciences* 109, no. 47 (November 20, 2012): 19408–13.

Lodish, Harvey, Arnold Berk, S. Lawrence Zipursky, Paul Matsudaira, David Baltimore, and James Darnell. *Molecular Cell Biology*. 4th ed. W. H. Freeman, 2000.

Lotharius, Julie, and Patrik Brundin. “Impaired Dopamine Storage Resulting from A-synuclein Mutations May Contribute to the Pathogenesis of Parkinson’s Disease.” *Human Molecular Genetics* 11, no. 20 (October 1, 2002): 2395–2407.

Lpopis J. et al. (1998) Measurement of cytosolic, mitochondrial, and Golgi pH in single living cells with green fluorescent proteins. *Proccedings of the National Academy of Sciences of the USA*. **95** (12): 6803-6808

Macmillan, *Quantitative Chemical Analysis*., 2010. Chapter 13. Fundamentals of Electrochemistry. p.279 - 307

Mai, L. M., K. R. Shieh, and J. T. Pan. “Circadian Changes of Serum Prolactin Levels and Tuberoinfundibular Dopaminergic Neuron Activities in Ovariectomized Rats Treated with or without Estrogen: The Role of the Suprachiasmatic Nuclei.” *Neuroendocrinology* 60, no. 5 (November 1994): 520–26.

Manfredsson, F.P., Burger, C., Sullivan, L.F., Muzyczka, N., Lewin, A.S., and Mandel, R.J. (2007). rAAV-mediated nigral human parkin over-expression partially ameliorates motor deficits via enhanced dopamine neurotransmission in a rat model of Parkinson’s disease. Exp. Neurol. *207*, 289–301.

Manfredsson, Fredric P., Corinna Burger, Layla F. Sullivan, Nicholas Muzyczka, Alfred S. Lewin, and Ronald J. Mandel. “rAAV-Mediated Nigral Human Parkin over-Expression Partially Ameliorates Motor Deficits via Enhanced Dopamine Neurotransmission in a Rat Model of Parkinson’s Disease.” *Experimental Neurology* 207, no. 2 (October 2007): 289–301.

Manfredsson, Fredric P, Nihal Tumer, Benedek Erdos, Tessa Landa, Christopher S Broxson, Layla F Sullivan, Aaron C Rising, et al. “Nigrostriatal rAAV-Mediated GDNF Overexpression Induces Robust Weight Loss in a Rat Model of Age-Related Obesity.”

Molecular Therapy: The Journal of the American Society of Gene Therapy 17, no. 6 (June 2009): 980–91.

Manthripragada, Angelika D., Sadie Costello, Myles G. Cockburn, Jeff M. Bronstein, and Beate Ritz. "Paraoxonase 1, Agricultural Organophosphate Exposure, and Parkinson Disease:" *Epidemiology* 21, no. 1 (January 2010): 87–94.

Manyam BV. 1990. Paralysis agitans and levodopa in "Ayurveda":Ancient Indian medical treatise. Mov Disord 5:47–48.

Markey, S.P., Johannessen, J.N., Chiueh, C.C., Burns, R.S., and Herkenham, M.A. Intraneuronal generation of a pyridinium metabolite may cause drug-induced parkinsonism. Nature. 1984; 311:464-467

Maroteaux, L., and R. H. Scheller. "The Rat Brain Synucleins; Family of Proteins Transiently Associated with Neuronal Membrane." *Brain Research. Molecular Brain Research* 11, no. 3–4 (October 1991): 335–43.

Marsden, C. D. "Pigmentation in the Nucleus Substantiae Nigrae of Mammals." *Journal of Anatomy* 95, no. Pt 2 (April 1961): 256–61.

Martinez-Vicente, Marta, Zsolt Talloczy, Susmita Kaushik, Ashish C. Massey, Joseph Mazzulli, Eugene V. Mosharov, Roberto Hodara, et al. "Dopamine-Modified α-Synuclein Blocks Chaperone-Mediated Autophagy." *The Journal of Clinical Investigation* 118, no. 2 (February 1, 2008): 777–88.

Matzuk, Martin M., and Clifford B. Saper. "Preservation of Hypothalamic Dopaminergic Neurons in Parkinson's Disease." *Annals of Neurology* 18, no. 5 (November 1, 1985): 552–55.

McCormack, Alison L., Jennifer G. Atienza, Louisa C. Johnston, Julie K. Andersen, Susan Vu, and Donato A. Di Monte. "Role of Oxidative Stress in Paraquat-induced Dopaminergic Cell Degeneration." *Journal of Neurochemistry* 93, no. 4 (May 1, 2005): 1030–37.

McCormack, Alison L., Mona Thiruchelvam, Amy B. Manning-Bog, Christine Thiffault, J. William Langston, Deborah A. Cory-Slechta, and Donato A. Di Monte. "Environmental Risk Factors and Parkinson's Disease: Selective Degeneration of Nigral Dopaminergic Neurons Caused by the Herbicide Paraquat." *Neurobiology of Disease* 10, no. 2 (July 2002): 119–27.

McFarland, Nikolaus R., Jeng-Shin Lee, Bradley T. Hyman, and Pamela J. McLean. "Comparison of Transduction Efficiency of Recombinant AAV Serotypes 1, 2, 5, and 8 in the Rat Nigrostriatal System." *Journal of Neurochemistry* 109, no. 3 (May 2009): 838–45.

Mizuno Y et al. Inhibition of mitochondrial respiration by 1-methyl-4-phenyl-1,2,3,6-tetrahydropyridine in mouse brain *in vivo*. *Neurosci Lett*. 1988; **91**: 349-353

Mizuno, Y., Ohta, S., Tanaka, M., Takamiya, S., Suzuki, K., Sato, T., Oya, H., Ozawa, T., and Kagawa, Y. (1989). Deficiencies in Complex I subunits of the respiratory chain in Parkinson's disease. Biochemical and Biophysical Research Communications *163,* 1450–1455.

Mizuno, Y., Suzuki, K., Sone, N., and Saitoh, T. (1988). Inhibition of mitochondrial respiration by 1-methyl-4-phenyl-1,2,3,6-tetrahydropyridine (MPTP) in mouse brain in vivo. Neurosci. Lett. *91*, 349–353.

Mizuno, Y., N. Hattori, H. Mori, T. Suzuki, and K. Tanaka. "Parkin and Parkinson's Disease." *Current Opinion in Neurology* 14, no. 4 (August 2001): 477–82.

Mizuno, Yoshikuni, Nobuhito Sone, Keiji Suzuki, and Tomohiko Saitoh. "Studies on the Toxicity of 1-methyl-4-phenylpyridinium Ion (MPP+) Against Mitochondria of Mouse Brain." *Journal of the Neurological Sciences* 86, no. 1 (August 1988): 97–110.

Moore, K E, K T Demarest, and K J Lookingland. "Stress, Prolactin and Hypothalamic Dopaminergic Neurons." *Neuropharmacology* 26, no. 7B (July 1987): 801–8.

Morgan, I.G. Synaptosomes and cell separation. *Neuroscience* 1, 159–165 (1976).

Moss, J., and Bolam, J.P. (2008). A Dopaminergic Axon Lattice in the Striatum and Its Relationship with Cortical and Thalamic Terminals. J. Neurosci. *28*, 11221–11230.

Murphy, Michael P. "How Mitochondria Produce Reactive Oxygen Species." *Biochemical Journal* 417, no. Pt 1 (January 1, 2009): 1–13.

Nakamura H et al. Mitochondria covered with a net of parallel and latticed filaments in nigral neurons of monkeys with experimental parkinsonism. *Acta Neuropathol*. 1989; **77**: 489-493.

Nakamura, H., Kato, S., and Tanaka, J. (1989). Mitochondria covered with a net of parallel and latticed filaments in nigral neurons of monkeys with experimental parkinsonism. Acta Neuropathol. *77*, 489–493.

Nakatogawa, Hitoshi, Yoshinobu Ichimura, and Yoshinori Ohsumi. "Atg8, a Ubiquitin-like Protein Required for Autophagosome Formation, Mediates Membrane Tethering and Hemifusion." *Cell* 130, no. 1 (July 13, 2007): 165–78. doi:10.1016/j.cell.2007.05.021.

Narendra, Derek P., Seok Min Jin, Atsushi Tanaka, Der-Fen Suen, Clement A. Gautier, Jie Shen, Mark R. Cookson, and Richard J. Youle. "PINK1 Is Selectively Stabilized on Impaired Mitochondria to Activate Parkin." *PLoS Biol* 8, no. 1 (January 26, 2010): e1000298.

Narendra, Derek, Atsushi Tanaka, Der-Fen Suen, and Richard J. Youle. "Parkin Is Recruited Selectively to Impaired Mitochondria and Promotes Their Autophagy." *The Journal of Cell Biology* 183, no. 5 (December 1, 2008): 795–803.

Nicklas WJ, Youngster SK, Kindt MV, Heikkila RE. MPTP, MPP+ and mitochondrial function.Life Sci. 1987;40(8):721-9.

Nishioka, Kenya, Shin Hayashi, Matthew J. Farrer, Andrew B. Singleton, Hiroyo Yoshino, Hisamasa Imai, Toshiaki Kitami, et al. "Clinical Heterogeneity of A-synuclein Gene Duplication in Parkinson's Disease." *Annals of Neurology* 59, no. 2 (February 1, 2006): 298–309.

Noble J, Bailey M. Quantitation of protein. Methods Enzymol. 2009;463:73–95.

Noda, Nobuo N., Yoshinori Ohsumi, and Fuyuhiko Inagaki. "Atg8-family Interacting Motif Crucial for Selective Autophagy." *FEBS Letters*, Autophagy, 584, no. 7 (April 2, 2010): 1379–85.

Noyce, Alastair J., Jonathan P. Bestwick, Laura Silveira-Moriyama, Christopher H. Hawkes, Gavin Giovannoni, Andrew J. Lees, and Anette Schrag. "Meta-Analysis of Early Nonmotor Features and Risk Factors for Parkinson Disease." *Annals of Neurology* 72, no. 6 (December 1, 2012): 893–901.

Olzmann, James A., Lian Li, Maksim V. Chudaev, Jue Chen, Francisco A. Perez, Richard D. Palmiter, and Lih-Shen Chin. "Parkin-mediated K63-linked Polyubiquitination Targets Misfolded DJ-1 to Aggresomes via Binding to HDAC6." *The Journal of Cell Biology* 178, no. 6 (September 10, 2007): 1025–38.

Ott. Rotenone. "A Brief Review of its Chemistry. Environmental Fate, and Toxicity of Rotenone Formulations." Accessed October 14, 2014. http://www.newmexicotu.org/Rotenone%20summary.pdf

Outeiro, Tiago Fleming, and Susan Lindquist. "Yeast Cells Provide Insight into Alpha-synuclein Biology and Pathobiology." *Science (New York, N.Y.)* 302, no. 5651 (December 5, 2003): 1772–75.

Ozawa, T. "Oxidative Damage and Fragmentation of Mitochondrial DNA in Cellular Apoptosis." *Bioscience Reports* 17, no. 3 (June 1997): 237–50.

Palacino, J.J., Sagi, D., Goldberg, M.S., Krauss, S., Motz, C., Wacker, M., Klose, J., and Shen, J. (2004). Mitochondrial dysfunction and oxidative damage in parkin-deficient mice. J. Biol. Chem. *279*, 18614–18622.

Park, Jeehye, Sung Bae Lee, Sungkyu Lee, Yongsung Kim, Saera Song, Sunhong Kim, Eunkyung Bae, et al. "Mitochondrial Dysfunction in Drosophila PINK1 Mutants Is Complemented by Parkin." *Nature* 441, no. 7097 (June 29, 2006): 1157–61.

Parkinson, James. *An Essay on the Shaking Palsy*. Whittingham and Rowland, 1817.

Passmore, Lori A, and David Barford. "Getting into Position: The Catalytic Mechanisms of Protein Ubiquitylation." *Biochemical Journal* 379, no. Pt 3 (May 1, 2004): 513–25.

Perez, F.A., and Palmiter, R.D. (2005). Parkin-deficient mice are not a robust model of parkinsonism. PNAS *102*, 2174–2179.

Petit, Agnes, Toshitaka Kawarai, Erwan Paitel, Nobuo Sanjo, Mary Maj, Michael Scheid, Fusheng Chen, et al. "Wild-type PINK1 Prevents Basal and Induced Neuronal Apoptosis, a Protective Effect Abrogated by Parkinson Disease-related Mutations." *Journal of Biological Chemistry* 280, no. 40 (October 7, 2005): 34025–32.

Pendergrass, W., Wolf, N., and Poot, M. (2004). Efficacy of MitoTracker GreenTM and CMXrosamine to measure changes in mitochondrial membrane potentials in living cells and tissues. Cytometry Part A *61A*, 162–169.

Polosa, P.L. & Attardi, G. Distinctive pattern and translational control of mitochondrial protein synthesis in rat brain synaptic endings. J. Biol. Chem. 266, 10011-10017 (1991).

Polymeropoulos, M. H., J. J. Higgins, L. I. Golbe, W. G. Johnson, S. E. Ide, G. Di Iorio, G. Sanges, et al. "Mapping of a Gene for Parkinson's Disease to Chromosome 4q21-q23." *Science (New York, N.Y.)* 274, no. 5290 (November 15, 1996): 1197–99.

Poole, Angela C., Ruth E. Thomas, Laurie A. Andrews, Heidi M. McBride, Alexander J. Whitworth, and Leo J. Pallanck. "The PINK1/Parkin Pathway Regulates Mitochondrial Morphology." *Proceedings of the National Academy of Sciences* 105, no. 5 (February 5, 2008): 1638–43.

Preti A. Vanoxerine national institute on drug abuse. Curr Opin Invistig Drugs. 2000;1(2):241-51.

Ramsay RR, Dadgar J, Trevor A, Singer TP. Energy-driven uptake of N-methyl-4-phenylpyridine by brain mitochondria mediates theneurotoxicity of MPTP. Life Sci. 1986 Aug 18;39(7):581-8.

Ramsay RR, Kowal AT, Johnson MK, Salach JI, Singer TP. The inhibition site of MPP+, the neurotoxic bioactivation product of 1-methyl-4-phenyl-1,2,3,6-tetrahydropyridine is near the Q-binding site of NADH dehydrogenase. Arch Biochem Biophys.1987;259(2):645-9.

Ramsay, R. R., and T. P. Singer. "Energy-dependent Uptake of N-methyl-4-phenylpyridinium, the Neurotoxic Metabolite of 1-methyl-4-phenyl-1,2,3,6-tetrahydropyridine, by Mitochondria." *The Journal of Biological Chemistry* 261, no. 17 (June 15, 1986): 7585–87.

Rana, A., Rera, M., and Walker, D.W. (2013). Parkin overexpression during aging reduces proteotoxicity, alters mitochondrial dynamics, and extends lifespan. PNAS *110*, 8638–8643.

Richter, C., J. W. Park, and B. N. Ames. "Normal Oxidative Damage to Mitochondrial and Nuclear DNA Is Extensive." *Proceedings of the National Academy of Sciences* 85, no. 17 (September 1, 1988): 6465–67.

Rogers GW, Brand MD, Petrosyan S, Ashok D, Elorza AA, et al. (2011) High Throughput Microplate Respiratory Measurements Using Minimal Quantities of Isolated Mitochondria. PLoS ONE 6(7): e21746.

Ross, Owen A., Mathias Toft, Andrew J. Whittle, Joseph L. Johnson, Spiridon Papapetropoulos, Deborah C. Mash, Irene Litvan, et al. "Lrrk2 and Lewy Body Disease." *Annals of Neurology* 59, no. 2 (February 1, 2006): 388–93.

Royden Jones, Netter's Neurology, Chapter 47. Parkinson's disease, (Elsevier Inc. 2005), p.402-415

Royden Jones, Netter's Neurology, Chapter 57. Surgical treatments for movement disorders, (Elsevier Inc. 2005), p.475-477

Sanchez-Ramos J, Barrett JN, Goldstein M, Weiner WJ, Hefti F. 1-Methyl-4- phenylpyridinium (MPP+) but not 1-methyl-4-phenyl-1,2,3,6-tetrahydropyridine (MPTP) selectively destroys dopaminergic neurons in cultures of dissociated rat mesencephalic neurons. Neurosci Lett. 1986;72(2):215-20.

Sancho, Rosa M., Bernard M. H. Law, and Kirsten Harvey. "Mutations in the LRRK2 Roc-COR Tandem Domain Link Parkinson's Disease to Wnt Signalling Pathways." *Human Molecular Genetics* 18, no. 20 (October 15, 2009): 3955–68. doi:10.1093/hmg/ddp337.

Sandyk, R. (1993). The relationship between diabetes mellitus and Parkinson's disease. Int. J. Neurosci. *69*, 125–130.

Santa Cruz Biotechnology, Inc.2007.HEPES (CAS 7365-45-9). http://www.scbt.com/datasheet- 29097-hepes.html, September 2014

Satake, Wataru, Yuko Nakabayashi, Ikuko Mizuta, Yushi Hirota, Chiyomi Ito, Michiaki Kubo, Takahisa Kawaguchi, et al. "Genome-wide Association Study Identifies Common Variants at Four Loci as Genetic Risk Factors for Parkinson's Disease." *Nature Genetics* 41, no. 12 (December 2009): 1303–7. doi:10.1038/ng.485.

Sauerbeck, A., Pandya, J., Singh, I., Bittman, K., Readnower, R., Bing, G., and Sullivan, P. (2011). Analysis of regional brain mitochondrial bioenergetics and susceptibility to mitochondrial inhibition utilizing a microplate based system. J Neurosci Methods *198*, 36–43.

Schapira, A.H.V., Cooper, J.M., Dexter, D., Jenner, P., Clark, J.B., and Marsden, C.D. (1989). Mitochondrial complex I deficiency in parkinson's disease. The Lancet *333*, 1269.

Schmidt. “Medicalneurophys.” *Medicalneurophys*. (2012). Accessed July 16, 2014. http://medicalneurophys.wordpress.com/.

Scotcher, K.P., Irwin, I., DeLanney, L.E., Langston, J.W., and Di Monte, D. (1990). Effects of 1-methyl-4-phenyl-1,2,3,6-tetrahydropyridine and 1-methyl-4-phenylpyridinium ion on ATP levels of mouse brain synaptosomes. J. Neurochem. *54*, 1295–1301.

Scotcher KP, Irwin I, DeLanney LE, Langston JW, Di Monte D. Mechanism of accumulation of the 1-methyl-4-phenylpyridinium species into mouse brain synaptosomes. J Neurochem. 1991;56(5):1602-7.

Seaman, Matthew N. J., Michael E. Harbour, Daniel Tattersall, Eliot Read, and Nicholas Bright. “Membrane Recruitment of the Cargo-selective Retromer Subcomplex Is Catalysed by the Small GTPase Rab7 and Inhibited by the Rab-GAP TBC1D5.” *Journal of Cell Science* 122, no. 14 (July 15, 2009): 2371–82. doi:10.1242/jcs.048686.

Sherer T.B., R. Betarbet, *and* J. T. Greenamyre, Environment, mitochondria, and Parkinson's disease. *Neuroscientist.2002;8(*3):*192*–197

Sherer, Todd B., Jason R. Richardson, Claudia M. Testa, Byoung Boo Seo, Alexander V. Panov, Takao Yagi, Akemi Matsuno-Yagi, Gary W. Miller, and J. Timothy Greenamyre. “Mechanism of Toxicity of Pesticides Acting at Complex I: Relevance to Environmental Etiologies of Parkinson’s Disease.” *Journal of Neurochemistry* 100, no. 6 (March 1, 2007): 1469–79. doi:10.1111/j.1471-4159.2006.04333.x.

Shieh, K. R., and J. T. Pan. “An Endogenous Cholinergic Rhythm May Be Involved in the Circadian Changes of Tuberoinfundibular Dopaminergic Neuron Activity in Ovariectomized Rats Treated with or without Estrogen.” *Endocrinology* 136, no. 6 (June 1995): 2383–88. doi:10.1210/endo.136.6.7750459.

Shimoji, K., Ravasi, L., Schmidt, K., Soto-Montenegro, M.L., Esaki, T., Seidel, J., Jagoda, E., Sokoloff, L., Green, M.V., and Eckelman, W.C. (2004). Measurement of Cerebral Glucose Metabolic Rates in the Anesthetized Rat by Dynamic Scanning with 18F-FDG, the ATLAS Small Animal PET Scanner, and Arterial Blood Sampling. J Nucl Med *45*, 665–672.

Sigma-Aldrich, 2014. Dimethyl Sulfoxide. http://www.sigmaaldrich.com/catalog/product/sigma/d8418?lang=en&region=US, September 2014

Simón-Sánchez, Javier, Claudia Schulte, Jose M. Bras, Manu Sharma, J. Raphael Gibbs, Daniela Berg, Coro Paisan-Ruiz, et al. “Genome-wide Association Study Reveals Genetic Risk Underlying Parkinson’s Disease.” *Nature Genetics* 41, no. 12 (December 2009): 1308–12.

Simonsen, Anne, Robert C. Cumming, Andreas Brech, Pauline Isakson, David R. Schubert, and Kim D. Finley. “Promoting Basal Levels of Autophagy in the Nervous System Enhances

Longevity and Oxidant Resistance in Adult Drosophila." *Autophagy* 4, no. 2 (February 2008): 176–84.

Singer TB et al. Biochemistry of the neurotoxic action of MPTP: or how a faulty batch of'designer drug' led to parkinsonism in drug abusers. Trends Biochem. Sci. 1987;12: 266-270

Singleton, A B, M Farrer, J Johnson, A Singleton, S Hague, J Kachergus, M Hulihan, et al. "alpha-Synuclein Locus Triplication Causes Parkinson's Disease." *Science (New York, N.Y.)* 302, no. 5646 (October 31, 2003): 841. doi:10.1126/science.1090278.

Smeyne, Richard Jay, and Vernice Jackson-Lewis. "The MPTP Model of Parkinson's Disease." Molecular Brain Research, Molecular Mechanisms in Parkinson's Disease, 134, no. 1 (March 24, 2005): 57-66.

Sudhof, T.C. (2004). "The synaptic Vesicle Cycle". Annual Review of Neuroscience 27: 509-547.

Smith, Y., Bennett, B.D., Bolam, J.P., Parent, A., and Sadikot, A.F. (1994). Synaptic relationships between dopaminergic afferents and cortical or thalamic input in the sensorimotor territory of the striatum in monkey. The Journal of Comparative Neurology *344*, 1–19.

Smith, Wanli W., Zhong Pei, Haibing Jiang, Darren J. Moore, Yideng Liang, Andrew B. West, Valina L. Dawson, Ted M. Dawson, and Christopher A. Ross. "Leucine-Rich Repeat Kinase 2 (LRRK2) Interacts with Parkin, and Mutant LRRK2 Induces Neuronal Degeneration." *Proceedings of the National Academy of Sciences of the United States of America* 102, no. 51 (December 20, 2005): 18676–81.

Spencer, Brian, Rewati Potkar, Margarita Trejo, Edward Rockenstein, Christina Patrick, Ryan Gindi, Anthony Adame, Tony Wyss-Coray, and Eliezer Masliah. "BECLIN 1 GENE TRANSFER ACTIVATES AUTOPHAGY AND AMELIORATES THE NEURODEGENERATIVE PATHOLOGY IN ?-SYNUCLEIN MODELS OF PARKINSON'S AND LEWY BODY DISEASE." *The Journal of Neuroscience : The Official Journal of the Society for Neuroscience* 29, no. 43 (October 28, 2009): 13578–88.

Spina, M B, and G Cohen. "Dopamine Turnover and Glutathione Oxidation: Implications for Parkinson Disease." *Proceedings of the National Academy of Sciences of the United States of America* 86, no. 4 (February 1989): 1398–1400.

Starkov, Anatoly A. "The Role of Mitochondria in Reactive Oxygen Species Metabolism and Signaling." *Annals of the New York Academy of Sciences* 1147, no. 1 (December 1, 2008): 37–52.

Stephans SE, Miller GW, Levey AI, Greenamyre JT. Acute mitochondrial and chronic toxicological effects of 1-methyl-4-phenylpyridinium in humanneuroblastoma cells. Neurotoxicology. 2002;23(4-5):569-80.

St-Pierre, Julie, Julie A. Buckingham, Stephen J. Roebuck, and Martin D. Brand. "Topology of Superoxide Production from Different Sites in the Mitochondrial Electron Transport Chain." *The Journal of Biological Chemistry* 277, no. 47 (November 22, 2002): 44784–90.

Sun, X., Liao, N.-K., and Yu, J.-J. (2012). Prognostic Value of a Mitochondrial Functional Score in Prostate Cancer. J. Int. Med. Res. *40*, 371–376.

Taiz L. Zeiger E. 2010. *Plant physiology*. 5th edition. Sinauer Associates, Inc.

Takahashi, Nobuyuki, Lucinda L. Miner, Ichiro Sora, Hiroshi Ujike, Randal S. Revay, Vladimir Kostic, Vernice Jackson-Lewis, Serge Przedborski, and George R. Uhl. "VMAT2 Knockout Mice: Heterozygotes Display Reduced Amphetamine-conditioned Reward, Enhanced Amphetamine Locomotion, and Enhanced MPTP Toxicity." *Proceedings of the National Academy of Sciences* 94, no. 18 (September 2, 1997): 9938–43.

Takahashi, H., E. Ohama, S. Suzuki, Y. Horikawa, A. Ishikawa, T. Morita, S. Tsuji, and F. Ikuta. "Familial Juvenile Parkinsonism: Clinical and Pathologic Study in a Family." *Neurology* 44, no. 3 Pt 1 (March 1994): 437–41.

Tanaka A. Parkin-mediated selective mitochondrial autophagy, mitophagy: Parkin purges damaged organelles from vital mitochondrial network. FEBS let. 2010;584:1386-1392

Tang, Fei, Bin Wang, Na Li, Yanfang Wu, Junying Jia, Talin Suo, Quan Chen, Yong-Jun Liu, and Jie Tang. "RNF185, a Novel Mitochondrial Ubiquitin E3 Ligase, Regulates Autophagy through Interaction with BNIP1." *PLoS ONE* 6, no. 9 (September 9, 2011): e24367.

Tanida I. Ueno T. Kominami E. LC3 and autophagy. Methods Mol Biol. 2008; 445: 77-88.

Tanner, C. M., and S. M. Goldman. "Epidemiology of Parkinson's Disease." *Neurologic Clinics* 14, no. 2 (May 1996): 317–35.

Tenenbaum, L., A. Chtarto, E. Lehtonen, T. Velu, J. Brotchi, and M. Levivier. "Recombinant AAV-Mediated Gene Delivery to the Central Nervous System." *The Journal of Gene Medicine* 6, no. S1 (February 1, 2004): S212–S222.

Thomas, Kelly Jean, Melissa K. McCoy, Jeff Blackinton, Alexandra Beilina, Marcel van der Brug, Anna Sandebring, David Miller, Dragan Maric, Angel Cedazo-Minguez, and Mark R. Cookson. "DJ-1 Acts in Parallel to the PINK1/parkin Pathway to Control Mitochondrial Function and Autophagy." *Human Molecular Genetics* 20, no. 1 (January 1, 2011): 40–50.

Tolkovsky, Aviva M, Luzheng Xue, Graham C Fletcher, and Vilma Borutaite. "Mitochondrial Disappearance from Cells: a Clue to the Role of Autophagy in Programmed Cell Death and Disease?" *Biochimie* 84, no. 2–3 (February 2002): 233–40.

Tong, Youren, Hiroo Yamaguchi, Emilie Giaime, Scott Boyle, Raphael Kopan, Raymond J. Kelleher, and Jie Shen. "Loss of Leucine-Rich Repeat Kinase 2 Causes Impairment of Protein Degradation Pathways, Accumulation of ?-Synuclein, and Apoptotic Cell Death in Aged Mice." *Proceedings of the National Academy of Sciences of the United States of America* 107, no. 21 (May 25, 2010): 9879–84.

Torres GE, Gainetdinov RR, Caron MG (2003). "Plasma membrane monoamine transporters: structure, regulation and function". Nat. Rev. Neurosci. 4 (1): 13-25.

Trempe, Jean-François, and Edward A Fon. "Structure and Function of Parkin, PINK1, and DJ-1, the Three Musketeers of Neuroprotection." *Frontiers in Neurology* 4 (2013): 38.

Turrens, J. F., A. Alexandre, and A. L. Lehninger. "Ubisemiquinone Is the Electron Donor for Superoxide Formation by Complex III of Heart Mitochondria." *Archives of Biochemistry and Biophysics* 237, no. 2 (March 1985): 408–14.

Uhl, G.R., Walther, D., Mash, D., Faucheux, B., and Javoy-Agid, F. (1994). Dopamine transporter messenger RNA in Parkinson's dis ease and control substantia nigra neurons. Ann. Neurol.35, 494–498.

UniProt Consortium, "Large neutral amino acids transporter small subunit 1, Q01650." Accessed June 10, 2014. http://www.uniprot.org/uniprot/Q01650.

Valente, Enza Maria, Anna Rita Bentivoglio, Peter H. Dixon, Alessandro Ferraris, Tamara Ialongo, Marina Frontali, Alberto Albanese, and Nicholas W. Wood. "Localization of a Novel Locus for Autosomal Recessive Early-Onset Parkinsonism, PARK6, on Human Chromosome 1p35-p36." *The American Journal of Human Genetics* 68, no. 4 (January 4, 2001): 895–900.

Van der Zee P. HS Koger. J. gootjes. Hespe W. Aryl 1,4-dialk(en)ylpiperaziones as selective and very potent inhibitors of dopamine uptake. European J Pharmacol.1980; 86:303.

Van Duijn, C. M., M. C. J. Dekker, V. Bonifati, R. J. Galjaard, J. J. Houwing-Duistermaat, P. J. L. M. Snijders, L. Testers, et al. "PARK7, a Novel Locus for Autosomal Recessive Early-Onset Parkinsonism, on Chromosome 1p36." *The American Journal of Human Genetics* 69, no. 3 (January 9, 2001): 629–34.

Vercammen, L., Van der Perren, A., Vaudano, E., Gijsbers, R., Debyser, Z., Van den Haute, C., and Baekelandt, V. (2006). Parkin protects against neurotoxicity in the 6- hydroxydopamine rat model for Parkinson's disease. Mol. Ther. *14*, 716–723.

Vila, Miquel, and Serge Przedborski. "Genetic Clues to the Pathogenesis of Parkinson's Disease" 10 (July 1, 2004): S58–S62.

Vilariño-Güell, Carles, Christian Wider, Owen A. Ross, Justus C. Dachsel, Jennifer M. Kachergus, Sarah J. Lincoln, Alexandra I. Soto-Ortolaza, et al. "VPS35 Mutations in Parkinson Disease." *The American Journal of Human Genetics* 89, no. 1 (July 15, 2011): 162–67.

Vincow, E.S., Merrihew, G., Thomas, R.E., Shulman, N.J., Beyer, R.P., MacCoss, M.J., and Pallanck, L.J. (2013). The PINK1-Parkin pathway promotes both mitophagy and selective respiratory chain turnover in vivo. Proc. Natl. Acad. Sci. U.S.A. *110*, 6400–6405.

Virmani A, Gaetani F, Binienda Z, Xu A, Duhart H, Ali SF.. Role of mitochondrial dysfunction in neurotoxicity of MPP+: partial protection of PC12 cells byacetyl-L-carnitine. Ann N Y Acad Sci. 2004;1025:267-73.

Wang, Qing Jun, Yaomei Ding, D. Stave Kohtz, Stave Kohtz, Noboru Mizushima, Ileana M. Cristea, Michael P. Rout, et al. "Induction of Autophagy in Axonal Dystrophy and Degeneration." *The Journal of Neuroscience: The Official Journal of the Society for Neuroscience* 26, no. 31 (August 2, 2006): 8057–68.

Wang, Xinglong, Michael H. Yan, Hisashi Fujioka, Jun Liu, Amy Wilson-Delfosse, Shu G. Chen, George Perry, Gemma Casadesus, and Xiongwei Zhu. "LRRK2 Regulates Mitochondrial Dynamics and Function through Direct Interaction with DLP1." *Human Molecular Genetics* 21, no. 9 (May 1, 2012): 1931–44.

Wider, C., L. Skipper, A. Solida, L. Brown, M. Farrer, D. Dickson, Z. K. Wszolek, and F. J. G. Vingerhoets. "Autosomal Dominant Dopa-responsive Parkinsonism in a Multigenerational Swiss Family." *Parkinsonism & Related Disorders* 14, no. 6 (August 2008): 465–70.

Wimalasena, K. (2011). "Vesicular monoamine transporters: structure-function, pharmacology, and medicinal chemistry." Med Res Rev 31 (4):483-519.

Whittaker, V.P. Thirty years of synaptosome research. J. Neurocytol. 22, 735-742 (1993).

Whittaker, V.P. & Gray, E.G. The synapse: biology and morphology. Br. Med. Bull. 18, 223-228 (1962)

Wolf ME. Kaptos G. Flow cytometric analysis of rat striatal nerve terminals. J. Neurosci. 1989; 9(1):94-105.

Xiao, Xiao, Juan Li, and Richard Jude Samulski. "Production of High-Titer Recombinant Adeno-Associated Virus Vectors in the Absence of Helper Adenovirus." *Journal of Virology* 72, no. 3 (March 1, 1998): 2224–32.

Xie, L., H. Kang, Q. Xu, M. J. Chen, Y. Liao, M. Thiyagarajan, J. O'Donnell, et al. "Sleep Drives Metabolite Clearance from the Adult Brain." *Science* 342, no. 6156 (October 18, 2013): 373–77.

Xu, Q., Y. Park, X. Huang, A. Hollenbeck, A. Blair, A. Schatzkin, and H. Chen. "Physical Activities and Future Risk of Parkinson Disease." *Neurology* 75, no. 4 (July 27, 2010): 341–48.

Yang, Yi, Koji Fukui, Tatsuro Koike, and Xiaoxiang Zheng. "Induction of Autophagy in Neurite Degeneration of Mouse Superior Cervical Ganglion Neurons." *The European Journal of Neuroscience* 26, no. 10 (November 2007): 2979–88.

Youle RJ. Narendra DP. Mechanisms of mitophagy. Nat Rev Mol Biol. 2011;12(1):9-14

Zamzami N et al. (2000) Quantitation of Mitochondrial transmembrane potential in cells and in isolated mitochondria. *Methods in enzymology*. **322**: 208-213

Zecca, L, D Tampellini, M Gerlach, P Riederer, R G Fariello, and D Sulzer. "Substantia Nigra Neuromelanin: Structure, Synthesis, and Molecular Behaviour." *Molecular Pathology* 54, no. 6 (December 2001): 414–18.

Zhang, Bicheng, Jun Huang, Hong-Liang Li, Ting Liu, Yan-Yi Wang, Paul Waterman, Ai-Ping Mao, et al. "GIDE Is a Mitochondrial E3 Ubiquitin Ligase That Induces Apoptosis and Slows Growth." *Cell Research* 18, no. 9 (September 2008): 900–910.

Zhang, L., L. Yu, and C. A. Yu. "Generation of Superoxide Anion by Succinate-Cytochrome c Reductase from Bovine Heart Mitochondria." *The Journal of Biological Chemistry* 273, no. 51 (December 18, 1998): 33972–76.

Zhang, Pingzhao, Long Yu, Jie Gao, Qiang Fu, Fangyan Dai, Yong Zhao, Lu Zheng, and Shouyuan Zhao. "Cloning and Characterization of Human VPS35 and Mouse Vps35 and Mapping of VPS35 to Human Chromosome 16q13–q21." *Genomics* 70, no. 2 (December 1, 2000): 253–57.

Zhang Z-X, Dong Z-H,Roma´n GC. 2006. Early descriptionsof Parkinson's disease in ancient China. Arch Neurol 63:782–784.

Zimprich, Alexander, Anna Benet-Pagès, Walter Struhal, Elisabeth Graf, Sebastian H. Eck, Marc N. Offman, Dietrich Haubenberger, et al. "A Mutation in VPS35, Encoding a Subunit of the Retromer Complex, Causes Late-Onset Parkinson Disease." *The American Journal of Human Genetics* 89, no. 1 (July 15, 2011): 168–75.